BIOSYNTHESIS OF GOLD NANOPARTICLES FOR BREAST CANCER TARGETED DRUG DELIVERY

DISSERTATION

Submitted to the Graduate School

In Partial Fulfillment of the Requirement for the

Degree of Doctor of Philosophy in the

Department of Materials Science and Engineering

African University of Science and Technology, Abuja-Nigeria

By

DOZIE-NWACHUKWU STELLA OBIAGELI (ID No: 70084)

December, 2016.

PhD Dissertation Committee:

Prof. Wole Soboyejo (Princeton University, NJ, USA)

Dr. O. Shola Odusanya (SHESTCO, Abuja, Nigeria)

Dr. Karen Malatesta (Princeton University, NJ, USA)

Dr. Nicolas Anuku (Princeton University, NJ, USA)

BIOSYNTHESIS OF GOLD NANOPARTICLES FOR BREAST CANCER TARGETED DRUG DELIVERY

By:

DOZIE-NWACHUKWU STELLA OBIAGELI

A THESIS APPROVED BY THE MATERIALS SCIENCE AND ENGINEERING DEPARTMENT

RECOMMENDED: ……

Supervisor, Professor Wole Soboyejo

……..

Co-supervisor, Dr. O. Shola Odusanya

…….

Head, Dept. of Materials Science and Engineering

Approved: …….

Chief Academic Officer

Date: ……..

DEDICATION

With thanks to Almighty God,

This dissertation is dedicated to my darling husband, Chiedozie Nwachukwu and my lovely children, Justin and Kamsy

ABSTRACT

Although there have been significant efforts in breast cancer treatment over the past many decades, current therapeutic approaches are limited by non-specific systemic distribution, inadequate drug concentrations reaching the tumor and multidrug resistance. This dissertation presents the results of experimental and theoretical studies of the potential applications of biosynthesized gold nanoparticles (AuNPs) and micro encapsulated prodigiosin in targeted drug delivery for the treatment of breast cancer. Gold nanoparticles possess unique physicochemical properties, such as large surface area to mass ratio, and high surface reactivity, presence of surface plasmon resonance (SPR) bands, biocompatibility and ease of surface functionalization, which enables them to diffuse with greater ease inside the tumor cells delivering a high amount of drug selectively to tumor cells with significant reduced toxicity. In this work, the biosynthesis of gold nanoparticles (AuNPs) from plant (Nauclea latifolia) and bacteria (Serratia marcescens) were elucidated. The Nauclea latifolia extract was used to synthesize AuNPs in a record time of < 30 sec, and the sizes of the nanoparticles were in the range of 10 nm – 60 nm. The AuNPs were characterized with UV-visible (UV-Vis) spectroscopy, while the nanoparticle shapes, sizes and polydispersity were elucidated via transmission electron microscopy (TEM) and dynamic light scattering (DLS), respectively. Selected area electron diffraction (SAED) patterns of the AuNPs showed the four-fringe pattern of gold nanoparticles, which corresponds to the face centered cubic (fcc) metal structure of gold ((111), (200), (220), (311)), which confirmed the formation of pure metallic gold nanoparticles. The biosynthesized nanoparticles were functionalized with some molecular recognition units (MRU) (Luteinizing Hormone Releasing Hormone, LHRH and Folic Acid), through thiol linkages or carbodiimide chemistry. The adhesion force between LHRH- or Folate- conjugated AuNPs and the breast cancer cell line

MDA-MB-231 was determined through atomic force microscopy (AFM). Furthermore, Helium Ion Microscopy (HIM) was used to visualize the clear ring of attachment of the ligands to the gold core. The encapsulation of prodigiosin in chitosan microspheres was equally studied for localized drug delivery. The water-in-oil emulsion technique in which glutaraldehyde was used as a cross-linker was adopted. The morphologies of the resulting microspheres were then studied using scanning electron microscopy (SEM). The average sizes of the microspheres were between 40 µm and 60 µm, while the percentage yields were found to be between 42±2% and 55.5±3%. The resulting encapsulation efficiencies were between 66.7±3% and 90±4%. The in- vitro drug release from the microspheres were characterized using Higuchi and Korsmeyer-Peppas models. The implications of these results are then discussed with a view of developing suitable drug delivery systems that will go a long way to solving the problem of breast cancer in the world, with particular reference to Africa.

Table of Contents

Contents **Pages**

Acknowledgements

My greatest thanks go to Almighty God for His overwhelming kindness, divine mercies and protection, and above all for seeing me to the end of this study. To you oh Lord be honor, adoration and praise forever and ever…Amen!

I am highly indebted and will ever remain grateful to my advisor, Prof. Wole Soboyejo. I count myself to be greatly honored to have a world class professor as my supervisor. In him I found not just an advisor, but a father, friend and mentor, who was always there for me to patiently guide, support and encourage me, even during the tough times in this Ph.D. pursuit. May God Almighty who knows how best to reward continually favor, protect and bless you and your wonderful family.

My sincere gratitude goes to Dr. Shola Odusanya who apart from being my co-advisor, is also my boss in the office where I work. He has been strongly behind me with his full support, constant encouragement, criticisms, advice and guidance throughout the period of this study. He is more like a brother and friend to me. I pray that God will always grant you open doors of favor and kindness.

I would like to thank my thesis committee members, Prof. W.O. Soboyejo, Dr. S.O. Odusanya, Dr. Karen Malatesta, and Dr. Nicolas Anuku, whose meaningful contributions and questions broadened my horizon in the new frontiers of nanomedicine. I also wish to acknowledge my Head of Department, Prof. Peter Onwualu, for his moral support and fatherly advice.

Some of the characterization done in this dissertation would not have been possible without the help of friends like Mr. Gerald Poiriere, Cathy Chi, Jingjie Hu, Vanessa Uzonwanne, and Dr. John Obayemi, all of Princeton University, New Jersey. I am indeed very grateful to you all. I am particularly grateful to the Biomedical Research Group and the entire Soboyejo Research

Group at the African University of Science and Technology, Abuja-Nigeria for their care, support and encouragement when the going was tough.

At this point, I wish to acknowledge the World Bank STEP- B program, and the World Bank African Centers of Excellence Program, The African University of Science and Technology, The African Development Bank, The African Capacity Building Foundation and the Nelson Mandela Institution (NMI) for financial support.

I am also grateful to the technical staff at Princeton Institute of Science and Technology of Materials (PRISM) for their assistance with materials characterization, the staff of the Central workshop and the Biotechnology Advanced Research Center of Sheda Science and Technology complex (SHESTCO) for their technical support. I wish to express my gratitude to the Director General of SHESTCO, Prof. S.A. Thomas for his encouragement and support.

I would like to thank my family members, my loving, supportive, encouraging, and patient husband, Dozie, whose faithful support during this Ph.D. is so much appreciated, my children, Justin and Kamsy, my brothers and sisters, especially, Mrs. Vivian Opara, my brothers-in-law, sisters-in-law, my dearly mother-in-law, my cousins, nieces and nephews. Thank you all for your love and encouragement.

Lastly, I bless the name of the Lord for my parents, Chief and Lolo Charles .O. Iwuoha (of the Blessed Memory). Though you did not live to see me attain this academic height, but it had always been your wish for me. And I know it is your prayers with the angels that saw me through. I am proud to be your daughter.

PEER REVIEWED PUBLICATIONS IN PHD FOCUS

1. **S.O. Dozie-Nwachukwu,** Y. Danyuo, J.D. Obayemi, O.S. Odusanya , K. Malatesta, W.O. Soboyejo. Extraction and encapsulation of prodigiosin in chitosan microspheres for targeted drug delivery. ELSEVIER; J. of Mater. Sci. and Engr. C (MSEC). Ref. No.: MSEC-D-16-01152R1, http://dx.doi.org/10.1016/j.msec.2016.09.078

2. **S. O. Dozie-Nwachukwu,** J. D. Obayemi,Y. T. Danyuo, G. Etuk-Udo, Y. Chi, J. Hu, N. Anuku,O.S. Odusanya, K. Malatesta, and W.O. Soboyejo. Biosynthesis of Gold Nanoparticles And Gold/Prodigiosin Nanoparticles with Serratia Marcescens Bacteria. Springer Journals; Waste Biomass Valor (2016), WAVE-D-15-00229R4

3. **S. O. Dozie-Nwachukwu**, J. D. Obayemi, Y. Danyo, G. Etuk-Udo, N. Anuku, O.S. Odusanya, K. Malatesta, C. Chi and W.O. Soboyejo. Biosynthesis of Gold Nanoparticles with *Serratia Marcescens* Bacteria. Advanced Materials Research Vol. 1132 (2015) pp 19-35; doi:10.4028/www.scientific.net/AMR.1132.19.

4. **S. O. Dozie-Nwachukwu,** G. Etuk-Udo, J. D. Obayemi, N. Anuku, O.S Odusanya, K. Malatesta, C. Chi and W.O. Soboyejo. Biosynthesis of Gold Nanoparticles from *Nauclea Latifolia* Leaves. Advanced Materials Research Vol. 1132 (2015) pp 36-50; doi:10.4028/www.scientific.net/AMR.1132.36

5. **S. O. Dozie-Nwachukwu,** J. D. Obayemi, Y. Danyuo, G. Etuk-Udo, N. Anuku, O.S Odusanya, K. Malatesta, J. Hu, Y. Chi, and W.O. Soboyejo. Adhesion of Biosynthesized Gold and Conjugated Gold/Prodigiosin Nanoparticles to Triple Negative Breast Cancer Cells. Publisher Springer Journals; Waste Biomass Valor (under review). Manuscript Number: WAVE-D-15-00242R2

6. Y. Danyuo, C. J. Ani, J. D. Obayemi, **S. Dozie-Nwachukwu** O. S. Odusanya , Y. Oni , N. Anuku, K. Malatesta and W. O. Soboyejo. Prodigiosin Release from an Implantable Biomedical Device: Effect on Cell Viability. Advanced Materials Research Vol. 1132 (2015) pp 3-18; doi:10.4028/www.scientific.net/AMR.1132.3

7. Y. Oni, K. Hao, **S. Dozie-Nwachukwu**, J. D. Obayemi, O. S. Odusanya, N. Anuku, and W. O. SoboyejoGold nanoparticles for cancer detection and treatment: The role of adhesion.Publisher (AIP) Journal of Applied Physics 115, 084305 (2014); doi: 10.1063/1.4863541

8. J. D. Obayemi, **S. Dozie-Nwachukwu,** Y. Danyuo, O. S. Odusanya, N. Anuku, K. Malatesta and W. O. Soboyejo. "Biosynthesis and the Conjugation of Magnetite Nanoparticles with Luteinizing Hormone Releasing Hormone (LHRH)". ELSEVIER; J.

of Mater. Sci. and Engr. C (MSEC).46 (2015) 482-496. DOI: 10.1016/j.msec.2014.10.081.

9. Y. Danyuo, J. D. Obayemi, **S. Dozie-Nwachukwu**, C. J. Ani, O. S. Odusanya, Y. Oni, N. Anuku, K. Malatesta and W. O. Soboyejo. "Prodigiosin Release from an Implantable Biomedical Device: Kinetics of Localized Cancer Drug Release". Publisher (ELSEVIER); Journal of Materials Science and Engineering C (MSEC), Vol. 42, Issue (1) (2014) pp734 - 745. Doi:10.1016/j.msec.2014.06.008.

10. Y. Danyuo, **S. Dozie-Nwachukwu**, J. D. Obayemi, C. J. Ani, O. S. Odusanya, Y. Oni, N. Anuku, K. Malatesta and W. O. Soboyejo. "Swelling of Poly (N-isopropyl acrylamide) (PNIPA)-Based Hydrogels with Bacterial-Synthesized Prodigiosin for Localized Cancer Drug Delivery". Publisher (ELSEVIER); Journal of Materials Science and Engineering C (MSEC) Vol. 59, (1) (2016), pp 19–29. Doi:10.1016/j.msec.2015.09.090.

11. J.D. Obayemi, Y. Danyuo, **S. Dozie-Nwachukwu,** O.S. Odusanya, N. Anuku, K. Malatesta, W. Yu, K.E. Uhrich, W.O. Soboyejo. PLGA-based microparticles loaded with bacterial-synthesized prodigiosin for anticancer drug release: Effects of particle size on drug release kinetics and cell viability. ELSEVIER ; Materials Science and Engineering: C Vol. 66, 1 September 2016, Pages 51–65 http://dx.doi.org/10.1016/j.msec.2016.04.071

12. J. D. Obayemi, Y. Danyuo, **S. Dozie-Nwachukwu,** O. S. Odusanya, N. Anuku, K. Malatesta, W. Yu, K. E. Uhrich and W. O. Soboyejo. "Injectable Biodegradable Prodigiosin-Loaded Microparticles for Localized Cancer Drug Delivery". Publisher (ELSEVIER); Journal of Materials Science and Engineering C (MSEC) (under review). Manuscript Number: MSECD- 15-00246.

LIST OF CONFERENCE PRESENTATIONS

1. **S.O. Dozie-Nwachukwu,** Y. Danyuo, J. Ani, G. Etuk-Udo, J.D Obayemi, N. Anuku, O. S. Odusanya, K. Malatesta and W.O. Soboyejo Biosynthesized Gold Nanoparticles and Microparticles for Cancer detection and treatment. 1st Us/Africa Workshop on Cancer Research, Princeton University, New Jersey, USA (26th -29th June, 2016).

2. **S.O. Dozie-Nwachukwu,** Y.T. Danyuo, J. Ani, G. Etuk-Udo, J.D Obayemi, N. Anuku, O. S. Odusanya, K. Malatesta and W.O. Soboyejo. Functionalization of gold nanoparticles for cancer therapy and diagnosis. The 8th International Conference of the African Materials Research Society, Accra, Ghana (7th – 10th December, 2015).

3. **S.O. Dozie-Nwachukwu,** J.D Obayemi, Y.T. Danyuo, J. Ani, G. Etuk-Udo, N. Anuku, O. S. Odusanya, K. Malatesta and W.O. Soboyejo. *In-vitro* release of prodigiosin encapsulated into chitosan microspheres. 1st AUSTECH International Conference, held at AUST, (12th – 13th October, 2015).

4. **Stella. O. Dozie-Nwachukwu**, Winston Wole Soboyejo and O. S. Odusanya. "Biosynthesis of Gold Nanoparticles for Breast Cancer Targeted Drug Delivery and Laser-Induced Hyperthermia", AUST PhD Colloquium 2015. Book of Proceedings (22nd January 2015).

5. **S.O. Dozie-Nwachukwu**, G. Etuk-Udo, J.D Obayemi, Y.T. Danyuo, N. Anuku, O. S Odusanya, K. Malatesta and W.O. Soboyejo. Folate-Conjugated Gold Nanoparticles an Approach for targeting Triple Negative Breast Cancer. The 7th International Conference of the African Materials Research Society, Addis-Ethiopia, (07-14th December, 2013).

6. **S.O. Dozie-Nwachukwu,** G. Etuk-Udo, J.D Obayemi, Y.T. Danyuo, N. Anuku, O. S. Odusanya, K. Malatesta and W.O. Soboyejo. Biosynthesis of gold nanoparticles: A comparison of plants and bacterial methods. A Presentation at the 1st International Conference of the NANOMEDICINE Society of Nigeria and the Nigerian Engineered Materials Conference at AUST-Abuja.". (25th – 29th November, 2013).

7. **S.O. Dozie-Nwachukwu.,** G. Etuk-Udo., J.D. Obayemi., N. Anuku., O.S.,Odusanya., K. Malatesta and ,O.W Soboyejo. Biosynthesis of Gold Nanoparticles with *Nauclea latifolia*

leaves and its application in Cancer Therapy. Nigerian Engineered Materials Conference at Obafemi Awolowo University, Ile Ife. (20^{th} – 24^{th} November, 2012).

8. **S. Dozie-Nwachukwu** and Y. Danyuo. "Nanoparticles and BioMEMS for Cancer Detection and Treatment". Presentation at AUST, during the Visit of World Bank Vice President, 2012.

9. Danyuo Yiporo, **S.O. Dozie-Nwachukwu**, G.A. Etuk-Udo, O. Oberiafor, M. C. Ilouno., T.M. Meshack, A. Agwu, O. S. Odusanya and W. O. Soboyejo. BIOMEMS for breast cancer drug delivery. Nigerian Engineered Materials Conference at Akure (20^{th} – 24^{th} November, 2011).

List of Figures

LIST OF TABLES

CHAPTER 1

1.0 Background / Introduction

1.1 Problem of Cancer

Cancer is a worldwide problem! [1] It is the second leading cause of death among other diseases [2, 3]. There is hardly any community in the world today without a cancer patient. According to the International Agency for Research on Cancer (IARC) [4], there were 14 million new cancer cases in 2012, worldwide, of which 5.6 million occurred in economically developed countries and 7.1 million in economically developing countries. A corresponding number of deaths also occurred in 2012 in the tune of 8.2 million (about 21,000 cancer deaths a day), 2.9 million in economically developed countries and 5.3million in economically developing countries. By 2030, this global burden is expected to grow to 21.7 million new cancer cases and 13 million cancer deaths due to the growth and aging of the population, as well as reductions in childhood mortality and deaths from infectious diseases in developing countries [2].

Cancer has a lot of economic implications. The immediate cost includes the money paid for the treatment and care/rehabilitation related to the illness [5]. The indirect costs include the loss of economic output due to days missed from work (morbidity costs) and premature death (mortality costs) [6]. There are also hidden costs of cancer, such as health insurance premiums and nonmedical expenses (transportation, child or elder care, house-keeping assistance etc.) [5-10]. According to a report by the American Cancer Society on the global economic cost of cancer (2010) [11], the total economic impact of premature death and disability from cancer was estimated to be as high as $895 billion worldwide, not including the direct cost of treating cancer. By implication, the study stated that 83 million years of healthy life were lost due to

death and disability from cancer in 2008 [11]. It was also found that the top three cancers that had the most economic impact are lung cancer ($188 billion), colon/rectal cancer ($99 billion) and breast cancer ($88 billion) [12, 13, 14].

Breast cancer is the most common cancer in women worldwide. Nearly 1.7 million new cases were diagnosed in 2012 [15]. This represents about 12% of all new cancer cases and 25% of all cancers in women [15]. Between 1980 and 2010, the number of women diagnosed with breast cancer in the USA increased more than two and a half times from 641,000 to 1.6 million a year [16]. The highest growth rates have been in North Africa, the Middle East, Oceania, South-East Asia, Western Sub-Saharan Africa and Central America [14]. The number of cases has risen most slowly in the rich, developed countries. The United Kingdom has one of the lowest growth rates of new cases of cancer at 1% a year **[16].** In 2016, an estimated 246,660 new cases of invasive breast cancer are expected to be diagnosed in women in the U.S., along with 61,000 new cases of non-invasive (in situ) breast cancer [17, 18].

In Africa as a whole, breast cancer is currently one of the most commonly diagnosed cancers among women in Africa, and also the leading cause of death due to cancer [19]. Breast cancer rates were highest in the Northern Africa and Southern Africa regions (32.7 per 100,000 and 38.1 per 100,000 respectively) [20]. According to a report [19], breast cancer incidence is on the increase, as compared to previous decades in which cervical cancer was the most commonly diagnosed cancer in many of these countries. The reasons for this shift include an increase in the prevalence of risk factors for breast cancer such as early menarche, later child-bearing, having fewer children, and obesity – factors that are associated with higher economic development [21]. In Uganda, breast cancer incidence has doubled from 11 per 100,000 in 1961 to 22 per 100,000 in 1995 [22]. This increase has been attributed to the adoption of westernized lifestyles;

however, improvements in data collection and reporting may also be contributing factors [23-24]. The factors contributing to the high mortality rates (fewer than half of women with breast cancer survive beyond 5 years in Gambia, Uganda and Algeria, compared with nearly 90% in the USA) include lack of appropriate screening services, lack of awareness about the symptoms of breast cancer, and the stigma that is often still associated with having cancer [25-26].

In Nigeria, breast cancer is the most common type of cancer in Nigerian women [27-28]. The incidence rate increased from 13.8–15.3 per 100,000 in the 1980s, to 33.6 per 100,000 in 1992 and 116 per 100,000 in 2001 [29]. The increase has been ascribed to changes in the demography, socio-economic parameters, epidemiologic risk factors, better reporting and increased awareness of the disease. Whereas the rate of mortality is declining in the developed countries such as America, Australia and Western Europe as a result of early diagnosis, screening, and improved cancer treatment programs, the reverse is the case in Africa and other developing countries [30-32]. Between 1960 and 1980, cervical cancer had 19.9% prevalence while breast cancer had 11.2% but between 1981 and 1995, breast cancer has taken over the lead with 25.7% while cervical cancer followed closely with 22.7% [33]. These statistics shows the incidence of breast cancer to be rated first among all other cancers.

Though breast cancer occurs at various ages, in 15% of the cases the women are under 30 years with the youngest age of 16 years being recorded in Lagos State [29]. The menace of breast cancer afflicting young women has been consistently reported among Africans including African Americans [34-41].

Most women present in advanced stages, retrospective studies have showed that 70 –90% of African women present with Stage III or IV of the disease. [34,36,37,42-43]. This could be as a

result of several factors ranging from lack of awareness, stigmatization, religious beliefs, family issues and socioeconomic factors which have been noted to influence the choice and outcome of treatment among women with late stages of breast cancer [22,37,44-46].

The biggest problem facing the cure of cancer is that of early detection [47 - 48], because the existing methods of detection such as biopsy, ductogram, and mammogram are limited in spatial resolution. Another major problem is the severe effects of existing cancer treatment methods e.g. radiation, surgery and chemotherapy. However, experts insist that early detection in order to improve breast cancer outcome and survival remains the cornerstone of breast cancer control.

1.2 Nanoparticles for the detection and treatment of cancer

Nanotechnology is the science that deals with matter at the scale of 1 billionth of a meter (i.e.,$10^{-}9$ m = 1 nm)[49]. A nanoparticle is a small object that measures between 1-100 nm and behaves as a whole unit with respect to its transport and properties [50]. Metallic nanoparticles have different physical and chemical properties from bulk metals, which make them attractive in various industrial applications. Such properties include; lower melting points, higher specific surface areas, specific optical properties, mechanical strengths, and specific magnetizations [49]. The particles have wide variety of potential applications in biomedical, optical and electronic fields [51-53]. Nanoparticles often have unexpected visible properties because they are small enough to confine their electrons and produce quantum effects. For example gold nanoparticles appear deep red to black in solution. Nanoparticles also have a very high surface area to volume ratio; this makes them to be more reactive to some other molecules than the bulk material.

Research in the field of nanoscience and nanotechnology has experienced unprecedented growth in recent time. There is hope that nanotechnology, as applied to medicine, will lead to significant

improvements in the area of diagnosis and treatment of disease. Nanoparticles (NPs) are attractive for medical purposes because of some unique features, such as high surface to mass ratio, quantum properties and ability to adsorb and carry other compounds such as drugs, probes and proteins [54].

One of the major applications of nanotechnology is in the field of medicine. Nanoparticles can be engineered as platforms for effective targeted drugs delivery and imaging labels by overcoming the many biological, biophysical, and biomedical barriers [55-56]. There are some barriers that limit the application of nanoparticles in preclinical and clinical use, such as biocompatibility, in vivo kinetics, tumor targeting efficacy, acute and chronic toxicity, ability to escape the reticuloendothelial system (RES), and cost-effectiveness [57-58].

Effective cancer therapy remains one of the greatest challenges to the scientific community. A major limitation inherent to most conventional anticancer chemotherapeutic agents is their lack of tumor selectivity. The use of nanoparticles as drug delivery vehicles for anticancer therapeutics has great potential to change the future of cancer therapy [59]. Tumor architecture allows nanoparticles to preferentially accumulate at the tumor site through enhanced permeation and retention effect (EPR) [60-61]. Using nanoparticles as drug delivery vectors results in the localization of a greater amount of the drug load at the tumor site thereby improving cancer therapy and reducing the harmful nonspecific side effects of chemotherapeutics [62-63]. In addition, formulation of these nanoparticles with imaging contrast agents provides a very efficient system for cancer diagnostics [62]. Early detection is the major factor in cancer treatment. Breast cancer is usually asymptomatic, such that by the time symptoms appear, the tumor would have metastasized beyond the breast. On the other hand, if breast cancers are

detected early, they tend to be smaller and still confined within the breast [64]. Some of the symptoms (Figure 1.1) of breast cancer include; (1) a lump or area of thickened tissue in either breast, (2) a change in the size or shape of one or both breasts, (3) discharge from either of your nipples (especially blood), (4) a lump or swelling in either of your armpits (5) dimpling on the skin of your breasts, (6) a rash on or around your nipple (7) a change in the appearance of your nipple, such as becoming sunken into your breast.

The size of a breast cancer and how far it has spread are two of the most important factors that determine the prognosis of a woman with this disease [65]. Presently, the common methods of diagnosis includes self -examination, biopsy, magnetic resonance imaging (MRI), mammogram, and ultra sound. Among all these, the mammogram is the gold standard [66], because it offers an effective means to detect breast cancer early. It is noninvasive, relatively inexpensive, and has reasonable sensitivity (72–88%) that increases with age [67-68]. Its primary advantage is the ability to detect tumors less than 1 cm in size and before they become clinically palpable [69]. The mammogram has the challenge of not being able to distinguish between benign and malignant lesions [70]. Thus, a biopsy is required to confirm or rule out cancer. Another drawback for the mammogram is that it is difficult to detect tumors in dense or scarred breast tissue or in augmented breasts is by mammography. Studies have revealed that mammography fails to detect 10% to 25% of breast cancers [71-72].

The conventional methods employed in the treatment of breast cancer include; surgery, radiotherapy, chemotherapy, hormonal therapy, gene therapy and immunotherapy [73-74]. These have been in use over many years but there are serious issues with them that hinder their efficacy at different levels. The main problems with conventional methods include; (i) they are not site-specific (ii) they have high toxicity, (iii) they have devastating short- and long-term side effects, (iv) low efficacy with less than 1% of drug making it to tumor cells. And also (v) they lack specificity.

The emergence of nanoparticles has come to offer solutions to these problems of early diagnosis and more specified treatment of cancer. More so, the ideal technology will be inexpensive and rapid and can be accomplished with little or no discomfort to the patient. Nano-medicine involves the use of precisely engineered materials within the range of 1 – 100nm length scale to develop novel therapeutic and diagnostic materials [75-76].

Gold nanoparticles have been widely used in biomedical science including tissue or tumor imaging, drug delivery, photo thermal therapy and immunochromatographic identification of pathogens in clinical specimens due to the surface plasmon resonance (SPR) [77]. The choice of gold nanoparticles results from their unique physiochemical properties including, large surface area to mass ratio, high reactivity unlike the bulk materials of the same composition, shape, biocompatibilities and surface carrier capabilities which enables different ligands to be attached thereby making them suitable for drug delivery. These properties are being used to overcome some of the limitations found in traditional therapeutic and diagnostic agents [78-79]. Because of their unique properties, nanoparticles have found use in medicine in areas of targeted drug delivery, as diagnostics and in the production of improved biocompatible materials [80]. Gold nanoparticles can be employed in immunohistochemistry to identify protein-protein interaction [81-83]. Also, through surface enhanced Raman scattering spectroscopy they can be used for detection and identification of single dye molecules [84]. Gold nanoparticles have also been employed for many other applications such as time-of-flight secondary ion mass spectrometry [85], capillary electrophoresis [86], and detection of cancer cells [87-88]. Dynamic light scattering (DLS) has been employed in the quantitative estimation of the concentration of intravenously injected gold nanoshells in mouse blood [89]. In another study, the use of gold

nanoshells as optical biosensors for real-time detection of streptavidinbiotin interactions in diluted human blood was evaluated [90].

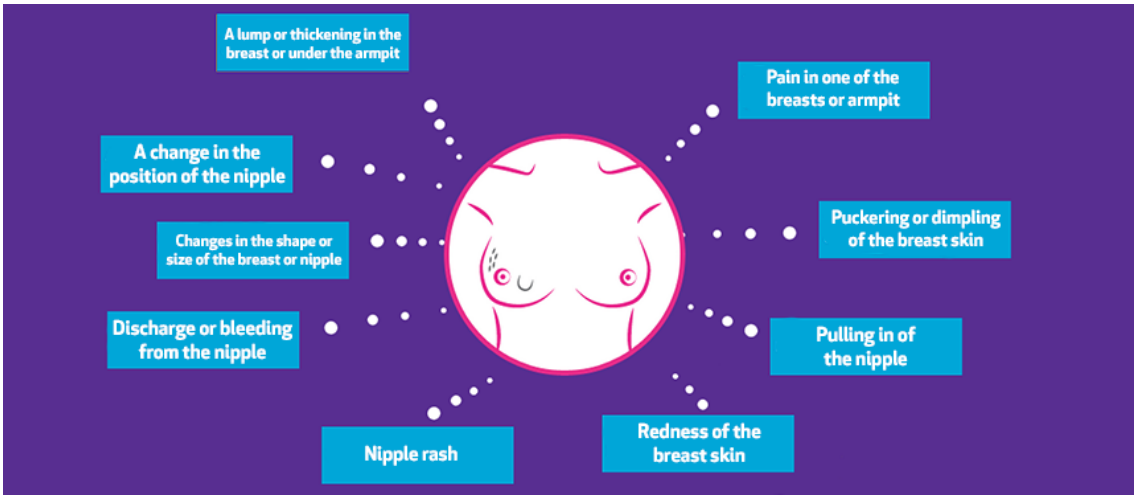

Figure 1.1: A schematic representation of the symptoms of breast cancer

1.3 Research Objectives

The major challenges of breast cancer are that of early detection and treatment regime. These constitute the issues that nanoparticles set to address. This thesis, which is focused on the biosynthesis of gold nanoparticles for breast cancer targeted drug delivery, has the following specific objectives;

- To biosynthesize gold nanoparticles from plants (*Nauclea latifolia*)
- To biosynthesize gold nanoparticles from bacteria *(Serretia marcescens).*
- To understand the mechanism for the formation of gold nanoparticles
- To ascertain the effects of pH and time on the shapes and sizes of the biosynthesized AuNPs

- To functionalize the gold nanoparticles by conjugating with some ligands (LHRH and folic acid) and drug of interest (prodigiosin).
- To carry out *in vitro* targeting of breast cancer cells (MDA-MB-231) using the AuNPs - drug design
- To determine the adhesion and pull-off forces between the conjugated gold nanoparticles and breast cancer cells by using the AFM cantilever method.
- To extract and purify prodigiosin, an anti-cancer agent, from the bacteria, *Serratia marcescens*
- To encapsulate prodigiosin in chitosan microspheres for localized drug delivery
- To study the drug release profile from the microspheres

It is important to consider the possible adverse effects of residual material after the drug delivery. Gold nanoparticles being biocompartible makes them a good candidate in this respect. Also, the choice of chitosan for microencapsulation is equally good since chitosan is biodegradable [91]

This research is therefore aimed at using the combined action of gold nanoparticles targeted drug delivery and localized drug delivery using drug encapsulated microspheres to ensure complete cure of breast cancer.

1.4 Scope of Thesis work

This thesis comprises experimental and theoretical work aimed at using biosynthesized gold nanoparticles in conjunction with chitosan microspheres as drug delivery devices at the nano- and micro-scales for the treatment of breast cancer. We present the results of our efforts to biologically synthesize gold nanoparticles from locally sourced materials, to design novel drug delivery systems that can kill breast cancer cells. It also contains fundamental studies involving

the robustness of current strategies that are being employed in drug delivery systems. This chapter introduces the problems associated with cancer, followed by nanoparticles for the detection and treatment of cancer, the research objectives and the scope of the thesis. Chapter 2 presents a survey of relevant literatures, while chapter 3 proceeds to introduce the synthesis of gold nanoparticles with *Nauclea latifolia* leaf extracts, a plant of local origin, and the adhesion of the conjugated AuNPs to breast cancer cells. Also in Chapter 4, we present the biosynthesis of gold nanoparticles and gold/prodigiosin nanoparticles with *Serratia marcescens* bacteria, a local isolate. Chapter 5 discusses the ligand conjugation of gold nanoparticles with special reference to triple negative breast cancer and cell adhesion, while in Chapter 6, the encapsulation of prodigiosin in chitosan microspheres, the drug release and swelling studies are presented. Salient conclusions are summarized in Chapter 7 along with suggestions for future work.

1.5 Summary

Breast cancer is the second greatest killer disease among women all over the world. In Africa, it is the major killer disease for women. Though the incidence rate of breast cancer is higher in the western word and Europe, than the developing countries, the rate of mortality is higher in the developing countries with particular reference to Africa. Normally, the age of occurrence is 40 years and above, but in Africa and African-Americans, breast cancer begins early in premenopausal women (30 years and above). Most times the type of breast cancer (triple negative breast cancer) that occurs among women of African origin is very virulent with limited prognosis.

The aims of this thesis are to biosynthesize gold nanoparticles and functionalize them with some ligands for targeted drug delivery to breast cancer cells. Indigenous biomaterials (plant leaves

and bacteria) were used for the synthesis which will go a long way to reducing the cost of treatment. Another interesting part of this work is the fact that the anti-cancer drug (prodigiosin) we are using was extracted from the bacteria, *Serratia marcescens*, which we isolated locally from soil at Sheda Science and Technology Complex, Abuja, Nigeria. This will also result in the reduction in the final cost of treatment and ensure availability of the drug.

REFERENCES

1. Ma, X., Yu, H.: Global Burden of Cancer. The Yale Journal of Biology and Medicine 79 (3-4) 85–94 (2006).

2. Ferlay J, Shin HR, Bray F, Forman D, Mathers CD, Parkin D. GLOBOCAN 2008, Cancer Incidence and Mortality Worldwide: IARC Cancer Base No.10 Lyon, France: International Agency for Research on Cancer. Available from: http://globocan.iarc.fr (2010).

3. Renee, T : Cancer Surpasses Heart Disease as Leading Cause of Death for All But the Very Elderly. JNCI J Natl Cancer Inst. 97 (5): 330-331(2005).

4. International Agency for Research on Cancer (IARC), Latest world cancer statistics. press release N° 223, 1-3 (2013).

5. Yabroff, K. R., Lund, J., Kepka, D., Mariotto, A. Economic Burden of Cancer in the US: Estimates, Projections, and Future Research. Cancer Epidemiology, Biomarkers & Prevention : A Publication of the American Association for Cancer Research, Cosponsored by the American Society of Preventive Oncology, 20(10), 2006–2014.

6. Warren, J.,L, Yabroff, K.R, Meekins, A, Topor M, Lamont EB, Brown ML. Evaluation of trends in the cost of initial cancer treatment. J Natl Cancer Inst.100:888–897 (2008).

7. Tangka, F.K, Trogdon, J.G., Richardson, L.C., Howard, D., Sabatino, S.A., Finkelstein, E.A. Cancer treatment cost in the United States. Cancer.116:3477–3484 (2010).

8. Woodward, R.M., Brown, M.L., Stewart, S.T., Cronin, K.A., Cutler, D.M. The value of medical interventions for lung cancer in the elderly: results from SEER-CMHSF. Cancer. 110:2511–2518 (2007).

9. Howard, D.H., Kauh, J., Lipscomb, J. The value of new chemotherapeutic agents for metastatic colorectal cancer. Arch Intern Med. 170:537–542 (2010).

10. Wong, Y-N., Meropol, N.J., Speier, W., Sargent, D., Goldberg, R.M., Beck, J.R. Cost implication of new treatments for advanced colorectal cancer. Cancer. 115:2081–2091 (2009).

11. American cancer society: the economic cost of cancer, 2010. http://www.cancer.org/acs/groups/content/

12. Ortega-Ortega, M., Oliva-Moreno, J., Jiménez-Aguilera, J. D., Romero-Aguilar, A., Espigado-Tocino, I.: Productivity loss due to premature mortality caused by blood cancer: a study based on patients undergoing stem cell transplantation. Gac Sanit. 29(3):178-83, (2015)

13. Hanly, P.A., Sharp, L.: The cost of lost productivity due to premature cancer-related mortality: an economic measure of the cancer burden BMC Cancer. 26;14:224 (2014) .

14. Ekwueme, D.U, Guy, G.P Jr., Rim, S.H., White, A., Hall, I.J., Fairley, T.L., Dean, H.D. Health and economic impact of breast cancer mortality in young women, 1970-2008. Am J Prev Med. 46(1):71-79 (2014)

15. World Cancer Research Fund International. Available from http://www.who.int/cancer/detection/breastcancer/en/index4.html accessed on the 6th May, 2016.

16. Forouzanfar, M.H., Foreman, K.J., Delossantos, A.M., Lozano, R., Lopez, A.D., Murray C.J., Naghavi, M. Breast and cervical cancer in 187 countries between 1980 and 2010: a systematic analysis. Lancet. 378(9801):1461-1484 (2011).

17. Breast cancer.org. US breast cancer statistics Available from http://www.breastcancer.org/symptoms/understand_bc/statistics accessed on 12th May, 2016.

18. Ueno NT, Buzdar AU, Singletary SE, Ames FC, McNeese MD, Holmes FA, Theriault RL, Strom EA, Wasaff BJ, Asmar L, Frye D, Hortobagyi GN. Combined-modality treatment of inflammatory breast carcinoma: twenty years of experience at M. D. Anderson Cancer Center. Cancer Chemother Pharmacol 40 (4): 321-9, (1997).

19. Ahmedin Jemal, Freddie Bray, Melissa M. Center, Jacques Ferlay, Elizabeth Ward, David Forman, Global Cancer Statistics, CA Cancer J Clin; 61: 69 –90 (2011).

20. International Agency for Research on Cancer. Globocan 2000: cancer incidence, mortality and prevalence worldwide. Lyon, France: IARC Press. (2001).

21. Rabia Tariq, Sadia Huma, Mariam Zaka Butt, Fatima Amin. Risk factors and prevalence of breast cancer: a review. J Pak Med Assoc. 63,(8), (2013).

22. Uganda Breast Cancer Working Group, "Breast cancer guidelines for Uganda," The African Health Sciences, 3, 47–50, (2003).

23. Fregene, A., Newman, L.A.: "Breast cancer in sub-Saharan Africa: how does it relate to breast cancer in African-American women?" Cancer, 103,(8):1540–1550,(2005).

24. . Parkin, M. D., Fernández, M. G. "Use of statistics to assess the global burden of breast cancer," The Breast Journal, 12, (1): S70–S80, (2006).

25. Boder, J. M. E., Abdalla, F. B. E., Elfageih, M. A. Abusaa, A., Buhmeida, A., Collan, Y "Breast cancer patients in Libya: comparison with European and central African patients," Oncology Letters, 2(2) 323–330, (2011).

26. Ikpatt, O. F., Kronqvist, P., Kuopio, T., Ndoma-Egba, R., Collan, Y. "Histopathology of breast cancer in different populations: Comparative analysis for Finland and Africa," Electronic Journal of Pathology and Histology, 8, (4), 24011–24018, (2002)

27. Mandong, B.M., Manasseh, A.N., Echejoh, G.O. Cancer in Nigerian Women: A Critical Need for Prevention Strategy. Nigerian Medical Practitioner 56, (1-2) (2009)

28. Adebamowo, C.A, Adekunle, O.O. Case controlled study of the epidemiological risk factors for breast cancer in Nigeria. Br J Surg; 86: 665 - 668 (1999).

29. Adebamowo, C.A., Ajayi, O.O. Breast cancer in Nigeria. West African Journal of Medicine; 19(3):179-91 (2000).

30. Adesunkanmi, A.R., Lawal, O.O, Adelusola, K.A, Durosimi, M.A. The severity, outcome and challenges of breast cancer in Nigeria. Breast 15(3):399-409 (2006).

31. Hisham, A.N., Yip, C.H. Overview of breast cancer in Malaysian women: a problem with late diagnosis. Asian Journal of Surgery 27(2):130-133 (2004) .

32. Parkin, D.M., Bray, F., Ferlay J, Pisani, P. Global cancer statistics, 2005. CA: a Cancer Journal for Clinicians 55(2):74-108 (2005).

33. Adetifa, F. A., Ojikutu, R. K. Prevalence and Trends in Breast Cancer in Lagos State, Nigeria. African Research Review, 3 (5), 1-15 (2009).

34. Amir, H., Kitinya, J.N., Parkin, D.M. A comparative study of carcinoma of the breast in an African population. East Afr Med J. 71:215–218 (1994).

35. Anyanwu, S.N. Breast cancer in eastern Nigeria: a ten year review. West Afr J Med.;19: 120 –125 (2000).

36. Hassan, I, Onukak, E.E, Mabogunje, O.A. Breast cancer in Zaria, Nigeria. J R Coll Surg Edinb.37:159 –161 (1992).

37. Muguti GI. Experience with breast cancer in Zimbabwe. J R Coll Surg Edinb.38:75–78 (1993).

38. Amir, H., Makwaya, C.K., Aziz, M.R, Jessani, S. Breast cancer and risk factors in an African population: a case referent study. East Afr Med J. 75:268 –270 (1998).

39. Adebamowo, C.A., Ogundiran, T.O., Adenipekun, A.A., Oyesegun, R.A., Campbell, O.B., Akang, E.U., Rotimi, C.N., Olopade, O.I. Obesity and height in urban Nigerian women with breast cancer. Ann Epidemiol. 13:455– 461 (2003) .

40. Yawitch, T.M., van Rensburg, E.J., Mertz, M., Falkson, C.I. Absence of commonly recurring BRCA1 mutations in black South African women with breast cancer. S Afr Med J. 90:788 (2000).

41. Ihekwaba, F.N. Breast cancer in Nigerian women. Br J Surg. 79:771–775 (1992).

42. Amir, H., Azizi, M.R., Makwaya, C.K, Jessani, S. TNM classification and breast cancer in an African population: a descriptive study. Cent Afr J Med. 43:357–359 (1997).

43. Hassan, I., Muhammed, I., Attah, M.M., Mabogunje, O. Breast cancer during pregnancy and lactation in Zaria, Nigeria. East Afr Med J. 72:280 –282 (1995).

44. Jones, S.B. Cancer in the developing world: a call to action. BMJ. 319:505–508 (1999).

45. Othieno-Abinya, N.A., Nyabola, L.O., Abwao, H.O., Ndege, P. Postsurgical management of patients with breast cancer at Kenyatta National Hospital. East Afr Med J. 79:156 –162 (2002).

46. Odusanya, O.O., Tayo, O.O. Breast cancer knowledge, attitudes and practice among nurses in Lagos, Nigeria. Acta Oncol. 40:844 – 848 (2001).

47. Richards, M.A., Westcombe, A.M., Love, S.B., Littlejohns, P., Ramirez, A.J. Influence of delay on survival in patients with breast cancer: a systematic review. Lancet. 353:1119–1126 (1999).

48. Olesen, F., Hansen, R.P., Vedsted, P. Delay in diagnosis: the experience in Denmark. Br J Cancer. 101 Suppl 2:S5–S8 (2009).

49. Satoshi, H., Nick, S. Introduction to Nanoparticles, in: Microwaves in Nanoparticle Synthesis, First Edition. Edited by Satoshi Horikoshi and Nick Serpone. Published by Wiley-VCH Verlag GmbH & Co. KGaA (2013).

50. Aiden E. K., Gabriel T. D. Nanoparticles: Properties, Classification, Characterization, and Fabrication. Nova Science Publishers, Inc. (2010).

51. Taylor, R., Coulombe, S., Otanicar, T., Phelan, P., Gunawan, A., Lv, Wei; Rosengarten, Gary; Prasher, Ravi; Tyagi, Himanshu "Small particles, big impacts: A review of the diverse applications of nanofluids". Journal of Applied Physics 113: 011301 (2013).

52. Taylor, R. A; Otanicar, T., Rosengarten, G. "Nanofluid-based optical filter optimization for PV/T systems". Light: Science & Applications 1 (10): e34. (2012).

53. Hewakuruppu, Y. L., Dombrovsky, L. A., Chen, C., Timchenko, V., Jiang, X., Baek, S., Taylor, R. A. "Plasmonic "pump–probe" method to study semi-transparent nanofluids". Applied Optics 52 (24): 6041–6050. (2013).

54. De Jong, W. H., Borm, P. J.A. Drug delivery and nanoparticles: Applications and hazards. Int J Nanomedicine. 3(2): 133–149 (2008).

55. Grodzinski, P., Silver, M., Molnar, L.K. Nanotechnology for cancer diagnostics: promises and challenges. Expert Rev Mol Diagn. 6:307–318 (2006)

56. Sahoo SK, Parveen S, Panda JJ. The present and future of nanotechnology in human health care. Nanomedicine. 3:20–31 (2007)

57. Cai W, Chen X. Nanoplatforms for targeted molecular imaging in living subjects. Small. 3:1840–1854 (2007).

58. Cai, W., Chen, X. Multimodality imaging of tumor angiogenesis. J Nucl Med. 49:113S–128S (2008)

59. W. Cai, T. Gao, H. Hong, J. Sun. Applications of gold nanoparticles in cancer nanotechnology. Nanotechnol Sci Appl.(1): (2008) . doi:10.2147/NSA.S3788.

60. Duncan, R., Sat Y.-N. "Tumour targeting by enhanced permeability and retention (EPR) effect". Ann. Oncol. 9 (Suppl.2): 39 (1998).

61. Vasey, P.A, Kaye SB, Morrison R, Twelves C, Wilson P, Duncan R, Thomson AH, Murray LS, Hilditch T.E, Murray,,T, Burtles, S., Fraier, D., Frigerio E, Cassidy J. "Phase I clinical and pharmacokinetic study of PK1 [N-(2hydroxypropyl)methacrylamide copolymer doxorubicin]: first member of a new class of chemotherapeutic agents-drug-polymer conjugates. Cancer Research Campaign Phase I/II Committee". Clinical Cancer Research 5 (1): 83–94 (1999).

62. van Vlerken, L.E .,an M.M Amiji. Multi-functional polymeric nanoparticles for tumour-targeted drug delivery Expert Opin. Drug Deliv. (2006) 3(2):205-216

63. Kumar Bishwajit Sutradhar and Md. Lutful Amin, "Nanotechnology in Cancer Drug Delivery and Selective Targeting," ISRN Nanotechnology, vol. 2014, Article ID 939378, 12 pages, 2014. doi:10.1155/2014/939378

64. American Cancer Society. Breast Cancer Prevention and Early Detection Available at http://www.cancer.org/acs/groups/cid/documents/webcontent/003165-pdf.pdf. Accessed on 18th May, 2016.

65. Cianfrocca , M., Goldstein, L.J. Prognostic and Predictive Factors in Early-Stage Breast Cancer . The Oncologist. 9 (6) 606-616 (2004)

66. Drukteinis, J. S., Mooney, B. P., Flowers, C. I., Gatenby, R. A. Beyond Mammography: New Frontiers in Breast Cancer Screening. The American journal of medicine, 126, (6), 472–479 (2013).

67. Poplack, S.P., Tosteson, A.N., Grove, M.R., Wells, W.A., Carney, P.A. Mammography in 53,803 women from the New Hampshire Mammography Network. Radiology. 217:832–840 (2000).

68. Linver, M.N., Paster, S.B. Mammography outcomes in a practice setting by age: prognostic factors, sensitivity, and positive biopsy rate. J Natl Cancer Inst Monogr. 22:113–117 (1997).

69. Miller, R. G. Breast Cancer Screening, Can We Talk? J Gen Intern Med. 16(3): 206–207 (2001).

70. Heller, S. L., Moy, L., Lavianlivi, S., Moccaldi, M., Kim, S. Differentiation of Malignant and Benign Breast Lesions Using Magnetization Transfer Imaging and Dynamic Contrast-enhanced MRI. J Magn Reson Imaging. 37(1): 138–145 (2013).

71. Bird, R.E., Wallace, T.W., Yankaskas, B.C., Analysis of cancers missed at screening mammography. Radiology. 184:613–617 (1992).

72. Birdwell, R.L., Ikeda, D.M., O'Shaughnessy, K.F., Sickles, E.A. Mammographic characteristics of 115 missed cancers later detected with screening mammography and the potential utility of computer-aided detection. Radiology. 219:192–202 (2001).

73. Arruebo, M., Vilaboa, N., Sáez-Gutierrez, B., Lambea, J., Tres, A., Valladares, M., González-Fernández, A. Assessment of the Evolution of Cancer Treatment Therapies. Cancers (Basel). 3(3): 3279–3330 (2011).

74. Rafsanjani, B. Z., Mosleh-Shirazi, M. A., Faghihi, R., Mosalaei, A., Omidvari, S., K. Hadad, K., Karbas, S.i. Breast Cancer and its Radiotherapeutic Methods. Iranian Journal of Medical Physics 9, (2), 75-85 (2012).

75. Nikalje, A.P. Nanotechnology and its Applications in Medicine. Med chem 5: 081-089 (2015).

76. Chen, G., Roy, I., Yang, C., Prasad, P.N. Nanochemistry and Nanomedicine for Nanoparticle-based Diagnostics and Therapy. Chem. Rev., 116 (5), 2826–2885 (2016).

77. Chithrani, D.B., Dunne, M., Stewart, J., Allen, C., Jaffray, D.A. Cellular uptake and transport of gold nanoparticles incorporated in a liposomal carrier. Nanomed: Nanotechnol Biol Med 6: 161-169 (2010).

78. Patra, C. R., Bhattacharya, R., Mukhopadhyay, D., Mukherjee, P. Fabrication of Gold Nanoparticles for targeted therapy in pancreatic cancer. Adv Drug Deliv Rev. 8; 62(3): 346–361 (2010).

79. Patel, N.V., Sheth, N. R. Newer Developments in the Nanoparticles for Cancer Treatment. Research and Reviews: Journal of Pharmaceutics and Nanotechnology, 2 (4) (2014)

80. De Jong, W. H., Borm, P. J.A. Drug delivery and nanoparticles: Applications and hazards Int J Nanomedicine. 3(2): 133–149 (2008).

81. Cao, Y.C., Jin, R., Nam, J.M., Thaxton, C.S., Mirkin, C.A. Raman dye-labeled nanoparticle probes for proteins. JACS. 125: 14676–14677 (2003).

82. Salata, O.V. Applications of nanoparticles in biology and medicine. J Nanobiotechnology. 2: 3 (2004).

83. Phillips, R.L., Miranda, O.R., You, C.C., Rotello Uwe, V. M., Bunz, H.F. Rapid and efficient identification of bacteria using gold-nanoparticle-poly(para-phenyleneethynylene) constructs. Angew. Chem. Int. Ed. 47, 2590 (2008).

84. Y. Wang, J. Irudayaraj. Surface-enhanced Raman spectroscopy at single-molecule scale and its implications in biology. Philos Trans R Soc Lond B Biol Sci. 368(1611): 20120026 (2013).

85. Kim, Y.P., Oh, E., Hong, M.Y., Lee, D., Han, M.K., Shon, H.K., Moon, D.W., Kim, H.S., Lee, T.G. Gold nanoparticle-enhanced secondary ion mass spectrometry imaging of peptides on self-assembled monolayers. Anal Chem. 78(6):1913-1920 (2006).

86. Tseng, W.L., Huang, M.F., Huang, Y.F., Chang, H.T., Nanoparticle-filled capillary electrophoresis for the separation of long DNA molecules in the presence of hydrodynamic and electrokinetic forces. Electrophoresis. 26(16):3069-3075 (2005)

87. Kah, J.C., Kho, K.W., Lee, C.G., James, C., Sheppard, R., Shen, Z.X., Soo, K.C., Olivo, M.C. Early diagnosis of oral cancer based on the surface plasmon resonance of gold nanoparticles. Int J Nanomedicine; 2(4):785-98(2007).

88. Medley, C.D., Smith, J.E., Tang, Z., Wu, Y., Bamrungsap, S., Tan, W. Gold nanoparticle-based colorimetric assay for the direct detection of cancerous cells. Anal Chem. 80(4):1067-72 (2008)

89. Xie, H., Gill-Sharp, K.L., O'Neal, D.P. Quantitative estimation of gold nanoshell concentrations in whole blood using dynamic light scattering. Nanomedicine. 3(1):89-94 (2007).

90. Wang, Y., Qian, W., Tan, Y., Ding, S. A label-free biosensor based on gold nanoshell monolayers for monitoring biomolecular interactions in diluted whole blood. Biosens Bioelectron. 23(7):1166-1170 (2008).

91. Saber, A., Strand, S.P., Ulfendahl, M. Use of the biodegradable polymer chitosan as a vehicle for applying drugs to the inner ear. Eur J Pharm Sci.;39 (1-3):110-115 (2010).

CHAPTER 2

2.0 Literature Review

2.1 Introduction

The increase in the incidence of breast cancer in the world today and the high mortality rate with particular reference to African women, has led to the involvement of philanthropists, financiers and researchers in a search of better strategies for the eradication of this dreaded disease [1]. Nanotechnology comprises the synthesis, characterization of materials and design of functionally organized devices in nanoscale (1-100nm) [2]. The application of nanostructured materials in medicine is termed Nanomedicine. The evolvement of Nanomedicine has brought many changes in healthcare and drug delivery. The nanoscale constructs are being utilized to provide a range of multiple, essentially new properties, which can be exploited in ways that improve the detection, treatment and monitoring of disease states [3].

Nanomaterials have a high surface to volume ratio, which enables the attachment of other materials such as drugs or other molecules leading to the formation of multifunctional nanomaterials [3]. Nanomaterials can be engineered to have different shapes, sizes and surface chemistry; as a result, nanomaterials have a wide range of applications in drug delivery, in vivo and in vitro diagnostics, biomaterials, active implants, in vivo imaging, bio-sensing, cell labeling, and tissue engineering [4-6].

This chapter presents an overview of prior work on drug delivery, with a focus on localized drug delivery and targeted delivery using nanoparticles and microparticles. The studies involving biosynthesis of gold nanoparticles (AuNPs), ligand conjugation, drug encapsulation, breast cancer treatment and combination therapy are also discussed.

2.2 CANCER AND CANCER GENETICS

Cancer is a group of diseases that cause cells in the body to change and grow out of control [7]. Most types of cancer cells eventually form a lump or mass called a solid tumor, and are named after the part of the body where the tumor originates. Cancer results from a series of molecular events that alter the normal properties of cells [8]. The normal control systems that prevent cell overgrowth and the invasion of other tissues are disabled in cancer cells [8]. As such, these altered cells divide and grow in the presence of signals that normally inhibit cell growth. Hence, cancer cells no longer require special signals to induce cell growth and division. The result is that these cells grow and develop new characteristics, including changes in cell structure, decreased cell adhesion, and production of new enzymes [9]. The overall effect is that the cell and its progeny divide and grow, even in the presence of normal cells which typically inhibit the growth of nearby cells. These changes allow cancer cells to spread and invade other tissues in the process of metastasis [10].

A small fraction of the approximately 35,000 genes in the human genome are associated with the development of cancer [11]. Alterations in the same gene often result in different forms of cancer [10]. The genes which malfunction can be categorized into three groups. First is the group called proto-oncogenes, which produce proteins that enhance cell division or inhibit normal cell death. The mutated forms of these genes are called oncogenes. The second group is tumor suppressor genes. These genes make proteins that usually prevent cell division or cause cell death. The third group contains DNA repair genes, which helps to prevent mutations that lead to cancer. Cell growth is usually regulated by a control of proto-oncogenes, which accelerate growth, and tumor suppressor genes, which slow or prevent cell growth. Mutations that produce oncogenes

accelerate growth [12], while those that affect tumor suppressors prevent the normal inhibition of growth. When any of these mutations occur, uncontrolled cell growth results [13].

2.2.1 Tumor:

A tumor is a mass of tissue made up from abnormal cells [10]. Tumors are divided into two types, benign and malignant.

2.2.2 Benign Tumors

A benign tumor is a mass of cells that lacks the ability to invade neighboring tissue or metastasize. These may form in various parts of the body. Benign tumors grow slowly, and are not cancerous and are not usually life-threatening (depends on where the tumor develops. If tumor develops in brain, it can cause illness or death because size of cranium is limited) [14]. They often do no harm if they are left alone. However, some benign tumors can cause problems, if tumor is allowed to continue to grow and further mutations occur, the tumor can become malignant. For example, some grow quite large and may cause local pressure symptoms, or look unsightly. Also, some benign tumors that arise from cells in hormone glands can make too much hormone, which can cause unwanted effects [15].

2.2.3 Malignant Tumors

Malignant tumors tend to grow quite quickly, and invade nearby or far away tissues and organs, where they can cause damage. Tumors normally develop in one original site - the primary tumor. Malignant tumors may also spread to other parts of the body to form secondary tumors (metastases). This happens if some cells break off from the primary tumor and are carried in the bloodstream or lymph channels to other parts of the body. These secondary tumors may then grow, invade and damage nearby tissues, and spread again. Not all cancers form solid tumors.

For example, in cancer of the blood cells (leukemia), many abnormal blood cells are made in the bone marrow and circulate in the bloodstream.

2.2.4 How Cancer Develops

Cancer cells behave as independent cells, growing without control to form tumors [16]. Tumor formation takes place in stages. Initially a point mutation occurs in one of the genes of the cell. This leads to hyperplasia due to uncontrolled cell division [17, 18]. At this stage the cells appear normal, but changes have occurred that result in some loss of control of growth (Figure 2.1). The next step is dysplasia, resulting from further growth, followed by abnormal changes to the cells. Additional changes in the cells still occur generating more abnormal cells which can now spread over a wider area of tissue. The cells then become anaplastic and begin to lose their original function. At this stage, the tumor is still contained within its original location (in situ) and is not invasive (benign). The last step occurs when the cells in the tumor metastasize, that is, they can invade surrounding tissue, including the bloodstream, and spread to other locations. This is the most serious type of tumor, but not all tumors progress to this point.

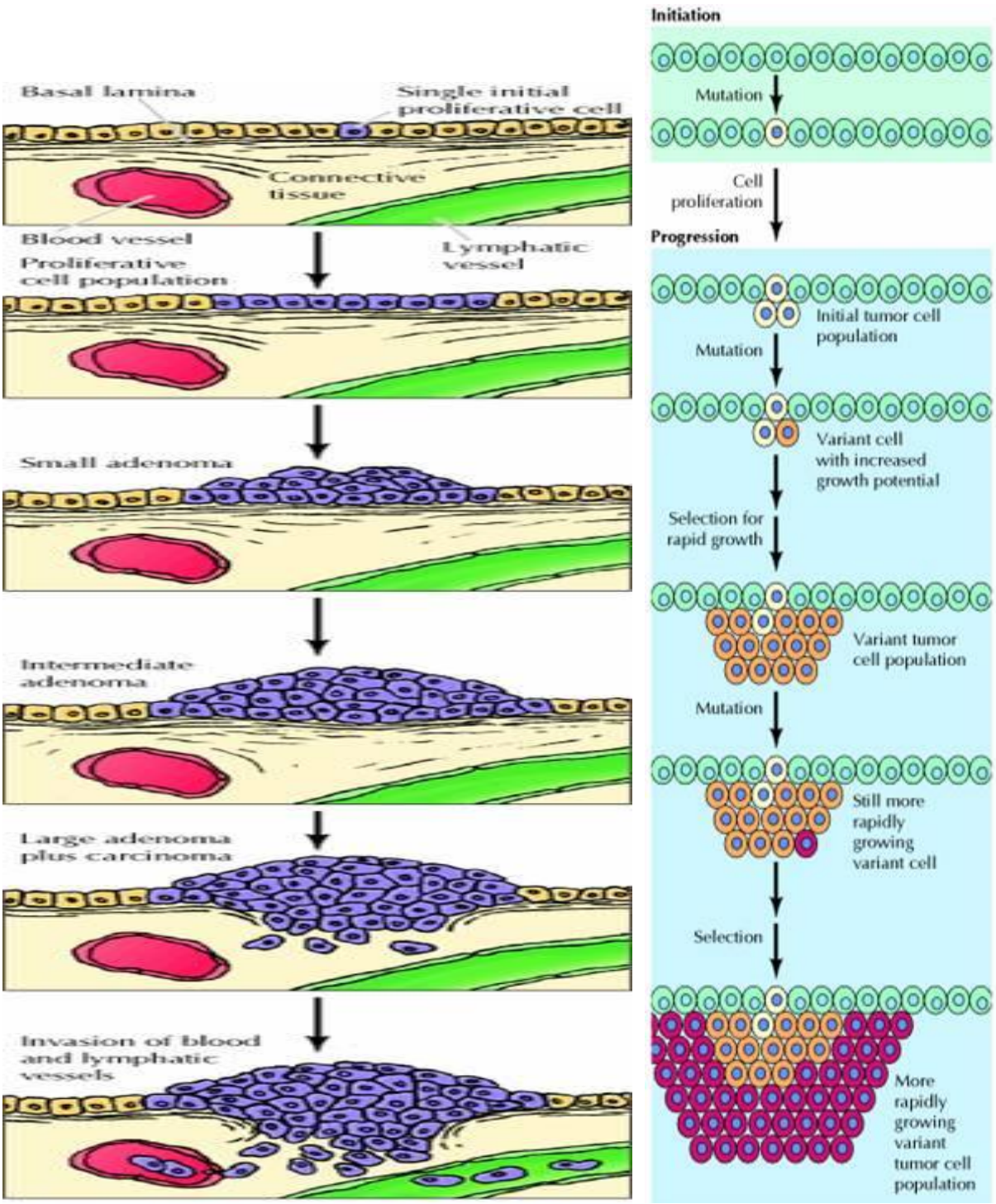

Figure 2.1: stages of cancer development

2.3 BREAST CANCER:

Breast cancer is a malignant neoplasm originating from breast tissue, most commonly from the inner lining of milk ducts or the lobules that supply the ducts with milk [19]. Some of the masses are benign; that is, they are not cancerous, do not grow uncontrollably or spread, and therefore are not life-threatening [20]. Some breast cancers are confined within the ducts and are known as ductal carcinoma in situ (DCIS) or in the lobules, called lobular carcinoma in situ (LCIS). Most times, LCIS (also known as lobular neoplasia) is not regarded as a true cancer, but an indicator of increased risk for developing invasive cancer in either breast [21]. The majority of in situ breast cancers are DCIS, and these account for about 83% of in situ cases diagnosed during 2004-2008 [22, 23]. Some breast cancers are invasive, that is, they break through the duct or glandular walls to invade the surrounding tissue of the breast. Triple-negative breast cancer (TNBC) is a subtype of invasive breast cancer with cells that lack estrogen receptors, progesterone receptors and human epithelial receptor 2 (HER 2). TNBC tends to appear more often in younger women and African-American women [24-28].

2.3.1 The Normal Breast

To understand breast cancer, it helps to have some basic knowledge about the normal structure of the breasts (Figure 2.2). The female breast is made up mainly of lobules (milk-producing glands), ducts (tiny tubes that carry the milk from the lobules to the nipple), and stroma (fatty tissue and connective tissue surrounding the ducts and lobules, blood vessels, and lymphatic vessels). Most breast cancers begin in the cells that line the ducts (ductal cancers). Some begin in the cells that line the lobules (lobular cancers), while a small number start in other tissues.

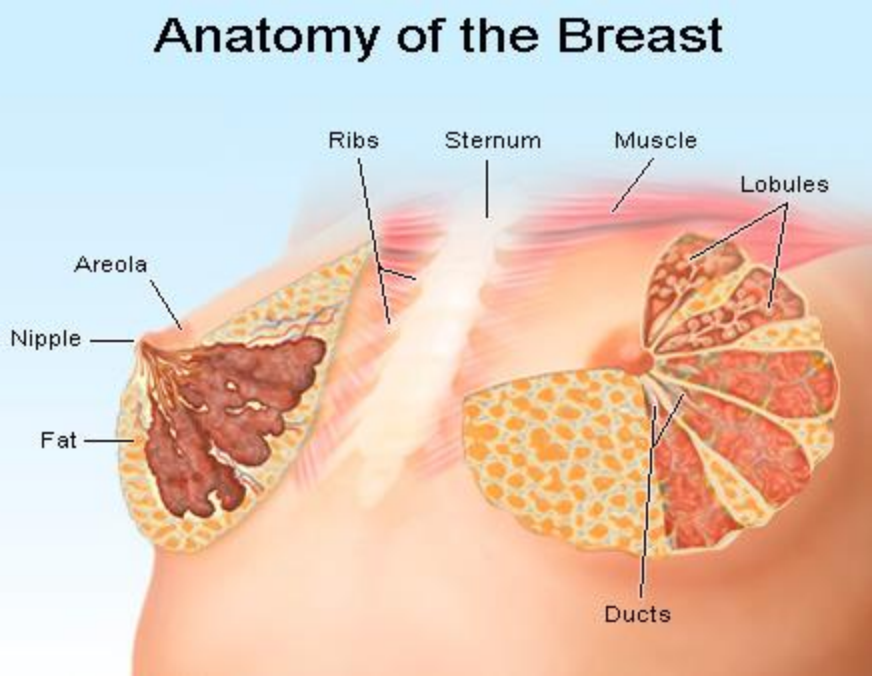

Figure 2.2: The Anatomy of the Breast

2.3.2 Risk Factors of Breast Cancer

It is not easy to pinpoint the main causes of breast cancer, however, some risk factors have been identified, which include;

- **Gender:** Breast cancer occurs mostly in women, though a small fraction of men occasionally develops breast cancer.
- **Age:** The older a woman gets, the higher is her risk of developing breast cancer. Over 80% of all female breast cancers occur among women aged 50+ years (after menopause) [29, 30].

- **Genetics:** Women who have a close relative who has/had breast or ovarian cancer are more likely to develop breast cancer. If two close family members develop the disease, it does not necessarily mean they shared the genes that make them more vulnerable, because breast cancer is a relatively common cancer. The majority of breast cancers are not hereditary. Women who carry the BRCA1 and BRCA2 genes have a considerably higher risk of developing breast and/or ovarian cancer. These genes can be inherited. TP53, another gene, is also linked to greater breast cancer risk [31-33].
- **A history of breast cancer:** Women who have had breast cancer, even non-invasive cancer, are more likely to develop the disease again, compared to women who have no history of the disease.
- **Having had certain types of breast lumps:** Women who have had some types of benign (non-cancerous) breast lumps are more likely to develop cancer later on. Examples include atypical ductal hyperplasia or lobular carcinoma in situ.
- **Dense breast tissue:** Women with denser breast tissue have a greater chance of developing breast cancer.
- **Estrogen exposure:** Women who started having menstrual periods at an earlier age or entered menopause later than usual have a higher risk of developing breast cancer. This is because their bodies have been exposed to estrogen for longer. Estrogen exposure begins when periods start, and drops dramatically during menopause [34, 35].
- **Obesity:** Post-menopausal obese and overweight women may have a higher risk of developing breast cancer. Experts say that there are higher levels of estrogen in obese menopausal women, which may be the cause of the higher risk [36, 37].

- **Height:** Taller-than-average women have a slightly greater likelihood of developing breast cancer than shorter-than-average women.
- **Alcohol consumption:** The more alcohol a woman regularly drinks, the higher her risk of developing breast cancer is. It is advised that if a woman wants to drink, she should not exceed one alcoholic beverage per day [38, 39].
- **Radiation exposure:** Undergoing X-rays and CT scans may raise a woman's risk of developing breast cancer slightly. Scientists found that women who had been treated with radiation to the chest for a childhood cancer have a higher risk of developing breast cancer [40].
- **Hormone Replacement Therapy (HRT):** Both forms, combined and estrogen-only HRT therapies may increase a woman's risk of developing breast cancer slightly. Combined HRT causes a higher risk [41, 42].

.

2.3.3 Symptoms of Breast Cancer

In the early stage, breast cancer is usually asymptomatic; hence early detection is usually eluded, thus making treatment to be difficult. However, as the tumor progresses, some of signs and symptoms may be noticed. These include, breast pain or heaviness; persistent changes to the breast, such as swelling, thickening, or redness of the breast's skin; and nipple abnormalities such as spontaneous discharge (especially if bloody), erosion, inversion, or tenderness. It is important to note that pain (or lack thereof) does not indicate the presence or the absence of breast cancer.

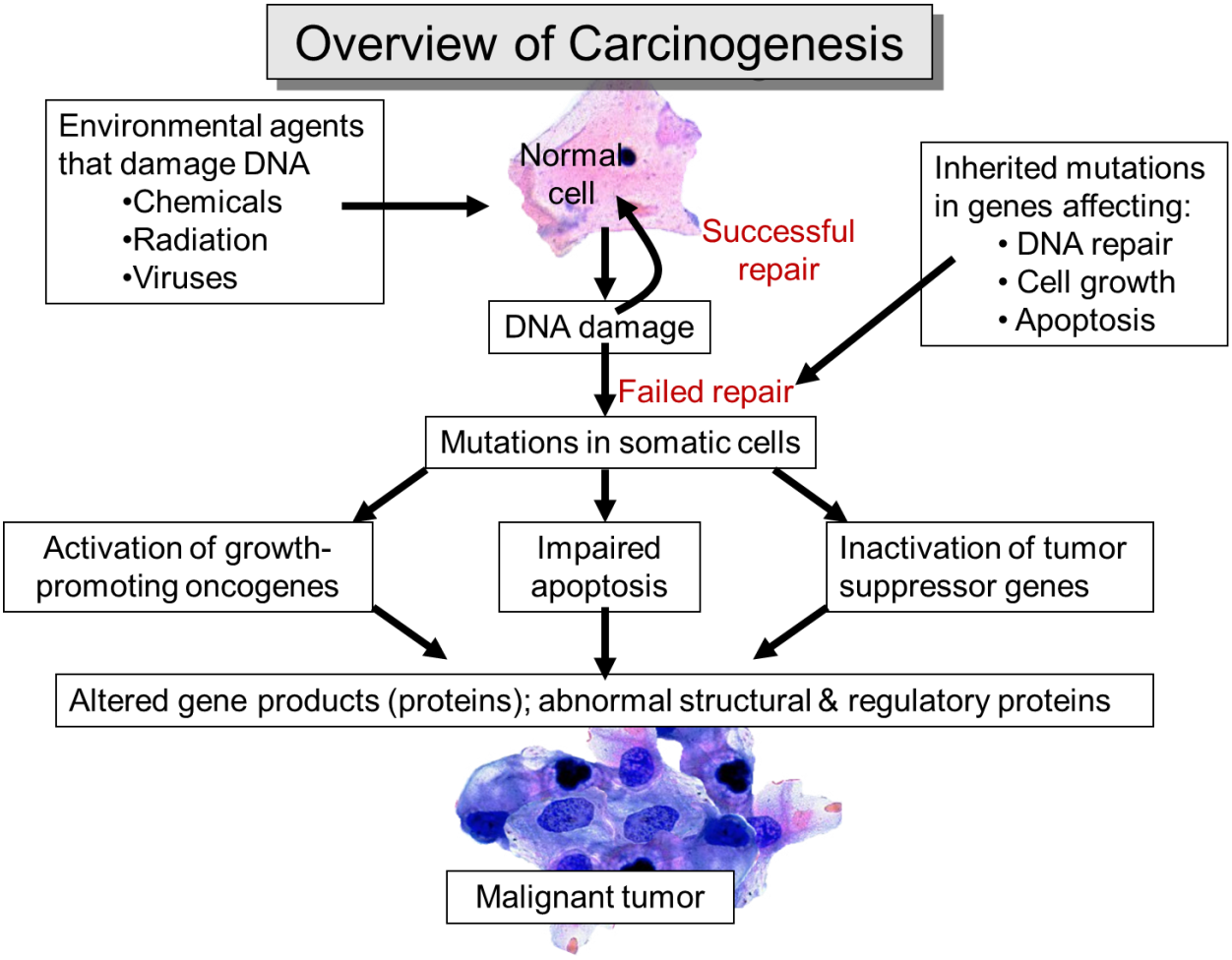

Figure 2.3: Summary of the Process of Cancer Formation

2.4 Gold Nanoparticles for Targeting of Breast Cancer

Despite the fact that research in the field of cancer biology has significantly increased in the past two decades, cancer is still a major health problem worldwide and remains the second leading cause of death [43]. Every year, more than 10 million new cases and over 5 million deaths result from the disease [44]. A diagnosis of cancer is usually considered terminal (However, some cancers, such as lymphoma, are not detected until they are stage IV, but the cure rate is usually

high) but, if detected early, the outcome may be favorable. Most times, a good number of cancer patients are asymptomatic until they are in the late stages of the disease.

The conventional methods of treatment of breast cancer usually fall into one of the following categories: surgery, radiation, chemotherapy, immune-therapy, hormone therapy, or gene therapy [45]. Chemotherapy is the most frequently used of these methods. The transport of anti-cancer drugs depends largely on the physicochemical properties of the molecules including size, configuration, charge and hydrophobicity [46]. Generally speaking, the conventional methods of treatment have so many pitfalls, which include, nonspecific systemic distribution of antitumor agents, inadequate drug concentrations reaching the tumor site, intolerable cytotoxicity, limited ability to monitor therapeutic responses, and development of multiple drug/heat resistance and devastating short- and long-term side effects [47, 48].

Due to inadequate therapies and clinical procedures for overcoming multi-drug resistant cancer, it becomes pertinent that new technologies emerge for accurate early detection and treatment of cancer. One of such technologies is the development of nanotechnology for targeted drug delivery. Gold nanoparticles have proved valuable in addressing some of these problems due to their unique characteristics. They have enhanced permeability and retention in tumor tissue, they exhibit surface plasmon resonance in near-infrared light, their interaction with radiation generates secondary electrons, and they also have the ability to be conjugated with drugs or other agents. The unique combination properties of gold nanoparticles allow them to act as highly multifunctional anticancer agents [49, 50]. Gold nanoparticles are used for both detecting and destroying cancer cells, as they can carry chemicals to destroy a cancer cell or they can be used with radiation to kill cancer cells. Targeting gold nanoparticles to the cancer cell and irradiating the nanoparticles with a laser has been shown to be a promising tool in fighting cancer [51]. The

heated nanoparticles heat the cancer cell up which would destroy the cancer cell without harming healthy cells. Using gold nanoparticles, Gibson *et al.,* [52] discovered a way to load dozens of molecules of paclitaxel onto tiny gold spheres that are barely wider than a strand of DNA without chemically altering the drug. Eghtedari *et a*l., (2009) [53] described a novel technique to functionalize gold nanorods (GNRs) allowing for in- vivo targeting of breast cancer tumors grown in athymic nude mice. GNRs were functionalized by covalent attachment of Herceptin (HER), a monoclonal antibody that enables molecular recognition of breast cancer cells expressing highly specific tumor associated antigens.

Among the benefits of targeted drug delivery are that it ensures specific delivery of the anti-cancer agent to the cancer, reduction in toxicity while maintaining therapeutic effects, greater safety and biocompatibility, reduction in the frequency of the dosages taken by the patient, providing a more uniform effect of the drug, reduction of drug side effects and reduced fluctuation in circulating drug levels (Figure 2.3). Some other unique features of targeted drug delivery by AuNPs include small size, large surface area, biocompatibility, stability, environmental friendliness, and ease of manufacture. The large surface area is employed in the modification of gold nanoparticles with targeting molecules or specific biomarkers, for targeted delivery. [54, 55] The strong binding attraction for thiols, proteins [55], carboxylic acid [56] aptamers [57] and disulfides makes AuNPs a suitable candidate for targeted drug delivery. Also, the surface plasmon resonance (SPR) of gold nanoparticles is being employed in photo thermal therapy and tumor imaging [58].

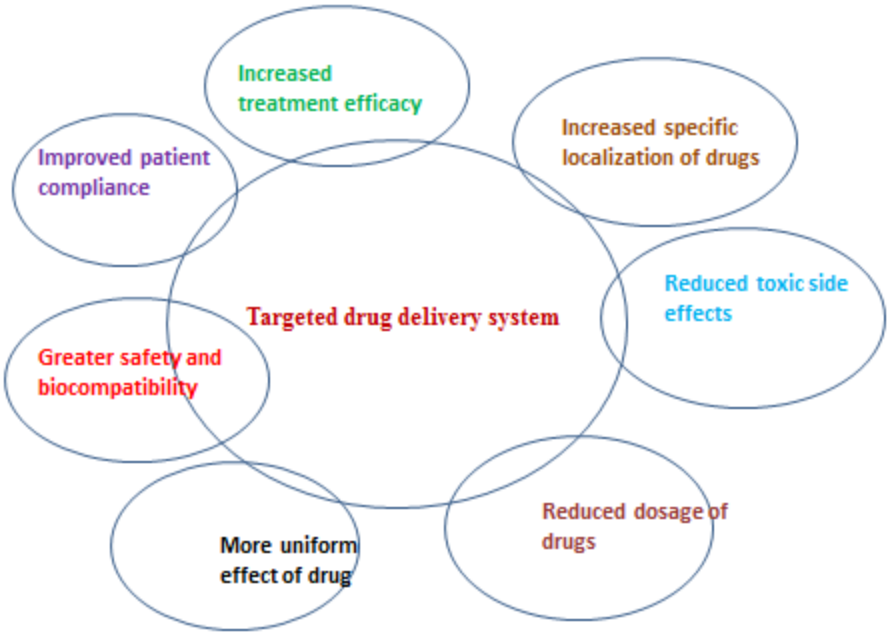

Figure 2.4: A chart showing the roles of targeted drug delivery

2.4.1 Mode of Targeting

The success of any delivery system depends on the ability of a nanocarrier to arrive at the targeted tissues after administration into the circulatory system through the penetration of barriers in the body with minimal loss of their volume or activity in the blood circulation. Secondly, after reaching the tumor tissue, drugs should have the ability to selectively kill tumor cells without affecting normal cells with a controlled release mechanism. [59]

Two approaches of targeting have been identified. They are, passive targeting and active targeting. [60]

2.4.2 Passive Targeting

This is a type of targeting that relies on the pathophysiological features of solid tumors which enable nanoparticles to selectively accumulate in tumor tissues [61]. Through the process of

angiogenesis, new blood vessels are developed for the growth and repair of cells in the body. This normal process is usually disturbed in the event of angiogenic diseases such as cancer, inflammatory, ischaemic, infectious and immune disorders. [62, 63] Cancer cells grow very rapidly, leading to increased demand of oxygen and nutrients. [62] The resultant effect of disturbance of the angiogenic process is that the blood vessels surrounding the tissue grow larger and become more permeable (leaky) than healthy vessels thereby increasing the porosity of the vasculature. This feature, termed the enhanced permeability and retention effect, is being employed as a means of passive targeting of cancer cells (and other angiogenic diseases) with gold nanoparticles. More so, as a result of the fast growing cancer cells, more oxygen and nutrients are required, so the glycolytic pathway is activated to release more energy. This leads to an acidic environment [64]. Taking advantage of this, some researchers have developed pH-sensitive liposomes designed to be stable at physiological pH 7.4, but degraded to release drug molecules at the acidic pH [65].

However, certain problems have been identified which affect the use of passive targeting as a means of drug delivery. These include,

1. The nanoparticles may be stopped by a mucosal barrier
2. There may be non-specific uptake of the nanoparticles
3. Also there may be non-specific delivery of the drug

2.4.2 Active Targeting

As a result of the shortcomings of passive targeting**,** researchers developed another mechanism that is more specific and delivers the drugs to the particular site of interest. This method is termed the active targeting. This phenomenon involves attaching of ligands (antibodies, [66] peptides [67], aptamers [68] or small molecules [69] that only bind to specific receptors on the

cell surface) to the gold nanoparticles through any of the conjugation methods available. The nanocarriers recognize and bind to target cells through ligand–receptor interactions. In order to achieve high specificity, the receptors should be more highly expressed on tumor cells than on normal cells, or if possible should be totally absent on the normal cells.

The internalization of the drug carriers takes place through a process called receptor-mediated endocytosis. This involves the binding of the nanocarriers to the receptor followed by the plasma membrane engulfing the receptor and nanocarrier forming the early endosome (Figure 2). The newly formed endosome is transferred to specific organelles. The pH within the endosome becomes acidic, so there will be dissociation and cleavage of the ligand and receptors. Then the drug particles are released which spread and enter the cytoplasm. The liberated receptors then move back to the cell surface where they attach and again partake in receiving more ligand conjugates [59].

For the folate receptor, when a folate-targeted conjugate binds with folate receptor on the cell surface, the invaginating plasma membrane envelopes the complex of the receptor and ligand forming an endosome. The endosomes are transferred to target organelles. As the pH value in the interior of the endosome diminishes to become acidic and lysozymes are activated, the drug is released from the conjugate and enters the cytoplasm, provided that it has the acceptable physicochemical properties for crossing the endosomal membrane. Released drug is then carried by its target organelle depending on the drug. Meanwhile, the folate receptor is set free from the conjugate and returns to the cell membrane, for another cycle of transport by attaching to folate-targeted conjugates [70].

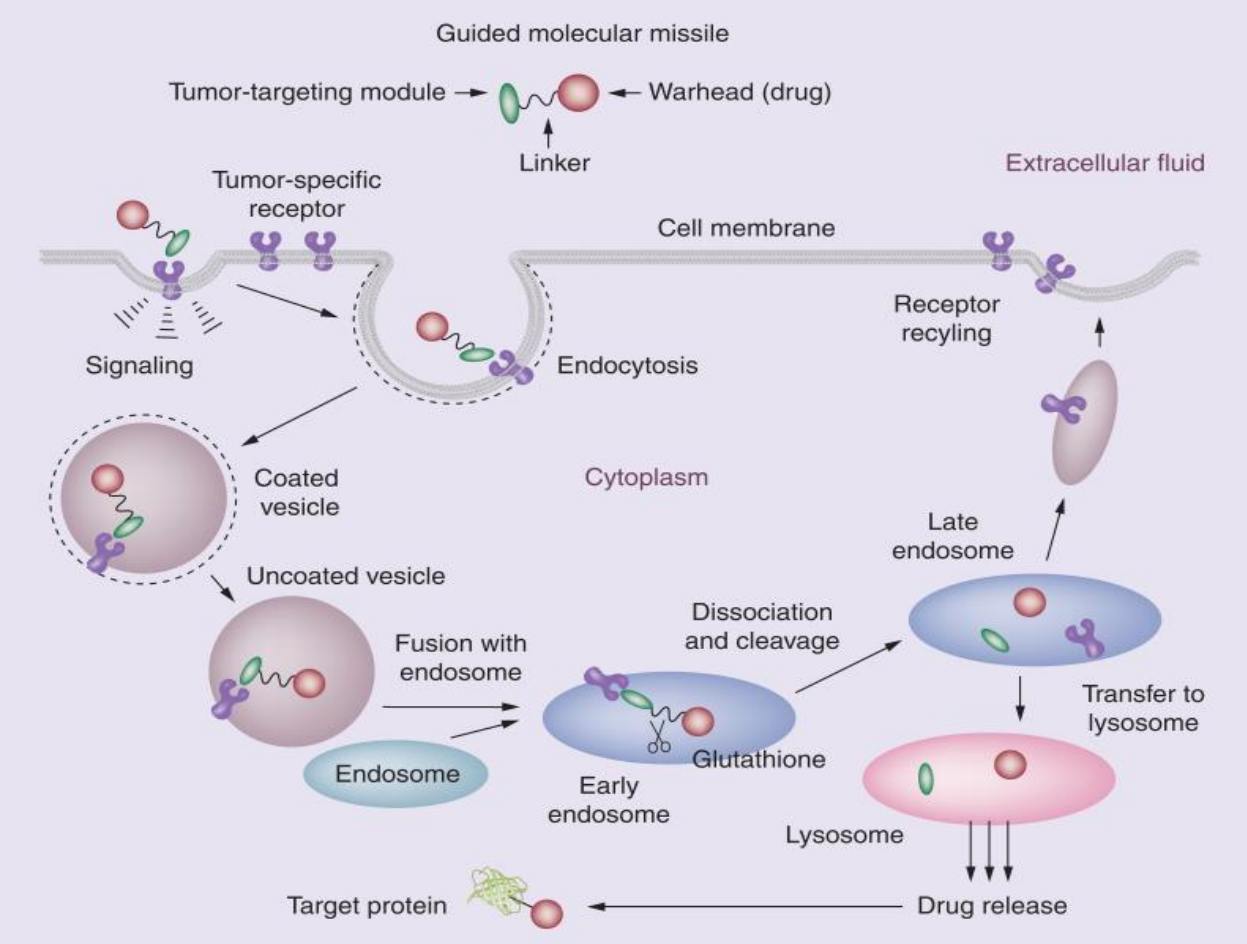

Figure 2.5: Processes involved in receptor-mediated endocytosis

2.4.3 Receptors on Cell Membranes

Cell surface receptors are receptors on the surface of a cell that act in cell signaling by receiving (binding to) extracellular molecules. Receptors are specialized integral membrane proteins that allow communication between the cell and the outside world. This type of receptor spans the plasma membrane and performs signal transduction, converting an extracellular signal into an intracellular signal or response. Thus, ligands that interact with cell-surface receptors do not have to enter the cell that they affect. Cell-surface receptors are also called cell-specific proteins or

markers because they are specific to individual cell types. Each cell-surface receptor has three main components: an external ligand-binding domain (extracellular domain), a hydrophobic membrane-spanning region, and an intracellular domain inside the cell [71].

Receptors on cell membranes allow specific interaction of drug carriers with cells facilitating their uptake via receptor-mediated endocytosis [72]. Folate receptors, which are differentially overexpressed in cells of cancers of epithelial origin, are applied to tumor-specific drug delivery in cancers including breast, ovary, brain, and lung malignancies. Further, as peptide receptors are expressed in gigantic quantities in some tumor cells, peptides/peptide analogs are conjugated to a drug carrier to allow tumor-specific targeting of cytotoxic agents, ensuring interaction with peptide receptors.

2.5. Biosynthesis of Gold Nanoparticles

The synthesis of metallic nanoparticles using biological systems as efficient means of producing nanoparticles is receiving great attention in modern nanotechnology. The conventional chemical and physical approaches for the synthesis of gold nanoparticles are based on either a top-down or bottom-up approaches. In using the top-down approach, bulk metal is decomposed into nanoparticles using high laser ablation [73] pyrolysis or attrition [74]. These techniques lack the ability to control the size of the nanoparticles [75] and also to maintain the surface structure, which accounts for the physicochemical and catalytic properties of the AuNPs [74]. More so, this laser ablation method is very expensive due to the complex and hi-tech equipment required. [73].

In the bottom-up approach, AuNPs are constructed atom by atom starting from a precursor gold (Au) salt solution, using either ultrasound [76] radiation [77], high temperature [78], lithography [79] or chemical/electrochemical methods [80,81,82] . The chemical synthesis method makes use of non-polar solvents, which are toxic and so not environmental friendly. [83] Physical methods

on their own, usually operate at high temperatures and pressures, which leads to increased energy consumption and high cost of production. Nanoparticles for biomedical application should be prepared only with biocompatible chemicals to minimize their toxic effect and increase their safe usage [84]

In contrast, the biosynthesis of gold nanoparticles from plants [85] and microbes [86] is cost effective, eco-friendly [87] and can also enable increased control over the formation of nanoparticles with different shapes and sizes [88,89,90]. Green synthesis helps to overcome the toxicity issues associated with chemical synthesis. Some researchers have advanced reasons why microorganisms synthesize nanoparticles. They suggested that microorganisms like bacteria, algae and fungi synthesize nanomaterials to benefit from their mechanical strength and chemical properties [91]. Diatoms, for instance, mineralize silica to build their cell walls [92], coccolithophore algae mineralize calcium carbonate to form calcite plates and build their exoskeleton [93] and magnetotactic bacteria (e.g. *Magnetospirillum gryphiswaldense*) synthesize magnetite nanoparticles [94] to enable the bacteria to migrate along a magnetic field towards low oxygen environments [95].

Microorganism can synthesize metal nanoparticles through metal bio-reduction to remove soluble metals from the surrounding environment, thus decreasing their toxicity and bioavailability. Most metal ions are toxic for bacteria, and, therefore, the bio-reduction of ions or the formation of water insoluble complexes is a defense mechanism developed by the bacteria to overcome such toxicity [96–99]. In metal-contaminated environments, only microorganisms that are capable of bio-reduction can survive there. *Shewanella oneidensis* can grow in presence of sub-Mm concentrations of Ag^{+}[100], *Geobacter sulfurreducens* can reduce in few hours soluble

U6+ to insoluble U4+ [101] and Fe3+-reducing mixed cultures can tolerate high concentrations of Ni, Cu, Cd, Zn, and Co [102].

The use of parts or whole plants, in the synthesis of gold nanoparticles is an exciting possibility that is relatively underexploited [87,89,103-104]. Using plants for synthesis of nanoparticles has a lot of advantages over other environmentally friendly biological methods. This is because using plants eliminates the cumbersome process of maintaining microbial cultures. Furthermore, the scale up of the biosynthesis of nanoparticles is relatively easy compared to the chemical synthesis.

Some plants have been used for synthesis of gold nanoparticles [105]. These include: the leaf extracts of geranium (*Pelargonium graveolens*),[105] lemongrass (*Cymbopogon flexuosus*)[106] *Cinnamommum camphora*,[107] neem (*Azadirachta indica*),[108] *Aloe vera*,[109] tamarind (*Tamarindus indica*)[110] and fruit extract of *Emblica officinalis.*[111] These have been shown to have the potential to reduce Au^{3+} to form gold nanoparticles (Au^{0}). The use of plants which have been found to possess anticancer or other therapeutic activity in biosynthesis of gold nanoparticles may yield drug conjugated nanoparticles with biological pendant groups which are lethal to malignant cells but do not affect normal cells.

2.5.1 The Mechanism for the Formation of Gold Nanoparticles

The mechanism leading to the formation of AuNPs is r reduction reaction that involves electron transport that goes on in the cell membrane of the bacteria. The cell-free extracts contain reducing agents (antioxidants such as vitamin C precursors, cytochrome oxidase, vitamin B complex and porphyrins) [112, 113, 114]. Among these, the cytochrome complex and the porphyrins stand out as possibilities for the reduction of $HAuCl_4$. The mechanism leading to the

formation of AuNPs is a reduction reaction that involves electron transport that goes on in the cell membrane of the bacteria.

Cytochrome complexes, a class of hemoproteins, play a great role in electron transport. These proteins can change the valence of the heme iron, alternating between ferrous (Fe^{2+}) and ferric (Fe^{3+}) states (equation 1). Cytochrome oxidase is a transmembrane protein complex found in bacteria and the mitochondrion of eukaryotes [115]. Cytochrome oxidase receives an electron from each of four cytochrome c molecules, and transfers them to one oxygen molecule, converting molecular oxygen to two molecules of water as shown in equation (2).

$$Fe^{2+} \longrightarrow Fe^{3+} + e^{-} \quad (1)$$

$$4\ \text{Cyt}\ c_{red} + O_2 + 8\ H^{+}_{\text{matrix}} \longrightarrow 4\ \text{Cyt}\ c_{ox} + 2\ H_2O + 4\ H^{+}_{\text{intermembrane}} \quad (2)$$

In the process, cytochrome oxidase binds four protons from the inner aqueous phase to make water, and in addition translocate four protons across the membrane, helping to establish a transmembrane difference of proton electrochemical potential that the ATP synthase then uses to synthesize ATP. Equation 3 is a combination of equations1 and 2 showing the complete reaction that go on in the cell membrane during electron transport.

$$4\ Fe^{2+}\text{-cytochrome } c + 8\ H^{+}_{\text{in}} + O_2 \longrightarrow 4\ Fe^{3+}\text{-cytochrome } c + 2\ H_2O + 4\ H^{+}_{\text{out}} \quad (3)$$

In the presence of $HAuCl_4$, cytochrome c reduces Au^{3+} in place of Fe^{3+} thereby forming gold nanoparticles

$$HAuCl_4 + 3e^- \longrightarrow Au + 4Cl^- + H^+ \quad (4)$$

$$Au^{3+}(aq) + 3e^- \longrightarrow Au^0(s)$$

2.6 Ligand Conjugation

Gold nanoparticles, being inert and relatively non-cytotoxic, are extensively used for various biomedical (or nano-medical) applications including drug and gene delivery [116–118]. However, due to their size, gold nanoparticles can easily penetrate various cells, and this non-specific penetration is one of the greatest challenges in using these nanoparticles for targeted delivery to specific tissues. To overcome this problem, researchers have been conjugating these nanoparticles with various biomolecules and ligands to develop strategies for targeted delivery. Bioconjugation simply involves the linking of biomolecules to nanoparticles by chemical or biological means [119]. It includes the conjugation of antibodies, nucleic acids and liposomal components or other biologically active molecules with nanoparticles. The outcome is several molecular combination that have useful properties. The conjugation of different moieties to the nanoparticles widens their application fields and provides the nanoparticles with new or enhanced properties [120]. The use of AuNPs in biological applications has demonstrated the importance of the conjugation of AuNPs with biological molecules [121, 122]. The biological molecules not only provide the interfaces for interactions between nanoparticles and the biological environment, but also contribute their biological functions, such as tumor cell targeting [123], cell penetration [124], antibody- antigen recognition [125], and many others. As a result of their well-defined surface chemistry [126], AuNPs can be modified and functionalized with a wide variety of biological molecules, such as peptides [127], proteins [128], oligonucleotides [129,130], carbohydrates [131], and even whole viral capsids [132-137].

Peptides represent a viable targeting moiety with favorable characteristics over antibodies and antibody analogues and fragments, including low molecular weight (around 1kDa), ideal tissue penetration ability, lack of immunogenicity, ease of production and relative flexibility in chemical conjugation processes [138]. Various peptides that recognize cancer-specific epitopes that are over-expressed on tumor cells and vasculature have been used as targeting moieties for drugs and drug nanorcarriers, one of which is luteinizing hormone releasing hormone (LHRH).

To prepare conjugates from nanoparticles and biomolecules, the surface chemistry of the nanoparticles must be such that the stabilizing ligands are fixed to the nanoparticle and possess terminal functional groups that are available for biochemical coupling reactions if required. The binding to the nanoparticle surface is frequently done through thiol groups [139-141]. Prior works by Carls *et al.*, [142-147] described the formation of self-assembled monolayers (SAM) of alkanethiolates via adsorption of alkanethiols onto the surfaces of gold colloids in aqueous dispersions. When an alkanethiol solution is added into gold nanoparticles, thiols will spontaneously bind to the surface of the gold with the SH head groups via a strong gold-sulfur interaction resulting in a closely packed monolayer, thus exposing the end groups at the layer/medium interface. Tailoring the terminated chemical identity of self-organized assemblies provides an effective means to functionalize gold and tune the surface physical or chemical properties to meet specific requirements.

In this work, the ligands; luteinizing hormone- releasing hormone (LHRH) and folic acid were characterized for their ability to target AuNPs.

2.6.1 Luteinizing Hormone-Releasing Hormone (LHRH)

Luteinizing hormone-releasing hormone (LHRH) is a decapeptide containing pGlu-His-Trp-Ser-Tyr- Gly-Leu-Arg-Pro-Gly-NH2 [148]. LHRH binds to receptors in the pituitary gland, stimulating the release of luteinizing hormone (LH) and follicle stimulating hormone (FSH). LH and FSH stimulate the gonads to synthesize steroid hormones [149]. A continuous supply of LHRH, as opposed to the naturally occurring pulsatile pattern, causes down- regulation of the LHRH receptors, resulting in a marked decrease in androgens in males and estrogens in females [150]. LHRH is being used to treat hormone-dependent tumors, through the desensitization of LHRH receptors. This also forms the basis for the hormonal treatment of prostate cancer, benign prostatomegaly, endometriosis, hysteromyoma, metrofibroma, precocious puberty, or breast cancer [151-154].

Over expression of luteinizing hormone releasing hormone (LHRH) receptors in hormone-associated cancers makes LHRH an attractive target for the selective delivery of chemotherapeutics. In the mid-1980s, analogs of LHRH peptide were introduced to target LHRH receptor in prostate [155] and breast [156] cancers. Since then this class of peptides has been extensively tested as carriers of chemotherapeutic agents to cancer cells. For example, LHRH analogs were conjugated to doxorubicin (DOX) (conjugate AN-152) or its counterpart 2-pyrollino-DOX (conjugate AN-207) resulting in targeted therapeutic conjugates in various cancer models [157–169]. In the work done by Obayemi *et al* [170], LHRH was successfully conjugated to magnetite nanoparticles for targeting of breast cancer cells. LHRH receptors are overexpressed on these cancerous tissues and so this peptide can be used as a targeting moiety.

2.6.2 Folic Acid (Folate)

Folate, also known as pteroylglutamate, is a water-soluble B vitamin that is critical to DNA synthesis, methylation, and repair (folate is used to synthesize thymine) [155-173]. Folic acid is a small molecule (441 Da), stable over a broad range of temperatures and pH values, inexpensive, and non-immunogenic [174]. Research has shown that Folate binding protein a glycosylphosphatidylinositol (GPI) anchored cell for folate (folate receptor), is overexpressed in some human tumors including ovarian, breast and lung cancers,[171, 175] while it is highly restricted in normal tissues [176]. This knowledge has been exploited in targeted drug delivery, by conjugating folate with a number of nanotechnology platforms, such as gold nanoparticles and chemotherapeutic agents. When these nano-conjugates are deposited at the tumor site a variety of methods to eradicate the cancer cells can be used, such as thermal ablation, drug release or delivery, or even coating the cancer cells with a high affinity antigen, which the body's immune system can detect and mount a defense against [173].

Conjugation of folate to gold nanoparticles can be achieved through succinimidyl ester amine chemistry, which results in a stable amide linkage [177-179]. Folate must be conjugated to nanoparticles *via* its γ−carboxyl group in order to retain its receptor-binding activity [180]. Covalent conjugation of small molecules, proteins, and even liposomes to the γ−carboxyl moiety of folic acid does not alter its ability to bind the folate receptor and undergo endocytosis by receptor bearing cells [181-183].

Our interest in folate is based on the findings of some researchers that folate can be used to target triple negative breast cancer. In the work done by O'Shannessy *et al.* [184] they reported that in metastatic breast cancer, folate receptor -α (FRA) was expressed in 86% of TNBC patients.

These results support the claim that FRA expression is enriched in the TNBC subtype of breast cancer and represents a new therapeutic target for this devastating disease. Similarly, Tacha and Bremer [185] , found that 50% of the population of breast cancer patients they tested who expressed folate receptors had triple negative breast cancer (TNBC).

2.7 Cell Adhesion Measurement

Adhesion plays a very vital role in cell communication and regulation, and also in the development and maintenance of tissues. Cell adhesion is the ability of a single cell to stick to another cell or the extracellular matrix (ECM). *In vitro*, most mammalian cells are anchorage-dependent and attach firmly to the substrate [186]. The greater adhesion that a cell has, the greater number of chemical bonds it has on its surface [187,188]. Cell adhesion also helps in stimulating signals that control cell differentiation, cell cycle, cell migration, and cell survival [189]. The adhesion of cells to substrate is a crucial consideration in biomaterial design and development. Cell adhesion is also essential in cell communication and regulation, and becomes of fundamental importance in the development and maintenance of tissues. Changes in cell adhesion can be the defining event in a wide range of diseases including arthritis [190,191], cancer [189,192,193], osteoporosis [194,195], and atherosclerosis [196,197]. Cell adhesiveness is generally reduced in human cancers. This reduced intercellular adhesiveness makes the cancer cells lose orderliness, leading to the destruction of histological structure, which is the morphological mark of malignant tumors [193]. Generally, tumor cells are characterized by changes in adhesivity to ECM, which may be related to the invasive and metastatic potential [198].

To measure the force of adhesion between the cell and the substrate, the Atomic Force Microscope (AFM) is used. The AFM measures the deflection of a cantilever spring with a sharp AFM tip (the tip radius is about 10-100 nm) as a function of displacement from a horizontal position which is driven by a piezo. The deflection of the cantilever is monitored by a laser-photodiode system and it relates to the forces acting between a probing tip and a substrate [199]. When the cantilever is far from the surface of the sample, the AFM-tip is force free, that is, there is no interaction. However, as the tip approaches the surface, electrostatic forces are generated which attracts the tip towards the substrate. At a distance of nanometers to atomic level ($\sim 20\text{nm}$)[200], Van der Waals and capillary forces acting on the surface becomes higher than the spring constant of the cantilever and the tip "jumps" onto the sample surface.

The piezo drive pushes the AFM-tip further onto the surface until a point of repulsion is reached and the motion of the piezo is reversed. The cantilever deflects towards the surface due to adhesion force before the tip breaks contact with the surface. The sudden pull off causes free vibrations of the cantilever. The force acting on the cantilever immediately before coming out of contact is a measure for the adhesion force between the AFM tip and the surface [201-203].

The pull-off force, which is a measure of the force of adhesion, was determined from the equation:

$$F = K x \qquad (1)$$

Where K is the spring constant of the cantilever and x is the maximum deflection of cantilever during the tip-substrate adhesion.

2.8 Breast Cancer Treatment

Different factors come into consideration when deciding which treatment option is best. Some of these factors include, the type of breast cancer, the size of the breast tumor, the stage of the breast cancer, the grade of the cancer cells, whether menopause has set in, whether the cancer cells have receptors for particular cancer drugs and generally the health status of the patient. There is no single treatment that is best for ball types of cancer, and patients often receive a combination of therapies and palliative care. Treatments usually fall into one of the following categories: surgery, radiation, chemotherapy, immunotherapy, hormone therapy, or gene therapy.

One of the most critical points in breast cancer treatment is early stage diagnosis, before tumor cells metastasize. In addition current diagnostic and therapeutic approaches rely predominantly on surgery and crude, non-specific techniques such as irradiation and chemotherapeutic agents [204,205]. Unfortunately, cancer therapies are limited by inadequate drug concentrations reaching the tumor. The rapid elimination and widespread distribution of the drug into targeted organs and tissues requires its administration in large quantities which often results in systemic toxicity and adverse effects [206,207]. Moreover, the majority of anti-cancer drugs is water insoluble and need to be dissolved in an organic solvent in order to be administered as an injectable solution. These organic solvents may be toxic and have their own side effects [208].

The development of resistance to chemotherapeutic agents is one of the major challenges in effective cancer treatment. Tumor cells are able to generate multi-drug resistance (MDR) to the majority of anti-cancer drugs [209]. Resistance to treatment results from a variety of factors including individual variations and somatic cell genetic differences in tumors, even those from the same tissue. The most common reason for acquisition of resistance to a broad range of

anticancer drugs is the expression or over-expression of one or more energy-dependent transporters that detect and eject anticancer drugs from cells [210].

The application of nanotechnology to medicine (nanomedicine) has the potential to offer solutions to these current obstacles in cancer therapies. The unique size (1-100nm) and large surface-to-volume ratios of nanoparticles [211] offer the ability to convert insoluble or poorly soluble drugs into soluble suspensions, thus eliminating the need for toxic organic solvents. The incorporation of anticancer drugs into nanoparticles not only has the potential to decrease their adverse cytotoxic effects, but also to increase the accumulation of the drug in the tumor vasculature [211-213]. Therefore, cancer nano-therapeutics are rapidly progressing and are being implemented to solve several limitations of conventional drug delivery systems [214]. Nanoparticles can be engineered to incorporate a wide variety of chemotherapeutic agents and target the delivery of these agents directly and specifically to the tumor site for better efficacy and less toxicity [215,216]. Combining types of passive encapsulation and release modalities with surface modifications (i.e. hydrophilic coatings) or tumor-specific targeting moieties could potentially increase the efficacy of nanoparticulate formulations several-folds. In this way, nanoparticles with enhanced surface properties may be able to deliver a high amount of drug selectively to tumor sites [217]. Obviously, nanoparticles have the ability to accumulate in cells without being recognized by P-glycoprotein (P-gp), one of the main mediators of multidrug resistance, resulting in an increased intracellular concentration of drugs [218]. In our study, we used prodigiosin, extracted from the indigenously isolated bacterium, *Serratia marcescens* as the anti-cancer drug of choice.

2.9 Prodigiosin

Prodigiosin is a red pigment produced as a secondary metabolite from certain species of microorganisms, such as *Serratia, Pseudomonas and Streptomyces* [219,220]. It is an alkaloid with a unique tripyrrole chemical structure.

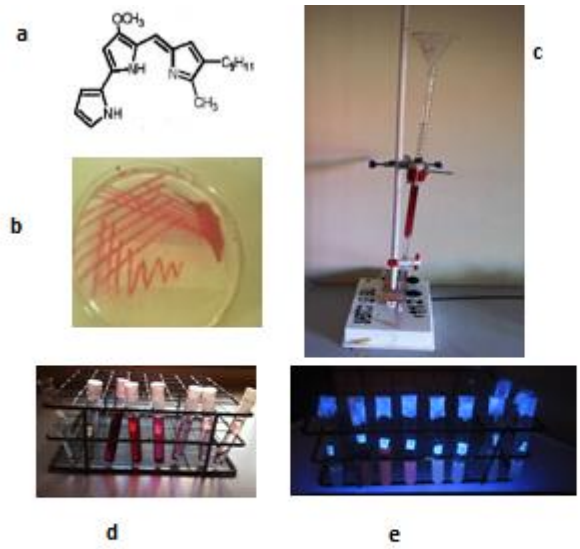

Figure 2.6:
(a) structure of prodigiosin (5[(3-methoxy-5-pyrrol-2-ylidene-pyrrol-2-ylidene)-methyl]-2-methyl-3-pentyl-1Hpyrrole),
(b) red pigment (prodigiosin) produced by *Serratia marcescens* on a petri dish,
(c) column chromatography for prodigiosin purification,
(d) different fractions collected from the chromatography and
(e) the collected fractions when illuminated with UV light, prodigiosin fluoresces.

Prodigiosin has three rings forming a pyrrolylpyrromethane skeleton with a C-4 methoxy group, a molecular formula C20H25N3O and a molecular weight of 323.44 Da (Figure 2.6) [220-222]. It is sensitive to light and insoluble in water. It is moderately soluble in alcohol and ether, and soluble in chloroform, methanol, acetonitrile and DMSO [223,224] . Prodigiosin has several biological activities such as immunomodulatory, antibacterial, anti-mycotic and antimalarial activities [225,226]. Recently, many studies [227-230] imply that prodigiosin has a massive potential in cancer chemotherapy, which draws increasing public attention. The studies on the anticancer effect of prodigiosin mainly focus on its ability to induce apoptosis. It has been

reported that prodigiosin can induce apoptosis in various kinds of cancer cells, such as haematopoietic, colorectal and gastric cancer cells [227–229]. Apoptosis is a form of cell death in which cells actively participate in their own destruction. This process is characterized by morphological [231-233] and biochemical/molecular [234,231,233] criteria. Cells undergoing apoptosis shrink and lose their normal intercellular contacts and subsequently exhibit cytoplasmic and chromatin condensation and internucleosomal cleavage of DNA. In the final stages of apoptosis, cells become fragmented into small apoptotic bodies, which are then eliminated by phagocytosis.

2.10 Drug encapsulation

Microencapsulation is a process by which individual particles or droplets of solid or liquid material (the core) are coated with a continuous film of polymeric material to produce capsules in the nanometer to micrometer size range, known as nanospheres or microspheres.[235,236] The coating materials suitable for microencapsulation should possess these qualities; able to stabilize the core material, be inert toward active ingredients, capable of controlled release under specific conditions, be film-forming, pliable, tasteless and stable, be non-hygroscopic, no high viscosity, and also economical. In addition, the coating materials should be equally soluble in an aqueous media or solvent, and the coating can be flexible, brittle, hard or thin [237,238]. Microencapsulation includes Bio encapsulation which is more restricted to the entrapment of a biologically active substance (DNA, cell or group of cells) generally to improve its performance and enhance its shelf life [239,240].

Drugs are encapsulated for taste and odor masking, to stabilize the drug, improve gastrointestinal (GI) tolerance, and provide sustained-release after oral administration [240]. Drug encapsulation

can be used to overcome some of the issues associated with conventional therapy which include non-site-specific to tumor, high toxicity, devastating short- and long-term side effects, low efficacy, <1% of drug making it to tumor cells [241,242]. To obtain maximum therapeutic efficacy, there is need to deliver the agent to the target tissue in an optimal amount and at the right time [243,244]. There are various approaches to delivering a therapeutic substance to the target site in a sustained controlled release fashion. One such approach is using microspheres as carriers for drugs. Microspheres are characteristically free flowing powders consisting of proteins or synthetic polymers which are biodegradable in nature and ideally having particle size less than 200 μm [245]

2.10.1 Types of Drug Release Mechanisms

The ultimate goal of drug encapsulation is to make the drug available at the site of interest at a particular time and in a required quantity. To achieve this, some workable systems have been developed by some researchers through which drugs can be released from microspheres. These include;

1. Degradation controlled monolithic system

Here, the drug is dissolved in a matrix and is distributed uniformly throughout the matrix. The drug is strongly attached to the matrix and is released on degradation of the matrix. The diffusion of the drug is slow as compared with degradation of the matrix.

2. Diffusion controlled monolithic system

Here the active agent is released by diffusion prior to or concurrent with the degradation of the polymer matrix. The rate of release also depends on whether the polymer degrades by a homogeneous or a heterogeneous mechanism.

3. Diffusion controlled reservoir system

Here the active agent is encapsulated by a rate controlling membrane through which the agent diffuses, and the membrane erodes only after its delivery is completed. In this case, drug release is unaffected by the degradation of the matrix.

4. **Erosion**

Erosion of the coat due to pH and enzymatic hydrolysis causes drug release with certain coat materials like glyceryl monostearate, beeswax and steryl alcohol [246-249].

2.10.2 Mechanism of drug release from swellable matrix tablets

Controlled drug release is based on diffusion through polymers, erosion of polymers and other polymer characteristics such as osmotic and ion exchange properties. When a glassy (or dry) polymer comes into contact with water or any other medium within which it is thermodynamically compatible, the solvent penetrates into the free spaces on the surface between the macromolecular chains. When enough solvent has entered into the matrix, the glass transition temperature (Tg) of the polymer drops to the level of the experimental temperature (which is usually 37^{o}C). The presence of solvent in the glassy polymer causes stresses, which are then accommodated by an increase in the radius of the gyration and end to end distance of the polymer molecules, which is seen macroscopically as swelling [250].

References

1. Jemal, A., Siegel, R., Ward, E., Hao, Y., Xu, J., Thun, M.J. Cancer Statistics. CA Cancer J Clin 59(4):225–249 (2009).

2. Klapper, M., Clark, C. G., Müllen, K. Application-directed syntheses of surface-functionalized organic and inorganic nanoparticles. Polymer International 57, 181-202 (2008)

3. Dreaden, E.C., Austin, L.A., Mackey, M.A., El-Sayed, M. A. Size matters: gold nanoparticles in targeted cancer drug delivery. Therapeutic delivery. 3(4):457-478 (2012).

4. Logothetidis S., Nanotechnology in Medicine:The Medicine of Tomorrow and Nanomedicine, Aristotle University, HIPPOKRATIA, 10(1), 7-21 (2006).

5. Svennersten, K., Larsson, K., Berggren, M., Dahlfors,A. Organic Bioelectronics in nanomedicine, Biochimica et Biophysica Act, 1810, pp 276 – 285 (2011).

6. P. Boisseau and B. Loubaton, Nanomedicine, Nanotechnology in Medicine, ComptesRendus de l′Académie des Sciences, 1-27 (2011)

7. American Cancer Society. Available at http://www.cancer.org/cancer/cancerbasics/what-is-cancer. Accessed on 20/11/2015.

8. Rediscovering biology available at https://www.learner.org/courses/biology/support/8_cancer.pdf. Accessed on 29/7/2015.

9. Sharma, R., Talukdar , D., Malik ,P., Mukherjee, T. K. Failure of immunological cells to eradicate tumor and cancer cells: an overview. Turk J Biol 38: 786-799 (2014)

10. Fearon, E.R., Vogelstein, B. "A genetic model for colorectal tumorigenesis". Cell. 61 (5): 759–67 (1990).

11. Venter, J.C., Adams M.D., Myers E.W., Li P.W., Mural R.J., Sutton G.G., Smith H.O., Yandell M., Evans C.A., Holt R.A., et al. The sequence of the human genome. Science 291:1304–1351 (2001).

12. David Polsky and Carlos Cordon-Cardo. Oncogenes in melanoma. Oncogene 22, 3087–3091(2003).

13. Guo, X. E., Ngo, B., Modrek, A. S., Lee, W.-H. Targeting Tumor Suppressor Networks for Cancer Therapeutics. Current Drug Targets, 15(1), 2–16 (2014).

14. Wilson, K. A., Waugh, A., Chambers, G., Grant, A., Ross, J.: Ross and Wilson anatomy and physiology in health and illness. Edinburgh: Churchill Livingstone. 53–54 (2006).

15. American cancer society. Available at http://www.cancer.org/cancer/pituitarytumors/detailedguide/pituitary-tumors-what-is pituitary-tumor. Accessed on 8/7/15.

16. Klein CA. "Cancer. The metastasis cascade". Science. 321 (5897): 1785–7 (2008).

17. Foulds, L, ed. Neoplastic Development, Vol. 1, London, Academic Press (1969).

18. Correa P. Morphology and natural history of cancer precursors. In: Schottenfeld D, Fraumeni JF, eds, Cancer Epidemiology and Prevention, New York, Oxford University Press, 45-64 (1996).

19. Sariego, J. Breast cancer in the young patient. Am Surg. 76(12):1397-400 (2010) .

20. Clark, W.H. "Tumour progression and the nature of cancer". Br. J. Cancer. 64 (4): 631–44 (1991).

21. Felipe, C. G., Jorge, S. R., David, J. D. Lobular Neoplasia and Invasive Lobular Carcinoma Breast Pathology, 21, 380-411 (2012)

22. Ward, E.M., DeSantis, C. E., Lin, C. C., Kramer, J. L., Jemal, A., Kohler, B., Brawley, O. W., Gansler, T. Cancer Statistics: Breast Cancer in Situ. CA CANCER J CLIN 65:481–495 (2015).

23. Gregory, D. L., Swain S. M.: Ductal Carcinoma in Situ, Complexities and Challenges NCI J Natl Cancer Inst 96 (12): 906-920 (2004).

24. Ihemelandu, C.U, Leffall, L.D. Jr, Dewitty, R.L, Naab TJ, Mezghebe HM, Makambi KH, Adams-Campbell L, Frederick WA. Molecular breast cancer subtypes in premenopausal African-American women, tumor biologic factors and clinical outcome. Ann Surg Oncol. 14(10):2994-3003, (2007).

25. Bowen, R.L., Duffy, S.W., Ryan, D.A., Hart, I.R., Jones, J.L. Early onset of breast cancer in a group of British black women. Br J Cancer. 98(2):277-81, (2008).

26. Lund, M.J., Trivers, K.F., Porter, P.L, Coates, R.J., Leyland-Jones, B., Brawley, O.W., Flagg, E.W., O'Regan, R.M., Gabram, S.G., Eley, J.W.: Race and triple negative threats to breast cancer survival: a population-based study in Atlanta, GA. Breast Cancer Res Treat. 113(2):357-70, (2009).

27. Shinde, S.S, Forman, M.R., Kuerer, H.M., Yan K, Peintinger F, Hunt KK, Hortobagyi GN, Pusztai L, Symmans WF. Higher parity and shorter breastfeeding duration: association with triple-negative phenotype of breast cancer. Cancer. 116(21):4933-43,(2010)

28. Stark, A., Kleer, C.G., Martin, I., Awuah , B., Nsiah-Asare ,A., Takyi, V., Braman, M., Quayson, S.E., Zarbo R, Wicha ,M., Newman, L. African ancestry and higher prevalence of triple-negative breast cancer: findings from an international study. Cancer. 116(21):4926-32, (2010).

29. National Cancer Institute. Breast Cancer Risk in American Women. Available at https://www.cancer.gov/types/breast/risk-fact-sheet accessed on 5/8/2014.

30. American Cancer Society (ACS). Cancer Facts & Figures 2009, Atlanta, GA: American Cancer Society (2009).

31. Turnbull, C., Rahman, N. Genetic predisposition to breast cancer: past, present, and future. Annu Rev Genomics Hum Genet. 9:321-345 (2008).

32. Antoniou, A., Pharoah, P.D., Narod, S, Risch HA, Eyfjord JE, Hopper JL, Loman N, Olsson H, Johannsson O, Borg A, Pasini B, Radice P, Manoukian S, Eccles DM, Tang N, Olah E, Anton-Culver H, Warner E, Lubinski J, Gronwald J, Gorski B, Tulinius H, Thorlacius S, Eerola H, Nevanlinna H, Syrjäkoski K, Kallioniemi OP, Thompson D, Evans C, Peto J, Lalloo F, Evans DG, Easton DF. Average risks of breast and ovarian cancer associated with BRCA1 or BRCA2 mutations detected in case Series unselected for family history: a combined analysis of 22 studies. Am J Hum Genet. 72(5):1117-1130 (2003).

33. Chen, S., Parmigiani, G. Meta-analysis of BRCA1 and BRCA2 penetrance. J. Clin Oncol. 25 1329-1333(2007).

34. Chlebowski, R.T., Anderson, G.L., Gass, M, , Lane DS, Aragaki AK, Kuller LH, Manson JE, Stefanick ML, Ockene J, Sarto GE, Johnson KC, Wactawski-Wende J, Ravdin PM, Schenken R, Hendrix SL, Rajkovic A, Rohan TE, Yasmeen S, Prentice RL; WHI Investigators. Estrogen plus progestin and breast cancer incidence and mortality in postmenopausal women. JAMA. 304 (15):1684-1692 (2010).

35. Chlebowski, R.T., Kuller, L.H., Prentice, R.L., Stefanick, M.L., Manson, J.E., Gass, M., Aragaki, A.K., Ockene ,J.K, Lane ,D.S., Sarto, G.E., Rajkovic, A., Schenken, R., Hendrix, S.L., Ravdin, P.M., Rohan, T.E, Yasmeen, S., Anderson, G; WHI Investigators. Breast Cancer after Use of Estrogen Plus Progestin in Postmenopausal Women. N Engl J Med. 360(6) 573-587 (2009).

36. Conroy, S.M., Maskarinec, G., Wilkens, L.R, White, K.K, Henderson, B.E, Kolonel, L.N. Obesity and breast cancer survival in ethnically diverse postmenopausal women: the Multiethnic Cohort Study. Breast Cancer Res Treat, 129(2):565-574. (2011).

37. Kerlikowske, K., Walker, R., Miglioretti, D. L., Desai, A., Ballard-Barbash, R., Buist ,D.S. Obesity, mammography use and accuracy, and advanced breast cancer risk", J Natl. Cancer Inst.100(23) 1724-1733 (2008)

38. Baan, R., Straif, K., Grosse, Y., Secretan, B., El Ghissassi, F., Bouvard, V., Altieri, A., Cogliano, V.: Carcinogenicity of alcoholic beverages. Lancet Oncol. 8:292–293 (2007)

39. Singletary, K.W., Gapstur, S.M. Alcohol and breast cancer: review of epidemiologic and experimental evidence and potential mechanisms. JAMA. Nov 7 2001;286(17):2143-2151

40. Preston, D.L., Mattsson, A., Holmberg, E., Shore, R., Hildreth, N.G., Boice, J.D., Jr. Radiation effects on breast cancer risk: a pooled analysis of eight cohorts. Radiat Res. Aug 158(2):220-235 (2002) .

41. Hemminki , E., Kyyronen, P., Pukkala, E. Postmenopausal hormone drugs and breast and colon cancer: Nordic countries 1995-2005. Maturitas. 61(4):299-304 (2008).

42. Cummings, S. R., Tice, J. A., Bauer S., Browner, W.S., Cuzick, J., Ziv, E., Vogel, V., Shepherd, J., Vachon, C., Smith-Bindman, R., Kerlikowske, K. Prevention of Breast Cancer In Postmenopausal Women: Approaches to Estimating and Reducing Risk. J Natl Cancer Inst. 101(6) 384-398 (2009)

43. Jemal, A., Siegel, R., Ward, E., Hao, Y., Xu, J., Thun, M. J. Cancer Statistics. CA Cancer J Clin 59(4):225–249 (2009).

44. Stewart, B.W., Coates, A.S. Cancer Prevention: A Global Perspective. J Clin Oncol 23(2):392–403 (2005).

45. Sudhakar, A. "History of cancer, ancient and modern treatment methods". Journal of Cancer Science and Therapy 01 (02): 1–4, (2009)

46. Jain, R.K. Transport of molecules in the tumor interstitium: a review. Cancer Res. , 47(12):3039–3051 (1987)

47. Rezende, T.S, Andrade, G.R.S, Barreto, L.S., Costa, Jr. N.B., Gimenez ,I.F., Almeida, L.E. Facile preparation of catalytically active gold nanoparticles on a thiolated chitosan. Mater Lett 64: 882-884 (2010).

48. Chen, K-S., Hung, T-S., Wu H-M, Wu J-Y, Lin M-T, Feng CK. Preparation of thermosensitive gold nanoparticles by plasma pretreatment and UV grafted polymerization. Thin Solid Films. 518: 7557-7562 (2010).

49. Dreaden, E. C., Austin, L. A., Mackey, M. A., & El-Sayed, M. A. Size matters: gold nanoparticles in targeted cancer drug delivery. Therapeutic Delivery, 3(4), 457–478 (2012).

50. Khan, A.K., Rashid, R., Murtaza, G., A Zahra A. Gold Nanoparticles: Synthesis and Applications in Drug Delivery. Tropical Journal of Pharmaceutical Research July 2014; 13 (7): 1169-1177

51. Kostoff, R.N., Koytcheff, R.G., Lau, C.G.Y. Structure of the nanoscience and nanotechnology applications literature. J. Technol. Transfer, 33: 472-484 (2008).

52. Gibson, J.D., Khanal, B.P., Zubarev, E.R. Paclitaxel functionalized gold nanoparticles. J Am Chem Soc. 129: 11653-11661 (2007).

53. Eghtedari, M., Liopo, A.V., Copland, J.A., Oraevsky, A.A., Motamedi, M. Engineering of hetero-functional gold nanorods for the in vivo molecular targeting of breast cancer cells. Nano Lett. 9 (1):287–291 (2009).

54. Guo Q, G. Q., Yuan, J., Zeng, J. Biosynthesis of gold nanoparticles using a kind of flavonol: Dihydromyricetin. Colloids and Surfaces A: Physicochemical and Engineering Aspects 441: 127-132 (2014).

55. Lee, K, Lee, H, Bae, K.H, Park, T.G. Heparin immobilized gold nanoparticles for targeted detection and apoptotic death of metastatic cancer cells. Biomater 31: 6530-6536 (2010).

56. Deb, S., Patra, H.K., Lahiri, P, Dasgupta, A.K., Chakrabarti K, Chaudhuri U. Multistability in platelets and their response to gold nanoparticles. Nanomed: Nanotechnol Biol Med. 7: 376-384 (2011).

57. Tarnawski, R., Ulbricht, M. Amphiphilic gold nanoparticles: Synthesis, characterization and adsorption to PEGylated polymer surfaces. Colloid Surfac A: Physicochem Engineer Aspects 374: 13-21 (2011).

58. Chithrani, D.B., Dunne, M., Stewart, J., Allen, C., Jaffray, D.A. Cellular uptake and transport of gold nanoparticles incorporated in a liposomal carrier. Nanomed: Nanotechnol Biol Med 6: 161-169, (2010).

59. Cho, K., Wang, X., Nie, S., Chen, Z., Shin, D.M. Therapeutic nanoparticles for drug delivery in cancer. Clin. Cancer Res.14, 1310–1316 (2008).

60. Sinha, R., Kim, G.J., Nie, S., Shin, D.M. Nanotechnology in cancer therapeutics: bioconjugated nanoparticles for drug delivery. Mol. Cancer Ther.5(8),1909–1917 (2006).

61. Maeda, H. The enhanced permeability and retention (EPR) effect in tumor vasculature: the key role of tumor-selective macromolecular drug targeting. Adv Enzyme Regul; 41:189 (2001)

62. Carmeliet, P., Jain, R. K. Angiogenesis in cancer and other diseases. Nature 407, 249-257 (2000).

63. Carmeliet, P. Angiogenesis in life, disease and medicine. Nature 438, 932-936 (2005).

64. Pelicano, H., Martin, D.S., Xu, R.H., Huang, P. Glycolysis inhibition for anticancer treatment. Oncogene25, 4633–4646 (2006).

65. Yatvin, M.B., Kreutz, W., Horwitz, B.A, Shinitzky, M. pH-sensitive liposomes: possible clinical implications.Science210 (4475), 1253–1255 (1980).

66. Sudimack, J., Lee, R.J. Drug targeting via the folate receptor. Adv. Drug Deliv. Rev.41,147–162 (2000).

67. Arap, W., Pasqualini, R., Ruoslahti, E. Cancer treatment by targeted drug delivery to tumor vasculature in a mouse model. Science 279(5349), 377–380 (1998).

68. Wu, Y., Sefah, K., Liu, H., Wang, R., Tan, W. DNA aptamer-micelle as an efficient detection/delivery vehicle toward cancer cells. Proc. Natl Acad. Sci. USA107,5–10 (2010).

69. Leamon, C.P, Reddy, J.A. Folate-targeted chemotherapy. Adv. Drug Deliv. Rev.56, 1127–1141 (2004).

70. Kumar Khanna, V. (2012). Targeted Delivery of Nanomedicines. ISRN Pharmacology, 2012, 571394. http://doi.org/10.5402/2012/571394

71. Boundless Biology.Types of Receptors.Available at https://www.boundless.com/biology/textbooks/boundless-biology-textbook/cell-communication-9/signaling-molecules-and-cellular-receptors-83/types-of-receptors-381-11607/. Accessed on 10/10/2016.

72. Vasir, J.K., Reddy, K.M., Labhasetwar, D.V. Nanosystems in drug targeting: opportunities and challenges. Current Nanoscience. 1:47–64, (2005).

73. Amoruso, S., Nedyalkov, N.N., Wang, X., Ausanio, G., Bruzzese, R., and Atanasov, P.A. Ultrashort-pulse laser ablation of gold thin film targets: theory and experiment. Thin Solid Films 550: 190–198 (2014).

74. Thakkar, K.N., Mhatre, S.S., and Parikh, R.Y. Biological synthesis of metallic nanoparticles. Nanomedicine 6: 257–262 (2010).

75. Mafuné, F., Kohno, J., Takeda, Y., Kondow, T. of gold nanoparticles by laser ablation in aqueous solution of surfactant. J Phys Chem B 105: 5114–5120, (2001).

76. Okitsu, K., Mizukoshi, Y., Yamamoto, T.A., Maeda, Y., Nagata, Y. Sonochemical synthesis of gold nanoparticles on chitosan. Mater Lett 61: 3429–3431, (2007).

77. Meyre, M.E., Treguer-Delapierre, M., Faure, C. Radiation-induced synthesis of gold nanoparticles within lamellar phases. Formation of aligned colloidal gold by radiolysis. Langmuir 24: 4421–4425, (2008).

78. Nakamoto, M., Kashiwagi, Y., Yamamoto, M. Synthesis and size regulation of gold nanoparticles by controlled thermolysis of ammonium gold (I) thiolate in the or presence of amines. Inorg Chim Acta 358: 4229–4236 (2005).

79. Wu, J., Zan, X., Li, S., Liu, Y., Cui, C., Zou, B., Zhang, W., Xu, H., Duan, H., Tian, D., Huang, W., Huo, F. In situ synthesis of large-area single sub-10nm nanoparticle arrays by polymer pen lithography. Nanoscale 6: 749–752 (2014).

80. Binupriya, A.R., Sathishkumar, M., Yun, S.I. Biocrystallization of silver and gold ions by inactive cell filtrate of Rhizopus stolonifer. Colloids Surf B Biointerfaces79: 531–534 (2010b).

81. Samal, A.K., Sreeprasad, T.S., Pradeep, T. Investigation of the role of NaBH4 in the chemical synthesis of gold nanorods. J Nanopart Res 12: 1777–1786 (2010).

82. Liu, X., Cu, C., Cheng, Y., Ma, H., Liu, D. Shape control technology during electrochemical synthesis of gold nanoparticles. Int J Min Met Mater 20: 486–493 (2013).

83. Narayanan, K.B., Sakthivel, N. Biological Synthesis of metal nanoparticles by microbes. Adv Colloid Interface Sci 156: 1–13 (2010).

84. Petrucci, O.D., Buck, D.C., Farrer, J.K., Watt, R.K. A ferritin mediated photochemical method to synthesize biocompatible catalytically active gold nanoparticles: size control synthesis for small (~ 2 nm), medium (~ 7 nm) or large (~ 17 nm) nanoparticles. RSC Adv 4: 3472–3481 (2014).

85. Arangasamy, L., Munusamy V. Tapping the unexploited plant resources for the synthesis of silver nanoparticles. African Journal of Biotechnology 7 (17), 3162-3165,(2008).

86. Mariekie Gericke and Anthony Pinches. Microbial Production of Gold Nanoparticles. Gold bulletin, 39,1 (2006).

87. Ankamwar B. Biosynthesis of Gold Nanoparticles (Green-Gold) Using Leaf Extract of Terminalia Catappa. E-Journal of Chemistry 7(4), 1334-1339 (2010).

88. Nair, B., Pradeep, T. Coalescence of Nanoclusters and Formation of Submicron Crystallites Assisted by Lactobacillus Strains Crystal Growth and Design, 2, 293 (2002).

89. Ahmad, A., Senapati, S., Khan, M.I., Kumar, R., Sastry, M. Extracellular biosynthesis of monodisperse gold nanoparticles by a novel extremophilic actinomycete, Thermomonospora sp. Langmuir 19:3550 (2003).

90. Mukherjee. P. Bioreduction of AuCl4− Ions by the Fungus, Verticillium sp. and Surface Trapping of the Gold Nanoparticles Formed Chem. Int. Edn. 40: 3585 (2001)..

91. Das, S.K., Dickinson, C., Laffir, F., Brougham, D.F., Marsili, E. Synthesis, characterization and catalytic activity of gold nanoparticles biosynthesized with Rhizopus oryzae protein extract. Green Chem 14: 1322–1344 (2012a).

92. Frigeri, L.G., Radabaugh, T.R., Haynes, P.A., Hildebrand, M. Identification of proteins from a cell wall fraction of the diatom Thalassiosira pseudonana. Insights into silica structure formation. Mol Cell Proteomics 5: 182–193 (2006).

93. Young, J.R., Davis, S.A., Bown, P.R., Mann, S. Coccolith ultrastructure and biomineralisation. J Struct Biol 126: 195–215 (1999).

94. Schüler, D. Formation of magnetosomes in magnetotactic bacteria. J Mol Microbiol Biotechnol 1: 79–86 (1999).

95. Crookes-Goodson, W.J., Slocik, J.M., Naik, R.R. Biodirected synthesis and assembly of nanomaterials. Chem Soc Rev 7: 2403–2412 (2008).

96. Klaus-Joerger, T., Joerger, R., Olsson, E., Granqvist, C. “Bacteria as workers in the living factory: metal-accumulating bacteria and their potential for materials science,” Trends in Biotechnology, 19, (1): 15–20, (2001)

97. Mullen, M. D., Wolf, D. C., Ferris, F. G., Beveridge, T. J., Flemming, C. A., Bailey, G. W. “Bacterial sorption of heavy metals,” Applied and Environmental Microbiology, 55, (12), 3143–3149, (1989).

98. He, S., Guo, Z., Zhang,Y., Zhang, S., Wang, J., Gu, N. “Biosynthesis of gold nanoparticles using the bacteria Rhodopseudomonas capsulata,” Materials Letters, 61, (18), 3984–3987, (2007).

99. Lengke, M. F., Fleet, M. E., Southam, G. “Biosynthesis of silver nanoparticles by filamentous cyanobacteria from a silver(I) nitrate complex,” Langmuir, 23, (5), 2694–2699, (2007).

100. Wang, H., Law, N., Pearson, G., van Dongen, B.E., Jarvis, R.M., Goodacre, R., Lloyd, J.R. Impact of silver (I) on the metabolism of Shewanella oneidensis. J Bacteriol 192: 1143–1150 (2010).

101. Orellana, R., Leavitt, J.J., Comolli, L.R., Csencsits, R., Janot, N., Flanagan, K.A., Gray, A.S., Leang, C., Izallalen, M., Mester, T., Lovley, D.R. U(VI) reduction by diverse outer surface c-type cytochromes of Geobacter sulfurreducens. Appl Environ Microbiol 79: 6369–6374 (2013).

102. Burkhardt, E.M., Bischoff, S., Akob, D.M., Buchel, G., Kusel, K. Heavy metal tolerance of Fe(III)-reducing microbial communities in contaminated creek bank soils. Appl Environ Microbiol 77: 3132–3136 (2011).

103. Huang, J., Li, Q., Sun, D., Lu, Y., Su, Y., Yang, X., Wang, H., Wang, Y., Shao, W., He, N., Hong, J., Chen, C. Biosynthesis of silver and gold nanoparticles by novel sundried Cinnanonum camphora leaf. Nanotechnology, 18(10), 105104 (2007).

104. Kasthuri, J., Kathiravan, K., Rajendiran, N. Phyllanthin-assisted biosynthesis of silver and gold nanoparticles: a novel biological approach. J Nanopart Res., 11(5), 1075-1085 (2009).

105. Shankar, S.S., Ahmad, A., Pasrichaa, R., Sastry, M. Bioreduction of chloroaurate ions by geranium leaves and its endophytic fungus yields gold nanoparticles of different shapes. J Mater Chem 13:1822–1826 (2003).

106. Shankar SS, Rai A, Ahmad A and Sastry M, Controlling the optical properties of lemongrass extract synthesized gold nanotriangles and potential application in infrared-absorbing optical coatings. Chem Mater 17:566–572 (2005).

107. Huang J, LiQ, Sun D, Lu Y, Su Y, Yang X, Wang, H., Wang, Y., Shao, W., He, N., Hong, J., Chen, C. Biosynthesis of silver and gold nanoparticles by novel sundried Cinnamomum camphora leaf. Nanotechnology 18:105104–105114 (2007).

108. Shankar, S.S., Rai, A., Ahmad, A., Sastry, M. Rapid synthesis of Au, Ag, and bimetallic Au core–Ag shell nanoparticles using neem (Azadirachta indica) leaf broth. J Colloid Interf Sci 275:496–502 (2004).

109. Chandran, S.P, Chaudhary, M., Pasricha, R., Ahmad, A., Sastry, M. Synthesis of gold nanotriangles and silver nanoparticles using Aloe vera plant extract. Biotechnol Prog 22:577–583 (2006).

110. Ankamwar, B., Chaudhary, M., Sastry, M. Gold nanotriangles biologically synthesized using tamarind leaf extract and potential application in vapor sensing. Synth React Inorg Metal-Org Nano- Metal Chem 35:19–26 (2005).

111. Ankamwar, B., Damle, C., Ahmad, A., Sastry, M. Biosynthesis of gold and silver nanoparticles using Emblica officinalis fruit extract, their phase transfer and transmetallation in an organic solution. J Nanosci Nanotechnol 5:1665–1671 (2005).

112. Bhumkar, D.R., Joshi, H.M., Sastry, M., Pokharkar, V.B. Chitosan reduced gold nanoparticles as novel carriers for transmucosal delivery of insulin. Pharm. Res., 24 1415-1426 (2007).

113. Mallikarjuna, N.N., Rajender, S.V. "Green Synthesis of Ag and Pd Nanospheres, Nanowires, and Nanorods Using Vitamin : Catalytic Polymerisation of Aniline and Pyrrole," Journal of Nanomaterials, Article ID 782358, (2008) 8 pages, (2008).

114. Kai, S., Jingxia, Q., Jiwei, L., Yuqing, M. Preparation and characterization of gold nanoparticles using ascorbic acid as reducing agent in reverse micelles. Journal of Materials Science. 44 (3), 754-758 (2007).

115. Lemberg, R., Barrett, J. Cytochromes (Academic New York), 277-279 (1973)

116. Connor, E.E., Mwamuka, J., Gole, A., Murphy, C.J., Wyatt, M.D. Gold nanoparticles are taken up by human cells but do not cause acute cytotoxicity. Small, 1, 325–327(2005).

117. Ghosh, P., Han, G., De, M., Kim, C.K., Rotello, V.M. Gold nanoparticles in delivery applications. Adv. Drug Deliv. Rev., 60, 1307–1315 (2008).

118. Pissuwan, D., Niidome, T., Cortie, M.B. The forthcoming applications of gold nanoparticles in drug and gene delivery systems. J. Contr. Release, 149, 65–71 (2009)

119. Susana Liébana, Guido A. Drago. Bioconjugation and stabilisation of biomolecules in biosensors. Essays In Biochemistry J, 2016, 60(1) 59-68.

120. Arruebo, M., Valladares M., González-Fernández, A. Antibody-Conjugated Nanoparticles for Biomedical Applications. Journal of Nanomaterials, 2009 Article ID 439389, 24 pages (2009).

121. Lynch, I., Dawson, K.A. Protein-nanoparticle interactions. Nano Today, 3:40–47 (2008).

122. Cedervall, T., Lynch, I., Lindman, S., Berggard, T., Thulin, E., Nilsson, H., Dawson, K.A., Linse, S. Understanding the nanoparticle-protein corona using methods to quntify exchange rates and affinities of proteins for nanoparticles. PNAS, 104:2050–2055 (2007)

123. Chanda, N., Kattumuri, V., Shukla, R., Zambre, A., Katti, K., Upendran, A., Kulkarni, R.R., Kan, P., Fent, G.M., Casteel, S.W., Smith, C.J., Boote, E., Robertson, J.D., Cutler, C., Lever, J.R., Katti, K.V., Kannan, R. Bombesin functionalized gold nanoparticles show in vitro and in vivo cancer receptor specificity. PNAS, 107:8760–8765 (2010).

124. Berry, C.C. Intracellular delivery of nanoparticles via the HIV-1 tat protein. Nanomedicine, 3:357–365 (2008).

125. El-Sayed, I.H., Huang, X., El-Sayed, M.A. Selective laser photo-thermal therapy of epithelial carcinoma using anti-EGFR antibody conjugated gold nanoparticles. Cancer Lett, 239:129–135 (2006).

126. Daniel, M.C., Astruc, D. Gold nanoparticles: assembly, supramolecular chemistry, quantum-size-related properties, and applications toward biology, catalysis, and nanotechnology. Chem Rev, 104:293–346 (2004) .

127. Aili, D., Enander, K., Rydberg, J., Lundstrom, I., Baltzer, L., Liedberg, B. Aggregation-induced folding of a de novo designed protein immobilized on gold nanoparticles. J Am Chem Soc, 128:2194–2195 (2006).

128. Bhattacharya, R., Patra, C.R., Wang, S.F., Lu, L.C., Yaszemski, M.J., Mukhopadhyay, D., Mukherjee, P. Assembly of gold nanoparticles in a rod-like fashion using proteins as templates. Adv Funct Mater, 16:395–400 (2006).

129. Alivisatos, A.P., Johnsson, K.P., Peng, X.G., Wilson, T.E., Loweth, C.J., Bruchez, M.P., Schultz, P.G. Organization of 'nanocrystal molecules' using DNA. Nature, 382:609–611 (1996).

130. Mirkin, C.A., Letsinger, R.L., Mucic, R.C., Storhoff, J.J. A DNA-based method for rationally assembling nanoparticles into macroscopic materials. Nature, 382:607–609 (1996).

131. Barrientos, G., De la Fuente, J.M., Rojas, T.C., Fernandez, A., PenadÈs, S. Gold glyconanoparticles: Synthetic polyvalent ligands mimicking glycocalyx-like surfaces as tools for glycobiological studies. Chem Eur J, 9:1909–1921 (2003).

132. Chen, C., Kwak, E.S., Stein, B., Kao, C.C., Dragnea, B. Packaging of gold particles in viral capsids. J Nanosci Nanotechnol, 5:2029–2033 (2005).

133. Chen, C., Daniel, M.C., Quinkert, Z.T., De, M., Stein, B., Bowman, V.D., Chipman, P.R., Rotello, V.M., Kao, C.C., Dragnea, B. Nanoparticle-templated assembly of viral protein cages. Nano Lett, 6:611–615 (2006).

134. Goicochea, N.L., De, M., Rotello, V.M., Mukhopadhyay, S., Dragnea, B. Core-like particles of an enveloped animal virus can self-assemble efficiently on artificial templates. Nano Lett, 7:2281–2290 (2007).

135. Aniagyei, S.E., DuFort, C., Kao, C.C., Dragnea, B. Self-assembly approaches to nanomaterial encapsulation in viral protein cages. J Mater Chem, 18:3763–3774 (2008).

136. Loo, L., Guenther, R.H., Basnayake, V.R., Lommel, S.A., Franzen, S. Controlled encapsidation of gold nanoparticles by a viral protein shell. J Am Chem. Soc., 128:4502–4503 (2006).

137. Loo, L., Guenther, R.H., Lommel, S.A., Franzen, S. Encapsidation of nanoparticles by red clover necrotic mosaic virus. J Am Chem Soc, 129:11111–11117 (2007).

138. Tai, W., Mahato, R., Cheng, K. The role of HER2 in cancer therapy and targeted drug delivery. J. Control Release, 146(3), 264-275 (2010).

139. Giersig, M., Mulvaney, P. Langmuir, 9, 3408 – 3413 (1993).

140. Brust, M., ink, J.F.,Bethe ll, D., Schiffrin, D. J., Kiely, C., J. Chem. Soc. Chem. Commun., 1655 -1656 (1995).

141. Galow, T.H., Boal, A.K., Rotello, V.M. Adv. Mater. 12: 576 -579 (2000).

142. Carl, S. WeisbeckerM, argaret V. Merritt,i and GeorgeM . Whitesidesx Molecular Self-Assembly of Aliphatic Thiols on Gold Colloids. Langmuir, 12, 3763-3772 (1996)

143. Troughton, E. B., Bain, C. D., Whitesides, G. M., Num, R. G., Allara, D. L., Porter, M. D. Longmuir, 4, 365-385 (1988).

144. Woods, R. In Flotation; Fuerstenau, M. C., Ed.; American Institute of Mining, Metallurgical, and Petroleum Engineers: Baltimore, (1976).

145. Nuuo, R. G., Allara, D. L. J. Am. Chem. Soc.,105, 4481-83 (1983).

146. Nuzzo, R. G., Zegarski, B. R., Dubois, L. H. J. Am. Chem. Soc., 109, 733-40 (1987).

147. Nuzzo, R. G., Fusco, F. A., Allara, D. L. J. Am. Chem. Soc. 1987,109,2358-2368

148. Tsai, P.S. Gonadotropin-releasing hormone in invertebrates: structure, function and evolution. Gen Comp Endocrinol. 148: 48-53 (2006).

149. Cheng, C.K., Leung, P.C.K. “Molecular Biology of Gonadotropin Releasing Hormone (GnRH)-I, GnRH-II, and Their Receptors in Humans”, Endocrine Reviews 26(2): 283-306 (2005)

150. Millar, R. P., Lu, Z. L., Pawson, A. J., Flanagan, C. A., Morgan, K., Maudsley, S. R. “Gonadotropin-Releasing Hormone Receptors,” Endocrine Reviews, 25, (2), 235-275 (2004)

151. Mezo, G., Manea, M. Luteinizing hormone-releasing hormone antagonists. Expert OpinTher Pat. 19:1771-85 (2009).

152. Akaza H. Future prospects for luteinizing hormone releasing hormone analogues in prostate cancer treatment. Pharmacology. 2010; 85:110-20.

153. Vercellini, P., Somigliana, E., Vigan, P., Abbiati, A., Barbara, G., Crosignani, P.G. Endometriosis: current therapies and new pharmacological developments. Drugs. 69: 649-75 (2009).

154. Hackshaw, A. Luteinizing hormone-releasing hormone (LHRH) agonists in the treatment of breast cancer. Expert Opin Pharmacother. 10:2633-2639 (2009) .

155. Schally, A.V., Comaru-Schally, A.M., Plonowski, A., Nagy, A., Halmos, G., Rekasi, Z. Peptide analogs in the therapy of prostate cancer. Prostate, 45, 158–166 (2000).

156. Miller, W.R., Scott, W.N., Morris, R., Fraser, H.M., Sharpe, R.M. Growth of human breast cancer cells inhibited by a luteinizing hormone-releasing hormone agonist. Nature 313, 231–233 (1985).

157. Szepeshazi, K., Schally, A.V., Nagy, A. Effective treatment of advanced estrogen-independent MXT mouse mammary cancers with targeted cytotoxic LH-RH analogs. Breast Cancer Res. Treat. 56, 267–276 (1999).

158. Bajo, A.M., Schally, A.V., Halmos, G., Nagy, A. Targeted doxorubicin-containing luteinizing hormone-releasing hormone analogue AN-152 inhibits the growth of doxorubicin-resistant MX-1 human breast cancers. Clin. Cancer Res. 9, 3742–3748 (2003).

159. Kahan, Z., Nagy, A., Schally, A.V., Halmos, G., Arencibia, J.M., Groot, K. Complete regression of MX-1 human breast carcinoma xenografts after targeted chemotherapy with a cytotoxic analog of luteinizing hormone-releasing hormone, AN-207. Cancer 85, 2608–2615 (1999).

160. Letsch, M., Schally, A.V., Szepeshazi, K., Halmos, G., Nagy, A. Preclinical evaluation of targeted cytotoxic luteinizing hormone-releasing hormone analogue AN-152 in androgen-sensitive and insensitive prostate cancers. Clin. Cancer Res. 9, 4505–4513 (2003).

161. Plonowski, A., Schally, A.V., Nagy, A., Groot, K., Krupa, M., Navone, N.M., Logothetis, C. Inhibition of in vivo proliferation of MDA-PCa-2b human prostate cancer by a targeted cytotoxic analog of luteinizing hormone-releasing hormone AN-207. Cancer Lett. 176, 57–63 (2002).

162. Grundker, C., Volker, P., Griesinger, F., Ramaswamy, A., Nagy, A., Schally, A.V., Emons, G. Antitumor effects of the cytotoxic luteinizing hormone-releasing hormone analog

AN-152 on human endometrial and ovarian cancers xenografted into nude mice. Am. J. Obstet. Gynecol. 187, 528–537 (2002).

163. Miyazaki, M., Nagy, A., Schally, A.V., Lamharzi, N., Halmos, G., Szepeshazi, K., Groot, K., Armatis, P. Growth inhibition of human ovarian cancers by cytotoxic analogues of luteinizing hormone-releasing hormone. J. Natl. Cancer Inst., 89, 1803–1809 (1997).

164. Miyazaki, M., Schally, A.V., Nagy, A., Lamharzi, N., Halmos, G., Szepeshazi, K., Armatis, P. Targeted cytotoxic analog of luteinizing hormone-releasing hormone AN-207 inhibits growth of OV-1063 human epithelial ovarian cancers in nude mice. Am. J. Obstet. Gynecol. 180, 1095–1103 (1999).

165. Arencibia, J.M., Bajo, A.M., Schally, A.V., Krupa, M., Chatzistamou, I., Nagy, A. Effective treatment of experimental ES-2 human ovarian cancers with a cytotoxic analog of luteinizing hormone-releasing hormone AN-207. Anticancer Drugs 13, 949–956 (2002).

166. Koppan, M., Nagy, A., Schally, A.V., Plonowski, A., Halmos, G., Arencibia, J.M., Groot, K. Targeted cytotoxic analog of luteinizing hormone-releasing hormone AN-207 inhibits the growth of PC-82 human prostate cancer in nude mice. Prostate 38, 151–158 (1999).

167. Nagy, A., Schally, A.V., Armatis, P., Szepeshazi, K., Halmos, G., Kovacs, M., Zarandi, M.; Groot, K., Miyazaki, M., Jungwirth, A., Horvath, J. Cytotoxic analogs of luteinizing hormone-releasing hormone containing doxorubicin or 2-pyrrolinodoxorubicin, a derivative 500–1000 times more potent. Proc. Natl. Acad. Sci. USA 93, 7269–7273 (1996).

168. Chatzistamou, L., Schally, A.V., Nagy, A., Armatis, P., Szepeshazi, K., Halmos, G. Effective treatment of metastatic MDA-MB-435 human estrogen-independent breast carcinomas with a targeted cytotoxic analogue of luteinizing hormone-releasing hormone AN-207. Clin. Cancer Res., 6, 4158–4165 (2000).

169. Kahan, Z., Nagy, A., Schally, A.V., Halmos, G., Arencibia, J.M., Groot, K. Administration of a targeted cytotoxic analog of luteinizing hormone-releasing hormone inhibits growth of estrogen-independent MDA-MB-231 human breast cancers in nude mice. Breast Cancer Res. Treat. 59, 255–262 (2000).

170. Obayemi, J.D., Dozie-Nwachukwu, S., Danyuo, Y., Odusanya, O.S., Anuku, N., Malatesta, K., Soboyejo, W.O. Biosynthesis and the conjugation of magnetite nanoparticles

with luteinizing hormone releasing hormone (LHRH). Materials Science and Engineering C 46 482–496 (2015).

171. Garin-Chesa, P., Campbell, I., Saigo, P.E., Lewis, J.L., Old, L.J., Rettig, W.J. Trophoblast and ovarian cancer antigen LK26: sensitivity and specificity in immunopathology and molecular identification as a folate-binding protein. Am J Pathol 142: 557-567 (1993).

172. Oaks, B.M., Dodd, K.W., Meinhold, C.L., Jiao, L., Church, T.R., Stolzenberg-Solomon, R.Z. Folate intake, post-folic acid grain fortification, and pancreatic cancer risk in the Prostate, Lung, Colorectal and Ovarian Cancer Screening Trial. Am J Clin Nutr 91: 449-455 (2010).

173. Mansoori, A., Brandenburg, K., Shakeri-Zadeth, A. A comparative study of two folate conjugated gold nanoparticles for cancer nanotechnology applications. Cancer 2: 1911-1928 (2010).

174. Muller, C., Schibli, R. Folic acid conjugates for nuclear imaging of folate receptorpositive cancer. J Nucl Med 52: 1-4 (2011).

175. Parker, N., Turk, M.J., Westrick, E., Lewis, J.D., Low, P.S., Leamon, C.P. Folate receptor expression in carcinomas and normal tissues determined by a quantitative radioligand binding assay. Anal Biochem ; 338: 284-293 (2005).

176. Yoo, H., Park, T. Folate-receptor-targeted delivery of doxorubicin nano-aggregates stabilized by doxorubicin-peg-folate conjugate. J Control Release 100: 247-256 (2004).

177. Prabaharan, M., Grailer, J.J., Pilla, S., Steeber, D.A., Gong, S.Q. Gold nanoparticles with a monolayer of doxorubicin-conjugated amphiphilic block copolymer for tumor-targeted drug delivery. Biomaterials, 30(30), 6065 – 6075 (2009).

178. Aslan, K., Luhrs, C.C., Perez-Luna, V.H. Controlled and reversible aggregation of biotinylated gold nanoparticles with streptavidin. J. Phys. Chem. B, 108(40), 15631-15639 (2004).

179. Aslan, K., Pérez-Luna, V. Nonradiative interactions between biotin functionalized gold nanoparticles and fluorophore-labeled antibiotin. Plasmonics, 1(2), 111-119 (2006).

180. Lee, R.J., Low, P.S. In Methods in Moleculer Medicine. G.E. F.; C. D. Eds.; Humana Press Inc.: Totowa, NJ, 25, 69-75 (2000).

181. Turek, J.J., Leamon, C.P., Low, P.S. Endocytosis of folate-protein conjugates: ultrastructural localization in KB cells, J. Cell.Sci. 106 (Pt 1) 423–430(1993).

182. Leamon, C.P., Low, P.S. Membrane folate-binding proteins are responsible for folate-protein conjugate endocytosis into cultured cells, Biochem. J. 291 (Pt 3) 855– 860 (1993).

183. Leamon, C.P., Low, P.S. Delivery of macromolecules into living cells: a method that exploits folate receptor endocytosis, Proc. Natl. Acad. Sci. U. S. A. 88, 5572–5576 (1991).

184. O'Shannessy, D. J., Somers, E. B., Maltzman, J., Smale, R., Fu, Y-S. Folate receptor alpha (FRA) expression in breast cancer: identification of a new molecular subtype and association with triple negative disease. SpringerPlus 1(22): 1-9 (2012).

185. Tacha, D., Bremer, R. Folate Receptor alpha is Frequently Expressed in Triple Negative Breast Cancers. Modern Pathology 26, Supplement 2: (71A): 1-4 (2013).

186. Sagvolden, G., Giaever, I., Pettersen, E.O., Feder, J. Cell adhesion force microscopy. Proc. Natl.Acad. Sci. USA, 96, 471–476 (1999).

187. Dembo, M., Torney, D., Saxman, K., Hammer, D. The kinetics of membrane-to-surface adhesion and detachment. Proc. R. Soc. 234, 55–83 (1988).

188. Shen, Y., Nakajima, M., Kojima, S., Homma, M., Kojima, M., Fukuda, T. Single cell adhesion force measurement for cell viability identification using an AFM cantilever-based micro putter. Meas. Sci. Technol. 22, 115802 (2011).

189. Huang, S.; Ingber, D.E. The structural and mechanical complexity of cell-growth control. Nat. Cell Biol. 1, E131 (1999).

190. Lasky, L.A., Singer, M.S., Dowbenko, D., Imai, Y., Henzel, W.J., Grimley, C.; Fennie, C.; Gillett, N., Watson, S.R., Rosent, S.D. An endothelial ligand for L-Selectin is a novel mucin-like molecule. Cell 69, 927–938 (1992).

191. Szekanecz, Z., Koch, A.E. Cell-cell interactions in synovitis: Endothelial cells and immune cell migration. Arthritis Res. 2, 368–373 (2000).

192. Okegawa, T., Pong, R.-C., Li, Y., Hsieh, J.-T. The role of cell adhesion molecule in cancer progression and its application in cancer therapy. Acta Biochim. Pol. 51, 445–457 (2004).

193. Hirohashi, S., Kanai, Y. Cell adhesion system and human cancer morphogenesis. Cancer Sci. 94, 575–581 (2003).

194. Perinpanayagam, H., Zaharias, R., Stanford, C., Keller, J., Schneider, G., Brand, R. Early cell adhesion events differ between osteoporotic and non-osteoporotic osteoblasts. J. Orthop. Res. 19, 993–1000 (2001).

195. Cho, P., Schneider, G.B., Kellogg, B., Zaharias, R., Keller, J.C. Effect of glucocorticoid-induced osteoporotic-like conditions on osteoblast cell attachment to implant surface microtopographies. Implant Dent. 15, 377–385 (2006).

196. Serhan, C.N., Savill, J. Resolution of inflammation: The beginning programs the end. Nat. Immunol. 6, 1191–1197 (2005).

197. Simon, S., Green, C.E. Molecular mechanics and dynamics of leukocyte recruitment during inflammation. Annu. Rev. Biol. 7, 151–185 (2005).

198. Khalili, A. A., Ahmad, M. R. A Review of Cell Adhesion Studies for Biomedical and Biological Applications. Int. J. Mol. Sci. 16, 18149-18184 (2015)

199. Butt, H., Cappella, B., Kappl, M.: Force measurements with the atomic force microscope:Technique, interpretation and applications. Surface Science Reports. 59 1–152, (2005).

200. Santner, E., Stegemann, B.: Adhesi)n measurements by AFM – a gateway to the basics of friction . Accessed from :www.academia.edu/7351106/Adhesion_measurements_by_AFM_a_gateway_to_the_basics_of_friction. on 30th March, 2016.

201. Bhushan, B. (Ed.), Handbook of Micro/Nanotribology. 2nd ed. CRC press, Boca Raton (1999).

202. Burnham, N.A., Colton, R.J, Pollock, H.M. Interpretation of force curves in force microscopy. Nanotechnology, 4: 64-80 (1993)

203. Cappella, B., Dietler, G. Force-distance curves by atomic force microscopy. Surf. Sci. Rep., 34(1-3): 1-104 (1999).

204. Duong A. and Mousa S.A. Current status of nucleoside antivirals in chronic hepatitis B. Drugs Today (Barc). 45: 751−761 (2009.

205. Fuller C.D., Thomas C.R. Chemoradiation for anal cancer: The more things change, the more they stay the same. Oncology. 24(5): 427-430 (2010).

206. Cho K., Wang X., Nie S., Chen Z., Shin D.M. Therapeutic nanoparticles for drug delivery in cancer. Clin Cancer Res. 14; 1310 (2008).

207. Baviskar, D.T., Chaudhari, R.D., Kale, M.T., Jain, D.K. Recent advances on tumor targeted drug delivery system an overview. Asian Journal of Biomedical and Pharmaceutical Sciences. 1 (4): 32-42 (2011).

208. Kwon, G.S. Polymeric micelles for delivery of poorly water soluble compounds. Crit Rev Ther Drug Carrier Syst. 2003; 20: 357–403.

209. Jabr-Milane, L.S., van Vlerken, L.E., Yadav, S., Amiji, M.M. Multifunctional nanocarriers to overcome tumor drug resistance. Cancer Treat Rev. 34(7): 592-602 (2008).

210. Gottesman, M.M. Mechanisms of cancer drug resistance. Annual Review of Medicine. 53: 615-627 (2002).

211. Singh, A.K., Pandey, A., Rai, R., Tewari, M., Pandey, H.P, Shukla, H.S. Nanomaterials as emerging tool in cancer diagnosis and treatment. Digest Journal of Nanomaterials and Biostructures. 3 (3): 135 – 140 (2008).

212. Matsumura, Y., Maeda, H. A new concept for macromolecular therapeutics in cancer chemotherapy: Mechanism of tumoritropic accumulation of proteins and the antitumor agent smancs. Cancer Res. 46: 6387–6392 (1986).

213. Iyer, A.K., Khaled, G., Fang, J., Maeda, H. Exploiting the enhanced permeability and retention effect for tumor targeting. Drug Discov Today. 11: 812–818 (2006).

214. Nam H.Y., Kwon S.M., Chung H., Lee S.Y., Kwon S.H., Jeon H. Cellular uptake mechanism and intracellular fate of hydrophobically modified glycol chitosan nanoparticles. J Control Release. 135: 259–267 (2009).

215. Liang, X.J., Chen, C., Zhao, Y., Wang, P.C. Circumventing tumor resistance to chemotherapy by nanotechnology. Methods Mol Biol. 596:467-488 (2010).

216. Brannon-Peppas L. and Blanchette J.O. Nanoparticle and targeted systems for cancer therapy. Adv Drug Deliver Rev. 56: 1649—1459 (2004).

217. Wang, M., Thanou, M. Targeting nanoparticles to cancer. Pharmacol Res. 62(2):90-99 (2010).

218. Bharalia, D.J., Mousaa, S.A. Emerging nanomedicines for early cancer detection and improved treatment. Current perspective and future promise. Pharmacology and Therapeutics. 128 (2): 324-335 (2010).

219. Giri, A.V., Anandkumar, N., Muthukumaran, G., Pennathur, G. A novel medium for the enhanced cell growth and production of prodigiosin from Serratia marcescens isolated from soil. BMC Microbiol. 4, 11-18 (2004).

220. Song, M.J., Bae, J., Lee, D.S., Kim, C.H., Kim, J.S., Kim, S.W., Hong, S.I. Purification and Characterization of Prodigiosin Produced by Integrated Bioreactor from Serratia sp. KH-95. J. Biosci. Bioeng. 101, 157-161 (2006).

221. Williamson, N.R., Fineram, P.C., Leeper, F.J., Salmond, G.P.C. The biosynthesis and regulation of bacterial prodiginines. Nat. Rev. Microbiol. 4, 887-899 (2006).

222. Harris, A.K.P., Williamson, N.R., Slater, H., Cox, A., Abbasi, S., Foulds, I., Simonsen, H.T., Leeper, F.J., Salmond, G.P.C. The Serratia gene cluster encoding biosynthesis of the red antibiotic, prodigiosin, shows species and strain-dependent genome context variation. Microbiol. 150, 3547-3560 (2004).

223. Khanafari, A., Assadi, M.M., Fakhr, F.A. Review of Prodigiosin, Pigmentation in *Serratia marcescens*. Online J. Biol. Sci. 1, 1-13 (2006).

224. Grimont, P.A.D., Grimont, F., Dulong, De Rosnay, H.L.C., Sneath, P.H.A. Taxonomy of the genus Serratia. J. Gen. Microbiol. 98, 39 (1977).

225. Pandey, R., Chander, R., Sainis, K.B. A novel prodigiosin-like immunosuppressant from an alkalophilic Micrococcussp. Int Immunopharmacol 3: 159–67 (2003).

226. Lazaro, J.E., Nitcheu, J., Predicala, R.Z., Mangalindan, G.C., Nesslany, F., Marzin, D., Concepcion, G.P., Diquet, B. Heptyl prodigiosin, a bacterial metabolite, is antimalarial in vivo and non-mutagenic in vitro. J Nat Toxins 11:367–77 (2002).

227. Montaner, B., Navarro, S., Pique,´ M., Viaseca, M., Martinell, M., Giralt, E., Gil, J., Pérez-Tomás, R. Prodigiosin from the supernatant of Serratia marcescens induces apoptosis in hematopoietic cancer cell lines. Br J Pharmacol 131:585–93 (2000).

228. Montaner, B., Pe´rez-Toma´s, R. Prodigiosin-induced apoptosis in human colon cancer cells. Life Sci 68:2025–36 (2001)

229. Dı´az-Ruı´z, C., Montaner, B., Pe´rez-Toma´s, R. Prodigiosin induces cell death and morphological changes indicative of apoptosis in gastric cancer cell line HGT-1. Histol Histopathol 16:415–21 (2001).

230. Montaner, B., Pe´rez-Toma´s, R. Activation of protein kinase C is required for protection of cells against apoptosis induced by the immunosuppressor prodigiosin. Biochem Pharmcol 63:1–7 (2002).

231. Rudd, B.A.M., Hopwood, D.A. A pigmented mycelial antibiotic in Streptomyces coelicolor: control by a chromosomal gene cluster. J. Gen. Microbiol., 119: 333-340 (1980).

232. Kerr, J.F.R., Winterford, C.M. Harmon, B.V. Apoptosis. Its significance in cancer and cancer therapy. Cancer, 73: 2013 – 2026 (1994).

233. Wickremasinghe, R.G. and A.V. Hoffbrand, Biochemical and genetic control of apoptosis: relevance to normal hematopoiesis and hematological malignancies. Blood, 93: 3587 – 3600 (1999).

234. Reed, J.C., Mechanisms of apoptosis avoidance in cancer. Curr. Opin. Oncol., 11: 68 – 75 (1999).

235. Alagusundaram, M., Chetty, M.S., Umashankari, C. Microspheres as a Novel drug delivery system – A review. Int J Chem. Tech. 12: 526-534 (2009).

236. Allen, L.V., Popovich, N.G., Ansel, H.C. Pharmaceutical Dosage Forms and Drug Delivery Systems. Delhi, India: BI Pubication, 8: 265 (2005).

237. Berger HL. Ultrasonic Liquid Atomization. 1St edition Hyde Park, NY: Partridge Hill Publishers; (1998).

238. Blanco, M.D., Alonso, M.J. Development and characterization of protein-loaded poly (lactideco-glycolide) nanospheres. Eur J Pharm Biopharm, , 43:287-294 (1997).

239. Banker G S, Rhodes C T. Modern pharmaceutics. In Parma Publication, 121: 501-527 (2002).

240. Bungenburg de Jong, H.G., Proc. Acad. Sci, Amsterdam, 41 646 (1938).

241. Deasy, P.B.. Evaluation of drug-containing microcapsules, J. Microencapsulation, 11 487–505 (1994)

242. Bhujbala, S.V., de Vosb, P., Nicloua, S.P. Drug and cell encapsulation: Alternative delivery options for the treatment of malignant brain tumors. Advanced Drug Delivery Reviews, 67–68, 10 ; 142–153 (2014)

243. Kita, K., Dittrich, C. Drug delivery vehicles with improved encapsulation efficiency: taking advantage of specific drug–carrier interactions. Expert Opinion on Drug Delivery, 8(3) 329-342 (2011).

244. Anusha, K., Sailaja, A.K. Preparation and evaluation of mefenamic acid loaded microspheres using synthetic and natural polymers. Der Pharmacia Lettre, 8 (1):197-205 (2016).

245. Rathod, S.S, Dev, A., Kumbhar, R.B. In vitro release and in vivo tissue localization of 5-flurouracil loaded Microspheres. Int J Pharm Pharm Sci, 6, (1), 78-83 (2015)

246. Ramtek,e, K.H, Jadhav V.B, Dhole S.N Microspheres: as carrieres used for novel drug delivery system. IOSR Journal of Pharmacy. 2, (4) 44- 48, (2012).

247. Brazel, S.C., Peppas, N.A. Modeling of drug release from swellable polymers. Eur J Pharm Biopharm, 49: 47–48 (2000).

248. Benita S, Donbrow M. Controlled drug delivery through microencapsulation, J. Pharm Sci, 71: 205–210 (1982)

249. Cassidy, JP, Landcert NM, Quardos E. Controlled buccal delivery of buprenorphine. J.control .Rel, 1993, 25: 21-29 (1993).

250. Gupta, P., Vermani, K., Garg, S. Hydrogels: from controlled release of pH responsive drug delivery. Drug Discovery Today, 7, 569-579 (2000).

CHAPTER 3

3.0 Plant synthesis of Gold nanoparticles with *Nauclea latifolia* leaf extract and Adhesion of Conjugated Gold/Prodigiosin Nanoparticles to Breast Cancer Cells

3.1.Introduction

Significant efforts have been made to develop gold nanoparticles (AuNPs) and conjugated AuNPs/cancer drug nanoparticles for the specific and selective targeting of cancer [1-3]. In most cases, gold has been used due to its photo-optical properties and biocompatibility [4]. AuNPs have also been synthesized by chemical, physical and biological pathways [5-8].

Although most of the prior efforts to synthesize AuNPs have used chemical synthesis [9] and physical synthesis [10], there is growing interest in the biosynthesis of AuNPs from plants [11-13], microbes [14] and fungi [15]. These approaches have been used to produce AuNPs with different sizes and shapes [16, 17]. Gold nanoparticles have also been shown to interact with laser beams to induce heat for hyperthermic cancer treatment [18], laser surgery [19] and drug delivery [20].

In most cases, fungi [21], actinomycetes [22], and bacteria [23] have been used to synthesize metallic nanoparticles [24]. Some prior work [13, 22, 25, 26] has also explored the use of parts of plants, or whole plants, in the synthesis of AuNPs. Such plant-based synthesis, using plant extracts, is relatively under-exploited. This method of synthesis could also be adapted in low-resource settings and developing countries for the synthesis of metallic nanoparticles.

Furthermore, the plant-based synthesis of AuNPs has been shown to be easier than the microbial-based synthesis of AuNPs. This is because the plant-based process occurs relatively quickly, and does involve the use of bioreactors, as in the case of microbial synthesis [27]. The use of plant extract method also is a technique that is relatively easy to scale up [28, 29].

A number of plants have been used to synthesize AuNPs [30-37]. They include: leaf extracts of Tamarind (*Tamarindus indica*) [31], cinnamon *Cinnamommum camphora* [32], lemongrass (*Cymbopogon flexuosus*) [33], geranium (*Pelargonium graveolens*) [34], extract of *Emblica officinalis* [35], Neem (*Azadirachta indica*) [36] and *Aloe vera* [37]. All of these plant extracts have been shown to have the potential to reduce Au^{3+} ions to AuNPs.

In our recent work [27], AuNPs were synthesized from *Nauclea latifolia* (NL) leaf extracts. The effects of pH on the sizes and shapes of the AuNPs were also explored. The AuNPs that were synthesized at pH values between 4.5 and 9.5 had sizes between 10 and 60 nm. Furthermore, extracts from the NL leaf were also shown to have anticancer activity and/or therapeutic activity [38-40]. These two-in-one effects suggest that the biosynthesis of AuNPs can be combined with the drugs to produce nanoclusters that are conjugated to attach specifically to receptors on cancer cells [41] or diseased cells [42]. There is, therefore, a potential to develop such AuNPs for the specific targeting and treatment of cancer and other diseases.

Although, AuNPs are being considered for potential applications in laser hyperthermia, significant efforts have also been made to develop Au/cancer drug nanoparticles that can be used for both laser hyperthermia and cancer drug release [43, 44]. There is, therefore an interest in the synthesis of Au/cancer drug nanoparticles that can be used for both cancer drug release and laser hyperthermia. Hence, in this paper we explore the synthesis of AuNPs/prodigiosin cancer drug for the specific targeting and treatment of triple negative breast cancer cells via localized drug delivery and laser hyperthermia.

Furthermore, in an effort to understand the specific targeting of breast cancer cells, the adhesion of the nanoparticles was studied along with the shapes and sizes of AuNPs/prodigiosin (PG) drug

prepared under different pH conditions. The AuNPs were characterized using transmission electron microscopy images and dynamic light scattering. The adhesion of LHRH-conjugated AuNPs is shown to be much greater than that of AuNPs to normal breast cancer cells. The increased adhesion of the LHRH-conjugated AuNPs and/or PG cancer drug is attributed to the increased incidence of LHRH receptors that are over-expressed on the surfaces of breast cancer cells. The implications of the results are discussed for the specific/selective targeting and the localized treatment of triple negative breast cancer cells.

3.1.1Theory of Adhesion Measurement

The technique of adhesion measurement involves the use of Atomic Force Microscope (AFM) to measure adhesion forces between nanoparticles coated on an AFM tip and breast cancer cells at a nanoscale. The force microscopy method involves bringing coated AFM tips close enough to a substrate for adhesive interactions to occur [Figures 3.1(a & b)]. Due to the presence of inherent Van der Waals forces present, the two components jump into contact [Figure 3.1(b)].

After contact, the tips get displaced further, as they undergo elasticity in the same direction [45-47]. Upon their retraction, the displacements are reversed, as the loads are reduced to zero. However, because of the presence of adhesion, the tips do not detach at zero load. The tips only get retracted when the applied force applied is sufficient to overcome the adhesion. When this happens, the pull-off of the AFM tips occurs from the substrates.

The resulting pull-off force, represented as F, is a measure of the adhesion between the nanoparticle/drug complex and the breast cancer/normal breast cells. This is given by Hooke's law to be:

$$F = k\delta \quad (1)$$

where k is the stiffness of the AFM cantilever and δ is the displacement of the AFM tip at the on onset of pull-off. The spring constants of the uncoated (bare) and coated AFM tips are usually determined experimentally using the thermal tune method [48]. Thermal tuning is done to obtain the actual spring constants (k) that are subsequently used to calculate the pull-off forces (adhesion forces) from Hooke's equation above. The k value is usually obtained at a temperature of 22°C and a steady relative humidity of 36–45%. Usually, prior to each adhesion measurement, the photodetector sensitivity was calibrated using a stiff quartz material.

It is important to note that measurements of pull-off (adhesion forces) have been used to measure forces in biological materials [49-51]. These have been shown to be sufficient to detect the differences between breast cancer cells and normal breast cells in recent work by Meng *et al.*, 2010 [46]. The adhesion forces have also been shown to reveal differences between the adhesive and cohesive interactions in different nanoclusters of gold nanoparticles in recent work by Oni *et al.*, 2014 [47].

However, although atomic force microscopy has been used to measure the adhesive forces between the constituents of nanoclusters, to the best of our knowledge, there have been no prior measurements of the adhesion forces between LHRH-conjugated gold nanoparticles and triple negative breast cancer cells/normal breast cells. These will, therefore, be measured in the current work, with the objective of determining the robustness of gold nanoparticle clusters for the specific targeting and treatment of cancer via localized chemotherapy and hyperthermia.

3.2 Experimental Procedures

3.2.1 Materials

The gold (III) chloride trihydrate, ACS reagent, ≥ 49.0% Au basis, was purchased from Sigma-Aldrich, St. Louis, USA, Lot number 127K1374. The other materials include: sterile distilled water and mature leaves of *Nauclea latifolia* (obtained from SHESTCO, Abuja, Nigeria). Phosphate buffer and Acetate buffer for synthesis were obtained from Sigma-Aldrich (St. Louis, MO, USA), and Thermo Fisher Scientific, Inc. (Waltham, MA, USA), respectively. Cyclohexane Mercaptan, 99% for conjugation work was purchased from Acros Organics, Thermo Fisher Scientific (New Jersey, USA).

The LHRH peptides that were used for the conjugation and the immuno-fluorescence staining of LHRH receptors were purchased from Sigma-Aldrich Co. LLC, (St. Louis, MO USA). In the case of the adhesion measurement, MDA-MB-231 breast cancer cell line, MCF-10A normal breast cell line, growth media (L15), and medium supplements (fetal bovine serum and penicillin/streptomycin) were all purchased from American Type Culture Collection (ATCC, Manassas, VA, USA). Also, uncoated antimony (n)-doped Si atomic force microscopy (AFM) tips (MPP-31100) were purchased from Bruker AFM Probes (Santa Barbara, CA USA).

3.2.2 Extraction and Synthesis of Gold Nanoparticles

Details of the procedures that were used to obtain plant extracts from *Nauclea latifolia* are provided in Ref. 27. Hence, we will only summarize the procedures for the extraction and synthesis of the AuNPs from the *Nauclea latifolia leaves.* Although extracts for AuNPs synthesis can be obtained from both fresh leaves and dry ones, fresh mature leaves of *Nauclea latifolia* were used in this study. These were collected from the Botanical Park at Sheda Science

and Technology Complex (SHESTCO), Gwagwalada, Abuja, Federal Capital Territory, Nigeria. Some of the leaves were sun dried for 2 days, ground into powder with a pestle and mortar, before storing the ground powder in a bottle and refrigerator.

In the case of the fresh leaves, they were washed with sterile distilled water and ground with a mortar and pestle. 1g of freshly ground leaves was placed in each of 7 beakers containing 20 ml of 0.5M Acetate buffer (pH 4.0, 5.5, 6.5) and 0.5M phosphate buffer solutions of pH ranges 7.5, 8.5 and 9.5, with the last flask containing distilled water, labelled as NLO (that is, without pH adjustment, though the pH was found to be 7.0). These were stirred at 500 rpm for 20 minutes on a magnetic stirrer. The leaf extracts were filtered through Whatmann filter paper No.1. The synthesis of AuNPs at pH 7.0 from *Nauclea latifolia* has been shown [27] to be promising for biomedical applications.

In the case of the dry leaves, 0.05g (0.25%) of the dried *Nauclea latifolia* leaf powder was soaked in 20 ml of the corresponding buffer solutions (at different pH) and stirred on a magnetic stirrer for 20 minutes. The solutions were then filtered accordingly to obtain the extract.

Synthesis of AuNPs was achieved by using the extracts from the leaves prepared as described above. 4 ml of each of the fresh *Nauclea latifolia* extracts were measured into corresponding test tubes. Subsequently, 1 ml of 2.5mM gold (III) chloride tri-hydrate was then added to each test tube at room temperature (28-30°C). The *Nauclea latifolia* leaf extract reacted with hydrogen tetra chloroaurate ($HAuCl_4$) within 30 seconds forming AuNPs. This was revealed by the visible color change that occurred as $HAuCl_4$ solution changed color from pale yellow to ruby red.

3.2.3 Ligand Conjugation of LHRH to Gold Nanoparticles

3.2.3.1 Thiolation of Gold Nanoparticles

The thiolation and conjugation was done using AuNPs that were formed at a pH of 7.0. The conjugation process involved the use of a self-assembled monolayer (SAM) method developed originally by Shiao-wen *et al.*, 2008 [52], with some modifications. Cyclohexane mercaptan, 99%, from Acros Organics was used. First, a 1 mM thiol solution was prepared by measuring 6µl of the cyclohexane thiol in a fume cupboard, into 50ml of 50% ethanol, and stirred at 500 rpm for 20 minutes to mix properly. In another 50ml beaker, 10 ml of 5mg/ml gold nanoparticles was added and placed on a magnetic stirrer that was set at 500 rpm. Then 2 ml of 1 mM thiol solution was then added and stirred for 30 minutes.

3.2.3.2 Conjugation with LHRH

A 1mg/ml solution of LHRH was freshly prepared in deionized water. Subsequently, 4ml of the already thiolated gold nanoparticles was then poured into a beaker, before adding 1 ml of the LHRH solution. This was then stirred on the magnetic stirrer for 30 minutes at a temperature of 4^{o}C. This resulted in the coupling of LHRH to the gold core (using a thiol linkage), either through an amino acid added at the C-terminus, or a D-amino acid placed in position 6 of the LHRH peptide sequence.

3.2.4.0 Prodigiosin Synthesis and Prodigiosin/AuNP Mixtures

3.2.4.1 Prodigiosin (PG) Synthesis

A method developed recently by Obayemi *et al.*, 2016 [53] for the synthesis and purification of prodigiosin (PG) was adopted for the synthesis and purification of the PG used in this work.

Hence, the synthesis and purification process will only be summarized in this paper. The extraction of PG was done from *Serratia marcescens* subsp. *marcescens* strain using the method described by Kamble *et al.* [54]. The extracted samples were then purified using size exclusion chromatography (using Sephadex G-50 superfine resin), prior to characterization with High Performance Liquid Chromatography (HPLC) using an HPLC system with a dual wavelength absorbance detector (Waters 2695 with 2487 Absorbance Detector, LabX, Midland, ON, Canada The PG content was determined from the HPLC analysis by comparing the peak areas (normalization), as well as the symmetrical increase of the peak areas, as a function of the retention time.

3.2.4.2 Mixture of Prodigiosin and Conjugated Gold Nanoparticles

PG was added to the gold nanoparticles-conjugate by means of physisorption, whereby the molecules were held in place by Van der Waals forces. 1 mg of prodigiosin was dissolved in 2 ml of methanol and added to the gold nanoparticles conjugate. The mixture was stirred at 500 rpm at a temperature of 4^{o}C (to prevent the denaturation of proteins) for 30 minutes.

3.2.5.0 Gold Nanoparticle Characterization

3.2.5.1 UV-Spectrophotometry Measurements

Following the synthesis and conjugation, an ultraviolet-visible spectrophotometer (UV-Vis) (CECIL 7500 Series, Buck Scientific Inc., East Norwalk, USA), with a range between 400 and 700 nm, was used to confirm the formation of gold nanoparticles. This was done using procedures described in detail in Ref. 27. The procedures were repeated at 20-minute intervals for total durations of 1 hour, 24 hours and 48 hours.

3.2.5.2 Transmission Electron Microscopy (TEM) and Electron Diffraction (ED)

The shapes and sizes of the nanoparticles produced by these reactions were characterized using transmission electron microscopy (CM100 Transmission Electron Microscope, Philips/FEI Corporation, Hillsboro, OR, USA), while the presence of gold was confirmed again using selected-area electron diffraction (SAED) patterns of the nanoparticles. Prior to TEM examination, drops of gold nanoparticle solutions were placed on copper grids. These were allowed to dry under ambient conditions (25^{o}C). They were then mounted on a CM100 Transmission Electron Microscope at the Princeton Institute of Science and Technology of Materials (PRISM) at Princeton University, New Jersey, USA. Subsequently, the nanoparticle sizes and shapes were further analyzed using ImageJ software package (NIH Image, Scion Image for Windows, National Institute of Health, Bethesda, Maryland, USA). In the case of SAED analysis, a selected-area aperture, with a diameter of 1 mm, was used. The resulting SAED patterns were then recorded and analyzed.

3.2.5.3 Dynamic Light Scattering (DLS)

A Malvern Instrument Zeta-sizer Nano Series (Malvern Instruments, Westborough, MA, USA) was used in the DLS measurements of the AuNPs as well as conjugated AuNPs/PG mixtures at room temperature (25^{o}C). The samples were first diluted 1:8 with distilled water. They were then filtered with a 0.22 micron filter and in each case 0.1 mL of the gold nanoparticles solution was added to the cuvette. The DLS instrument was run at a wavelength of 660 nm and the fixed scattering angle used was 90. Three runs per sample were performed for 2:00 minutes per run, giving a total of 6:00 minutes per sample.

3.2.5.4 Energy Dispersive X-ray Spectroscopy (EDS)

An Environmental Scanning Microscope (ESEM) (Model FEI Quanta 200F with Oxford-EDS system IE 250 X Max 80, Philips/FEI, Hillsboro, OR, USA) was used to obtain semi-quantitative estimates of the compositions of the AuNPs and LHRH-conjugated AuNPs/PG mixtures. Prior to EDS characterization, the AuNP solutions and the conjugated AuNP/PG mixtures were centrifuged at 12,000 rpm for 30 minutes to concentrate the nanoparticles. The nanoparticles were then placed on the SEM sample holder and air-dried before viewing them in the ESEM.

3.2.5.5 Adhesion Measurements

Prior to the adhesion measurements, a breast cancer cell line (MDA-MB-231cells) and a normal-breast cell line (MCF 10A cells) was cultured and prepared. About 20 µl of 5 x 10^4 cells/ml MDA-MB-231 cells was cultured in 60 x15 mm Falcon cell culture Petri dishes at 37°C. This was done under standard atmospheric pressure in L-15 medium supplemented with 100 I.U./mL penicillin/100 lg/mL streptomycin and 10% FBS.

In the case of the normal breast cells, 5 x 10^4 cells/ml of MCF10A breast cells was incubated at 37 ^{o}C in 5% CO_2 in DMEM/F12 medium (Invitrogen # 11330-032) supplemented with 5% horse serum (Invitrogen # 16050-122), 30 ng/ml murine Epidermal Growth Factor (Peprotech #315-09), 0.5 µg/ml hydrocortisone (Sigma, #H-0888), 100 ng/ml cholera toxin (Sigma #C8052-1MG), 10 µg/ml insulin (Sigma #I-882-100MG), 1% Penicillin-Streptomycin (Invitrogen #15070-063), and 0.2% amphotericin (Gemini Bioproducts, #400-104), respectively.

After 72 h of culturing, the cell confluence was about 70%. Both cell samples were then washed twice with PBS solution (1X PBS at 4°C) and fixed in 3.7% formaldehyde solution for 15 minutes. The fixed cells were then rinsed three times with PBS (1X PBS at 4^{o}C). This was followed by three rinses with distilled-deionized water (4^{o}C). This last rinse with water was used to remove possible salt deposits that may have resulted from the prior PBS rinses. Finally, the fixed cells were dried in a vacuum desiccator for two hours (at 25 - 30^{o}C).

Adhesion measurements were done using a Multimode Dimension DI Nanoscope IIIa Atomic Force Microscope (Bruker Instruments, Woodbury, NY, USA). The Atomic Force Microscope (AFM) tips were coated with the LHRH, AuNPs, prodigiosin drug (PG), LHRH-conjugated AuNPs and LHRH-conjugated AuNPs/PG mixture using a simple dip coating technique [47]. This was done under sterile conditions at a temperature of 22^{o}C, as reported by Oni *et al.* [47].

To ensure that the AFM tips were coated with LHRH or LHRH-AuNPs, the bare AFM tips and the nanoparticle coated AFM tips were imaged using environmental scanning electron microscopy (ESEM). The secondary electron images of the coated and bare AFM tips were obtained from a Phillips FEI Quanta 200 Field Emission Gun (FEG) Environmental-SEM (Philips Electronics N.V., Eindhoven, Netherlands). These images were used to confirm the presence of LHRH and nanoparticle coatings on the AFM tips, before and after the adhesion measurements. The different coated tips were brought into contact with the substrates (breast cancer cells and normal breast cells) during the AFM adhesion measurements.

As described in Section 2, the Atomic Force Microscope (AFM) measures the deflection of a cantilever spring with a sharp AFM tip (the tip radius is about 10-100 nm) as a function of displacement from a horizontal position, which is driven by a piezo-electric system. The

deflection of the cantilever is monitored using a laser-photodiode system. It relates the forces between the probe-tip and the substrate [55] to the displacement of the tip.

When the cantilever is far away from the surface of the sample, the AFM-tip is force free. Hence, there is no adhesive interaction between the tip and the substrate. However, as the tip approaches the surface, adhesion forces increase significantly. These attract the tip towards the substrate (See Figure 1b). At a distance of a few nanometers from the substrate (~ 20 nm), the secondary forces (Van der Waals forces and hydrogen bonds) acting on the surface become significant, causing the cantilever and the tip to jump into contact with the sample surface [56].

The piezo drive pushes the AFM-tip further on the surface until a point of repulsion is reached and the motion of the piezo is reversed. The cantilever deflects towards the surface due to adhesion force before the tip breaks contact with the surface. The sudden pull-off may cause free vibrations of the cantilever. The pull-off is described as the adhesion between the coated AFM tips and surface of the substrate [54-59].

The following adhesion measurements were made:

(i) Bare AFM tip to breast cancer/normal breast cells;

(ii) LHRH-coated AFM tip to breast cancer/normal breast cells;

(iii) PG drug coated AFM tip to breast cancer/normal breast cells;

(iv)AuNPs to breast cancer/normal breast cells;

(vi) AuNPs–LHRH to breast cancer/normal breast cells, and

(vii) AuNPs-LHRH/PG mixture to breast cancer/normal breast cells;

3.2.5.6 Confocal Fluorescence Microscopy of LHRH Receptors

Immuno-fluorescence staining of both breast cancer cells and normal breast cells were carried out using methods reported earlier by Meng *et al.*, 2010 [46]. Both triple negative breast cancer cells (MDA-MB-231 cells) and normal breast cancer cells (MCF-10A cells) were cultured on sterile glass cover slips (with inside cross sectional areas of 60 mm x15 mm) and Falcon cell culture Petri dishes in their respective growth media. After 48 h, the cells were fixed, stained and imaged, as reported by Meng *et al.*, 2010 [46].

3.3.0 Results and Discussion

3.3.1 Nanoparticle Synthesis, Conjugation and Characterization

Duration of 30 seconds was used to synthesize the AUNPs from the *Nauclea latifolia* leaf extract [27]. This was possible when gold aurochloride ($HAuCl_4$) reacted with the extract at a pH of about 7.0. The formation of AuNPs was revealed by the visible color change that occurred, as the $HAuCl_4$ solution changed from a pale yellow color to ruby red [27].

The production of gold nanoparticles has been correlated with the change in color of pale yellow plant extracts or bacterial cell suspensions to pink or purple [60,61]. This color change is as a result of the reduction of Au^{3+} to Au^0 [62]. Detailed results of the synthesis of AuNPs from *Nauclea latifolia* are reported by Dozie-Nwachukwu, *et al.* [27].

From the UV-Vis measurements, the peaks revealed that the AuNPs were synthesized within 30 seconds, with a plasmon resonance peak at 540 nm. The nanoparticles also remained stable with a peak at 540 nm, even after 48 hours. The peak remained stable although the absorbance increased with time. It was also observed that dried leaves of *Nauclea latifolia* resulted in a similar yield of AuNPs, compared to the yields under wet conditions. However, processing with

dried leaves required about 1/20th the weight of *Nauclea latifolia* that was used under wet conditions.

The UV results for both un-conjugated AuNPs and LHRH conjugated AuNPs showed evidence of the presence of AuNPs (Figure 3.2a). After conjugation, the UV-Vis spectra (Figure 3.2b) showed the presence of 2 peaks, one peak at 260 nm which confirms the presence of the peptide, LHRH [63] , and a second peak at 540nm which is the wavelength of AuNPs. The reaction schematics of conjugation of AuNPs to LHRH is represented below.

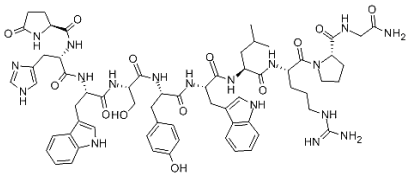

LHRH

+ AuNPs – SH ⟶ **LHRH-S-AuNPs** **(2)**

The TEM micrograph obtained for the AuNPs synthesized from *Nauclea latifolia* leaves, as well as the LHRH-conjugated AuNPs/PG mixtures, are presented in Figure 3.3. After conjugation with LHRH, the average size of the conjugated AuNPs was within the range of 51– 60 nm. Generally, the images of the AuNPs formed (Figure 3.3a) are combination of prismatic, octagonal, heptagonal and hexagonal shapes, with varying sizes.

Similar nanoparticle morphologies were also observed after conjugation and mixture with PG (Figure 3.3 b & c).These combination of shapes and sizes may be relevant for optimum surface plasmon resonance effect (SPRE) of AuNPs considering the incident angle and AuNPs-laser interaction. The TEM images and selected area electron diffraction (SAED) patterns also confirmed the formation and crystallization of nanoparticles. The SAED pattern presented in

Figure 3d represents the four-fringe pattern of gold nanoparticles, which corresponds to the face-centered cubic (fcc) crystal structure of gold [111, 200,220 311]. This confirms the formation of pure gold nanoparticles. The observed ring pattern is consistent with the reference to fcc gold, indicating that the biogenic nanoparticles seen in the TEM images are indeed crystalline gold. The Scherer ring pattern characteristic of face-centered cubic gold is clearly observed (figure 3.3 d), showing that the structures presented in the TEM images are nanocrystalline in nature.

Typical size distributions obtained from the image analyses of the TEM images are compared to those obtained from the DLS measurements in Figure 3.4. The hydrodynamic diameter measured with the DLS is presented in Figures 3.4 (c & d). The DLS measurements of the mean hydrodynamic diameters and the polydispersity indices of the AuNPs are represented in Figures 3.4(e) and 4(f). The hydrodynamic diameter of the AuNPs nanoparticles synthesized at a pH of 7.0 was 47.9 nm, while the polydispersity index (PDI) of the same nanoparticles was 0.23. The measured PDIs show that the representative samples of the biosynthesized AuNPs were relatively mono-dispersed. The measured hydrodynamic diameter describes the dimensions of a sphere that has the same diffusion coefficients within the same viscous environment. Furthermore, a comparison of the hydrodynamic diameters and the polydispersity index of the AuNPs synthesized (before and after conjugation) was studied. The Z average (which is the intensity weighted mean hydrodynamic size of the ensemble collection of particles measured by dynamic light scattering (DLS)), increased with the addition of the ligand, LHRH. The z-average also increased further when the anti-cancer drug, prodigiosin (PG), was added. This goes futher to confirm that conjugation actually took place.

In the case of AuNPs synthesized at a pH of 7.0, the z-averages before conjugation, after

conjugation with LHRH, and after the addition of prodigiosin, were 47.9 nm, 58.9 nm and 60.2 nm, respectively (Figure 3.4e). These are consistent with the findings of Takae *et al.* [64], who observed an increase in nanoparticle diameter (from 20 to 33.3 nm) after functionalization with 6,000 Mw PEG. Some other researchers also have reported that DLS measurements of the hydrodynamic diameters of AuNPs increase from 28.2 nm to 48.5 nm, with the addition of PEG coatings [65,66].

The results obtained from the DLS meaurements of the polydispersity index (PDI) showed that the PDI decreased with the addition of the ligands. This suggests that conjugation improves the dispersity of the particles. The AuNPs synthesized at a pH of 7.0 had a PDI of 0.23 before conjugation, a PDI of 0.29 after conjugation with with LHRH and a PDI of 0.08 after the addition of PG cancer drug (Figure 3.4f). In figure 3.4 (b and d), the size distributions of AuNPs were presented using results obtained from the TEM and DLS analyses. As discussed earlier, the TEM images correspond to electron transmission through the nanoparticles, while the DLS correspond to the hydrodynamic diameters.

The hydrodynamic diameters measured from the DLS were generally much greater than the effective diameters obtained from the TEM images. This is partly due to the adsorption of proteins and organic wastes onto the surfaces of the AuNPs, which is accounted for in the DLS measurements [67]. Such adsorption tends to promote the formation of nanoparticle clusters that increase the hydrodynamic radii. In the case of the TEM measurements, they only account for the electron transmission through the nanoparticle core. Thus, the high magnification TEM images required for the measurement of individual nanoparticle sizes may not necessarily reveal the statistical variations in the cluster sizes that are formed due to nanoparticle aggregation [67].

Typical EDS results obtained from the AuNPs synthesized at a pH of 7.0 are presented in Figure 3.5. The results show clear and predominant evidence of gold peaks at 540 nm, although peaks corresponding to some of the materials (used in the reactions) were also observed (Figure 3.5b). Note that the carbon and silicon peaks are attributed to the specimen mounting solution in the SEM grid [68]. The presence of gold peaks at 540 nm is consistent with the existence of AuNPs. The EDS analysis revealed the presence of gold (Au) and iron (Fe), which are usually attached to prodigiosin, as well as Cu and Si, which are most likely to be from the sample grid.

3.3.2 Adhesion Force Measurements

The SEM images of the bare AFM tip, AuNPs coated AFM tip, AuNPs-LHRH coated tips and LHRH-conjugated AuNPs/PG mixture coated tip are presented in Figure 3.6a – 3.6d, respectively. When coated with plain AuNPs, the attachment of the AuNPs was sparsely scattered on the tip, but the coating with AuNPs-LHRH conjugated AuNPs showed an even attachment as seen from the peeled off region in Fig. 3.6c. The SEM images of the coated tip clearly show the presence of AuNPs on the apex of the AFM tips [Figure 3.6(b-d)]. SEM images were used to ensure that the delamination of the coatings on the AFM tips did not occur during the pull-off/adhesion experiments. Figure 3.7 shows a typical AFM – force/distance curve measured by the AFM-cantilever versus tip sample distance. It indicates the AFM force-displacement behavior between AuNPs-LHRH coated AFM tips and MDA-MB- 231 breast cancer cells.

The measured adhesion force between the different constituents and breast cancer cells/normal breast cells are represented in Figure 3.8. The resulting pull-off/interaction forces between the bare AFM tip and the breast cancer cells (MDA-MB-231 cells) are slightly greater (the results

for breast cancer cells are actually over two-fold greater) than those between bare tips and normal breast cells. In the case of AuNPs coated AFM tips, the interaction between AuNP-coated AFM tips and breast cancer cells is more than two-fold greater than the interaction between AuNP-coated tips and normal breast cells (48.5 ± 2.5 nN compared to 18.6 ± 0.93 nN).

In the case of the adhesion forces between LHRH ligand and breast cancer cells or normal breast cells, the pull-off forces obtained were 105.6 ± 5.3 nN and 21.7 ± 1.8 nN, respectively. It is clear here that the interaction between LHRH coated AFM tip with breast cancer cells was greater than those of normal cells by a factor of about 5 (actually 4.8). This partly explains why LHRH specifically targets triple negative breast cancer cells [68-72].

In the case of therapeutics, the PG interaction to breast cancer cells or normal breast cells was measured. This result was important to understand the behavior of PG when used in a nanocluster of AuNPs-LHRH-PG. The adhesion forces between the PG drug and breast cancer cells or normal cells were relatively low, and within the same range (20.3 ±0.7nN and 13.5 ±1.6nN). Furthermore, the adhesion between LHRH-conjugated AuNPs and breast cancer cells or normal breast cells were measured to be 125.6 ± 6.3 nN and 35.3 ± 1.8 nN, respectively, which is about a three and a half-fold difference. These results clearly show that LHRH-conjugated AuNPs can be used for selective and specific targeting of triple negative breast cancer cells. Finally, the interaction between LHRH-conjugated AuNPs/PG mixtures to breast cancer cells was (118.4 ± 6 nN), which is almost 3-fold greater than for the interactions with normal breast cells (43.4 ± 2.7 nN).

The higher adhesion values obtained for the LHRH-conjugated AuNPs component to breast cancer cells are attributed to the over-expression of LHRH receptors on cancer cells compared to

normal cells (Figure 3.9). The increased adhesion between the LHRH-conjugated nanoparticles to breast cancer cells has been shown to be due to the increased incidence of LHRH-receptors on breast cancer cells [66, 68-72]. The results suggest that the over-expressed LHRH receptors, located on breast cancer cells, interact very strongly with LHRH peptides, respectively.

The current results suggest that force microscopy techniques incorporated with LHRH-conjugated AuNPs presented here may be used as a method for the fast screening of ligand-conjugated nanoparticles that can be used for the early detection of other forms of cancer and other diseased cells that over-express ligand receptors on their membrane surfaces. Such over-expression should increase the potential for the specific targeting and treatment of triple negative breast cancer.

3.4 Summary and Concluding Remarks

This paper presents the results of a study of adhesion of biosynthesized gold and gold/prodigiosin nanoparticles to triple negative breast cancer cells and normal breast cells. The AuNPs were synthesized from *Nauclea latifolia* leaf extracts, and the prodigoisin was purified from a local isolate of *Serratia marcencens*. We argue that such adhesion could increase the potential for specific targeting and cancer therapy. The adhesion results show that the adhesion force between LHRH-conjugated biosynthesized AuNPs and the breast cancer cell line MDA-MB-231 was greater (by a factor of five) than that of LHRH-conjugated AuNPs to normal breast cells. Similarly, in the case of the nanocluster of AuNPs-LHRH-PG mixture, the adhesion of the mixture to breast cancer cells is almost three-fold greater than that to normal breast cells. The increase in adhesion of the LHRH-conjugated gold nanoparticles is associated with the increased

incidence of LHRH receptors that are over-expressed on the surfaces of breast cancer cells. The increased incidence of LHRH receptors increased adhesive interactions by a factor of about five. It also increases the potential for use of AuNPs-LHRH-PG in the selective and specific targeting and treatment of breast cancer by localized cancer drug delivery, hyperthermia and laser surgery.

REFERENCES

1. Jennings, T., Strouse, G.: Past, present and future of gold nanoparticles. Adv Exp Med Biol. **620**, 34 – 47, (2007).

2. Holiday, R. Use of gold in medicine and surgery. Biomedical Scientist (The Official Gazette of the Institute of Biomedical science, UK), 962-63, (2008).

3. Dykman, L. A., Khlebtsov, N. G.: Gold Nanoparticles in Biology and Medicine: Recent Advances and Prospects. Acta Naturae. **3** (2), 34-55, (2011).

4. Chen, P.O., Mwakwari, S.C., Oyelere, A.K.: Gold nanoparticles: From nanomedicine to nanosensing. Nanotechnology, Science and Applications. **1**, 45–66, (2008).

5. Canizal, G., Ascencio, J.A., Gardea-Torresday, J., Jose-Yacaman, M. Multiple twinned gold nanorods grown by bio-reduction techniques. J.Nanoparticle Res. **3** 475-481, (2001).

6. Zhou, Y., Yu, S.H., Cui, X.P., Wang, C.Y., Chen, Z.Y.: Formation of Silver Nanowires by a Novel Solid- Liquid Phase Arc Discharge Method. Chem. Mater. **11,** 545-546, (1999).

7. Sun, Y., Mayers, B., Herricks, T., Xia, Y.: Polyol Synthesis of Uniform Silver Nanowires: A Plausible Growth Mechanism and the Supporting Evidence. Nano Lett. **3,** 955-960, (2003).

8. Mouxing, F., Qingbiao, L., Daohua, S., Yinghua, L., Ning, H., Xu, D., Huixuan, W., Jiale, H.: Rapid Preparation Process of Silver Nanoparticles by Bioreduction and Their Characterizations**.** Chin. *J. Chem. Eng.* **14**(1) 114- 117, (2006).

9. Selvakannan, P. R., Mandal, S., Pasricha, R., Adyanthaya, S. D., Sastry, M.: One-step synthesis of hydrophobized gold nanoparticles of controllable size by the reduction of aqueous chloroaurate ions by hexadecylaniline at the liquid-liquid interface. Chemical Communications, **13,** 1334–1335, (2002).

10. Okitsu, K., Yue, A., Tanabe, S., Matsumoto, H., Yobiko, Y.: Formation of colloidal gold nanoparticles in an ultrasonic field: control of rate of gold (III) reduction and size of formed gold particles. Langmuir. **17**(25), 7717–7720, (2001).

11. Singh, A., Jain, D., Upadhyay, M. K., Khandelwal, N., Verma, H. N.: Green synthesis of silver nanoparticles using *Argemone mexicana* leaf extract and evaluation of their antimicrobial activities. Digest Journal of Nanomaterials and Biostructures. **5** (2), 483-489 (2010).

12. Leela, A., Vivekanandan, M.: Tapping the unexploited plant resources for the synthesis of silver nanoparticles. African Journal of Biotechnology **7** (17), 3162-3165, (2008).

13. Balaprasad, A., Biosynthesis of Gold Nanoparticles (Green-Gold) Using Leaf Extract of Terminalia Catappa. E-Journal of Chemistry. **7**(4) 1334-1339, (2010)

14. Gericke, M., Pinches, A.: Microbial Production of Gold Nanoparticles. Gold bulletin. **39**(1) 22-28, (2006).

15. Sanghi, R., Verma, P., Puri, S.: Enzymatic Formation of Gold Nanoparticles Using *Phanerochaete Chrysosporium*. Advances in Chemical Engineering and Science. **1** (3) 154-162, (2011).

16. Sun, Y., Xia,Y.: Shape-controlled synthesis of gold and silver nanoparticles. Science. **298** (5601), 2176–2179, (2002).

17. Nair, B., Pradeep, T.: Coalescence of Nanoclusters and Formation of Submicron Crystallites Assisted by Lactobacillus Strains. Crystal Growth and Design, **2** 293, (2002).

18. Chatterjee, D.K., Diagardjane, P., Krishnan, S.: Nanoparticle-mediated hyperthermia in cancer therapy. Ther Deliv. **2**(8), 1001-14, (2011).

19. Mafune, F., Kohno, J., Takeda, Y.: Full Physical Preparation of Size-Selected Gold Nanoparticles in Solution: Laser Ablation and Laser-Induced Size Control. J. Phys. Chem. B. **106** (31), 7575–7577, (2002).

20. Cho, K., Wang, X., S. Nie, Z. (Georgia) Chen, Dong M. Shin, Therapeutic Nanoparticles for Drug Delivery in Cancer. Clin Cancer Res. **14**(5) 2008.

21. Mukherjee, P., Ahmad, A., Mandal, D., Senapati, S., Sainkar, S.R., Khan, M.I., Parischa, R., Ajayakumar, P.V., Alam, M., Kumar, R., Sastry, M.: Fungus mediated synthesis of silver nanoparticles and their immobilization in the mycelial matrix: A novel biological approach to nanoparticle synthesis. Nano Lett. **1**, 515-519, (2001).

22. Ahmad, A., Senapati, S., Khan, M.I., Kumar, R., Sastry, M.: Extracellular Biosynthesis of Monodisperse Fold Nanoparticles by a Novel Extremophilic Actinomycete Thermonospora sp. Langmuir. 19, 3550-3553, (2003).

23. Stephen, J.R., Maenaughton, S.J.: Developments in terrestrial bacterial remediation of metals. Curr Opin Biotechnol. **10**, 230-235 (1999).

24. Sastry, M., Ahmad, A., Khan, M.I., Kumar, R.: Biosynthesis of metal nanoparticles using fungi and actinomycete. Curr Sci. **85**, 162–170, (2003).

25. Huang, J., Li, Q., Sun, D., Lu, Y., Su, Y., Yang, X., Wang, H., Wang, Y., Shao, W., He, N., Hong, J., Chen, C.: Biosynthesis of silver and gold nanoparticles by novel sundried *Cinnamomum canphora* leaf, Nanotechnology. Nanotechnology, **18**(10) 105104-105115, (2007).

26. Kasthuri, J., Kathiravan, K., Rajendiran, N., Phyllanthin-assisted biosynthesis of silver and gold nanoparticles: a novel biological approach. J Nanopart Res. **11**(5) 1075-1085, (2009).

27. Dozie-Nwachukwu, S.O., Etuk-Udo, G., Obayemi, J.D., Anuku, N., Odusanya, O. S., Malatesta, K., Chi, C., Soboyejo, W.O.: Biosynthesis of Gold Nanoparticles from Nauclea latifolia Leaves; *Advanced Materials Research* 1132, 36-50, 2016.

28. Cho, K., Wang, X., S. Nie, Z. (Georgia) Chen, Dong M. Shin, Therapeutic Nanoparticles for Drug Delivery in Cancer. Clin Cancer Res. **14**(5) 2008.

29. Pellegrino, T., Kudera, S., Liedl, T., Muñoz Javier, A., Manna L., Parak, W. J.: On the Development of Colloidal Nanoparticles towards Multifunctional Structures and their Possible Use for Biological Applications. Small. **1,** 48-63 (2005).

30. Shankar, S.S., Ahmad, A. Pasrichaa, R., Sastry, M.: Bioreduction of chloroaurate ions by geranium leaves and its endophytic fungus yields gold nanoparticles of different shapes. J Mater Chem. **13,** 1822–1826, (2003).

31. Ankamwar, B., Chaudhary, M., Sastry, M.: Gold nanotriangles biologically synthesized using tamarind leaf extract and potential application in vapor sensing. Synth React Inorg Metal-Org Nano- Metal Chem. **35,** 19–26 (2005).

32. Huang, J., Li, Q., Sun, D., Lu, Y., Su, Y., Yang, X.: Biosynthesis of silver and gold nanoparticles by novel sundried *Cinnamomum camphora* leaf. Nanotechnology. **18** 105104–105114, (2007).

33. Shankar, S.S., Rai, A., Ahmad, A., Sastry, M.: Controlling the optical properties of lemongrass extract synthesized gold nanotriangles and potential application in infrared-absorbing optical coatings. Chem Mater. **17,** 566–572, (2005).

34. Shankar, S.S., Ahmad, A. Pasrichaa, R., Sastry, M.: Bioreduction of chloroaurate ions by geranium leaves and its endophytic fungus yields gold nanoparticles of different shapes. J Mater Chem. **13,** 1822–1826, (2003).

35. Ankamwar, B., Damle, C., Ahmad, A., Sastry M.: Biosynthesis of gold and silver nanoparticles using *Emblica officinalis* fruit extract, their phase transfer and transmetallation in an organic solution. J Nanosci Nanotechnol. **5,** 1665–1671, (2005).

36. Shankar, S.S., Rai, A., Ahmad, A., Sastry, M.: Rapid synthesis of Au, Ag and bimetallic Au core–Ag shell nanoparticles using neem (*Azadirachta indica*) leaf broth. J Colloid Interf Sci 275, 496–502, (2004).

37. Chandran, S.P., Chaudhary, M., Pasricha, R. Ahmad, A. Sastry, M.: Synthesis of gold nanotriangles and silver nanoparticles using *Aloe vera* plant extract. Biotechnol Prog. **22,** 577–583, (2006).

38. Umadevi, M., Sampath Kumar, K.P., Bhowmik, D., Duraive, S.: Traditionally Used Anticancer Herbs in India. Journal of Medicinal Plants Studies 1(3) 56-74, (2013).

39. Paul, J., Gnanam, R.M., Jayadeepa, R., Arul, L.: Anti-cancer activity on Graviola, an exciting medicinal plant extract vs various cancer cell lines and a detailed computational study on its potent anti-cancerous leads. Curr Top Med Chem **13**(14) 1666-1673, (2013).

40. Akpanabiatu, M.I., Umoh, I.B., Eyong, E.U., Udoh, F. V.: Influence of *Nauclea latifolia* Leaf Extracts on Some Hepatic Enzymes of Rats fed on Coconut oil and non-Coconut oil meals. Pharmaceutical Biology. **43**(2) , 153–157, (2005)

41. Brandenburg, K.S., Shakeri-Zadeh, A., Mansoori, G.A.: Folate-conjugated gold nanoparticlesfor cancer nanotechnology applications. Nanotech **3,** 404 – 407, (2011).

42. Gao, T., Hong, H., Sun, J.: Applications of gold nanoparticles in cancer nanotechnology. Nanotechnology, Science and Applications **1,** 17–32, (2008).

43. Chatterjee, D.K., Diagaradjane, P., Krishnan, S.: Nanoparticle-mediated hyperthermia in cancer therapy. Therapeutic delivery, 2(8):1001-1014, (2011).

44. Jain, S., Hirst, D.G., O'Sullivan, J.M. Gold nanoparticles as novel agents for cancer therapy. The British Journal of Radiology, 85(1010):101-113 (2012).

45. Hampp, E., Botah, R., Odusanya, S. O., Anuku, N., Malatesta, K., Soboyejo, W.O.: Biosynthesis and Adhesion of Gold Nanoparticles for Breast Cancer Detection and Treatment. Journal of Materials Research; 27 (22), 2891, (2012).

46. Meng, J., Paetzell, E., Bogorad, A., Soboyejo, W.O.: Adhesion between peptides/antibodies and breast cancer cells, J. Appl. Phys. 107, 114301,(2010).

47. Oni, Y., Hao, K., Dozie-Nwachukwu, S., Obayemi, J.D., Odusanya, O. S., Anuku, N., Soboyejo, W. O.: Gold nanoparticles for cancer detection and treatment: The role of adhesion. Journal of Applied Physics J. Appl. Phys. 115, 084305 (2014).

48. Gates, R.S., Osborn, W.A, Pratt, J.R.: Experimental determination of mode correction factors for thermal method spring constant calibration of AFM cantilevers using laser Doppler vibrometry. Nanotechnology, 24(25):255706, (2013).

49. Dupres,V., Menozzi, F.D., Locht, C., Clare, B.H., Abbott, N.L., Cuenot, S., Bompard, C., Raze, D., Dufrene, Y.F.: Nanoscale mapping and functional analysis of individual adhesins on living bacteria. Nat. Methods, 2, 515–520, (2005).

50. Wojcikiewicz, E.P., Zhang, X., Moy, V.: Force and Compliance Measurements on Living Cells Using Atomic Force Microscopy (AFM). Biol. Proced. Online 6, 1–9 (2004).

51. Li, F., Redick, S.D., Erickson, H. P., Moy, V. T.: Force Measurements of the α5β1 Integrin–Fibronectin Interaction. Biophys. J. 84, 1252–1262 (2003).

52. Shiao-Wen, T., Jiunn-Woei, T.L., Fu-Yin, H., Yi-Yun, C., Mei-Jhih, L., Ming-His Y.: Surface-Modified Gold Nanoparticles with Folic Acid as Optical Probes for Cellular Imaging. Sensors, 8, 6660-6673, (2008).

53. Obayemi, J.D., Danyuo, Y., Dozie-Nwachukwu, S., Odusanya, O.S., Anuku, N., Malatesta, K., Yu, W., Uhrich, K.E., Soboyejo, W.O.: PLGA-based microparticles loaded with bacterial-synthesized prodigiosin for anticancer drug release: Effects of particle size on drug release kinetics and cell viability. *Materials Science and Engineering C ;* 66, 51–65, (2016).

54. Kamble, K.D, Hiwarale, V.D., "Prodigiosin production from Serratia marcescens strains obtained from farm soil" International Journal of Environmental Sciences, 3 (1), 631-638, (2012).

55. Butt, H., Cappella, B., Kappl, M.: Force measurements with the atomic force microscope: Technique, interpretation and applications. Surface Science Reports. 59 1–152, (2005).

56. Santner, E., Stegemann, B.: Adhesion measurements by AFM – a gateway to the basics of friction Accessed from: www.academia.edu/7351106/Adhesion_measurements_by_AFM_a_gateway_to_the_basics_of_friction on 30th March, 2016.

57. Bhushan, B. (Ed.), Handbook of Micro/Nanotribology. 2nd ed. CRC press, Boca Raton (1999).

58. Burnham, N.A., Colton, R.J, Pollock, H.M. Interpretation of force curves in force microscopy. Nanotechnology, 4: 64-80 (1993).

59. Cappella, B., Dietler, G. Force-distance curves by atomic force microscopy. Surf. Sci. Rep., 34(1-3): 1-104 (1999).

60. Boham, A.B., Kocipai, A.A.: Flavonoids and condensed tannins from leaves of Hawaiian Vaccinium vaticulation and V. calycinium. Pacific Science. 48, 458 – 463, (1994).

61. Madhavi, R.B., Dighe, V.V.: Synthesis of Gold Nano particles using Putranjiva roxburghii Wall. Leaves Extract. International Journal of drug discovery and herbal research (IJDDHR). 2(1), 275-278, (2012).

62. Kundu , A., Layek, R.K., Kujla, A., Nandi A.K. : Highly fluorescent graphene oxide-poly (vinyl alcohol) hybrid: an effective material for specific Au^{3+} ion sensors. ACS Appl Mater Interface. **4**(10) 5576-82, (2012).

63. Rogošić, M., Mencer, H.J., Gomzi, Z.: Polydispersity index and molecular weight distributions of polymers. European Polymer Journal. 32, (11), 1337–1344 (1996).

64. Takae, S., Akiyama,Y., Otsuka, H., Nakamura, T., Nagasaki, Y., Kataoka, K. : Ligand density effect on biorecognition by PEGylated gold nanoparticles: regulated interaction of RCA120 lectin with lactose installed to the distal end of tethered PEG N strands on gold surface. Biomacromolecules 6(2) 818–824 (2005).

65. Hall, J.B., Dobrovolskaia, M.A., Patri A.K., McNeil, S.E.: Characterization of nanoparticles for therapeutics. Nanomedicine. 2(6) 789–803 (2007)

66. Arnida, A., Janát-Amsbury, M.M., Ray, A., Peterson, C.M., GhandehariH.: Geometry and surface characteristics of gold nanoparticles influence their biodistribution and uptake by macrophages. Eur J Pharm Biopharm: 77, 417–423 (2011).

67. Lim, J., Yeap, S.P., Che, H.X., S. C. Low; Characterization of magnetic nanoparticle by dynamic light scattering. Nanoscale Research Letters 2013 8:381.

68. Obayemi, J. D., Dozie-Nwachukwu, S., Danyuo,Y., Odusanya, O.S., Anuku, N., K. Malatesta, K., Soboyejo, W.O.: 'Biosynthesis and the Conjugation of Magnetite Nanoparticles with Luteinizing Hormone Releasing Hormone (LHRH)' : Journal of Materials Science and Engineering C, 46, 482–496, (2015).

69. Zhou, J., Leuschner, C., Kumar, C., Hormes J.F., Soboyejo, W.O.: Sub-cellular accumulation of magnetic nanoparticles in breast tumors and metastases. Biomaterials; 27(9):2001–2008, (2006).

70. Zhou, J., Leuschner, C., Kumar, C., Hormes J., Soboyejo, W.O.: A TEM Study of Functionalized Nanoparticles Targeting Breast Cancer Cells in Mice, Materials Science and Engineering C, 26, 1451-1455, (2006).

71. Leuschner, C., Kumar, C.S.S.R., Hansel, W., Zhou, J., Soboyejo, W.O., Hormes, J.: LHRH-Conjugated Magnetic Iron Oxide Nanoparticles for Detection of Breast Cancer Metasteses. Breast Cancer Res. Treat. Springer 2006 DOI 10.1007/s10549-006-9199-7. 99 163–176, (2006).

72. Meng J., Fana, J., Galiana, G., Branca, R.T , Clasen, P.L., Ma,S., Zhou, J., Leuschner, C., Kumar, C.S.S.R., Hormes, J., Otiti, T., Beye, A.C., Harmer, M.P.,

Kiely, C.J., Warren, W., Haataja, M.P. Soboyejo,W.O.:"LHRH-Functionalized Superparamagnetic Iron Oxide Nanoparticles for Breast Cancer Targeting and Contrast Enhancement in MRI" Materials Science and Engineering C 29, 1467–1479, (2009).

(a)

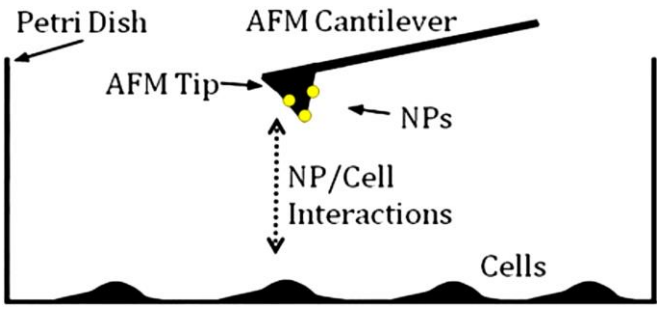

Fig. 3.1a: Ligand/receptor interactions. In the experimental setup, ligands on the dip-coated AFM tip interact with surface receptors on breast cancer cells (MDA-MB-231)/normal breast cells (MCF10A) seeded on a Petri dish ([Adapted from Ref. [45]).

(b)

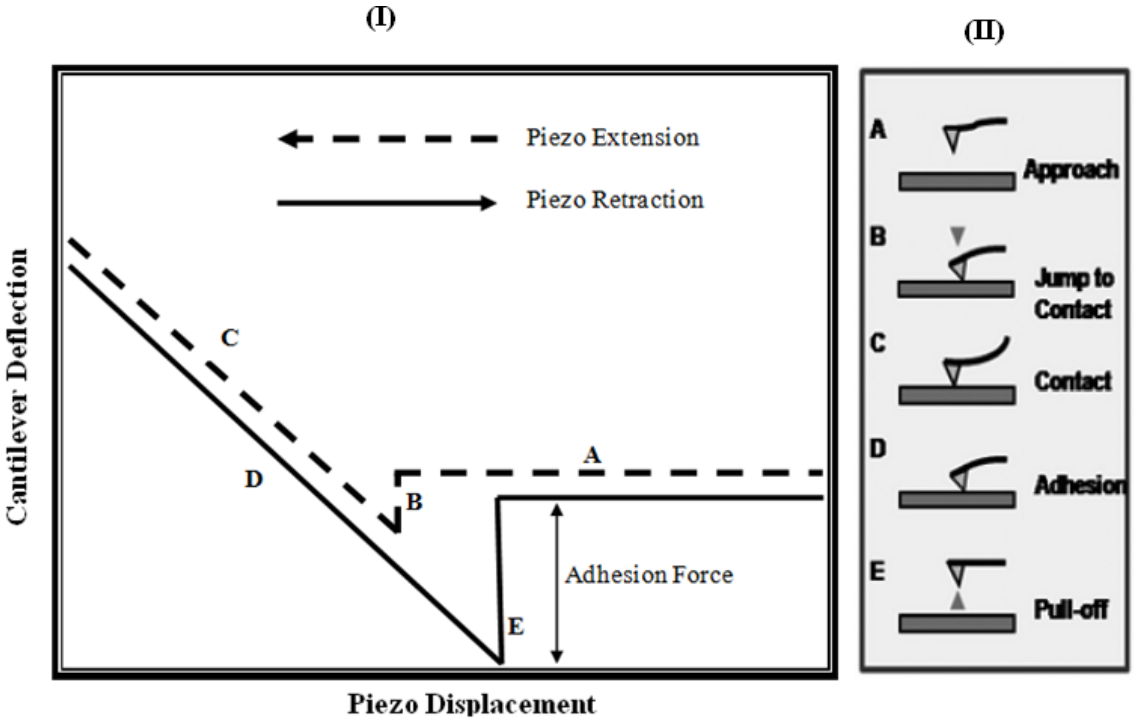

Fig. 3.1b: Schematic of typical force–displacement plot with corresponding stages of force displacement behavior. In one approach-retract cycle, the AFM tip approaches the surface of the sample (A), jumps to contact with the surface when significant van der Waals forces are felt (B), and undergoes elastic bending and is retracted (C, D). Due to adhesive interactions, the tip does not detach from the substrate until a force sufficient to pull the tip off of the surface is achieved (E). (Adapted from Ref. [43,45]).

(a)

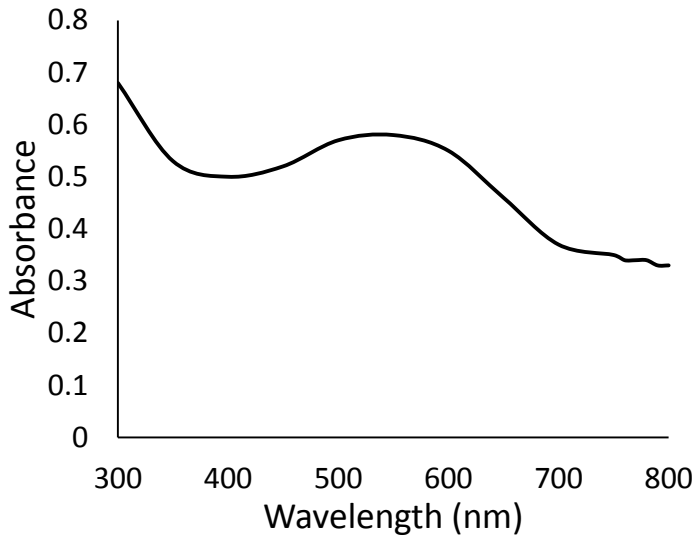

(b)

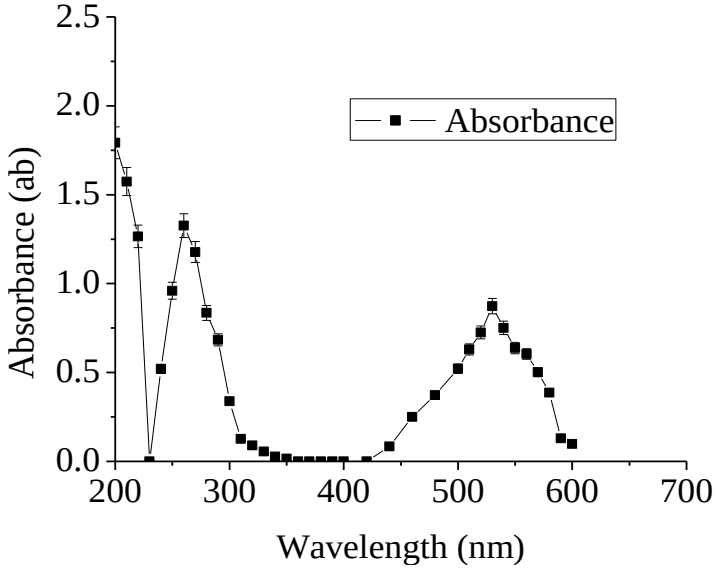

Fig.3. 2 (a) UV/Vis spectra obtained for AuNPs produced from *Nauclea latifolia* leaves at a pH of 7.0; (b) UV/Vis spectra obtained for LHRH-conjugated AuNPs Synthesized in (a) above.

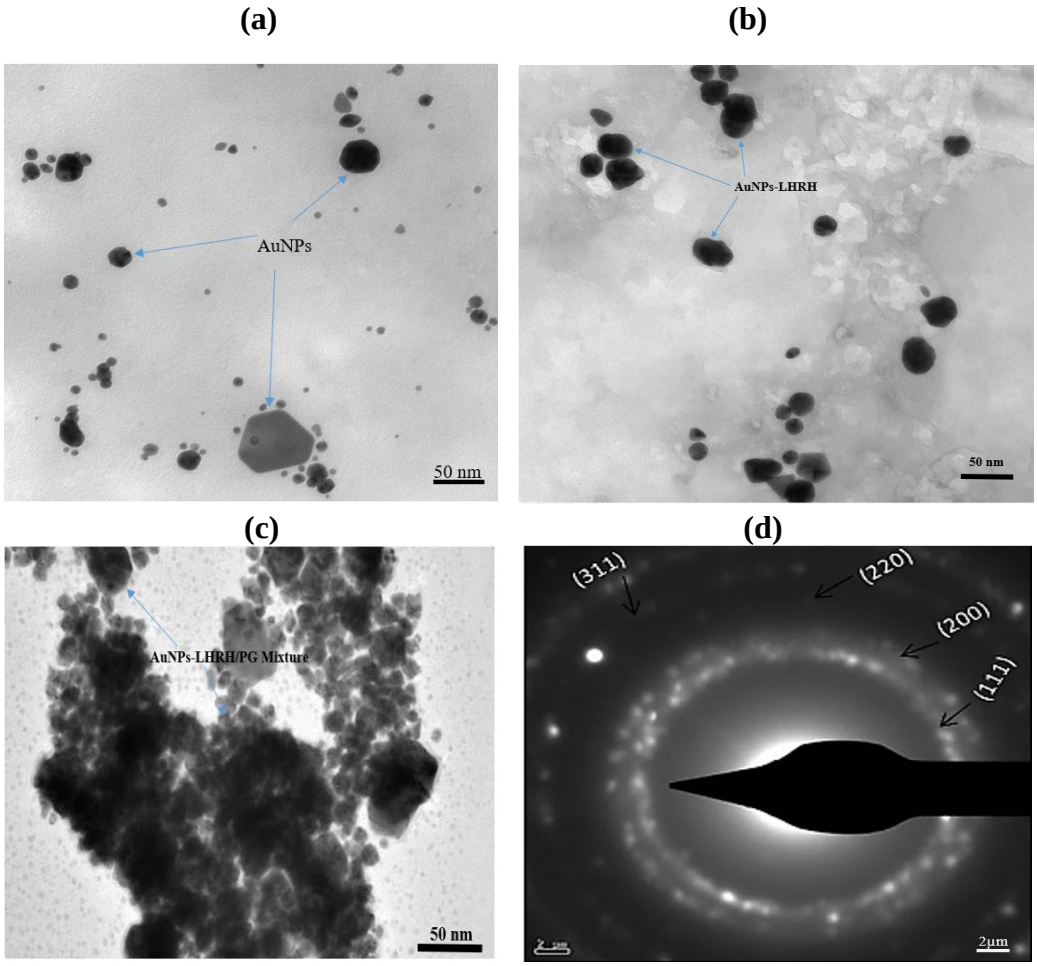

Fig. 3.3 TEM images of (a) AuNPs synthesized from *Nauclea latifolia* leaves at a pH of 7.0; (b) LHRH-conjugated AuNPs (c) LHRH-conjugated AuNPS with PG mixtures (d) The Scherer ring patterns indicating the fcc gold which is nanocrystalline in nature.

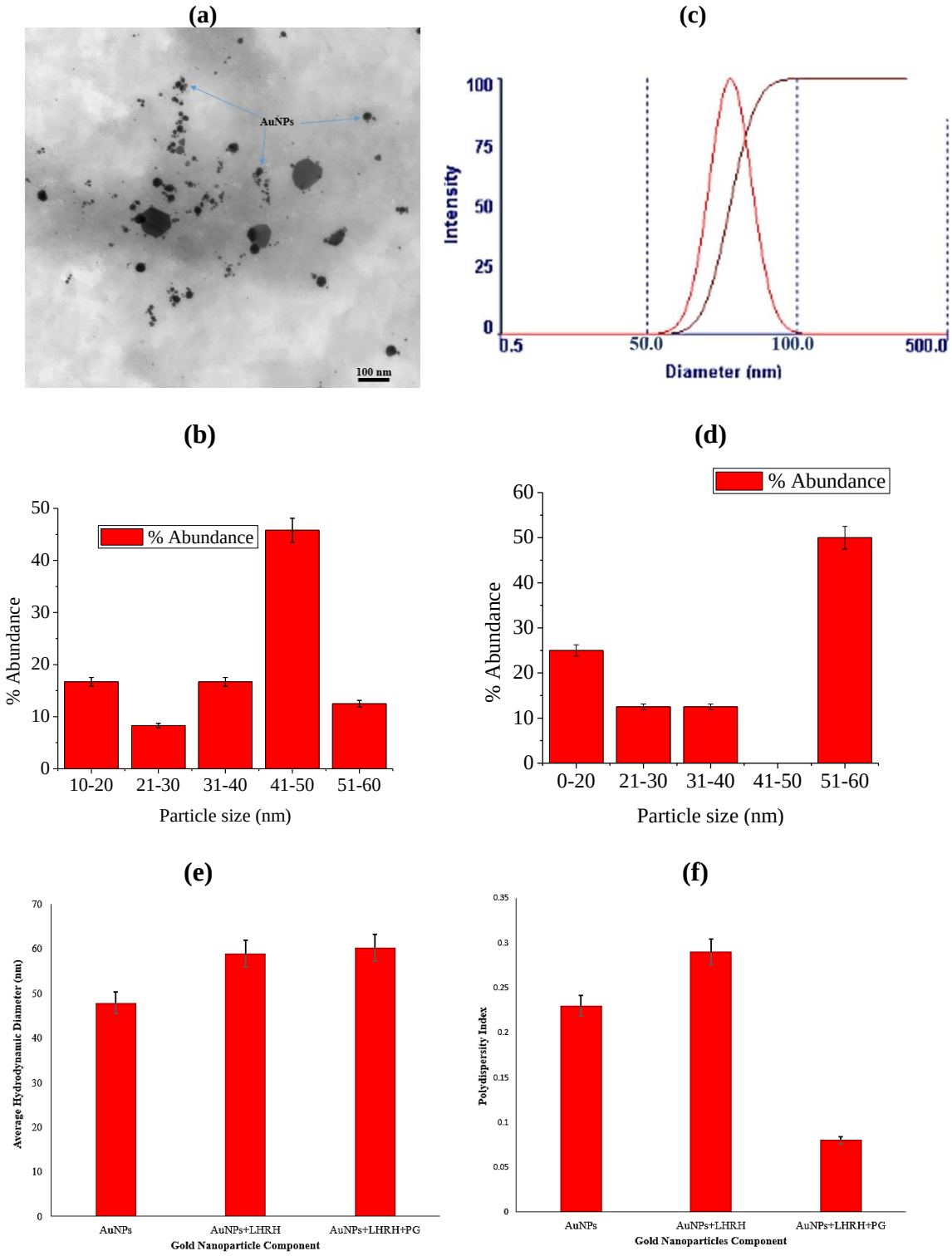

Fig. 3.4: (a) and (b) Typical TEM AuNPs size distribution (c) and (d) Typical DLS hydrodynamic diameter of size distribution of AuNPs synthesized from *Nauclea latifolia* leaves. (e) and (f) show the average distribution and polydispersity index of AuNPs, AuNPs-LHRH and AuNPs-LHRH-PG, respectively.

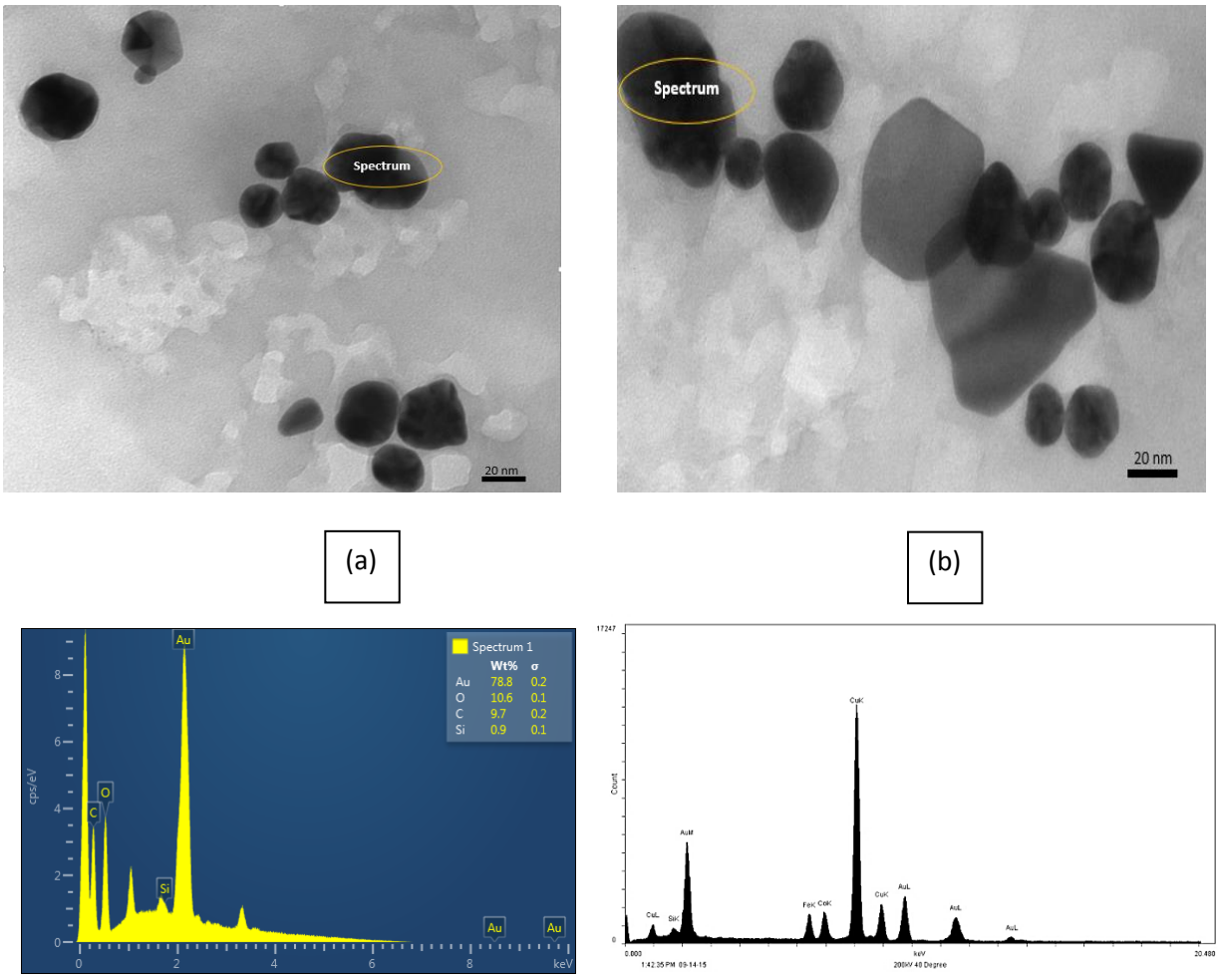

Fig. 3.5: EDX showing elemental composition of (a) AuNPs synthesized from *Nauclea latifolia* at a pH 7.0; (b) LHRH-conjugated AuNPs/PG mixture.

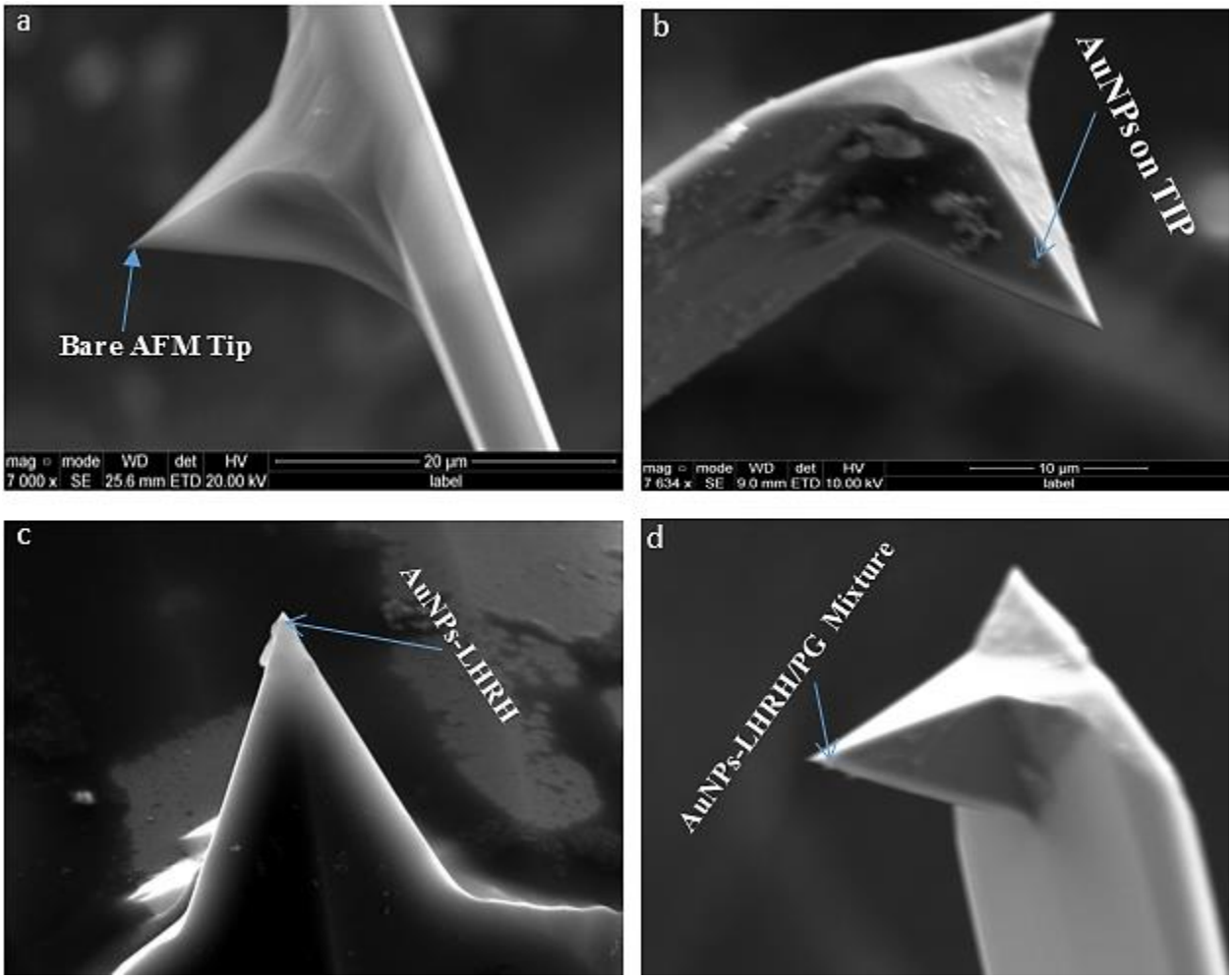

Fig. 3.6. Scanning Electron Microscopy image of AFM tips: (a) Bare tip (b) AuNPs coated AFM tip (c) LHRH-conjugated AuNPs coated AFM tip (d) AuNPs-LHRH/PG drug coated AFM tip.

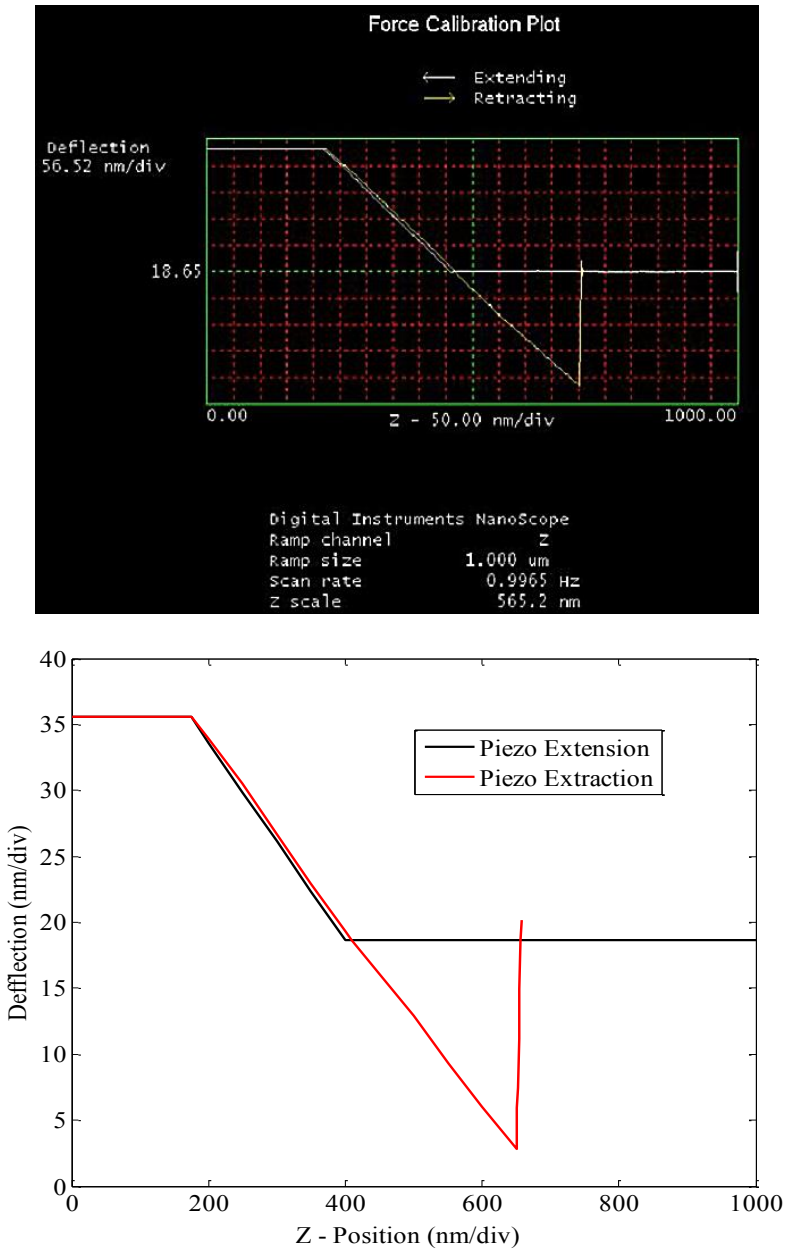

Fig. 3.7: Typical AFM force-displacement behavior between AuNPs-LHRH coated AFM tips to MDA-MB 231 breast cancer cells.

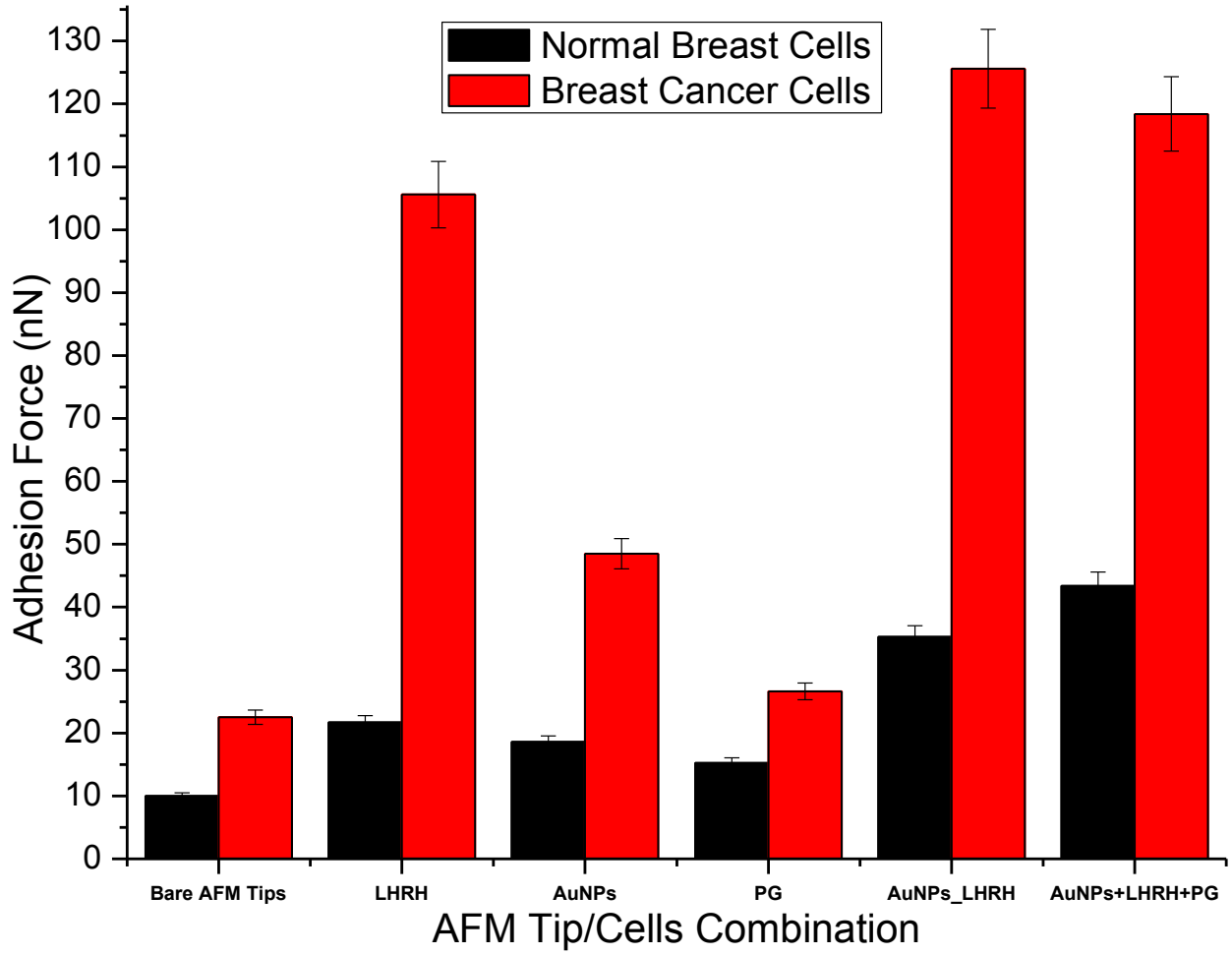

Fig.3. 8: Summary of adhesion force measurements between uncoated/bare AFM tip as well as different nanoparticles-coated AFM tips and breast cancer (MDA-MB-231) cells/normal breast (MCF 10 A) cells.

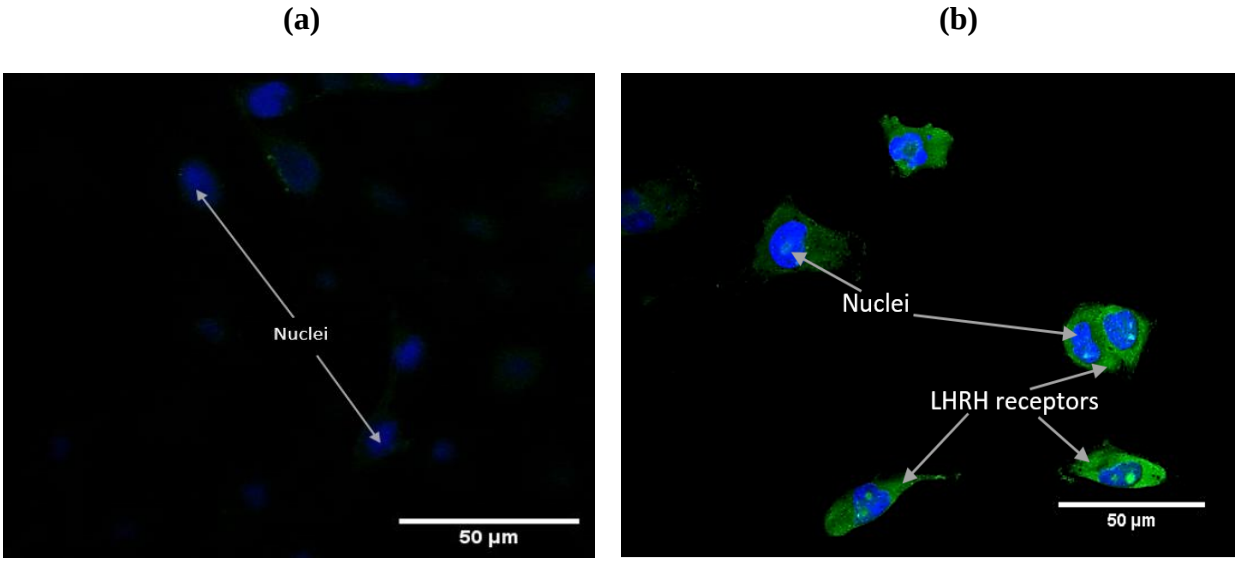

Fig. 3.9: Fluorescence confocal images of LHRH receptor distribution on (a) normal breast cells and (b) breast cancer cells. The images show the over-expression of LHRH receptors and nuclei designated by arrows.

Chapter 4

4.0 Biosynthesis of Gold Nanoparticles and Gold/Prodigiosin Nanoparticles with *Serratia marcescens* bacteria.

4.1 Introduction:

Since nanoparticles have large surface to volume ratios, their surface-related characteristics and surface properties are usually affected by slight changes in their size, shape and surrounding media [1]. Consequently, gold nanoparticles are very chemically reactive compared to bulk gold, which is known to be inert. Gold nanoparticles also have the potential for applications in: drug delivery; gene transfer; bio-probes in cells and tissue analysis; visualization of micro- and nano-objects, and also for the observation of biological processes at the nano-scale [2] and micro-scale [3].

In most cases, gold nanoparticles are synthesized using chemical methods [4-6] or physical methods [7]. However, these often require expensive equipment and chemicals and produce toxic by-products. There is, therefore, a need for alternative, less expensive methods, for the synthesis of gold nanoparticles. One of the alternatives is to use biological organisms, such as bacteria, [8] fungi [9] and plants, [10, 11] in biochemical processes that result in the formation of gold nanoparticles with different shapes and sizes that are relevant to optoelectronic devices, [12] nano- medicine [13] and catalysis. [14-16]

Microorganisms, such as bacteria [17- 19] and fungi, [20] have been used to synthesize gold nanoparticles in recent years [21- 24]. An earlier study by Beveridge and Murray, [25] found that *Bacillus subtilis* was able to reduce Au^{3+} ions to gold nanoparticles with a size range of 5-25 nm. The nanoparticles were produced inside the cell wall. Konishi *et al*. [23] also found that *Shewanella algae* were able to reduce Au^{3+} ions to form 10-20 nm gold nanoparticles. These were formed extracellularly with the assistance of hydrogen gas. Similarly, fungi (*Verticillium* sp.) [9], *Fusarium oxysporum* [26], Actinomycete (*Thermomonospora* sp. [17] and *Rhodococcus* sp.) [27] have been used to synthesize gold nanoparticles, intra- or extra-cellularly.

The AuNPs can also be used as contrast agents in optical coherence tomography as a result of the variations in their sizes and shapes, which allow for the precise tuning of their resonance wavelength [28]. Over the years, gold nanoparticles have also been used for both imaging and therapeutic purposes in several cancer models, both *in vitro* and *in vivo* [29- 31]. Mukherjee *et al.,* [32] have also reported the inhibition of angiogenesis by gold nanoparticles, through the direct binding of the particles to heparin-binding growth factors (vascular permeability factor/VEGF and FGF specifically), a property that is very useful in halting tumor proliferation.

Further, Hainfeld *et al.,* [33] have shown that gold nanoparticles can be used to enhance localized radiotherapy in order to prolong 1-year survival rates of mice bearing EMT6 mammary carcinomas (86% survival with gold nanoparticles versus 20% survival with X-rays alone). Nanoparticles have also been localized within cancerous cells through active targeting, in which nanoparticles are conjugated with small tumor-specific recognition molecules, like folic acid, [34] thiamine [35] and antibodies or lectins [36]. An antibody effectively used in conjugation is anti-HER2, [37, 29, 28] although it is possible to attach a wide variety of antibodies raised against tumor-specific markers.

In the field of nano-electronics, gold nanoparticles have been found to be very useful. Fabien *et al.,* [38] developed a transistor that can mimic the main functionalities of a synapse. This organic transistor is based on pentacene and gold nanoparticles and is known as a NOMFET (Nanoparticle Organic Memory Field-Effect Transistor). Gold nanostructures can also be incorporated into macro-porous scaffolds to increase the matrix conductivity and enhance the electrical signal transfer between cardiac cells [39]. Researchers are now trying to apply gold nanoparticles within the electronics industry for use in applications that range from data storage and touch screens, to printed text and conductive films [40].

The interactions between gold nanoparticles and biological cells have been studied recently using Atomic Force Microscopy [41- 43]. Hampp *et al.* [44] compared the adhesion forces between breast cancer cells and chemically-synthesized or bio-synthesized gold nanoparticles. They reported that the average adhesion force for the biologically synthesized AuNPs to breast cancer cells, with an average diameter of about 30 nm, is approximately 20 nN. These values were

found to be over three times larger than the average adhesion forces between breast cancer cells and chemically synthesized gold particles. Hampp *et al.* [44] attributed these differences (in adhesion values between the chemically synthesized and bio-synthesized AuNPs) to the presence of capping proteins on the biosynthesized AuNPs. They concluded that bio-synthesized nanoparticles are superior to chemically-synthesized nanoparticles, based on the greater adhesion forces to breast cancer cells than to normal cells.

In this paper, we explore the bio-synthesis of gold nanoparticles from *Serratia marcescens* bacteria. *Serratia marcescens* is a gram negative, motile bacillus of the family Enterobacteriaceae [45]. Its common habitat is in damp areas, such as bath rooms, soil around dirty gutters, and spoiled food, especially carbohydrates. It is also associated with urinary tract infections. Equally, we explored the synthesis of gold nanoparticles using prodigiosin.

Prodigiosin (PG) is a tripyrrole red pigment that is produced as a secondary metabolite by *Serratia marcescens* (SM) and some other bacteria. Studies have shown that, prodigiosin has anticancer, antiproliferative, cytotoxic and antibacterial properties. It can also be used for immunosuppressive activities [46-51]. It has been reported that prodigiosin induces apoptosis in hematopoietic cancer cells as well as in cells derived from other human cancers (e.g. gastric and colon cancers), with no marked toxicity in nonmalignant cell lines [47, 49, 50]. Moreover, Francisco and coworkers (2003) [51] reported the effect and mechanisms of action of PG against different human neuroblastoma cell lines (i.e. SH-SY5Y, LAN-1, IMR-32 (N-type) and SK-N-AS (S-type).

The bio-synthesized gold nanoparticles were characterized using UV-Visible spectroscopy (UV-Vis), Scanning Electron Microscopy (SEM), Energy dispersive X-ray Spectroscopy (EDX) and Transmission Electron Microscopy (TEM).

4.2.0. Experimental Procedures

4.2.1. Materials

The gold (III) chloride trihydrate, ACS reagent, ≥49.0% Au basis, was purchased from Sigma-Aldrich, St. Louis, USA, Lot number 127K1374. All the reagents used were Analar grade. The

basic equipment includes: Mortar and pestle, A Sanyo MSE Harrier 18/80 refrigerated Centrifuge (Sanyo, London, UK), an O'Haus PA64 analytical plus weighing balance (Switzerland), a water bath (Fisher Scientific, model 2321, Marletta Ohio,USA), a Transmission Electron Microscope (TEM)(CM100 Transmission Electron Microscope, Philips/FEI Corporation, Hillsboro, OR, USA) a UV-visible Spectrophotometer (CECIL 7500 Series, Buck Scientific Inc., East Norwalk, USA), and a rotary evaporator (BUCHI, Rotavapor® 114 with Water Bath B-480, Bristol, Wisconsin, USA).

4.2.2 Isolation and identification of *Serratia marcescens*

The bacteria, *Serratia marcescens (SM)* were obtained from soil at Sheda Science and Technology Complex (SHESTCO), Abuja, Nigeria. First, a soil sample was collected from a damp area at SHESTCO using a sterile bottle. 1g of the soil was weighed into a 50 ml conical flask and 10 ml of sterile distilled water was added to it, before mixing thoroughly. Serial dilution was then carried out on 1ml of the sample up to a dilution of 10^9. The $x10^4$ and $x10^5$ dilutions were inoculated into nutrient agar plates (Sigma Aldrich, St. Louis, USA). About 8 different organisms grew, but our interest was on the red pigmented colonies. Subsequently, we sub-cultured the red pigmented bacteria until we obtained a pure culture of the organism. Finally, the culture was sent to Deutsche Sammlung von Mikroorganismen und Zellkulturen (DSMZ), in Germany, for characterization and identification. They identified the organism as *Serratia marcescens marcescens* through sequence analysis and ribotyping.

4.2.3 Biosynthesis of gold nanoparticles using cell-filtrate and viable biomass

A loopful of *Serratia marcescens* growing on a petri plate was inoculated in a 250 ml conical flask containing 100 ml of sterile peptone-glycerol broth (PGB) The inoculated medium was incubated at 30°C in a rotary shaker at 160 revolutions per minute (rpm), for 48 hours. After 48 hours, the culture was centrifuged at 5000 rpm and 4°C for 15 minutes and further filtered through a 2µm membrane filter. The cell-free was collected in another flask, while the biomass was washed 3 times with sterile distilled water to remove all traces of the medium. Then, 1g (wet weight) of the biomass was re-suspended in 10 ml of sterile distilled water. The samples were placed in the test tubes as indicated in Table 4.1. The contents of the test tubes were then

mixed thoroughly and incubated in the water bath at 30°C for durations between 24 hours and 10 days.

4.2.4 Extraction and purification of prodigiosin (PG)

Prodigiosin was extracted from *Serratia marcescens (SM)* cultured on peptone glycerol agar (PGA) and purified using column chromatography. The percentage purity was equally determined with the aid of HPLC. This information can be seen in our recent publication, Danyuo et al., [52].

4.2.5 Biosynthesis of gold nanoparticles with prodigiosin

10 mg of the prodigiosin extract was dissolved in 5ml methanol and brought up to 50 ml with distilled water. 2 ml of the prodigiosin solution was reacted with 1 ml of 2.5mM $HAuCl_4$ and stirred for 10 minutes. A color change was observed as the bright red color of prodigiosin changed to a pale pink color in approximately 24 hours.

4.3.0 Characterization of gold nanoparticles

4.3.1 UV/Vis spectral analysis

The reduction of Au^{3+} to Au^0 was monitored using the UV-Vis spectrophotometer (UV-Vis) (CECIL 7500 Series, Buck Scientific Inc., East Norwalk, USA), equipment and vendor info). The Plasmon resonance frequency absorption characteristic of gold was monitored between wavelength ranges 400 – 700nm. The effects of time and pH on the synthesis of gold nanoparticles were also investigated.

4.3.2 Scanning Electron Microscopy (SEM) / Energy Dispersive X-ray Spectroscopy (EDS)

The SEM analysis of the synthesized gold nanoparticles was done using a FEI/Philips XL30 FEG-SEM, set at acceleration voltage of 15.00 kV, magnification of 102400x and a pressure of 3.91-5Torr. The gold nanoparticles solution was centrifuged at 12000 rpm for 30 minutes to pellet the nanoparticles. Samples of the pellet were placed on the SEM sample holder for observation. The elemental analyses of the samples were also made with EDS, using the same equipment and the same samples. When an electron beam is focused on the sample in a scanning electron microscope (SEM), the electrons from the primary beam penetrate the sample and

interact with the atoms from which it is made, and X-rays result from these interactions. The X-rays are detected by an Energy Dispersive detector which displays the signal as a spectrum of intensity versus X-ray energy. The energies of the characteristic X-rays allow the elements making up the sample to be identified, while the intensities of the characteristic X-ray peaks allow the concentrations of the elements to be quantified.

4.3.3 Transmission electron microscopy (TEM)

The sizes and shapes of the gold nanoparticles synthesized were determined with the Transmission Electron Microscope Microscope (CM100 Transmission Electron Microscope, Philips/FEI Corporation, Eindhoven, Holland). A copper grid (SPI supplies / structure probe, Inc., West Chester, USA) was placed on a glass slide, then a drop of gold nanoparticles solution was placed on the grid and allowed to air dry. It was then viewed in the TEM. The sizes of the particles were determined using the ImageJ software (NIH Image, Scion Image for Windows, National Institute of Health, Bethesda, Maryland, USA)

4.3.4 Helium Ion Microscopy (HIM)

Helium Ion Microscopy was carried out at the Microscopy facility in the Department of Physics at Rutgers University, Piscataway, New Jersey, USA using a Carl Zeiss Orion Helium Ion Microscope (ZEISS, Germany). The PG/gold nanoparticle complex was viewed with 1µm and 4 µm fields of view. The working distance was 7.3 mm, while the blanker current was 0.1 pA. The acceleration voltage was 30 kV, while the dwell time was 1 µs. The line averaging for the 1µm field of view image was 64, while that for the 4 µm field of view was 128.

The single most critical parameter in nanotechnology imaging is resolution. The helium ion microscope is a new type of microscope that uses helium ions for surface imaging and analysis. It works like the scanning electron microscope, but it uses a focused beam of helium ions instead of electrons [53]. The helium ions can be focused into a smaller probe size and provide a much smaller interaction volume at the sample surface compared to electrons. Also, it generates higher resolution images with better material contrast and improved depth of focus. The high resolution arises from the use of a finely sharpened needle and a process that strips individual atoms away from the source until an atomic pyramid is created with just three atoms at the very end of the

source tip. The HIM achieves a resolution of less than 0.3 nm at energy of 25-30 kV and can deliver beam currents between 1 fA and 25 pA. [54]

4.3.5 Dynamic Light Scattering (DLS)

A series of 1:10 dilutions of the samples was made with Dulbecco's Phosphate Buffer Saline (DPBS) (Sigma Aldrich, St. Louis, MO, USA. D8537) at pH 9 that was used for the DLS analysis. The machine used was a BIC 90 plus particle size analyzer that was equipped with a Brookhaven BI-9000 AT digital correlator (Brookhaven Instruments Corp., Holtsville, NY, USA). The light source was a solid-state laser operating at 658 nm with 30 mW power, while the signals were detected by a high-sensitivity avalanche photodiode detector. All of the measurements were conducted in triplicate at a fixed scattering angle of 90° at 25 ± 1 °C. Each sample was analyzed for 6 minutes (3 runs per sample at 2 minutes per run).

4.4.0 Results and Discussion

4.4.1 Nanoparticle Synthesis

After 24 hours of exposure to $HAuCl_4$, the almost colorless cell-free conditioned medium of *Serratia marcescens* changed color from pale yellow to pink or purple (Figure 4.1). Such color change is generally considered to be an indication that the $HAuCl_4$ has been reduced to Au^0 [55-59].

$$HAuCl_4 + 3e^- \longrightarrow Au + 4Cl^- + H^+ \qquad (1)$$

In contrast, the synthesis of gold nanoparticles by the cell biomass required a much longer duration. The color change to pink or purple was observed on the 6^{th} day. The control experiments (without either the cell-free extract or the biomass) remained pale yellow in color, indicating that the synthesis of gold nanoparticles did not occur in the absence of the cell-free conditioned medium or the cell biomass.

The formation of gold nanoparticles was initially monitored by visual observation and then characterized using various characterization techniques. To verify the reduction of gold ions, samples were withdrawn at different times and scanned in the range of 400-750 nm in a UV-visible spectrophotometer, which revealed the appearance of the peaks at 540-560 nm, which are characteristic of gold nanoparticles. UV-vis spectroscopy is one of the most important techniques

used to identify the formation and stability of the gold nanoparticles in aqueous solution. Gold nanoparticles are known to exhibit a maximum absorption in the range of 500 to 600 nm [60, 61].

4.4.2: Effects of pH on Biosynthesis of Gold Nanoparticles

We studied the effect of pH on synthesis of gold nanoparticles by *Serratia marcescens* using UV-Vis spectroscopy. Both the cell-free conditioned medium and biomass of *Serratia marcescens* were exposed for 10 days to a 2.5 mM $HAuCl_4$ solution, having adjusted the reaction medium to five pH values, i.e. 4.0, 5.5, 6.5, 7.5 and 8.5. This is consistent with the results of other prior researchers [62- 64], where variations in pH during exposure to gold ions, had an impact on the size, shape and number of particles produced per cell.

In the current work, plasmon resonance peaks were observed in the biomass at wavelengths close to ~ 550 nm and at pH levels of 4.0, 5.5, 6.5 and 7.5 on day 6, but by day 10, only pH 6.5 showed a plamon resonance of 570 nm with an increased absorption maxima of 1.90 (Figures 4.2a-4.2b and Table 4.2). No evidence of AuNPs formation was observed in the UV-Vis spectra of pH 8.5 for the biomass. This is similar to the findings of Joerger *et al*. [65] who observed that the optimum gold accumulation by microbial cells normally occurs in the pH range of 2 to 6.

In the synthesis reactions containing the cell-free conditioned medium, pH 4 resulted in peak absorbance at a wavelength of approximately 540 nm (Figures 4.3a – 4.3d). This suggests that moderately sized AuNPs were formed at this pH. In contrast, the pH of 6.5 resulted in a maximum absorbance at a wavelength of 570 nm. This is again consistent with the synthesis of large nanoparticle sizes (Figure 4.3b and Table 4.3) [66]. The effect of pH on the size distribution of gold nanoparticles synthetized by *Lactobacillus* sp. was already observed [67]. However, no plasmon resonance peaks were observed at the pH values of 5.5, 7.5 and 8.5, after exposure of cell-free extracts to $HAuCl_4$ for durations up to 96 hours.

The UV-Vis scans showed that the absorption maxima at the different pH were around 540 – 570 nm, depending on the sizes of the gold nanoparticles [68]. This is attributed to the Surface Plasmon Resonance (SPR) peak of gold nanoparticles. Smaller nanoparticles (sizes ~ 10 – 40 nm) have been shown to result in lower wavelengths (515 – 540 nm) at which maximum

absorptions are observed. Conversely, larger nanoparticles (sizes ~ 50 – 100 nm) are associated with higher wavelengths (550 – 570 nm), for maximum absorption / plasmon resonance [17, 69, 70].

It is important to note that gold nanoparticles were synthesized in the cell biomass after 6 days of exposure to $HAuCl_4$. The times taken for the color changes to occur are summarized in Tables 4.2 and 4.3. These show that the cell-free conditioned medium resulted in the fastest color changes, while the cell biomass required much longer durations for color changes to occur. Hence, from the color changes, we can deduce that the supernatant/ cell free medium is more efficient at synthesizing gold nanoparticles than the cell biomass. Furthermore, the UV-Vis results also show that the cell-free extract is more effective at producing gold nanoparticles than the cell biomass. The current results also demonstrate that the absorbance and the nanoparticle sizes increase with time. This is consistent with the red shift observed in the plasmon resonance peaks of the particles, with increasing time.

4.4.3 Characterization

4.4.3.1 Transmission Electron Microscopy (TEM)

The TEM images of the gold nanoparticles synthesized with the cell-free extract of *Serratia marcescens* at pH 4 and 6.5 are presented in Figures 4.4a-4.4b. They show the presence of gold nanoparticles of different shapes and sizes. The shapes observed range from spherical to prismatic and hexagonal nanoparticles. The average size of the particles (for a pH of 4) was between 21-30 nm (Figure 4.5a), and 31-40 nm (for a pH of 6.5) (Figure 4.5b). Therefore, the average size of nanoparticles seems to be dependent on the pH, with higher pH values producing nanoparticles of larger size. Also in Figures 4.4c- 4.4e, the TEM images of the gold nanoparticles synthesized using the biomass of *Serratia marcescens* were shown. Spherical shapes were predominant, similar to the shapes of nanoparticles synthesized from the cell-free conditioned medium. The sizes of the nanoparticles ranged from 20-120 nm, as shown in the histograms in Figures 4.5c-4.5e.

4.4.3.2 Scanning Electron Microscopy (SEM)

The synthesis of gold nanoparticles with cell biomass occurred intra-cellularly as shown in the SEM micrograph in Figure 6. This shows rod shaped bacteria, *Serratia marcescens,* decorated with gold nanoparticles within the cells. The image suggests that the reducing agent responsible for the reduction of $AuCl_4^-$ to Au^0 is actually within the bacteria. It also explains why the synthesis with the cell-free extract is faster, because the reducing agent (prodigiosin), a by-product of the bacteria, is released into the surrounding environment (media). Hence, possibly due to the higher concentration of the exudates in the media, it performs better as a reducing agent. Another possibility is that in the cell-free extract, the reducing agent has better access to the gold ions, which could be compartmentalized within the bacterial cell. Older publications show TEMs of bacteria containing gold nanoparticles, and the nanoparticles are located on the cell membrane or the cell wall within the bacteria. So, it's possible that if the nanoparticles are located in one of these compartments, they are not accessible to the reducing agent [71, 72]. In contrast, in the case of synthesis from biomass, additional time is needed to secrete and transport the by-products to react with the hydrogen aurochloride.

4.4.3.3 Energy Dispersive X-ray Spectrometry (EDS)

The EDS analyses also confirmed the presence of gold nanoparticles, as shown in Figure 4.7. In the case of the synthesis with the cell–free conditioned medium at a pH of 4 (Figure 4.7a), only 2 elements were present, gold (Au) and silicon (Si). Sharp peaks of gold were seen indicating high purity of the AuNPs. It also suggests that there was a complete reduction of $AuCl_4^-$ to AuNPs. At pH 6.5 (Figure 4.7b), using the cell-free extract, the elements Au, Si, carbon(C) and oxygen (O) were present. The C and Si are likely to be from the sample grid. In the case of synthesis with the biomass, on day 6 at pH 5.5 and 6.5 (Figures 4.7c-4.7d), the elements Au, C, O, Si and trace amount of sodium (Na) were observed. The Na is most likely to be an impurity from the sample grid. On day 10, for the biomass, the presence of Au, C and Si were seen.

From the results, the intensities of gold fractions in all the samples were higher than those of the other elements present, particularly the sample at pH 4, indicating high purity of the AuNPs.

4.4.3.4 Analysis of Gold /Prodigiosin Nanoparticles

The results of the analysis done on Gold/prodigiosin nanoparticles are presented in Figure 4.8. The UV-Vis spectra show the curves for only prodigiosin and after the synthesis of gold nanoparticles. The prodigiosin as extracted had a wavelength of 540nm and an absorbance of 1.23. After the synthesis of gold nanoparticles, the wavelength dropped to 535nm and an absorbance of 0.866. The reduction in the wavelength is an indication that the nanoparticles formed are within the range of 40-50nm, since wavelength is related to the size [73].

The TEM images revealed the nanoparticles to be mostly hexagonal in shape (Figure 4.8b). The result of the HIM analysis done for the gold/prodigiosin nanoparticles showed the gold nanoparticles were well dispersed (Figure 4.8c). The EDX analysis (Figure 4.9) showed the presence of Au and iron (Fe). The presence of Fe confirms the proposed mechanism that gold displaces Fe which is often in association with prodigiosin.

4.4.3.5 Dynamic Light Scattering (DLS)

Each of the AuNPs samples were diluted with distilled water in the ratio 1:8 and then filtered with 0.22 micron filter. Dynamic light scattering (DLS) is used to measure the size of particles suspended in a liquid. The average mean size (Z-Average) of synthesized gold nanoparticles at different pH were measured and the results are as follows (Figure 4.10); for the cell free conditioned medium at pH 4.0, the Polydispersity index (PDI), 0.25, shows that the sample is relatively monodispersed, but the sizes of the NPs are very large, about 270 nm. At pH 5.5, nanoparticles produced by the cell-free conditioned medium have a Z-average under 100 nm, but this is still large for bare AuNPs. The PDI indicates that the nanoparticles were mostly polydispersed. At pH 6.5, the nanoparticles are relatively monodispersed, but the mean size is large, with Z-average larger than 100 nm. The results of the DLS for gold nanoparticles from cell free extracts at pH 7.5, 8.5 and 9.5 revealed that they all have relatively moderate mean sizes with Z-average of 40.2nm, 43.6nm, 42.6nm respectively and equally a relatively low polydispersity, 0.27, 0.29 and 0.27 (refer to Table 4.4). These results are good for bare nanoparticles.

In comparing these results with the results of the UV-Vis scans, which indicated that AuNPs were not present at pH 8.5 and 9.5, one can infer that gold nanoparticles were actually present but that their concentration was too small to be detected; hence the DLS was able to detect them. The gold nanoparticles synthesized with the biomass were also analyzed. The sample at pH 4 had a very large Z-average of 120.5nm but the PDI was low at 0.21. At pH 5.5 the mean size was small, 39.0nm but the PDI was rather very high, 0.53, making the nanoparticles unsuitable for drug delivery.

The term polydispersity (or more recently dispersity without the poly, according to IUPAC recommendation) [74] is used to describe the degree of "non-uniformity" of a distribution. The polydispersity index represents the ratio of particles of different sizes to total number of particles. The higher the polydispersity index, the less monodispersed the particles will be. The Polydispersity Index is dimensionless and is scaled such that values smaller than 0.05 are rarely seen other than with highly monodisperse standards. Values greater than 0.7 indicate that the sample has very broad size distribution and is probably not suitable for the dynamic light scattering (DLS) technique [75].

4.4.4 The Formation of Gold Nanoparticles

The cell-free conditioned medium contain reducing agents (antioxidants such as vitamin C precursors, cytochrome oxidase, vitamin B complex and porphyrins) [76- 78]. Among these, the cytochrome complex and the porphyrins stand out as possibilities for the reduction of $HAuCl_4$. The mechanism leading to the formation of AuNPs is a reduction reaction that involves electron transport that occurs in the cell membrane of the bacteria.

Cytochrome complexes, a class of hemoproteins, play a great role in electron transport. These proteins can change the valence of the heme iron, alternating between ferrous (Fe^{2+}) and ferric (Fe^{3+}) states (equation 2). Cytochrome oxidase is a transmembrane protein complex found in bacteria and the mitochondrion of eukaryotes [79]. The cytochrome oxidase complex receives an electron from each of four cytochrome c molecules, and transfers them to one oxygen molecule, converting molecular oxygen to two molecules of water as shown in equation (3).

$$Fe^{2+} \longrightarrow Fe^{3+} + e^{-} \qquad (2)$$

$$4\ Cyt\ c_{red} + O_2 + 8\ H^+_{matrix} + 4e^- \longrightarrow 4\ Cyt\ c_{ox} + 2\ H_2O + 4\ H^+_{intermembrane} \quad (3)$$

In the process, the cytomchrome oxidase complex binds four protons from the inner aqueous phase to make water, and, in addition, translocate four protons across the membrane, helping to establish a transmembrane difference of proton electrochemical potential that the ATP synthase then uses to synthesize ATP. Equation 4 is a combination of equations 2 and 3 showing the complete reaction that go on in the cell membrane during electron transport.

$$4\ Fe^{2+}\text{-cytochrome } c + 8\ H^+_{in} + O_2 \longrightarrow 4\ Fe^{3+}\text{-cytochrome } c + 2\ H_2O + 4\ H^+_{out} \quad (4)$$

In the presence of $HAuCl_4$, the Fe^{2+}-cytochrome c reduces Au^{3+} thereby forming gold nanoparticles.

$$HAuCl_4 + 3e^- \longrightarrow Au + 4Cl^- + H^+ \quad (1)$$

$$Au^{3+}(aq) + 3e^- \longrightarrow Au^0(s)$$

As has already been stated, the process of gold nanoparticle formation is a reduction reaction. Generally, gold nanoparticles are produced in a liquid by reduction of hydrogen tetra chloroauric acid ($HAuCl_4$). As the reducing agent is added (conditioned medium), this causes Au^{3+} ions to be reduced to neutral gold atoms (Au^0). As more and more of these gold atoms form, the solution becomes supersaturated, and gold gradually starts to precipitate in the form of sub-nanometer particles, the rest of the gold atoms that form stick to the existing particles. This involves the process of nucleation and growth.

The shape and size of the nanoparticles formed are controlled by the pH of the solution. Ji *et al.*, [80] reported that the pathway by which gold particles are synthesized varies depending on pH. Other researchers, [81] also found that the pH is controlled by the concentration of trisodium citrate. For a low pH, pH 3.7−6.5, the particles form through an intermediate of $[AuCl_3(OH)]^-$ which undergoes nucleation within 10 s, a LaMer burst nucleation, followed by fast random attachment and finally intraparticle ripening. For a higher pH ∼6.5−7.7, the particles undergo reduction through $[AuCl_2(OH)]^{2-}$ and $[AuCl(OH)]^{3-}$ with a much longer nucleation of ∼60 s

followed by slow growth. In the synthesis of gold nanoparticles, it is somewhat unclear which chemical reaction is occurring and there are two separate pathways which the gold could undertake. The first is to bond as ions, and then have a reduction occur, or the reduction could occur first followed by a bonding of the gold atoms [82].

4.5 Summary and Concluding Remarks

We have demonstrated that *Serratia marcescens* can be used in the synthesis of gold nanoparticles both intra- and extra-cellularly. However, the use of cell-free extract proved to be more effective than the biomass, as it requires lower reaction times. Also, the study indicates that pH 4 is the optimum pH for the synthesis. In addition, the nanoparticle sizes at this pH (40-60 nm) are within the range that is suitable for applications in nano-medicine e.g. for cancer detection and treatment.

The SEM image revealed gold nanoparticles within the bacterial cells. This is a strong indication that the factor responsible for the reduction of gold chloride is located within the cell. With the ability of prodigiosin to synthesize gold nanoparticles, it therefore confirms that it is the prodigiosin, which is a secondary metabolite of the bacteria that is responsible for the reduction. Furthermore, the EDS results showed that the gold nanoparticles at this pH are pure, as indicated by the presence of high intensities of gold (Au) element, with a little amount of Silicon (Si), which most likely was from the sample grid.

The TEM images showed the cell-free nanoparticles to be well dispersed than those from biomass which appeared agglomerated. From the DLS results, it was seen that for pH 5.5, pH 8.5 and pH 9.5 of the cell-free synthesized gold nanoparticles and pH 5.5 of the biomass synthesized AuNPs has hydrodynamic size range of less than 50nm which is good for bare nanoparticles ready for conjugation. Most of the nanoparticles have PDI of between 0.2 and 0.3 meaning that they are mildly polydispersed. Thus, the gold nanoparticles produced by *Serratia marcescens* have properties that make them well-suited for drug delivery to diseased cells.

References:

1. Neeleshwar, S., Chen, C.L., Tsai, C.B., Chen, Y.Y., Chen, C.C., Shyu, S.G., Seehra, M.S.: Size-dependent properties of CdSe quantum dots. Phys Rev B. **71**, (201307), 1–4. (2005)

2. Deplanche, K., Macaskie, L.E.: Biorecovery of gold by Escherichia coli and Desulfovibrio desulfuricans. Biotechnol Bioeng, **99**, 1055- 1064, (2008).

3. Salata, O.V.: Application of nanoparticles in biology and medicine. J Nanobiotechnol. **2,** 3–9, (2004).

4. Tolles, W.M.: Nanoscience and nanotechnology in Europe. Nanotechnology. **7,** (2) 59, (1996).

5. Selvakannan, P.R., Mandal, S., Phadtare, S., Gole, A., Pasricha, R., Adyanthaya, S.D., Sastry, M.: Water-dispersible tryptophan-protected gold nanoparticles prepared by the spontaneous reduction of aqueous chloroaurate ions by the amino acid. J. Colloid Interface Sci. **269**, 97–102, (2004).

6. Sun, Y., Xia,Y.: Shape-controlled synthesis of gold and silver nanoparticles. Science **298** (5601), 2176-2179, (2002).

7. Okitsu, K., Yue, A., Tanabe, S., Matsumoto, H., Yobiko, Y.: Formation of colloidal gold nanoparticles in an ultrasonic field: control of rate of gold (III) reduction and size of 338 formed gold particles. Langmuir, **17**, 7717-7720, (2001).

8. Stephen, R., Macnaughton, S.J.: Developments in terrestrial bacterial remediation of metals. Curr. Opin. Biotechnol. **10,** 230–233, (1999).

9. Mukherjee, P., Ahmad, A., Mandal,D., Senapati, S., Sainkar, S.R., Khan, M.I., Parischa, R., Ajayakumar, P.V., Alam, M., Kumar, R., Sastry, M.: Fungus mediated synthesis of silver nanoparticles and their immobilization in the mycelial matrix: A novel biological approach to nanoparticle synthesis. Nano Lett, **15**, 15-519, (2001).

10. Singh, A., Jain, D., Upadhyay, M.K., Khandelwal, N., Verma, H.N.: Green synthesis of silver nanoparticles using Argemone mexicana leaf extract and evaluation of their antimicrobial activities. Digest Journal of Nanomaterials and Biostructures. **5** (2) 483-489, (2010).

11. Arangasamy, L., Munusamy, V.: Tapping the unexploited plant resources for the synthesis of silver nanoparticles. African Journal of Biotechnology 7 (17), 3162-3165, (2008).

12. Melanie, H., Ulrich, S.: On the application potential of gold nanoparticles in nanoelectronics and biomedicine. Phil. Trans. R. Soc. A, **368**, 1405–1453 (2010).

13. Rochelle, A., Resham, B., Mukherjee, P.: Gold nanoparticles: opportunities and challenges in nanomedicine. Expert Opinion on Drug Delivery. **7**(6) 753-763, (2010).

14. Valden, M., Lai, X., Goodman, D.W.: Onset of catalytic activity of gold clusters on Titania with the appearance of nonmetallic properties. Science. **281**(5383) 1647-1650 (1998).

15. Haruta, M., and Date, M Advances in the catalysis of Au nanoparticles, Appl. Catal., A. **222,** 427–437, (2001).

16. Kung, H.H., Kung, M.C., Costello, C.K.: Supported Au catalysts for low temperature CO oxidation. J. Catal., **216**, 425–432, (2003).

17. Ahmad, A., Senapati, S., Khan, M.I., Kumar, R., Sastry, M.: Extracellular Biosynthesis of Monodisperse Fold Nanoparticles by a Novel Extremophilic Actinomycete Thermonospora sp. Langmuir, **19**, 3550-3553, (2003).

18. Zhang, X., Yan, S., Tyagi, R.D., Surampalli, R.Y.: Synthesis of nanoparticles by microorganisms and their application in enhancing microbiological reaction rates. Chemosphere. **82**, 489-494, (2011).

19. Li, X., Xu, X.H., Chen, Z.S., Chen, G.: Biosynthesis of Nanoparticles by Microorganisms and Their Applications. J Nanomater. **2011**(2011). Article ID 270974, 16 pages, doi:10.1155/2011/270974.

20. Gole, A., Dash, C., Sainkar, S.R., Mandale, A.B., Rao, M., Sastry, M.: Extracellular biosynthesis of silver nanoparticles using the fungusFusarium oxysporum. Analytical Chemistry. **72**, 1401–1403(2000).

21. Husseiny, M.I., El-Aziz, M.A., Badr, Y., Mahmoud, M.A.: Biosynthesis of gold nanoparticles using Pseudomonas aeruginosa. Spectrochimica Acta Part A. **67** (3-4) 1003–1006, (2007).

22. He, S., Guo, Z., Zhang, Y., Zhang, S., Wang, J., Gu, N.: Biosynthesis of gold nanoparticles using the bacteria Rhodopseudomonas capsulate. Materials Letters. **61** (18) 3984–3987, (2007).

23. Konishi, Y., Tsukiyama, T., Tachimi, T., Saitoh, N., Nomura,T., Nagamine, S.: Microbial deposition of gold nanoparticles by the metal-reducing bacterium Shewanella algae, Electrochimica Acta. **53** (1), 186–192, (2007).

24. Mohanpuria, P., Rana, N.K., Yadav, S.: Biosynthesis of nanoparticles: technological concepts and future applications. Journal of Nanoparticle Research. **10** (3) 507–517, (2008).

25. Beveridge, T.J., Murray, G.E.: Sites of Metal Deposition in the Cell Wall of Bacillus subtilis. J. Bacteriol. **141**, 876-887, (1980).

26. Mukherjee, P., Senapati, S., Mandal,D., Ahmad, A., Khan, M.I., Kumar, R., Sastry, M.: Extracellular synthesis of gold nanoparticles by the fungus Fusarium oxysporum. Chembiochem **3,** 461–463, (2002).

27. Ahmad, A., Senapati, S., Khan, M.I., Ramani, R., V. Srinivas, V., Sastry, M.: Intracellular synthesis of gold nanoparticles by a novel alkalotolerant actinomycete, Rhodococcus species. *Nanotechnol.* **14,** 824-838, (2003a).

28. Chen, J., Saeki, F., Wiley, B.J., Cang, H., Cobb, M.J., Li, Z., Au, L., Zhang, H., Kimmey, M.B., Li, X., Xia,Y.: Gold nanocages: bioconjugation and their potential use as optical imaging contrast agents. Nano Lett. **5**(3) (2005) 473-477.

29. Loo, C., Lowery, A., Halas, N., West, J., Drezek, R.: Immunotargeted nanoshells for integrated cancer imaging and therapy. *Nano Lett* ; **5** 709–11, (2005)

30. Loo, C., Lin, A., Hirsch, L., Lee, M.H., Barton, J., Halas, N., West, J., Drezek, R.: Nanoshell-enabled photonics-based imaging and therapy of cancer. Tech. Cancer Res.Treat. **3**(1), 33-40, (2004)

31. Hirsch, L.R., Stafford, R.J., Bankson, J.A., Sershen, S.R., Rivera, B., Price, R.E.,. Hazle, J.D., Halas, N.J., West, J.L.: Nanoshell-mediated near-infrared thermal therapy of tumors under magnetic resonance guidance. Proc. Natl. Acad. Sci. USA. **100**(23) 13549-13554 (2003).

32. Mukherjee, P., Bhattacharya, R., Wang, P., Wang, L., Basu, S., Nagy, J.A., Atala, A., Mukhopadhyay, D., Soker, S.: Antiangiogenic properties of gold nanoparticles. Clin. Cancer Res. **11**(9), 3530-3534 (2005).

33. Hainfeld, J.F., Slatkin, D.N., Smilowitz, H.M.: The use of gold nanoparticles to enhance radiotherapy in mice. Phys. Med. Biol. **49**, N309-N315, (2004).

34. Reddy, J.A., Allagadda, V.M., Leamon, C. P.: Targeting therapeutic and imaging agents to folate receptor positive tumors. Curr. Pharm. Biotechnol. **6**(2) 131-150, (2005).

35. Cascante, M., Centelles, J.J., Veech, R.L., Lee, W.N., Boros, L.G.: Role of thiamin (vitamin B-1) and transketolase in tumor cell proliferation. Nutr. Cancer. 36(2), 150-154, (2000)

36. Park, J.W., Benz, C.C., Martin, F. J.: Future directions of liposome- and immunoliposome- based cancer therapeutics. Semin. Oncol. **31**(6 Suppl. 13) 196-205 (2004).

37. El-Sayed, I.H., Huang, X., El-Sayed, M. A.: Surface plasmon resonance scattering and absorption of anti-EGFR antibody conjugated gold nanoparticles in cancer diagnostics: applications in oral cancer. Nano Lett. **5**(5), 829-834,(2005)

38. Alibart, F., Pleutin, S., Guerin, D., Novembre, C., Lenfant, S., Lmimouni, K., Gamrat, C., Vuillaume, D.: An organic nanoparticle transistor behaving as a biological spiking synapse. Adv. Funct. Mat., **20** (2) 330–337, (2010).

39. Michal, S., Ben, M.M., Ron, F., Assaf, S., Tal, D.: Nanoengineering gold particle composite fibers for cardiac tissue engineering. J. Mater. Chem. B. **1**, 5210-5217, (2013).

40. Stoppa, M., Chiolerio. A.: Wearable Electronics and Smart Textiles: A Critical Review. Sensors, **14,** 11957-11992, (2014).

41. Benoit, M., Gaub, H.E.: Measuring cell adhesion forces with the atomic force microscope at the molecular level. Cell tissue organs. **172**(3), 174-189, (2002).

42. Helenius, J., Heisenberg, C.P., Gaub, H.E., Muller, D.L.: Single cell force spectroscopy. Journal of cell science. **121**(11), 1785-1791, (2008).

43. Benoit, M., Selhuber-unkel, C.: Measuring cell adhesion forces: theory and principles. Methods Mol Biol. **736,** 355-77, (2011).

44. Hampp, E., Botah, R., Odusanya, O.S., Anuku, N., Malatesta, K.A., Soboyejo, W.O.: Biosynthesis and adhesion of gold nanoparticles for breast cancer detection and treatment. Journal of Materials Research. **27** (22), 2891 -2901, (2012).

45. Don, J.B., Noel, R.K., James, T.S.: [1984 (Williams & Wilkins)]. George M. Garrity, ed. The Gammaproteobacteria. Bergey's Manual of Systematic Bacteriology 2B (2nd ed.). NewYork: Springer (2005) 1108.

46. Han, S. B., Kim, H. M., Kim, Y. H., Lee, C. W., Jang, E. S., Son, K. H., Kim, S. U., Kim, Y. K.: T Cell Specific Immunosuppression by Prodigiosin Isolated from *Serratia Marcescens*. Int J. Immunopharmacol. **20,** 1-13, (1998).

47. Montaner, B., Navarro, S., Piqué, M., Vilaseca, M., Martinell, M., Giralt, E., Gil, J., Pérez-Tomás, R.: Prodigiosin from the Supernatant of *Serratia Marcescens* Induces Apoptosis in Hematopoietic Cancer Cell Lines. British J. Pharmacol. **131,** 585-593, (2000).

48. Song, M. J., Bae, J., Lee, D. S., Kim, C. H., Kim, J. S., Kim, S. W., Hong, S. I.: Purification and Characterization of Prodigiosin Produced by Integrated Bioreactor from *Serratia Sp*. KH-95. J. Biosc. Bioeng. **101**, 157-161, (2006).

49. Montaner, B., Pérez-Tomás, R.: Prodigiosin Induces Caspase-9 and Caspase-8 Activation and Cytochrome. C Release in Jurkat T cells. Ann. NY Acad. Sci. **973,** 246-249, (2002).

50. Pérez-Tomás, R., Montaner, B., Llagostera, E., Soto-Cerrato, V.: The Prodigiosins, Proapoptotic Drugs with Anticancer Properties. Biochem. Pharmacol. **66,** 1447- 1452, (2003).

51. Francisco, R., Perez-Tomas, R., Gimenez-Bonafe, P., Soto-Cerrato, V., Gimenez-Xavier, P., Ambosio, S.: Mechanisms of Prodigiosin Cytotoxicity in Human Neurobblastoma Cell Lines. European Journal of Pharmacology. **572** (2-3), 111-119, (2007).

52. Danyuo, Y., Ani, C. J., Obayemi, J. D., Dozie-Nwachukwu, S., Odusanya , O. S., Oni, Y., Anuku, N., Malatesta, K., Soboyejo, W. O.: Prodigiosin Release from an Implantable Biomedical Device: Effect on Cell Viability. Advanced Materials Research, **1132,** 3-18, (2016).

53. Arey, B.W., Shutthanandan, V., Jiang, W.: Helium Ion Microscopy versus Scanning Electron Microscopy. W. R. Wiley Environmental Molecular Sciences Laboratory, Pacific Northwest National Laboratory, Richland, WA 99354 (2010)

54. Ward, B.W., Notte, J.A., Economou, N. P.: Helium ion microscope: A new tool for nanoscale microscopy and metrology. J. Vac. Sci. Technol. **24**, 2871, (2006).

55. Noruzi, M., Zare, D., Davoodi, D.: A rapid biosynthesis route for the preparation of gold nanoparticles by aqueous extract of cypress leaves at room temperature. Spectrochim Acta A Mol Biomol Spectrosc **94**: 84–88, (2012).

56. Malarkodi, C., Rajeshkumar, S., Vanaja, M., Paulkumar, K., Gnanajobitha, G., Annadurai, G.: Eco-friendly synthesis and characterization of gold nanoparticles using Klebsiella pneumoniae. J Nanostruct Chem **3,** 30, 1-7, (2013).

57. Sunkar, S., Valli Nachiyar, C.V., Renugadevi,K.: Endophytic Bacillus cereus mediated synthesis of gold nanoparticles and their stabilization using biopolymer chitosan J. Chem. Pharm. Res., **6** (11), 434 - 443, (2014).

58. Xia, Y., Halas, N.J., Shape-controlled synthesis and surface plasmonic properties of metallic nanostructures. MRS Bull. **30**, 338–348 (2005).

59. Khalil, M.M.H., Ismail, E.H., El-Magdoub, F.: Biosynthesis of Au nanoparticles using olive leaf extract: 1st nano updates. Arab J Chem **5,** 431–437, (2012)

60. Rastogi, L., Arunachalam, J.: Green synthesis route for the size controlled synthesis of biocompatible gold nanoparticles using aqueous extract of garlic (Allium sativum). Adv. Mat. Lett. **4**(7), 548-555, (2013).

61. Prevo, B.G., Esakoff, S.A., Mikhailovsky, A., Zasadzinski, J. A.: Scalable Routes to Gold Nanoshells with Tunable Sizes and Response to Near-Infrared Pulsed-Laser Irradiation. Small. **4**(8), 1183–1195, (2008).

62. Gericke, M., Anthony, P.: Microbial production of gold nanoparticles. Gold Bulletin **39** (1), 22-28, (2006).

63. Suryawanshi, M.L., Deshmukh, A.M.: Studies on aquatic actinomycetes from Shivaji Sagar, Ph. D. thesis, Shivaji University, Kolhapur, India (2008).

64. Kathiresan, K., Manivannan, S., Nabeel, M.A., Dhivya, B.: Studies on silver nanoparticles synthesized by a marine fungus, Penicillium fellutanum isolated from coastal mangrove sediment. Colloids and Surfaces B: Biointerfaces. **71**, 133-137, (2009).

65. Joerger, R., Klaus, T., Granqvist, C.G.: Biologically produced silver-carbon composite materials for optically functional thin-film coatings. Adv Mater **12,** 407-409(2000)

66. Mukherjee, P., Ahmad, A., Mandal, D., Senapati, S., Sainkar, S.R., Khan, M.I., Ramani, R., Parischa, R., Ajayakumar, P.V., Alam, M., Sastry, M., Kumar, R.: Bioreduction of AuCl(4)(-) Ions by the Fungus, Verticillium sp. and Surface Trapping of the Gold Nanoparticles. Angew Chem Int Ed Engl. **40**(19), 3585-3588,(2001).

67. Nair, B., Pradeep, T.: Coalescence of nanoclusters and formation of submicron crystallites assisted by Lactobacillus strains. Cryst. Growth Des. 2, 293-298, (2002)

68. Njoki, P.N., Lim, I.I.S., Mott, D., Park, H-Y., Khan, B., Mishra, S., Sujakumar, R., Luo, J., Zhong, C-J.: Size correlation of optical and spectroscopic properties for gold nanoparticles," Journal of Physical Chemistry C. **111**(40), 14664–14669, (2007).

69. Kumar, A., Vemula, P.K., Ajayan, P.M., John, G.: Silver-nanoparticle-embedded antimicrobial paints based on vegetable oil. Nat. Mater. 7, 236–241, (2008).

70. Xie, J., Zheng, Y., Ying, J.Y.: Protein-Directed Synthesis of Highly Fluorescent Gold Nanoclusters J. Am. Chem. Soc. 131(3), 888–889, (2009).

71. Dykman, L.A., Khlebtsov, N.G.: Gold Nanoparticles in Biology and Medicine: Recent Advances and Prospects. Acta Naturae 3(2), 34–55, (2011).

72. Chandran, K., Song, S., Yun,S.: Effect of size and shape controlled biogenic synthesis of gold nanoparticles and their mode of interactions against food borne bacterial pathogens. Arabian Journal of Chemistry in press, (2014).

73. Cytodianostics Inc. Accessed on 29 December, 2015 at http://www.cytodiagnostics.com/store/pc/Introduction-to-Gold-Nanoparticle-Characterization-d3.htm.

74. Stepto, R. F. T.: Dispersity in Polymer Science (IUPAC Recommendations 2009). Pure Appl. Chem., **81** (2), 351–353, (2009).

75. International Standard ISO13321 Methods for Determination of Particle Size Distribution Part 8: Photon Correlation Spectroscopy, International Organization for Standardization (ISO) (1996)

76. Bhumkar, D.R., Joshi, H.M., Sastry, M., Pokharkar, V.B.: Chitosan reduced gold nanoparticles as novel carriers for transmucosal delivery of insulin. Pharm. Res., 24 (2007) 1415-1426.

77. Mallikarjuna, N.N., Rajender, S.V.: Green Synthesis of Ag and Pd Nanospheres, Nanowires, and Nanorods Using Vitamin: Catalytic Polymerization of Aniline and Pyrrole, Journal of Nanomaterials. doi:10.1155/2008/782358 (2008).

78. Kai, Q., Jingxia, L., Jiwei, M., Yuqing.: Preparation and characterization of gold nanoparticles using ascorbic acid as reducing agent in reverse micelles. Journal of Materials Science. **44** (3), 754-758, (2007).

79. Lemberg, R., Barrett, J.: Cytochromes. Academic, New York, 277-279, (1973)

80. Ji, X.; Song, X.; Li, J.; Bai, Y.; Yang, W.; Peng, X. Size control of gold nanocrystals in citrate reduction: the third role of citrate. J. Am. Chem. Soc. 2007, 129, 13939.-13948

81. Chow, M.; Zukoski, C. J. Gold Sol Formation Mechanisms: Role of Colloidal Stability Colloid Interface Sci. 1994, 165, 97.

82. Yao, T.; Sun, Z.; Li, Y.; Pan, Z.; Wei, H.; Xie, Y.; Nomura, M.; Niwa, Y.; Yan, W.; Wu, Z.; Jiang, Y.; Liu, Q.; Wei, S. Insights into Initial Kinetic Nucleation of Gold Nanocrystals J. Am. Chem. Soc. 2010, 132, 7696.

(a) **(b)**

Before at zero hour (with cell free conditioned medium) After synthesis at 24 hours

Fig. 4.1 Photographs showing color changes (a) before and (b) after the synthesis of gold nanoparticles using *Serratia marcescens* at pH 4.0, 5.5, 6.5, 7.5, 8.5

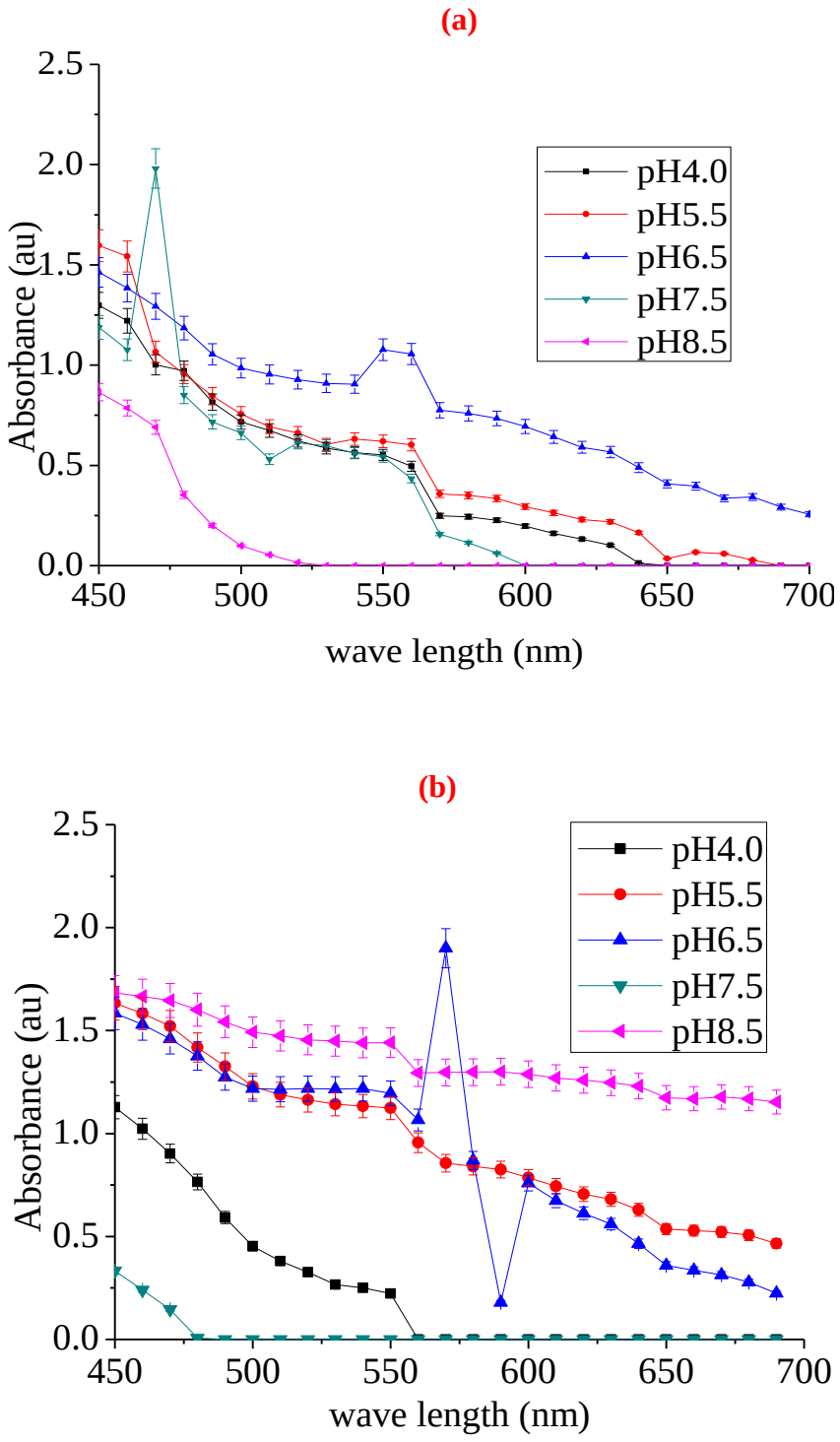

Fig 4.2 UV/Vis spectra of gold nanoparticles synthesis with the biomass at (a) 6 days, and (b) 10 days.

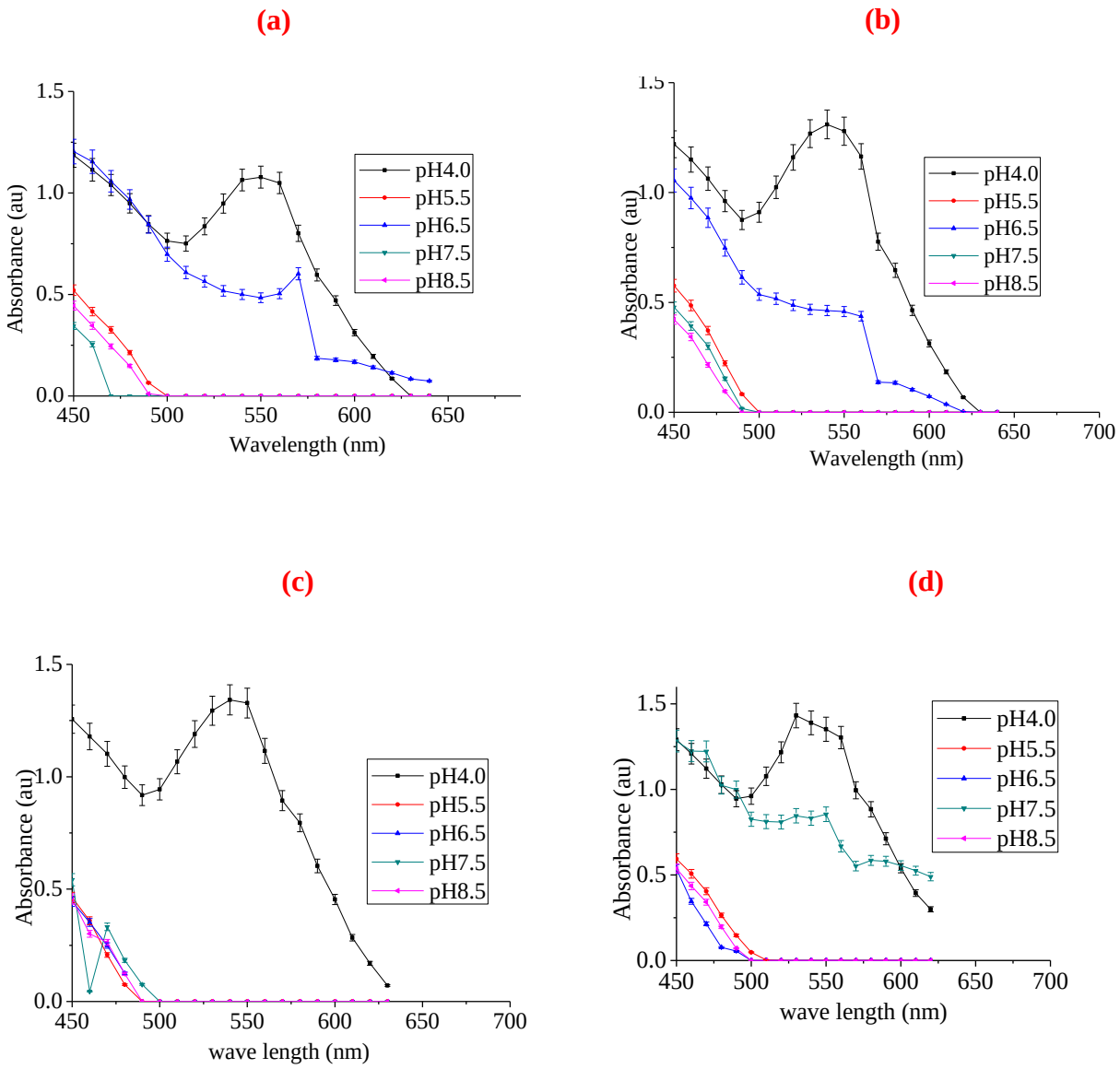

Fig. 4.3 Effects of pH on UV/Vis spectra of gold nanoparticles synthesis with the cell-free conditioned medium of *Serratia marcescens* at; (a) 24hrs; (b) 48hrs (c) 72hrs, and (d) 96hrs

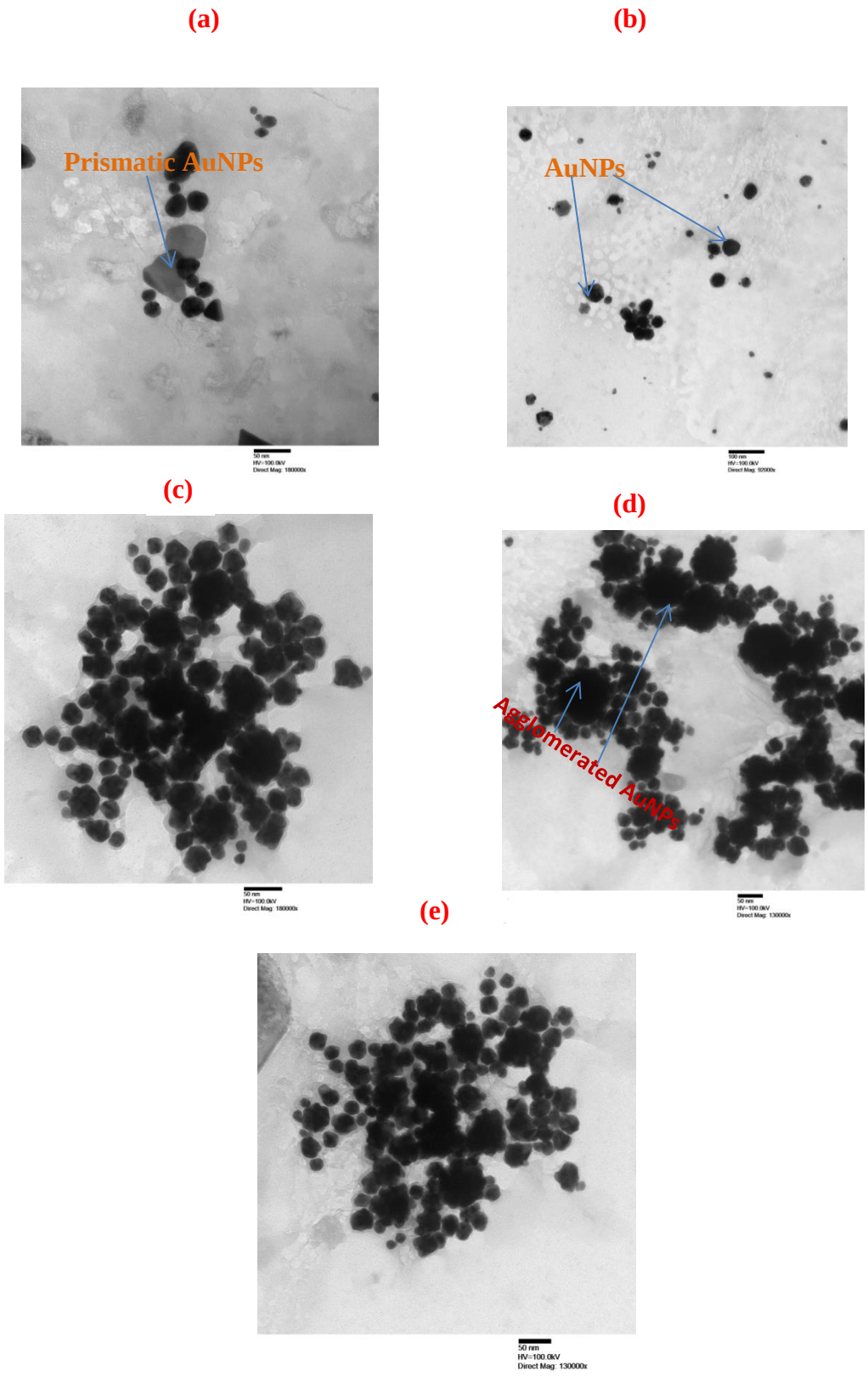

Fig.4. 4 TEM images of the biosynthesized gold nanoparticles obtained from cell-free conditioned medium of *Serratia marcescens* at: (a) pH 4 on day 1; (b) pH 6.5 on day 1. From biomass at: (c) pH 5.5 after 24 hours; (d) pH 6.5 on day 6, and (e) pH 6.5 on day 10.

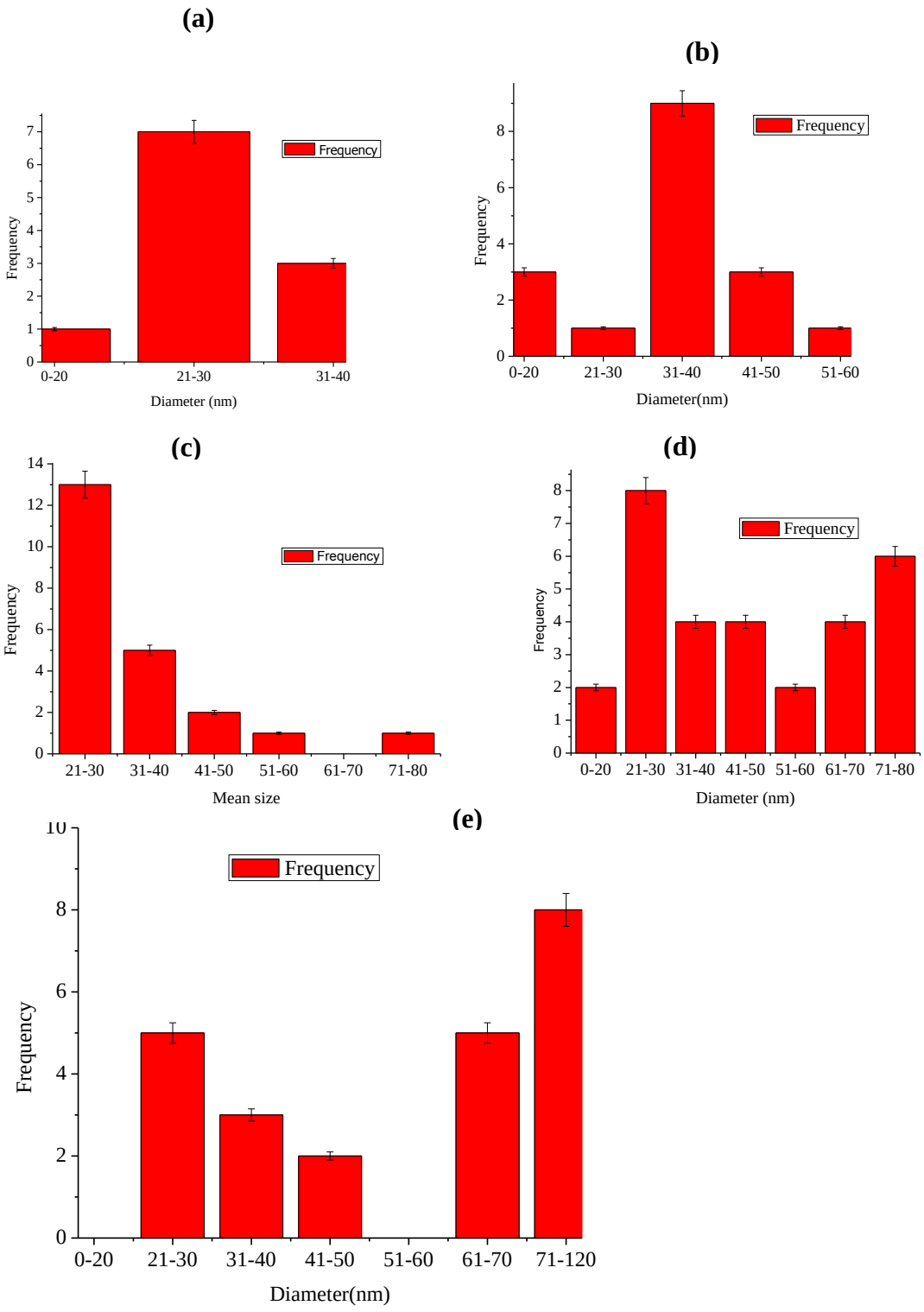

Fig. 4.5 Histograms showing the size distribution of the gold nanoparticles synthesized (a) from cell-free conditioned medium of *Serratia marcescens* at pH4 ; (b) at pH6.5 ; (c) from biomass of *Serratia marcescens* at pH 5.5 ; (d) pH 6.5 at day 6 and (e) pH 6.5 at day 10.

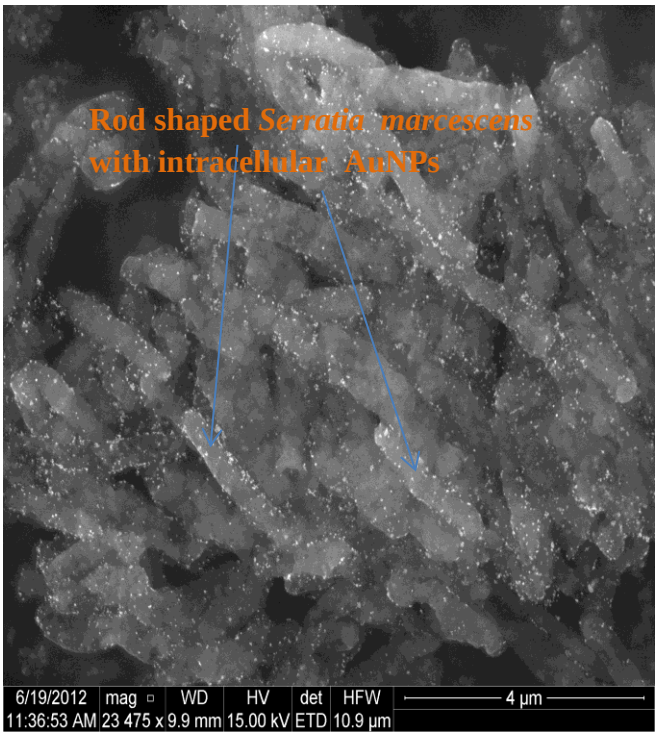

Fig. 4.6 SEM micrograph showing rod - shaped *Serratia marcescens* with intracellular gold nanoparticles after 24hr.

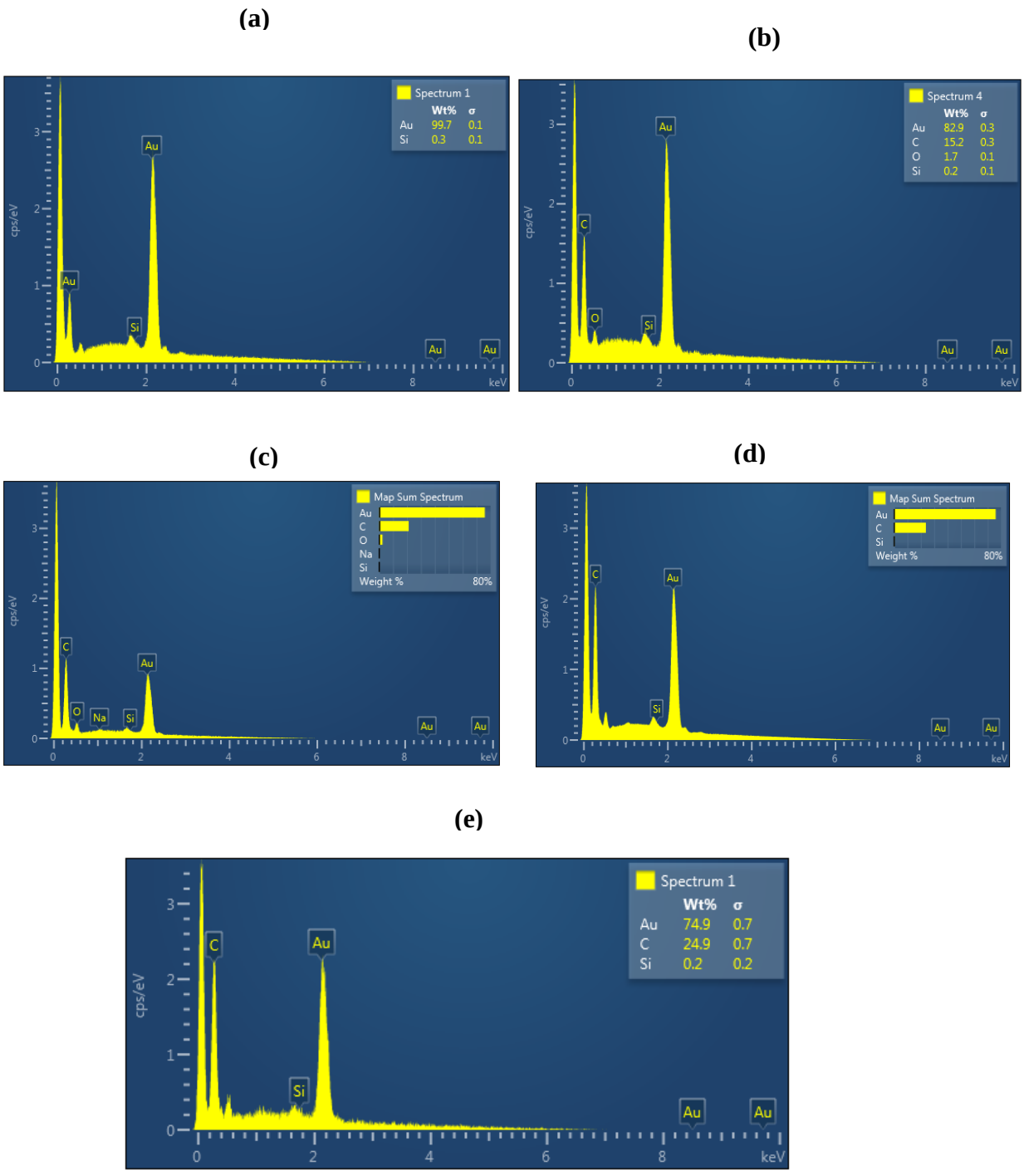

Fig. 4.7 EDS analysis of the synthesized AuNPs indicating the presence of elemental gold (a) AuNPs synthesis with the cell-free conditioned medium at pH4; (b) cell-free conditioned medium at pH 6.5; (c) EDS of AuNPs from biomass on day 6 at pH 5.5 ; (d) at pH 6.5 and (e) at pH 6.5 on day 10.

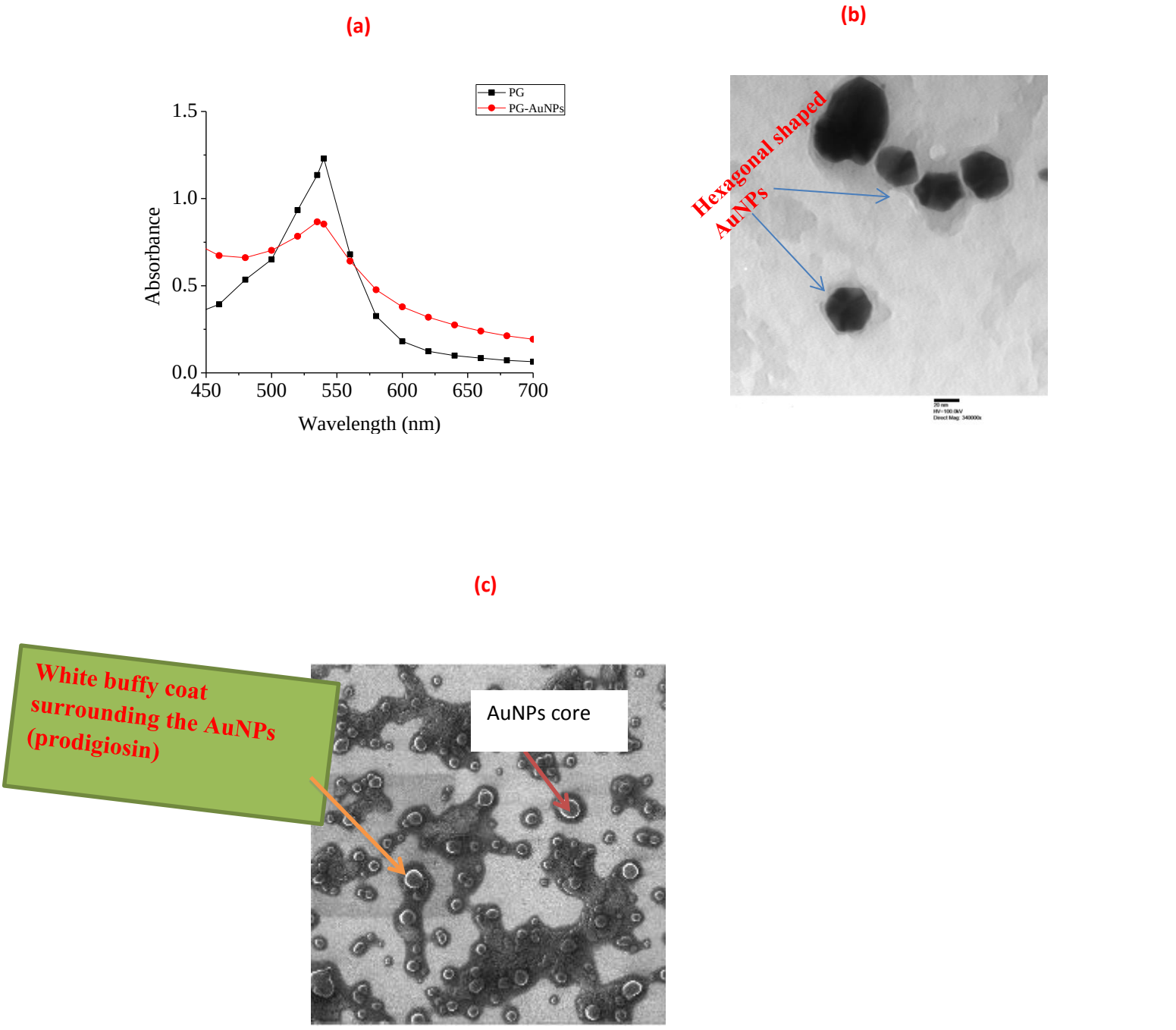

Fig. 4.8 Analysis of gold/prodigiosin nanoparticles (a) UV-Vis analysis of prodigiosin before and after the synthesis, (b) TEM image showing hexagonal shaped nanoparticles (c) HIM image analysis

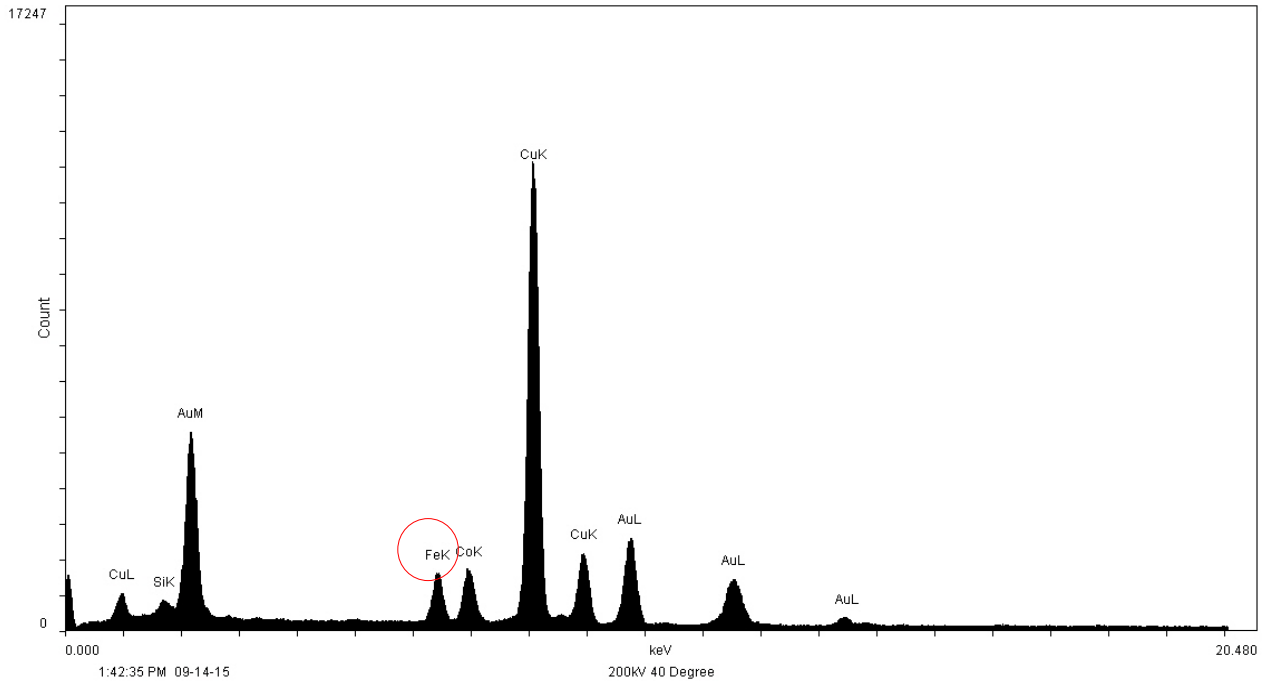

Fig.4. 9 EDX of prodigiosin-gold nanoparticles produced from *Serratia marcenscens* showing the presence of iron (Fe).

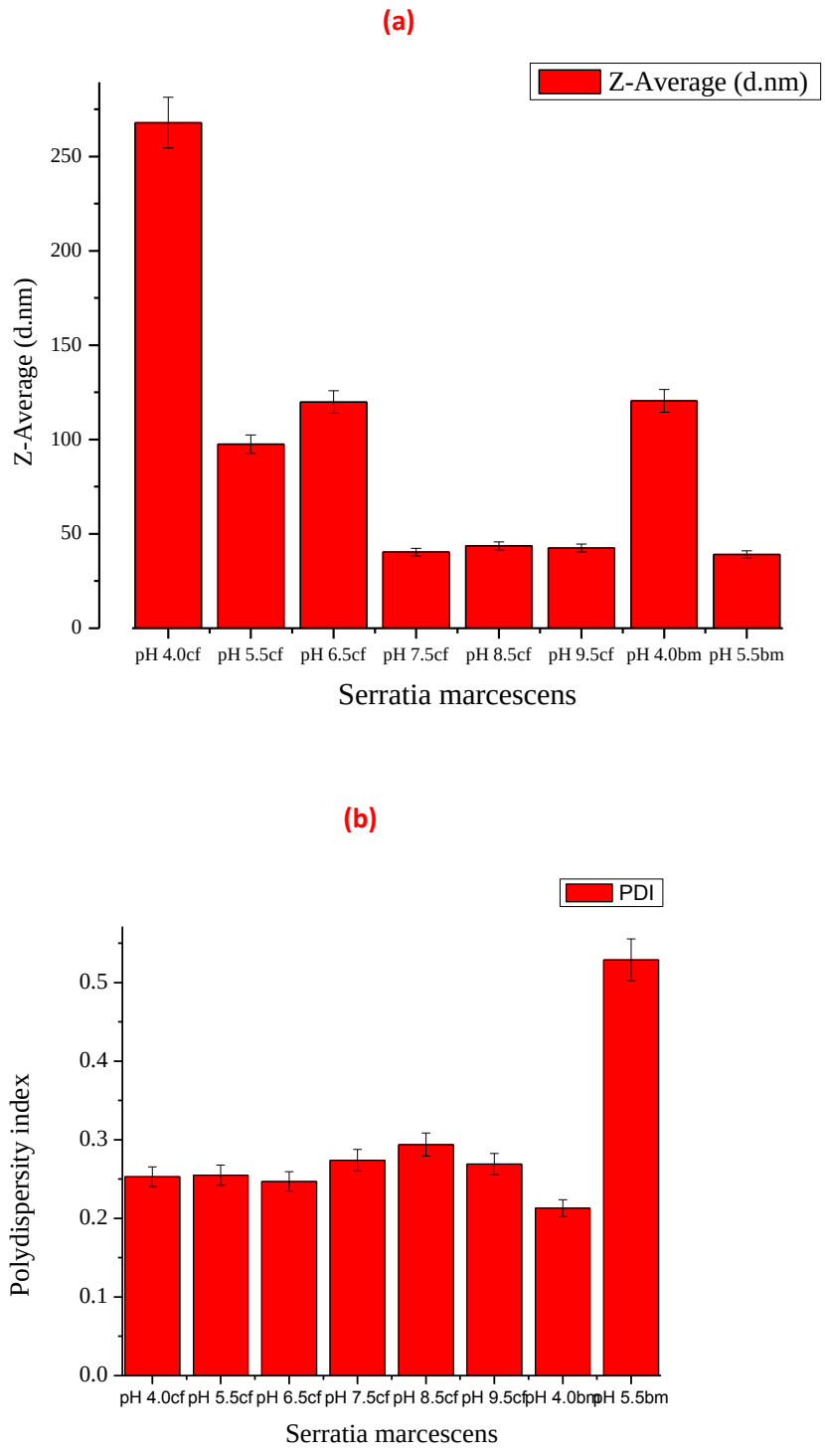

Fig.4.10 DLS Results of the *Serratia marcescens* synthesized gold nanoparticles at varying pH using the cell -free conditioned medium and biomass (a) Z-Average results and (b) PDI (cf = cell-free; bm = biomass)

TABLE 4.1 Procedure for biosynthesis of gold nanoparticles using viable biomass and cell-free conditioned medium.

	Biomass						Cell-free-Medium					
Test tubes	**Blank (0)**	**pH 4**	**pH 5.5**	**pH 6.5**	**pH 7.5**	**pH 8.5**	**Blank (0)**	**pH 4**	**pH 5.5**	**pH 6.5**	**pH 7.5**	**pH 8.5**
SAMPLE (ml)	1	1	1	1	1	1	1	1	1	1	1	1
Acetate buffer (ml)	-	1	1	1	-	-	-	1	1	1	-	-
Phosphate buffer (ml)	-	-	-	-	1	1	-	-	-	-	1	1
Sterile distilled H_2O (ml)	1	-	-	-	-	-	1	-	-	-	-	-
$HAuCl_4$ 2.5mM (ml)	-	1	1	1	1	1	-	1	1	1	1	1

TABLE 4.2 Effects of pH and time on the synthesis of gold nanoparticles from the biomass after 6 days incubation and 10 days incubation

Incubation time	**6 days**		**10 days**	
pH	Peak wavelength (nm)	Absorb.	Peak wavelength (nm)	Absorb.
4	-	-	-	-
5.5	540	0.631	-	-
6.5	550	0.543	570	1.900
7.5	520	0.613	-	-
8.5	-	-	-	-

TABLE 4.3 Effects of pH and time on the synthesis of gold nanoparticles from the cell-free conditioned medium of *Serratia marcescens***, pH** 4.0, **pH** 6.5 and **pH** 7.5

pH	**4.0**		**6.5**		**7.5**	
Time (h)	Peak wavelength (nm)	Absorb.	Peak wavelength (nm)	Absorb.	Peak wavelength (nm)	Absorb.
24	550	1.078	570	0.602	-	-
48	540	1.310	-	-	-	-
72	540	1.342	-	-	-	-
96	550	1.403	-	-	550	0.855

TABLE 4.4 DLS results of the *Serratia marcescens* synthesized gold nanoparticles showing the Z-Average and the PDI.

Serratia marcescens	**Z-Average (d.nm)**	**PDI**
pH 4.0cf	267.9±15.8	0.25±0.04
pH 5.5cf	97.5±0.4	0.26±0.01
pH 6.5cf	119.9±1.9	0.25±0.01
pH 7.5cf	40.4±0.5	0.27±0.01
pH 8.5cf	43.6±0.7	0.29±0.04
pH 9.5cf	42.6±0.4	0.27±0.01
pH 4.0bm	120.5±26.2	0.21±0.05
pH 5.5bm	39.0±1.7	0.53±0.03

Key: cf = cell-free; bm = biomass

CHAPTER 5

5.0 Folate-Conjugated Gold Nanoparticles: An Approach for Targeting Triple Negative Breast Cancer

5.1 Introduction.

Triple-negative breast cancer (TNBC) is a type of breast cancer that does not express the genes for estrogen receptor (ER), progesterone receptor (PR) and Her2. [1, 2] Approximately 15% of globally diagnosed breast cancers are designated as ER-, PR- and Her2/neu-negative. [3, 4, 5] Reports from earlier studies showed that TNBC affects mostly young women (before age 40 or 50, as compared to age 60 or older, as is the case with other types of breast cancer). TNBC is also more likely to recur earlier at distant sites. Overall, the prognosis is very poor [6, 1, 7, 8]. Also, women with TNBC are more likely to develop visceral metastases, including central nervous involvement [9].

An estimated 1 million cases of breast cancer were diagnosed worldwide in 2008 [4]. Of these, approximately 170,000 cases were of the triple-negative (ER–/PR–/HER2–) phenotype [4]. TNBC is the most prevalent type of breast cancer in Africa [10]. A report [11] suggested that about 39% of all African American pre-menopausal women diagnosed with breast cancer have TNBC. Hence, African American women are about 3 times more likely to develop TNBC than white women are [12].

Active targeting of drugs to specific regions of the body (e.g. cancer cells that over-express specific receptors) has become one of the most important objectives for the next generation of drug-delivery systems [13, 14, 15, 16, 17]. In recent times, it has been shown that new anti-cancer advances demonstrate that successful anti-cancer strategies can be developed by employing proper carrier systems that are better able to deliver probes, drugs, or genes to tumor

targets [18]. Many efforts are in progress to develop active drug targeting systems that can both allow for specific drug delivery into disease sites while also reducing the toxicological drawbacks due to nonspecific discharge of the therapeutic regimen.

Currently, most methods that are used for breast cancer treatment are based primarily on targeting cellular protein expression in tumors [19]. Estrogen receptor/progesterone receptor (ER/PR) expressing breast cancers are treated with endocrine therapy. However, the triple negative breast cancers (TNBC) that do not express ER, PR or Her2 are treated with traditional systemic cytotoxic chemotherapy alone [19]. There is therefore a need to develop new therapeutic approaches that improve the poor prognosis for TNBC. Folic acid has emerged as a promising new class of anticancer agent, and is particularly useful for TNBC [20]. Folic acid is a small vitamin, that interacts specifically with the folate binding protein (FBP) located in the caveole-like invaginations in its receptor, which is located on the cell surface [21, 22]. The folic acid-FBP complex is taken up by cells and transported through the many organelles involved in endocytotic transport, providing for cytosolic deposition [22].

The folic acid receptor is over-expressed by many types of tumor cells, including ovarian, endometrial, colorectal, breast, lung, renal, neuroendocrine carcinomas, and brain metastases [23]. By virtue of its ability to be taken up by folate receptor overexpressing tumor cells, folic acid has been widely investigated as a targeting molecule for active anticancer drug delivery. Folate, or vitamin B9, is an essential cofactor in the synthesis of purines and pyrimidines and other cellular methylation reactions, including DNA replication, proteins and lipid production [24].

The four folate receptors (folate receptor alpha, FRA; beta, FRB; gamma, FRG; and delta, FRD) constitute a family of proteins that, at least in part, mediate accumulation of folate into cells, regulate folate homeostasis and may have effects on cellular proliferation [24, 25]. FRA, a glycosylphosphatidylinositol (GPI)-anchored cell surface glycoprotein, has a very limited tissue distribution. In normal tissue, FRA is mainly expressed on the apical surface of a subset of polarized epithelial cells, including parotid, kidney, lung, thyroid and breast [20, 26-28]. Previous studies reported FRA to be expressed on carcinomas of the ovary and endometrium, non-small cell lung adenocarcinoma, clear cell renal carcinoma, colorectal carcinoma, and breast carcinoma [20, 26-34]. The limited tissue distribution of FRA and its specific expression on certain malignancies makes FRA an attractive agent for directed therapies. The different levels of expression of FRA on normal and cancerous tissues have been explored in cancer therapy. One of the cases involves drug delivery via folate-conjugated therapeutic compounds that binds both FRA and FRB [35, 36]. Another approach involves direct and tumor cell death via humanized anti-FRA monoclonal antibodies [37-39]

There is a correlation between the degree of FR expression and resistance to standard systemic chemotherapy. That is, tumors that survive standard therapy commonly have higher levels of FR, such as the triple negative breast cancer (TNBC). Hence, the idea of using folate targeting as a new approach for targeting triple negative breast cancer has developed recently. However, since some amount of folate receptors are also present in normal cells, this has raised doubts as regards the suitability of using the folate receptor as a targeting moiety [40]. However, the work done by Leamon and Reddy [41] cleared up these doubts. They found that, not only is the vasculature of normal tissue different from that of cancerous tissue, but also that the membrane localization of

the folate-receptor differs in normal and cancerous tissue. The membrane localization of folate receptors therefore plays a major role in helping to differentiate them. Epithelial cells, which form an outer layer known as skin, to protect the body's tissues from the outside and also line the interior cavities such as the gastrointestinal tract or lungs, have two distinct types of membranes. These are the basal membrane, which faces the internal tissues or the bloodstream and the apical membrane or luminal surface, which face either the environment or a cavity within the body.

The folate-receptors within normal tissues are localized on the apical membrane of the epithelial cells. This means that the folate-receptors in the choroid plexus are entirely expressed on the surface that faces toward the cerebrospinal fluid. Likewise, for the kidney and lungs, the folate-receptors are expressed on the surface that faces toward urine and air, respectively [41]. This was also reported to be true for the gastrointestinal tract. Another distinction lies in the differences between the vasculature of normal and cancerous tissues. The vasculature of tumors is filled with gaps or openings due to EPR effects, which are in the hundreds of nm size range, while the pores in the healthy tissue vasculature are much smaller, in the few nanometer size range. This means that any targeted nanotechnology treatment agent must be larger than 10 nm to prevent the particle from entering healthy tissue. Also, the treatment agent must be smaller than 100 nm to allow it to enter the tumor. Therefore, the size of the nanoparticle treatment agent should prevent it from accessing the folate-receptor in healthy tissue. This may not apply if the patient has tissue damage, where the vasculature is damaged, or has been exposed to permeability enhancers, such that pore size is increased in normal tissues. Since the nanoparticle treatment agent will be able to diffuse into the tumor through the defects in the tumor vasculature, the particles will only be exposed to the folate-receptor on the cancer cells [42].

In all, the limited and well localized tissue distribution of the folate-receptor within healthy tissues, the defects in tumor vasculature, and the high expression level within several types of cancer make folate an appropriate choice of targeting moiety for nanotechnology-based cancer treatment. In this paper, membrane-bound FR (FRA and FRB), which is linked to cell surfaces via a glycosyl-phosphatidylinositol (GPI) anchor [43] and internalizes folates by receptor-mediated endocytosis, was used as the targeting moiety.

Prodigiosin derived from cell-free medium of *Serratia marcescens* is used as the drug of choice in this work, due to the ease of its extraction and purification from *Serratia marcescens*. Prodigiosin is a secondary metabolite alkaloid with a unique tripyrrole chemical structure. It is a red pigment isolated from a few species, such as *Serratia*, *Pseudomonas* and *Streptomyces* [44, 45]. AuNPs synthesized using locally sourced materials of biological origin and functionalized with the ligand, folate, are being studied as a possible remedy for the treatment of triple negative breast cancer in resource poor environments.

5.2.0 Experimental Procedures

5.2.1 Conjugation of Gold Nanoparticles with Folate

5.2.1.1 Preparation of the N-Hydroxysuccinimide Ester of Folate (NHS-Folate)

This preparation was done according to the method of Li et al., 2012 [46] (Figure 5.1). Briefly, 1g of folic acid (Alfer Aesar, 30 Bond Street, Ward Hill, MA, USA. Lot No. F29X146) was dissolved in 20 ml dimethyl sulfoxide (DMSO) (Qualikems Fine Chem Pvt. Ltd. 5531, Basti Harphool Singh, Sadar Thana Road, Delhi, India. Product number: DO11112) in a 250 ml conical flask. Then, 0.5 ml of Triethylamine (Pharmacos Ltd, Southend-on-sea, Essex, England, Batch number 8233) was added, followed by 0.94g of N, N' Dicyclohexyl Carbodiimide (DCC)

(Sigma Aldrich, St. Louis, MO, USA. Lot # SHBC064V) and 0.52 g N- Hydroxysuccinamide (NHS) (Sigma Aldrich, St. Louis, MO, USA. Lot no. MKBK170V). The flask was stirred in the dark for 12 hours using a magnetic stirrer at 600 rpm. After this, the insoluble dicyclohexyl urea formed was filtered off using Whatman filter paper No 1. The filtrate was then poured into a flask containing ice-cold 98% diethyl ether (Fisher Scientific, Fair Lawn, NJ, USA), and subsequently 30% acetone (Merck KGaA 642771 Darmstadt, Germany. Index no.606-001-00-8) was then added to the flask. Instantly, precipitates of NHS-Folate were formed. The solution was centrifuged at 3000g for 5min at 4°C and then washed twice with ether. A yellow powder of NHS-Folate ester was obtained after drying at room temperature. It was then stored in the desiccator at room temperature (~25°C).

5.2.1.2 Thiolation of Gold Nanoparticles

The process of self-assembled monolayer (SAM) was adopted, following the method of Shiao-wen *et al.*, 2008 [47]. Cyclohexane Mercaptan, 99% (Acros Organics, New Jersey, USA. Lot no. A20234299) was used. First, 1 mM Thiol solution was prepared in a fume hood by measuring 6 µl of cyclohexane Thiol into a beaker containing 50 ml of 50% ethanol, and then stirred at 500 rpm for 20minutes to mix. In another 50 ml beaker, 10 ml of, AuNPs which we biologically synthesized from *Serratia marcescens* and *Nauclea latifolia*, as described earlier [48-49], was stirred using a magnetic stirrer that was set at 500 rpm. Then 2 ml of 1 mM Thiol (aqueous?) solution was added to the beaker containing the AuNPs before stirring continuously for 30 minutes at room temperature.

5.2.1.3 Conjugation of NHS-Folate with AuNPs

The method of Stella [50] was adopted in this work with some minor modifications. Briefly, 10 mg of NHS-Folate powder was prepared as described above. This was then weighed and dissolved in 200 µl DMSO in a 50 ml beaker. Subsequently, 4 ml of thiolated gold nanoparticles solution, with a concentration of 5 mg/ml, was added and stirred at 500 rpm with a magnetic stirrer at room temperature. The pH was adjusted to 9.0 with 5mM carbonate/bicarbonate buffer at pH 11.5. The reaction was allowed to go on for 1 hour, while still stirring. The resulting Folate-S-AuNPs was purified by size exclusion chromatography, using a 3x14 Column of Sephadex G-50 superfine and 5mM Carbonate / Bicarbonate buffer pH 9.0 was used to elute the sample.

The Folate-S-AuNPs conjugate was eluted in the void volume [50]. Different fractions were collected and UV/Visible spectroscopy was carried out to detect the fractions containing AuNPs-Folate (data not shown). The UV/Vis result was compared with that of the unconjugated AuNPs. The folate – AuNPs fractions were further purified by dialyzing against 5mM bicarbonate buffer pH 9.0 and double distilled water (DDH2O). Finally, the anti-cancer drug, prodigiosin, earlier extracted and purified [51], was added. One portion (half) was lyophilized to obtain the Folate-AuNPs-prodigiosin powder for long-term (up to 6 months) storage, while the other portion (half) was stored as a solution at 4°C for immediate use.

5.2.2 Characterization of the conjugated Gold Nanoparticles

5.2.2.1 UV-Vis Spectroscopy

UV/Vis Spectroscopic analysis was carried out at different stages of the conjugation process using Biochrom Libra 522 spectrophotometer (Cambridge, England). The absorbance of the

gold nanoparticles was thus measured before and after the conjugation. Plots of absorbance against wavelength for before and after conjugation were then made (Figure 5.2).

5.2.2.2 Fourier Transformed Infra Red spectroscopy (FTIR)

A SHIMAZU FTIR-8400S Infra Red spectrophotometer (SHIMADZU CORPORATION, International Marketing Division 3. Kanda-Nishikicho 1-chome, Chiyoda-ku, Tokyo 101-8448, Japan) was used to analyze both unconjugated and conjugated samples. Solutions of the nanoparticles were subjected to infrared analysis using the FTIR spectrophotometer. The IR spectrum was collected for the mid-IR range of 400 – 4000 cm-1 and analyzed using IR Pal software (Wolf's Shareware and Freeware Chemical Utilities, V 2.0 written by Wolf van Heeswijk, 2010, Bekijk het (Netherland)).

5.2.2.3 Transmission Electron Microscopy (TEM)

The shapes and sizes of the synthesized gold nanoparticles were studied in a transmission electron microscope (CM100 Transmission Electron Microscope, Philips/FEI Corporation, Hillsboro, OR, USA). Prior to TEM examination, drops of gold nanoparticle solutions were placed on copper grids (CF200-Cu, Electron Microscope Sciences, Hatfield, PA, USA) and allowed to dry under ambient conditions (28-30°C). The grids were then mounted and imaged in the Transmission Electron Microscope at the Princeton Institute for the Science and Technology of Materials (PRISM) at Princeton University, New Jersey, USA.

5.2.2.4 Dynamic Light Scattering (DLS)

A series of 1:10 dilution of the samples was made with Dulbecco's Phosphate Buffer Saline (DPBS) (Sigma Aldrich, St. Louis, MO, USA. D8537) at pH 9 that was used for the DLS analysis. The machine was a BIC 90 plus particle size analyzer that was equipped with a

Brookhaven BI-9000 AT digital correlator (Brookhaven Instruments Corp., Holtsville, NY, USA). The light source was a solid-state laser operating at 658 nm with 30 mW power, while the signals were detected by a high-sensitivity avalanche photodiode detector. All of the measurements were conducted in triplicate at a fixed scattering angle of 90° at 25 ± 1 °C. Each sample was analyzed for 6 minutes (3 runs per sample at 2 minutes per run).

5.2.2.5 Helium Ion Microscopy (HIM)

Helium Ion Microscopy (HIM) was carried out at the Microscopy facility in the Department of Physics at Rutgers University, Piscataway, New Jersey, USA. The folate conjugate sample was viewed with 1µm and 4 µm fields of view. The working distance was 7.3 mm, while the blanker current was 0.1 pA. The acceleration voltage was 30 kV, while the dwell time was 1 µs. The line averaging for the 1µm field of view image was 64, while that for the 4 µm field of view was 128.

The single most critical parameter in nanotechnology imaging is resolution. The helium ion microscope is a new type of microscope that uses helium ions for surface imaging and analysis. It works like the scanning electron microscope, but it uses a focused beam of helium ions instead of electrons [52]. The helium ions can be focused into a smaller probe size and provide a much smaller interaction volume at the sample surface compared to electrons. Also, it generates higher resolution images with better material contrast and improved depth of focus. The high resolution arises from the use of a finely sharpened needle and a process that strips individual atoms away from the source until an atomic pyramid is created with just three atoms at the very end of the source tip. The HIM achieves a resolution of less than 0.3 nm at energy of 25-30 kV and can deliver beam currents between 1 fA and 25 pA. [53]

5.2.3 Adhesion Measurement

5.2.3.1 AFM tip and substrate coating/characterization:

Prior to the adhesion measurements, a breast cancer cell line (MDA-MB-231cells) and a normal breast cell line (MCF 10A cells) were cultured and prepared. About 20 µl of 1 x 105 MDA-MB-231 cells was cultured in 60 x15 mm Falcon cell culture Petri dishes at 37°C. This was done under standard atmospheric pressure in an L-15 medium supplemented with 100 I.U./mL penicillin/100 lg/mL streptomycin and 10% FBS.

In the case of normal breast cells, 20 µl of 1 x 10^5 of MCF-10A breast cells was incubated at 37 ^oC in 5% CO_2 in DMEM/F12 medium (Invitrogen # 11330-032) supplemented with 5% horse serum (Invitrogen # 16050-122), 30 ng/ml murine Epidermal Growth Factor (Peprotech #315-09), 0.5 µg/ml hydrocortisone (Sigma, #H-0888), 100 ng/ml cholera toxin (Sigma #C8052-1MG), 10 µg/ml insulin (Sigma #I-882-100MG), 1% Penicillin-Streptomycin (ATCC #30-2300 or Invitrogen #15070-063), and 0.2% amphotericin (Gemini Bioproducts, #400-104), respectively.

After 72 h of culturing, the cell confluence was about 70%. Both cell samples were then washed twice with PBS solution (1X PBS at 4°C) and fixed in 3.7% formaldehyde (Guangzhou Langs Chemical Additives Company Limited, Guangdong, China # LX-5512) solution for 15 minutes. The fixed cells were then rinsed three times with PBS. This was followed by three rinses with distilled-deionized water. This last rinse with water was used to remove possible salt deposits that may have resulted from the prior PBS rinses. Finally, the fixed cells were dried in a vacuum desiccator for two hours.

The AFM tips were coated by a simple dip-coating method [54]. The bare AFM tips were dip-coated with gold nanoparticles, folate or prodigiosin (PG). This was done by immersing them into their respective solutions for about 10 s to maximize the AFM tip surface contact with the solution. The tips were then air-dried for less than a minute, after which they were dipped for a second time, again for 10 s. This procedure was repeated 3–5 times to complete the coating process. The folate-AuNPS conjugate and AuNPS solutions were used at a concentration of 0.5 mg/ml.

Subsequently, the coated AFM tips were air-dried for a minimum of 24 h. They were then observed under a scanning electron microscope. The prodigiosin, folate and AuNPs substrates were prepared by spreading each of the solutions on glass sheets to form thin layers. These were then allowed to dry in air for a minimum of 24 h. The surface morphologies of the coated substrates and the uncoated glass substrates (control surfaces) [55] were then characterized using a Dimension 3100 Atomic Force Microscope (AFM) that was operated in the tapping mode (Dimension 3100, Bruker Instruments, Woodbury, NY, USA).

In order to confirm that the AFM tip samples were coated with gold nanoparticles, the coated and bare tips were imaged under a Phillips Model FEI XL30 field emission gun scanning electron microscope (SEM) (Phillips Electronics N.V., Eindhoven, The Netherlands). The images were obtained using secondary electron imaging. The images of the coated AFM tips were obtained before and after the AFM experiments. In this way, possible detachment or delamination of the coatings could be observed on the coated AFM tips.

Hence, since pull-off forces were only accepted for cases in which the coatings were still present after the pulloff experiments, the measured pull-off forces were confirmed to be due to the intended bi-material pairs. The spring constants of the coated and uncoated tips were measured

using the thermal tune method [56, 57]. This was measured because the actual spring constants are needed to obtain the true adhesion forces from Eq. (1). This also accounts for batch-to-batch variations in the spring constants, as well as the effects of coatings on the cantilever stiffness [55,56] The pull-off measurements were obtained under ambient conditions (room temperature of 22–23 °C and a relative humidity of 40–45%).

The resulting pull-off force represented as F, is a measure of the adhesion between the nanoparticle/drug complex and the breast cancer/normal breast cells. This is given by Hooke's law to be:

$$F = k\delta \qquad (1)$$

where k is the stiffness of the AFM cantilever and d is the displacement of the AFM tip at the onset of pull-off.

5.3.0 Results and Discussion

5.3.1 UV-Vis Analysis

The UV-Vis spectroscopy of the biosynthesized AuNPs before conjugation and this showed a maximum absorption peak at 540 nm (Figures 5.2 a - 5.2 b). The measurements recorded after conjugation showed a broadening and decrease of the peak. There was also a red shift of the SPR from 540 nm to 550 nm. This red shift has been attributed to the intermolecular hydrogen bonding that exists within the molecules of AuNPs linked by different ligands [58-60]. It has also been observed that a second peak occurred at 365 nm (in 5.2 a) and 360 nm (in 5.2 b), which confirmed the attachment of folate to the gold nanoparticles. This is in agreement with the results of other researchers [61-63] who showed that the absorption maxima at 360 nm can be used for

confirming the covalent attachment of the folate to Atp-AuNP (4-aminothiophenol-gold nanoparticles).

5.3.2 FTIR Analysis

FTIR analysis was performed to further confirm the conjugation of Folate-S-AuNPs. Figure 5.3a shows the FTIR spectrum of gold nanoparticles produced from *Nauclea latifolia* before conjugation, while figure 5.3b shows the spectrum after conjugation. The results revealed carboxylic acid (C=O) stretching vibrations at 1670 cm-1 originating from folic acid. Figure 5.3b showed the appearance of double peaks at 1010 cm-1 and 930 cm-1 corresponding to carbonyl stretching (C=S) and –SH stretching. [62] This accounts for the presence of the thiol group in the reaction. Another observable difference between the conjugated and the unconjugated gold nanoparticles is the presence of a broad peak between 3200 – 3400 cm-1 (Figure 5.3a) Also the sharp peak at 3450 cm-1 (Figure 5.3b) corresponds to O-H stretching vibrations.

5.3.3 TEM Analysis

The TEM images of the conjugated gold nanoparticles obtained from both *Serratia marcescens* (SM), at pH 4.5 and 8.5, and *Nauclea latifolia* without pH adjustment (NLO) are presented in Figures 5.4a – 5.4c. The results revealed the SM pH 4.5 AuNPs had different shapes, ranging from hexagonal to prismatic shapes. These shapes provide larger surface areas for the specific attachment of ligands than spherical shapes do. In contrast, the nanoparticles obtained from the pH 8.5 samples were monodispersed and spherical. They also had an average diameter of ~ 21-30 nm (Figure 5.4b). The AuNPs from *Nauclea latifolia* (Figure 5.4c) had some unique shapes,

ranging from rectangular prisms to cuboidal and hexagonal prism shapes. According to Toy et al., [64] the shape of nanoparticles has been shown to dictate the interaction of nanoparticles with cell membranes. The shape of nanoparticles determines their clearance by macrophages of the reticuloendothelial organs, it also affects endocytosis by normal and cancer cells.

A histogram of the nanoparticle sizes is presented in Figure 5.5a. This shows that, at pH 4.5, most of the gold nanoparticles synthesized from *Serratia marcescens* had sizes in the range of 40-50 nm. This is in the size range that is most suitable for drug delivery [62-64] (Figure 5.5a). At a pH of 8.5, the average nanoparticle sizes were about 21 – 30 nm in diameter (figure 5.5b), while the gold nanoparticles obtained from *Nauclea latifolia* (without pH adjustment) (NLO), are smaller, with average sizes of ~11 - 20 nm (Figure 5.5c).

Selected area electron diffraction (SAED) patterns of the AuNPs are presented in Figures 5.6a-5.6b. These represent the four-fringe pattern of gold nanoparticles, which corresponds to the fcc metal structure of gold ((111), (200), (220), (311)). This analysis confirmed the formation of pure metallic gold nanoparticles. The observed ring pattern is consistent with the crystalline structure of face-centered cubic (FCC) gold. This confirms that the biogenic nanoparticles observed in the TEM images are crystalline gold. The Scherrer ring pattern characteristic of face-centered cubic gold was also clearly observed. This confirmed that the observed structures in the TEM images were nanocrystalline gold.

5.3.4 HIM Analysis on the NL nanoparticles

The images obtained from the Helium Ion Microscopy (HIM) are presented in Figures 5.7a – 5.7b. Figure 5.7a presents folate conjugated AuNPs, with 1 µm field of view, while Figure 5.7b presents folate conjugate with a 4µm field of view. The images show clearly that the nanoparticles are monodispersed, with evidence of attachment of folate in the surface of the

nanoparticles, as indicated by the presence of buffy coats around the nanoparticles. This further confirmed that the conjugation was actually successful. Figure 5.8 shows a histogram of the particle size distributions. Nanoparticles, with diameters of ~ 21-30 nm had the highest frequency, followed by those with sizes of ~ 31 – 40 nm. These sizes are in a range that is suitable for drug delivery [65-67].

5.3.5 Energy Dispersive X-ray (EDX)

The image shown in Figure 5.9 shows an energy-dispersive X-ray (EDX) spectrum recorded in the spot profile mode from folate conjugated *Serratia marcescens* gold nanoparticles synthesized at pH 8.5. Strong EDX signals were detected from the gold nanoparticles. EDX signals were also detected from Cu, Si, K, and Fe atoms. The Cu, signals are likely to be X-ray emission from the copper grids that were used to mount the samples. Also, the silicon signal is attributed to the glass used for sample preparation, while the Fe is from the prodigiosin that was attached to the gold nanoparticles. This result further confirmed that the gold nanoparticles were still intact after conjugation. They also confirmed that the anti-cancer drug, prodigiosin, was also present.

5.3.6 Dynamic Light Scattering (DLS)

The results of the DLS experiments are presented in Figures 5.10 a - 5.10 d, and also in Tables 5.1 and 5.2. For the gold nanoparticles synthesized with *Serratia marcescens* (SM), at pH 4.5, the hydrodynamic diameter for the conjugated samples, both with and without the anti-cancer drug (prodigiosin) were 57.93±0.24 nm and 58.71 ±0.39 nm, respectively. These diameters are considered to be good for drug delivery [63, 65, 68]. Their PDI, however, showed moderate polydispersity (Figures 5.10 a -5.10 b and Table 5.1). At a pH of 8.5 the z-average of the conjugated AuNPs for with and without prodigiosin was higher, having values of ~ 83.7 ±1.7 nm

and 85.4±1.1 nm. Their PDI were 0.191±0.014 and 0.166±0.003, which indicated they have a good level of monodispersity. AuNPs at a pH of 8.5, therefore, are better candidates for drug delivery than those produced at pH 4.5, based on the polydispersity index.

For the gold nanoparticles synthesized with *Nauclea latifolia* leaf extract, the Z-average and PDI were determined for samples produced at varying pH before conjugation, after conjugation and with prodigiosin. There was a consistent increase in the hydrodynamic diameter of the samples labeled NLO (AuNPs without pH adjustment), as shown by the Z-averages, which were 58.9±0.3nm, for gold nanoparticles before conjugation, 62.7±0.6nm after conjugation with folate, and 70.5±0.2nm, after attaching the prodigiosin drug (Figure 5.10c and Table 5.2). A similar increment was also noticed in pH 7.5, 8.5 and 9.5 which further confirms that when molecules are added to bare nanoparticles, the diameter increases [69].

The changes in the hydrodynamic diameters of the conjugated AuNPs produced in the current study are consistent with reports by other researchers [69] who have reported changes in the diameter of the AuNP to 48.5 nm, with the addition of PEG coatings. Takae *et al*., [70] have also observed an increase in nanoparticle diameter (from 20 to 33.3 nm) after functionalization with 6,000 Mw PEG. Furthermore, Arinda *et al.* [71] found that functionalization with 5,000 Mw PEG increased AuNP diameter from 50 to 89 nm.

The PDI of the sample NLO (Figure 5.10d and Table 5.2) was close to 0.2, even after conjugation, indicating moderate monodispersity. The PDI for the nanoparticles produced at other pH ranges varied. However, somewhat interestingly, it was observed that the PDI decreased with increasing prodigiosin content. In any case, hydrodynamic diameters are very important for understanding nanoparticle performance in different biological assays, as well as for understanding the in-vitro transport of nanoparticles in different biological fluids.

5.3.7 Adhesion measurements

The SEM images of the bare AFM tips and the coated tips are shown in Figure 5.11 (a & b), while the adhesion force measurement for a bare tip, and tips coated with AuNPs, folate and folate conjugated AuNPs are presented in Figure 5.11c. The force of adhesion between tips and normal breast cells and tips and breast cancer cells shown in table 5.3. The results showed that the bare tips had a force of 10 nN for the normal cells and 16 nN for cancerous cells. When the tips were coated with either AuNPs, folate, PG, or AuNPs conjugated with folate, a significant increase in the force of adhesion was observed. The highest adhesion was noticed in the AuNPs/folate conjugate, with the adhesion force rising up to 80nN for the interaction with the breast cancer cells and 25 nN with the normal breast cells. By implication, this shows that conjugation of gold nanoparticles to the ligands improves their attachment to the cells, with the force of adhesion being more than three-fold higher in the cancer cells than the normal cells. The higher adhesion observed in the cancerous cells than in the normal cells confirm the specificity of the ligands.

5.3.8 Implications

The prerequisite for every possible application of nanoparticles in nanomedicine is the proper surface functionalization of such nanoparticles, which determines their interaction with the environment [72]. In addition, these interactions ultimately affect the colloidal stability of the particles. They may also lead to a controlled assembly or delivery of nanoparticles to specific targets, e.g. by the specific attachment of functional groups to receptors on the cell surface(s). Thiol groups are considered to show the highest affinity to noble metal surfaces, such as gold. [73] Hence, in this work, an alkanethiol was linked to gold nanoparticles by a Self-Assembled

Monolayer (SAM) process that occurred via a physisorption reaction [74]. In this way, the targeting moieties were attached to the gold nanoparticles.

From the results, folate molecules were successfully conjugated to gold nanoparticles, as shown by the UV-Vis, the FTIR and the HIM results (Figures 5.2, 5.3 and 5.7). Dynamic light scattering was also used to monitor the hydrodynamic size and colloidal stability of the gold nanoparticles. [75]. The DLS revealed that the average dynamic size of the conjugated gold nanoparticles ranged from 57.93±0.24 nm and 58.71 ±0.39 nm, when using gold nanoparticles synthesized by *Serratia marcescens* and 62.7±0.6-82.3±7.9 nm with gold nanoparticles synthesized by *Nauclea latifolia.*

DLS provided statistically representative data about the hydrodynamic size of these nanomaterials. In- situ, real time monitoring of AuNPs suspension by DLS provides useful information regarding the kinetics of the aggregation process and, at the same time, gives quantitative measurements of the sizes of the particle clusters that were formed [53].

The PDI results showed that after conjugation with folate, the nanoparticles were moderately polydispersed, and can still be used for drug delivery. Also, from the current results, we can deduce that the conjugated gold-nanoparticles synthesized by SM at pH 8.5, and the gold nanoparticles synthesized by *Nauclea latifolia* (NLO), are the best candidates for drug delivery, based on their z-averages and PDI values. Furthermore, the DLS results can be used to probe the layer thicknesses of the macromolecules adsorbed onto the surfaces of the AuNPs while the SAED results further confirmed the presence of gold nanoparticles after conjugation. The adhesion force measurement with AFM indicated that the folate conjugated gold nanoparticles had a higher force of adhesion than the unconjugated gold nanoparticles to both breast cancer cells and normal cells.

With the successful conjugation of folate to the synthesized gold nanoparticles, the next step now is to carry out in-vitro targeting of triple negative breast cancer cells (MDA-MB-231). The folate conjugated AuNPs with the drug payload is expected to be transported into the cell cytoplasm via the endocytotic pathway, with the expected result of cell death.

5.4.0 Summary and Concluding Remarks

Gold nanoparticles synthesized from bacteria (*Serratia marcescens*) and plant, (*Nauclea latifolia*) were conjugated with folate molecules through gold-thiol linkages and carbodiimide chemistry. The conjugation was then confirmed using UV-Vis spectroscopy, which showed the presence of a second peak at 365 nm indicating the presence of folate. Helium ion microscopy also revealed the attachment of another layer to the gold core, while TEM, FTIR and DLS results all confirmed the conjugation of the gold core to folate. The PDI results points to the fact that after conjugation, the gold nanoparticles from SM synthesized at pH 8.5 were moderately monodipersed with PDI of 0.166±0.003. These nanoparticles also had a z-average of 85.44±1.07. Therefore, the gold nanoparticles synthesized by SM at pH 8.5 are the best candidate for the conjugation work because these nanoparticles have the best properties for drug delivery.

References

1. Dent, R., Trudeau,M., Pritchard, K.I., Hanna, W.M., Kahn, H.K., Sawka, C.A., Lickley, L.A., Rawlinson, E., Sun, P., Narod, S.A.: Triple-negative breast cancer: clinical features and patterns of recurrence. *Clin Cancer Res*. **13,** 4429-4434 (2007).
2. Perou, C.M., Jeffrey, S.S., van de Rijn, M., Rees, C.A., Eisen, M.B., Ross, D.T., Pergamenschikov, A., Williams, C.F., Zhu, S.X., Lee, J.C., Lashkari, D., Shalon, D., Brown, P.O., Botstein, D.: Distinctive gene expression patterns in human mammary epithelial cells and breast cancers. *Proc Natl Acad Sci USA*. **96,** 9212–9217 (1999).

3. Jemal, A., Bray, F., Center, M.M., Ferlay, J., Ward, E., Forman,D.: Global cancer statistics. CA. *Cancer J Clin*. 61, 69-90 (2011).

4. Anders, C.K., Carey, L.A.: Biology, metastatic patterns, and treatment of patients with triple-negative breast cancer. *Clin Breast Cancer*. **9,** S73- S81(2009).

5. Hudis, C.A., Gianni, L.: Triple-negative breast cancer: an unmet medical need. *Oncologist.* **16**, 1-11(2011).

6. Schneider, B.P., Winer, E.P., Foulkes, W.D., Garber, J., Perou, C.M., Richardson, A., Sledge, G.W., Carey, L.A.: Triple-negative breast cancer: risk factors to potential targets. *Clin Cancer Res.* **14,** 8010-8018 (2008).

7. De Laurentiis, M., Cianniello, D., Caputo, R., Stanzione, B., G. Arpino, G.,G S. Cinieri, V. Lorusso, S. De Placido: Treatment of triple negative breast cancer (TNBC): current options and future perspectives. *Cancer Treat Rev.* **36**, S80- S86 (2010).

8. Chacon, R.D., Costanzo, M.V.: Triple-negative breast cancer. *Breast Cancer Res*. **12,** S3 (2010).

9. Lin, N.U., Claus, E., Sohl, J., Razzak, A.R., Arnaout, A ., Winer, E.P.: Sites of distant recurrence and clinical outcomes in patients with metastatic triple-negative breast cancer: high incidence of central nervous system metastases. Cancer. 113, 2638–2645 (2008).

10. Foulkes, W.D., Smith, I.E., Reis-Filho, J.S.: Triple-negative breast cancer. *N Engl J Med*. **363**(20), 1938-48 (2010).

11. Carey, L.A., Perou, C.M., Livasy, C.A., Dressler, L.G., Cowan, D., Conway, K., Karaca, G., Troester, M.A., Tse, C.K., Edmiston, S., Deming, S.L., Geradts, J., Cheang, M.C., Nielsen, T.O., Moorman, P.G., Earp, H.S., Millikan, R.C.: Race, breast cancer subtypes, and survival in the Carolina Breast Cancer Study. JAMA. 295(21), 2492-2502 (2006).

12. Kaplan, H.G., Malmgren, J.A., Atwood, M.K.: Impact of triple negative phenotype on breast cancer prognosis. Poster presented at: 29th Annual San Antonio Breast Cancer Symposium,San Antonio, TX; (2006) .

13. Zeng, F., Lee , H., Allen, C.: Epidermal Growth Factor-Conjugated Poly(ethylene glycol)-block-Poly(delta-valerolactone) Copolymer Micelles for Targeted Delivery of Chemotherapeutics. *Bioconjugate Chemistry*. 17, 399-409(2006).

14. Shi,M., Wosnick, J. H., Ho, K., Keating, A., Shoichet, M. S. Angew. Chem. Int. Edn. 46, 6126 (2007).

15. Nasongkla, N., Bey, E., Ren, J., Ai,H., Khemtong,C., Guthi, J. S., Chin, S. F., Sherry, A. D., Boothman, D. A., Gao, J. *Nano Lett.* **6**, 2427(2006).

16. Torchilin, V. P. , Lukyanov, A. N., Gao, Z., Papahadjopoulos-Sternberg, B. Proc. Natl. Acad. Sci. USA. 100, 6039 (2003).

17. Allen, T. M. Ligand-targeted therapeutics in anticancer therapy.Nature Rev. *Cancer* **2**, 750 – 763 (2002).

18. Paolo, C., Stefano, S., Alessandra, S., Tommaso, C., Roberto, F., Maurizio, F., Marco , F., Sabrina, P.: Synthesis and Physicochemical Characterization of Folate-Cyclodextrin Bioconjugate for Active Drug Chem. Delivery. *Bioconjugate.* **14**, (8) 99-908 (2003).

19. Anders, C., Carey, L. A.. Understanding and Treating Triple-Negative Breast Cancer. *Oncology (Williston Park).* **22**(11) 1233–1243 (2008).

20. O'Shannessy, D.J., Yu, G., Smale, R., Fu, Y-S ., Singhal, S., Thiel, R.P., Somers, E.B., Vachani, A.: Folate Receptor Alpha Expression in Lung Cancer: Diagnostic and Prognostic Significance. *Oncotarget* 3(4), 414–425 (2012).

21. Antony, A.C.: Folate receptors. Annu. Rev. Nutr. 16, 501–521 (1996)

22. Armstrong, D.K., Bicher, A., Coleman, R.L., Gibbon, D.G., Glenn, D., Old, L., Senzer, N.N., Schneeweiss, A., Verheijen, R.H., White, A.J., Weil, S.: Exploratory phase II efficacy study of MORAb-003, a monoclonal antibody against folate receptor alpha, in platinum-sensitive ovarian cancer in first relapse. *J. Clin. Oncol*. 26, 5500 (2008).

23. Bagnoli, M., Canevari, S., Figini, M., Mezzanzanica, D., Raspagliesi, F., Tomassetti, A., Miotti, S.: A step further in understanding the biology of the folate receptor in ovarian carcinoma. *Gynecol. Oncol*. **88**, S140–S144 (2003)

24. Elnakat, H., Ratnam, M.: Distribution, functionality and gene regulation of folate receptor isoforms: implications in targeted therapy. *Adv Drug Deliv Rev* **56**(8) 1067–1084 (2004).

25. Kelemen, L.E. The role of folate receptor α in cancer development, progression and treatment: Cause, consequence or innocent bystander? *International Journal of Cancer* **119** (2) 243–250(2006).

26. Weitman, S.D., Lark, R.H, Coney, L.R., Fort, D.W. , Frasca, V., Zurawski V.R., Kamen, B.A.: Distribution of the folate receptor GP38 in normal and malignant cell lines and tissues. *Cancer Res.* **52**(12), 3396–3401(1992a)

27. Weitman, S.D, Weinberg, A.G., Coney, L.R., Zurawski, V.R., Jennings D.S., Kamen, B.A.: Cellular localization of the folate receptor: potential role in drug toxicity and folate homeostasis. *Cancer Res* **52**(23), 6708–6711(1992b)

28. O'Shaughnessy, J., Schwartzberg, L. S., Danso, M. A., Rugo, H. S., Miller, K., Yardley, D. A., Carlson, R. W., Finn, R. S., Charpentier, E., Freese, M., Gupta, S., Blackwood-Chirchir, A., Winer, E. P.: A randomized phase III study of iniparib (BSI-201) in

combination with gemcitabine/carboplatin (G/C) in metastatic triple-negative breast cancer. *J Clin Oncol*. **29**, Supplement 15 s): Abstract 1007(2011).

29. Franklin, W.A., Waintrub, M., Edwards, D, Christensen, K., Prendegrast,P., Woods, J., Bunn, P.A., Kolhouse, J.F. : New anti-lung-cancer antibody cluster 12 reactswith human folate receptors present on adenocarcinoma. *Int J Cancer Suppl*. **8**, 89–95(1994).

30. Ross, J.F., Chaudhuri, P.K., Ratnam, M.: Differential regulation of folate receptor isoforms in normal and malignant tissues in vivo and in established cell lines. Physiologic and clinical implications. *Cancer*. **73**(9), 2432–2443(1994)

31. Wu, M., Gunning, W, Ratnam, M.: Expression of folate receptor type alpha in relation to cell type, malignancy, and differentiation in ovary, uterus, and cervix. *Cancer Epidemiol Biomarkers Prev*. **8**(9), 775–782 (1999)

32. Bueno, R., Appasani, K., Mercer, H., Lester, S., Sugarbaker, D.: The alpha folate receptor is highly activated in malignant pleural mesothelioma. *J Thorac Cardiovasc Surg*. **121**(2), 225–233 (2001)

33. Parker, N., Turk, M.J., Westrick, E., Lewis, J.D., Low, P.S., Leamon, C.P.: Folate receptor expression in carcinomas and normal tissues determined by a quantitative radioligand binding assay. *Anal Biochem* **338** (2), 284–293 (2005)

34. Shia, J., Klimstra, D.S., Nitzkorski, J.R., Low, P.S., Gonen, M., Landmann, R., Weiser, M.R., Franklin, W.A., Prendergast, F.G., Murphy, L., Tang, L.H., Temple, L., Guillem, J.G., Wong, W.D. Paty, P.B. : Immunohistochemical expression of folate receptor alpha in colorectal carcinoma: patterns and biological significance. *Hum Pathol*. **39** (4) 498–505 (2008).

35. Low, P.S., Kularatne, S.A.: Folate-targeted therapeutic and imaging agents for cancer. *Curr Opin Chem Biol*. **13**(3) 256–262 (2009).

36. Dosio, F., Milla, P., Cattel, L.: EC-145, a folate-targeted Vinca alkaloid conjugate for the potential treatment of folate receptor-expressing cancers. *Curr Opin Investig Drugs*. **11**(12), 1424–1433 (2010).

37. Ebel, W., Routhier, E.L., Foley, B., Jacob, S., McDonough, J.M., Patel, R. K., Turchin, H.A., Chao, Q., Kline, J.B., Old, L.J., Phillips, M.D., Nicolaides, N.C., Sass, P.M., Grasso, L.: Preclinical evaluation of MORAb-003, a humanized monoclonal antibody antagonizing folate receptor alpha. *Cancer Immun*. **7**, 6 (2007)

38. Konner, J.A., Bell-McGuinn, K.M., Sabbatini, P., Hensley, M.L., Tew, W.P., Pandit-Taskar, N., Vander Els, N., Phillips, M.D., Schweizer, C., Weil, S.C., Larson, S.M., Old, L.J.: Farletuzumab a humanized monoclonal antibody against folate receptor alpha, in epithelial ovarian cancer: a phase I study. *Clin Cancer Res*. **16**(21) 5288–5295 (2010).

39. Elwood, P.C., Nachmanoff, K., Saikawa, Y., Page, S.T., Pacheco, P., Roberts, S., Chung, K-N.: The divergent 5 termini of the human folate receptor (hFR) mRNAs

originate from two tissue-specific promoters and alternative splicing: characterization of the hFR gene structure. *Biochemistry*. **36** 1467–1478 (1997).

40. Shakeri-Zadeh, A., Ghasemifard, M., Mansoori, G.A.: Structural and optical characterization of folate-conjugated gold-nanoparticles. Phys. E: Low-dim. Sys. Nanostr. 2009, doi:10.1016/j.physe. 10.039 (2009).

41. Leamon, C.P., Reddy, J.A.: Folate-targeted Chemotherapy. Adv. Drug Deliv. Rev. 56, 1127-1141 (2004).

42. Kumar, C.S.S.R.: Nanomaterials for Cancer Therapy (Nanotechnologies for the Life Sciences); ibid, Nanomaterials for Cancer Diagnosis (Nanotechnologies for the Life Sciences); Wiley-VCH: Berlin, German, (2007).

43. Spannuth, W.A., Sood, A.K., Coleman, R.L.: Farletuzumab in epithelial ovarian carcinoma. Expert Opin Biol Ther.;10(3):431–7 (2010).

44. Giri, A.V., Anandkumar, N., Muthukumaran, G., Pennathur, G.: A novel medium for the enhanced cell growth and production of prodigiosin from Serratia marcescens isolated from soil. BMC Microbiol. 4, 11-18 (2004).

45. Song, M.J., Bae, J., Lee, D.S., Kim, C.H., Kim, J.S., Kim, S.W., Hong, S.I.: Purification and Characterization of Prodigiosin Produced by Integrated Bioreactor from Serratia sp. KH-95. J. Biosci. Bioeng. 101, 157-161 (2006).

46. Li, Y., Zhao, X., Zu, Y., Han, X., Ge,Y., Wang, W., Yu, X.: A Novel Active Targeting Preparation, Vinorelbine Tartrate (VLBT) Encapsulated by Folate-Conjugated Bovine Serum Albumin (BSA) Nanoparticles: Preparation, Characterization and in Vitro Release Study. Materials 5, 2403-2422 (2012)

47. Tsai, S.-W., Liaw, J.-W., Hsu, F.-Y., Chen, Y.-Y., Lyu, M.-J., & Yeh, M.-H.: Surface-Modified Gold Nanoparticles with Folic Acid as Optical Probes for Cellular Imaging. Sensors (Basel, Switzerland), 8(10), 6660–6673 (2008).

48. Dozie-Nwachukwu, S. O., Obayemi, J. D., Danyo, Y., Etuk-Udo, G., Anuku, N., Odusanya, O.S., Malatesta, K., Chi, C., Soboyejo, . W.O. Biosynthesis of Gold Nanoparticles with Serratia Marcescens Bacteria. Advanced Materials Research, 1132, 19-35, (2015).

49. Dozie-Nwachukwu, S. O., Etuk-Udo, G., Obayemi, J. D., Anuku, N., Odusanya, O.S, Malatesta, K., Chi, C., Soboyejo, W.O.: Biosynthesis of Gold Nanoparticles from Nauclea Latifolia Leaves. Advanced Materials Research, 1132, 36-50, (2015).

50. Stella, B., Arpicco, S., Peracchia, M.T., Le, D. D., Hoebeke, J., Renoir, M., D'angelo, J., Cattel, L., Couvreur,P.: Design of Folic Acid-Conjugated Nanoparticles for Drug Targeting. Journal of Pharmaceutical Sciences. 89 (11), 1452–1464 (2000).

51. Dozie-Nwachukwu, S.O., Danyuo, Y., Obayemi, J.D., Odusanya, O.S., Malatesta, K., Soboyejo, W.O. Extraction and encapsulation of prodigiosin in chitosan microspheres for targeted drug delivery. ELSEVIER; J. of Mater. Sci. and Engr. C (MSEC). Ref. No.: MSEC-D-16-01152R1, http://dx.doi.org/10.1016/j.msec.2016.09.078.

52. Morgan, J., Notte, J., Hill, R., Ward, B.: Microscopy Today, 14 (4), 24 (2006)

53. Ward, B.W., Notte, J.A., Economou, N.P.: Helium ion microscope: A new tool for nanoscale microscopy and metrology. J. Vac. Sci. Technol., 24, (2006) 2871.

54. Meng, J., Paetzell, E., Bogorad, A., Soboyejo, W. O.: J. Appl. Phys.107, 114301 (2010).

55. Wolf, K. V., Zong, Z., Meng, J., Orana, A., Rahbar, N., Balss, N K. M., Papandreou, G., Maryanoff, C. A., Soboyejo,W.: Biomed. Mater. Res. Part A 87A, 272–281 (2008).

56. Hutter, J. L., Bechhoefer, J.: Rev. Sci. Instrum. 64, 1868–1873 (1993).

57. Matei, G. A., Thoreson, E. J., Pratt, J. R., Newell, D. B., Burnham, N. A.: Rev. Sci. Instrum. 77, 083703 (2006).

58. Mansoori, G.A: Synthesis of Nanoparticles by Fungi. US Patent application number: 20100055199, 1-12 (2010).

59. Smith, M.B., March, J.: March's Advanced Organic Chemistry: Reactions, Mechanisms, and Structure, 6th edition; John Wiley & Sons: NY, USA, (2007).

60. Pan, D., Turner, J.L., Wooley, K.L.: Folic acid-conjugated nanostructured materials designed for cancer cell targeting. Chem. Commun. (Camb), 7, 2400-2401 (2003).

61. ShakeriZadehA., Mansoori, G.A.: Cancerous Cells Targeting and Destruction Using Folate Conjugated Gold Nanoparticles. Dynamic Biochem. Proc. Biotech. Mol. Biol. 4, (1) 6-12 (2010).

62. Mansoori, G. A., Brandenburg, S. K., Shakeri-Zadeh, A.: A Comparative Study of Two Folate-Conjugated Gold Nanoparticles for Cancer Nanotechnology Applications. Cancers. 2, 1911-1928 (2010).

63. Zhang, Z., Zhou, F., Lavernia, E.J.: On the analysis of grain size in bulk nanocrystalline materials via X-ray diffraction. Metallurgical and Materials Transactions A 34, 1349-1355 (2003).

64. Toy, R., Peiris, P. M., Ghaghada, B.K.B., Karathanasis, E.: Shaping cancer nanomedicine: The effect of particle shape on the in vivo journey of nanoparticles. Nanomedicine (Lond). 9(1), 121–134 (2014).

65. Nikoobakht, B., El-Sayed, M.A.: Evidence for bilayer assembly of cationic surfactants on the surface of gold nanorods. Langmuir 17, 6368–6374 (2001).

66. Ahmad, A., Mukherjee, P., Mandal, D., Senapati, S., Khan, M.I., Kumar, R., Sastry, M.: Enzyme mediated extracellular synthesis of CdS nanoparticles by the fungus, Fusarium oxysporum. J Am Chem Soc. 124, 12108-12109 (2002).

67. Li, S.D., L. Huang, L.: Nanoparticles evading the reticuloendothelial system: role of the supported bilayer. Biochim Biphys Acta. 788(10) 2259–2266 (2009).

68. Tan, Y.,Wang, Y., JiangL., Zhu, D.:"Thiosalicylic Acid-Functionalized Silver Nanoparticles Synthesized in One-Phase System," Journal of Colloid and Interface Science, 249, (2) 336-345 (2002).

69. Hall, J.B., Dobrovolskaia, M.A., Patri, A.K ., McNeil, S.E.: Characterization of nanoparticles for therapeutics. Nanomedicine. 2(6) 789–803 (2007).

70. Takae, S., Akiyama, Y., Otsuka, H., Nakamura, T., Nagasaki, Y., Kataoka, K.: Ligand density effect on biorecognition by PEGylated gold nanoparticles: regulated interaction of RCA120 lectin with lactose installed to the distal end of tethered PEG N strands on gold surface. Biomacromolecules 6(2) 818–824 (2005).

71. Arnida, A., Janát-Amsbury, M.M., Ray, A., Peterson, C.M. Ghandehari, H.: Geometry and surface characteristics of gold nanoparticles influence their biodistribution and uptake by macrophages. Eur J Pharm Biopharm: 77, 417–423 (2011).

72. Sperling, R. A. , Parak, W. J.: Surface modification, functionalization and bioconjugation of colloidal inorganic nanoparticles. Phil. Trans. R. Soc. A. 368, 1333–1383 (2010).

73. Love, J.C., Estroff, L.A. , Kriebel, J.K., Nuzzo, R.G., Whitesides, G.M. . Self-assembled monolayers of thiolates on metals as a form of nanotechnology. Chem. Rev. 105, 1103–1169 (2005).

74. De Groot, M.T., Evers, T.H., Merkx, M., Koper, M.T.M.: Electron transfer and ligand binding to cytochrome c' immobilized on self-assembled monolayers. Langmuir. 23, 729-736 (2007).

75. Van de Hulst, H.C. Light Scattering by Small Particles. New York: Dover Publications, (1981).

(i) Esterification of Folic acid

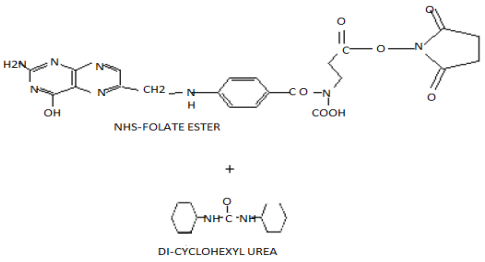

(ii) CONJUGATION REACTION

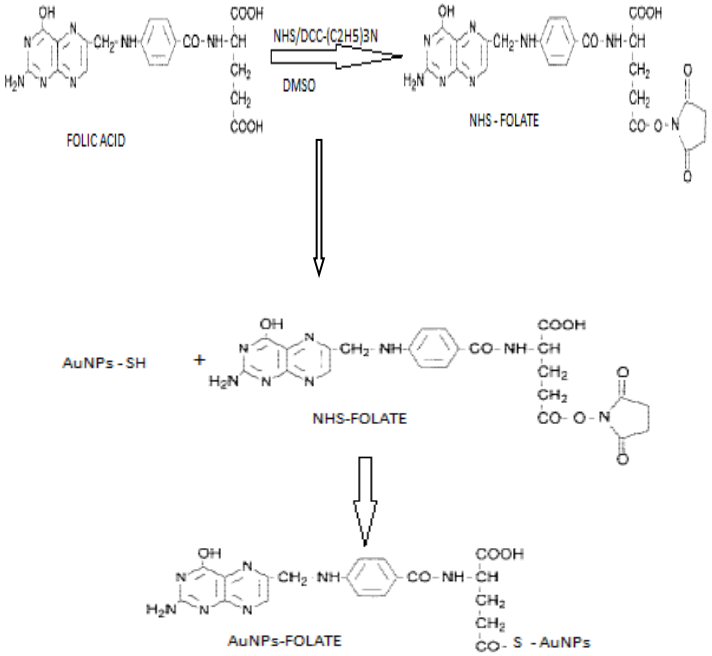

Fig.5.1: Steps involved in the conjugation of gold nanoparticles with folate receptors: (i) Esterification of folic acid, (ii) conjugation reaction of folic acid to gold nanoparticles.

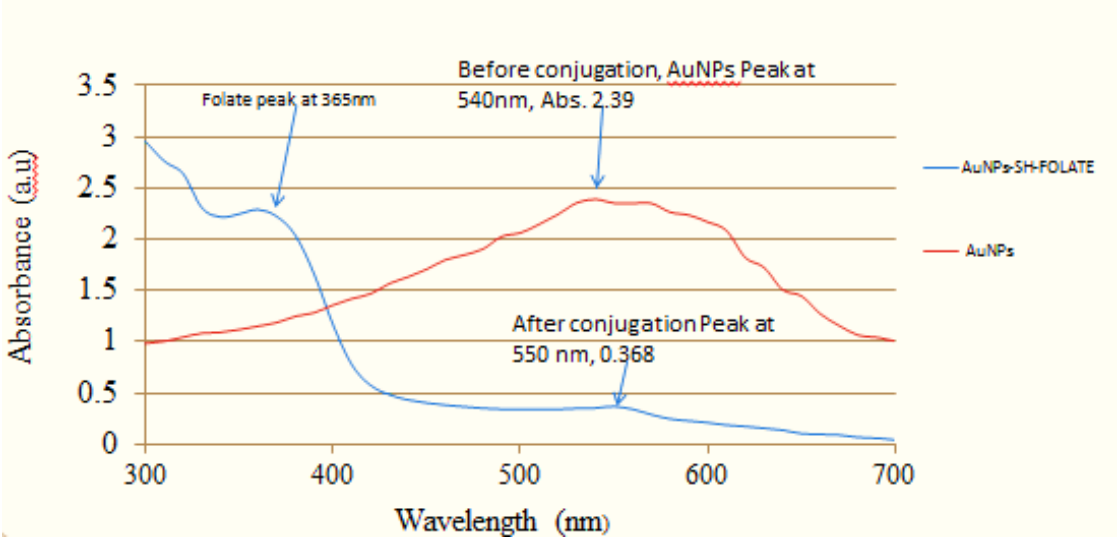

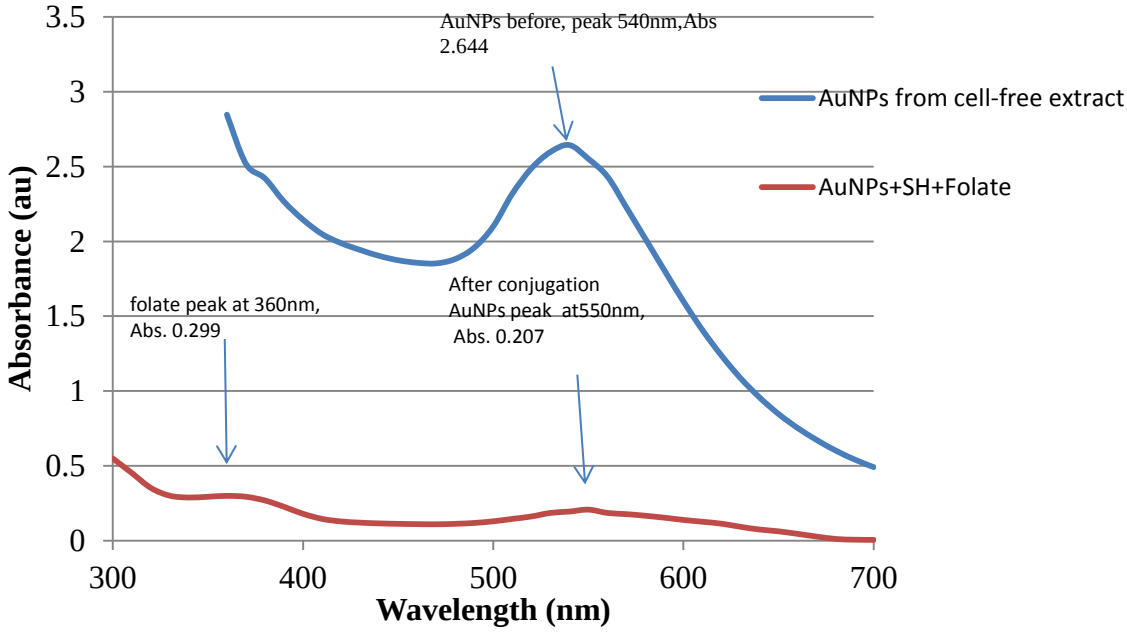

Fig. 5.2: UV-vis spectra of AuNPs from (a) *Nauclea latifolia* and (b) *Serratia marcescens.* Note the absorption peaks before conjugation with folate change in wavelength and absorbance after conjugation.

(a) AuNPs before conjugation

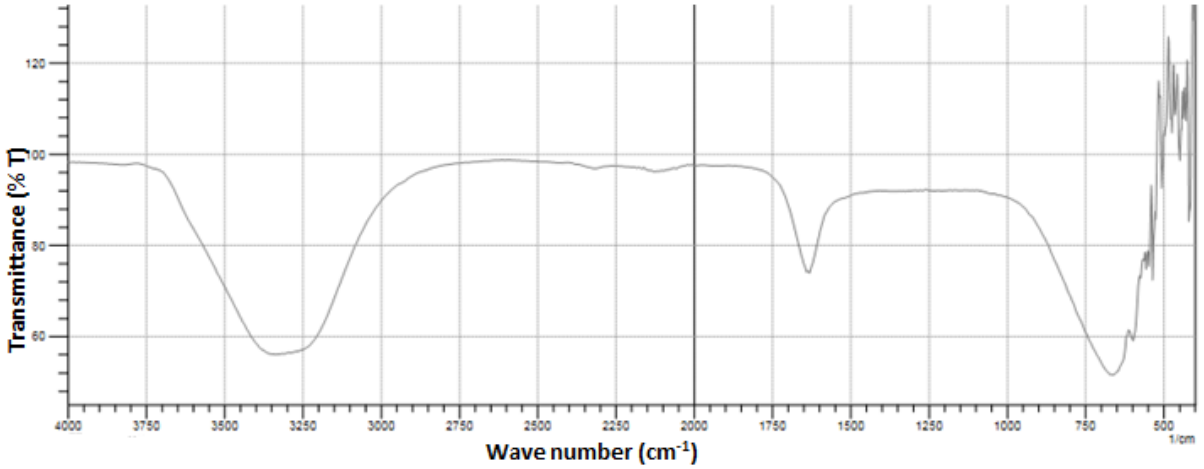

(b) AuNPs after conjugation

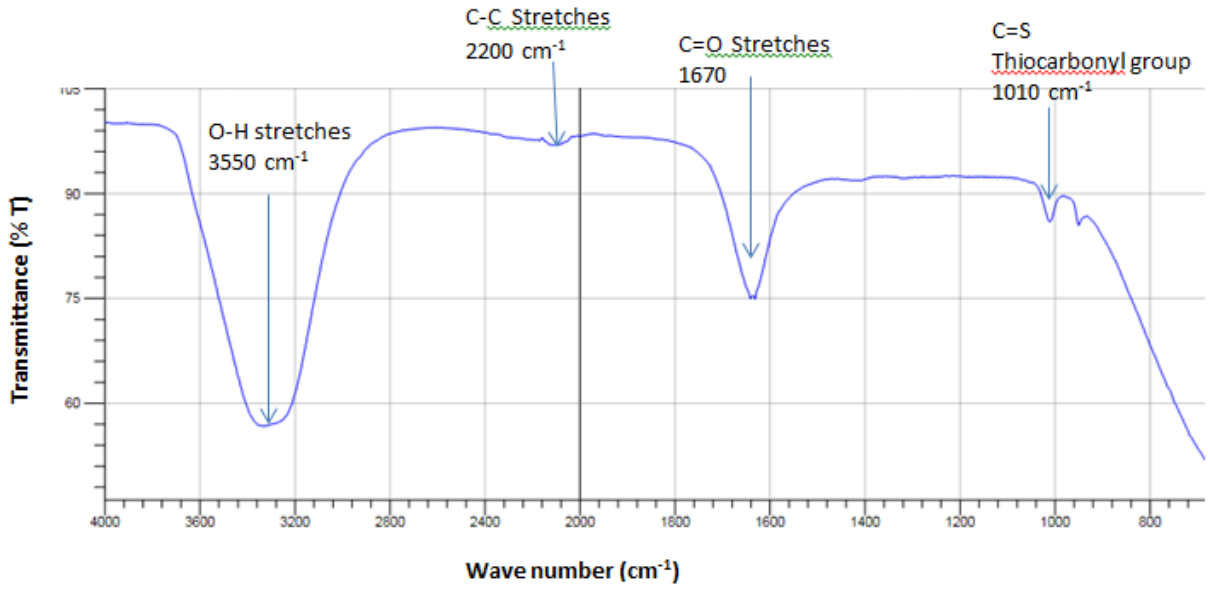

Fig. 5.3: Showing FTIR results obtained for AuNPs (a) before and (b) after conjugation with folate

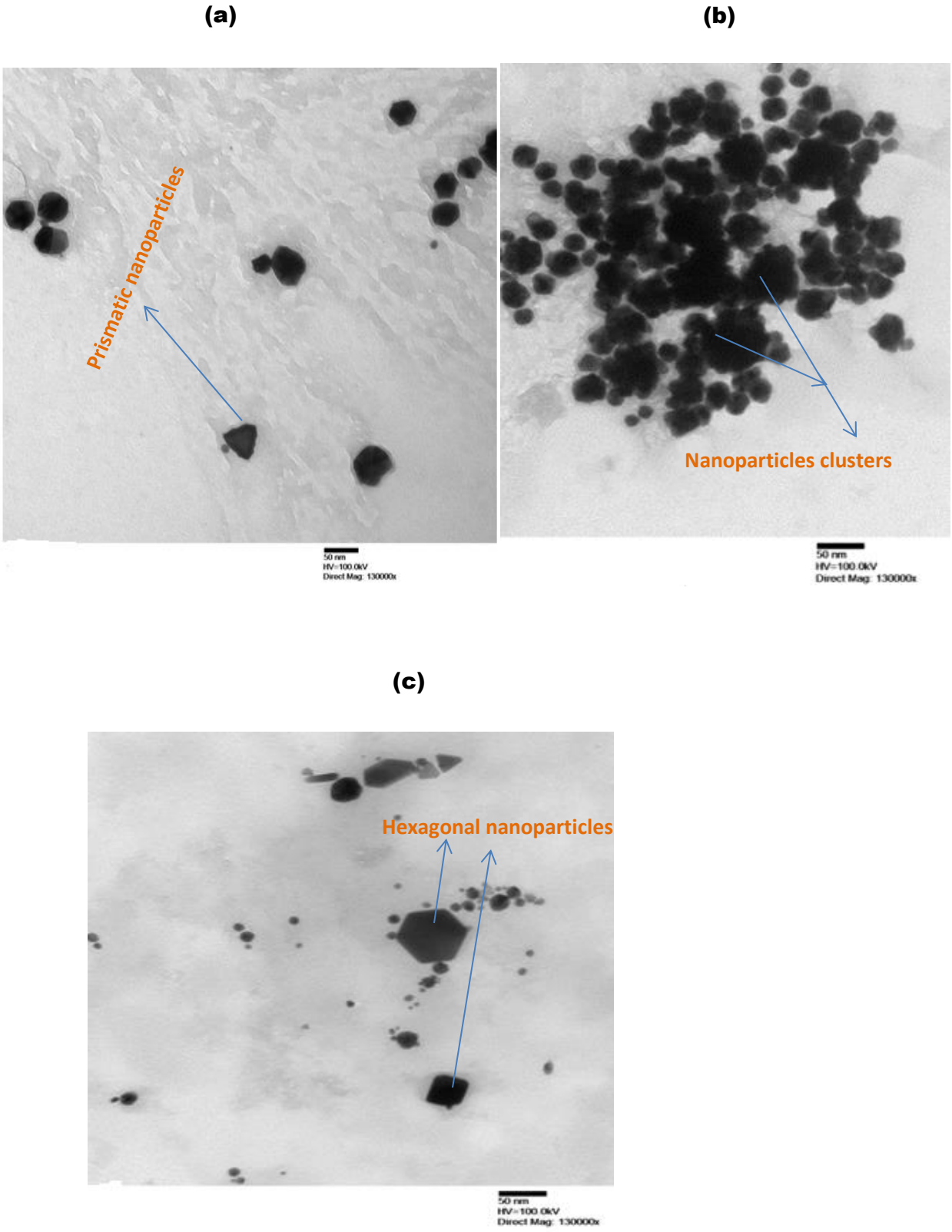

Fig.5.4: TEM images of folate conjugated gold nanoparticles from (a) *Serratia marcescens* at pH 4.5 (b) *Serratia marcescens* at pH 8.5 and (c) *Nauclea latifolia* (NLO + S + folate).

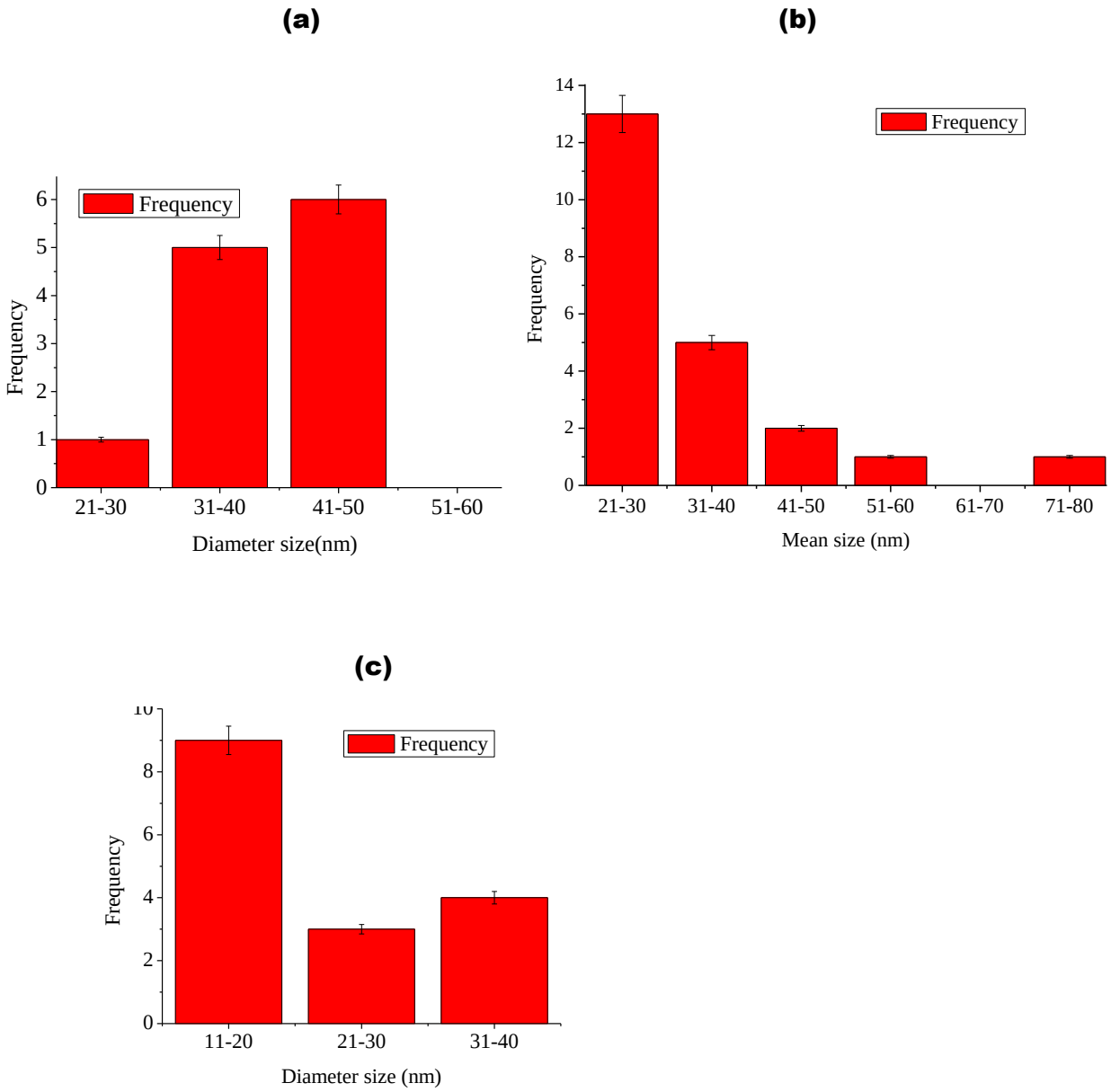

Fig. 5.5: Histograms of Folate conjugated gold nanoparticles from: (a) *Serratia marcescens* at pH of 4.5 (b) *Serratia marcescens* at pH of 8.5 and (c) *Nauclea latifolia* (NLO+S+Folate).

(a) (b)

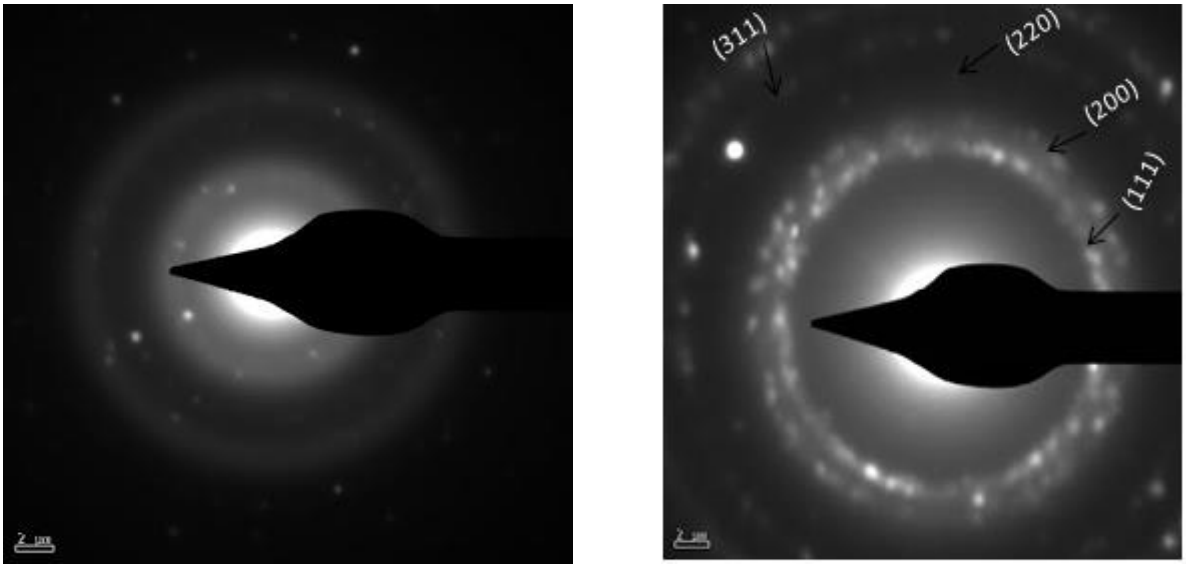

Fig. 5.6: SAED patterns for biosynthesized gold nanoparticles. The Scherrer ring patterns indicate the fcc gold which is nanocrystalline in nature. Diffraction rings attributed to (111), (200), (220), (311) planes of FCC Au can be found in the obtained diffraction images. (a) For *Nauclea latifolia* (NLO) synthesized AuNPs and (b) for *Serratia marcescens* synthesized AuNPs produced at pH 8.5

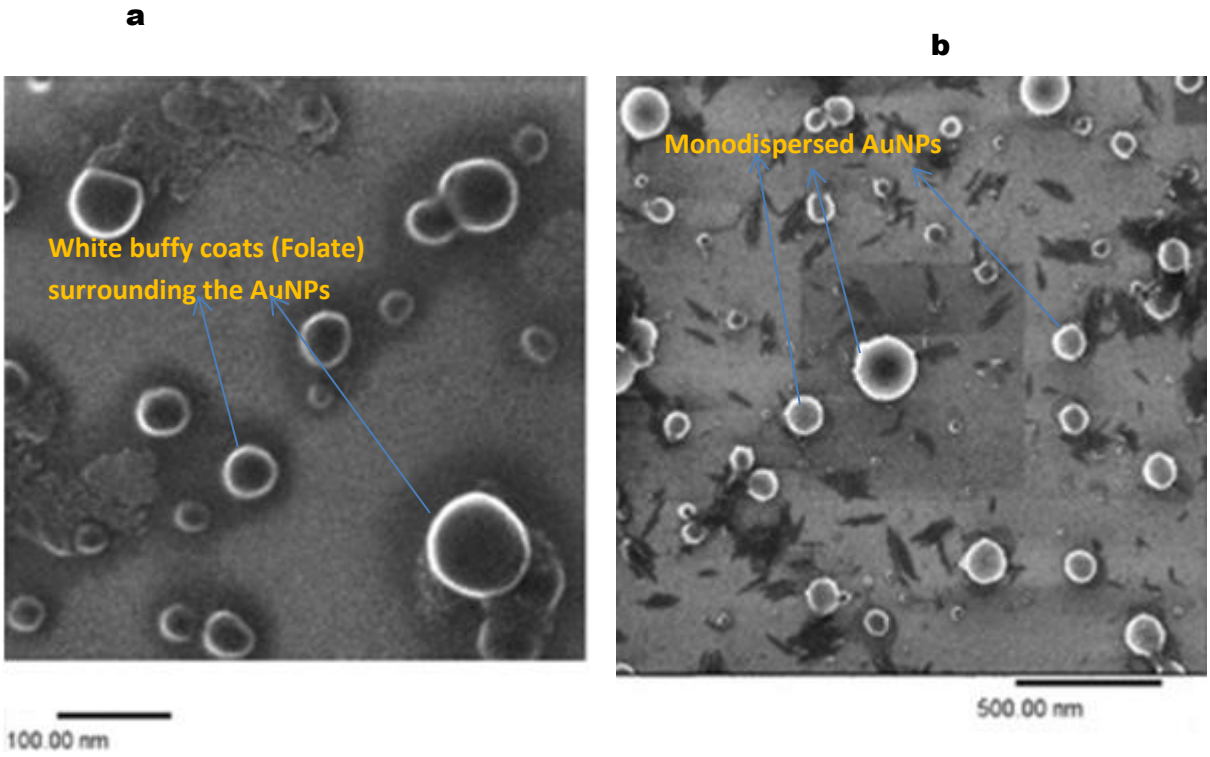

Fig. 5.7: Helium ion microscopy images of gold nanoparticles synthesized with NLO conjugated with folate (a) at 1 µm field of view, (b) at 4 µm field of view

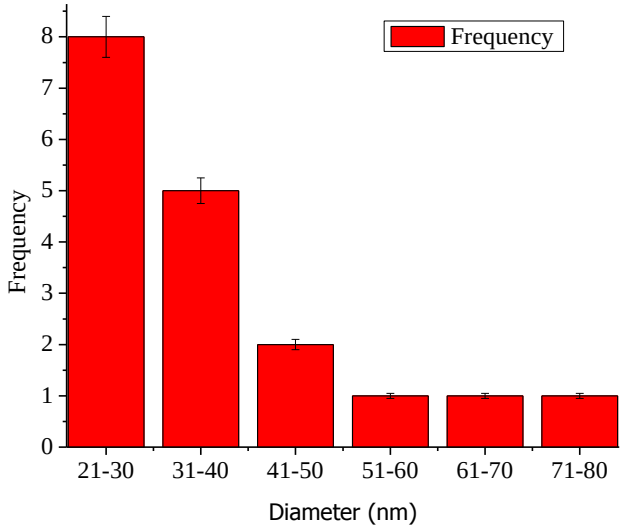

Fig. 5.8: Histogram of size distribution of Helium ion images of gold nanoparticles synthesized with NLO conjugated with folate

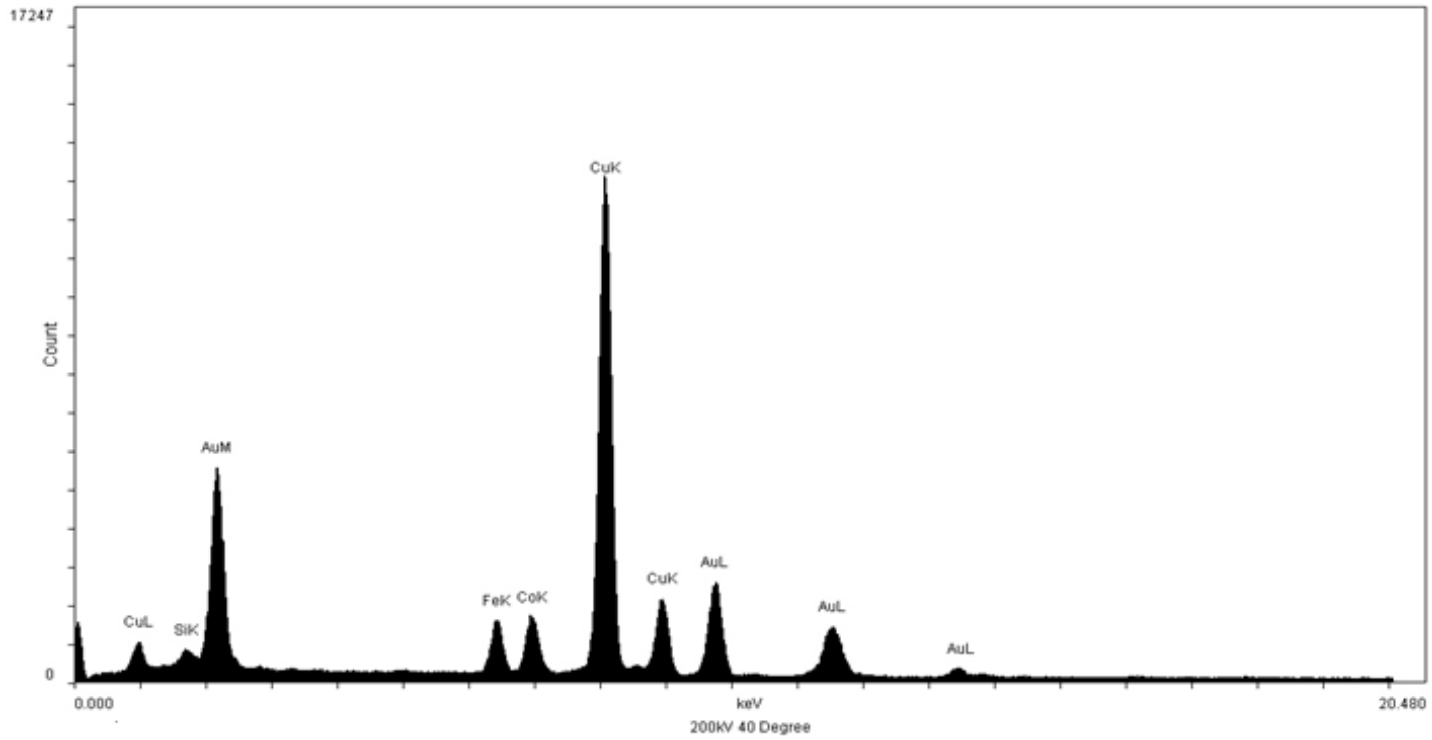

Fig.5.9: Shows the EDX (energy-dispersive X-ray) spectrum recorded in the spot-profile mode from one of the folate conjugated gold nanoparticles from *Serratia marcescens* produced at pH8.5.

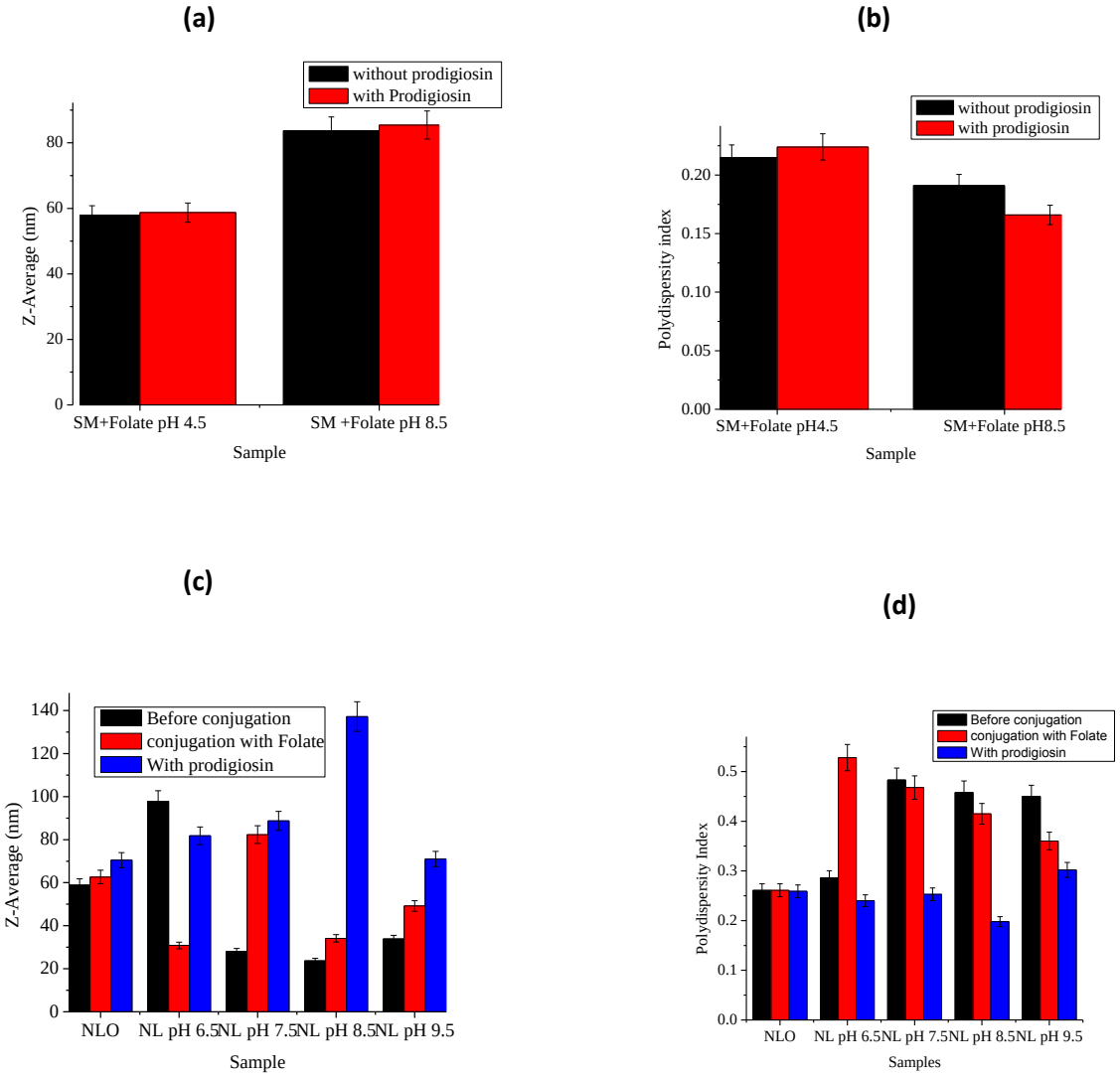

Fig. 5.10: Histograms of DLS results of gold nanoparticles synthesized with *Serratia marcescens (SM)* (a and b) and *Nauclea latifolia (Nl)* (c and d) comparing the effects of pH on the z-average and the PDI of AuNPs before and after conjugation with the ligand folate, with and without prodigiosin.

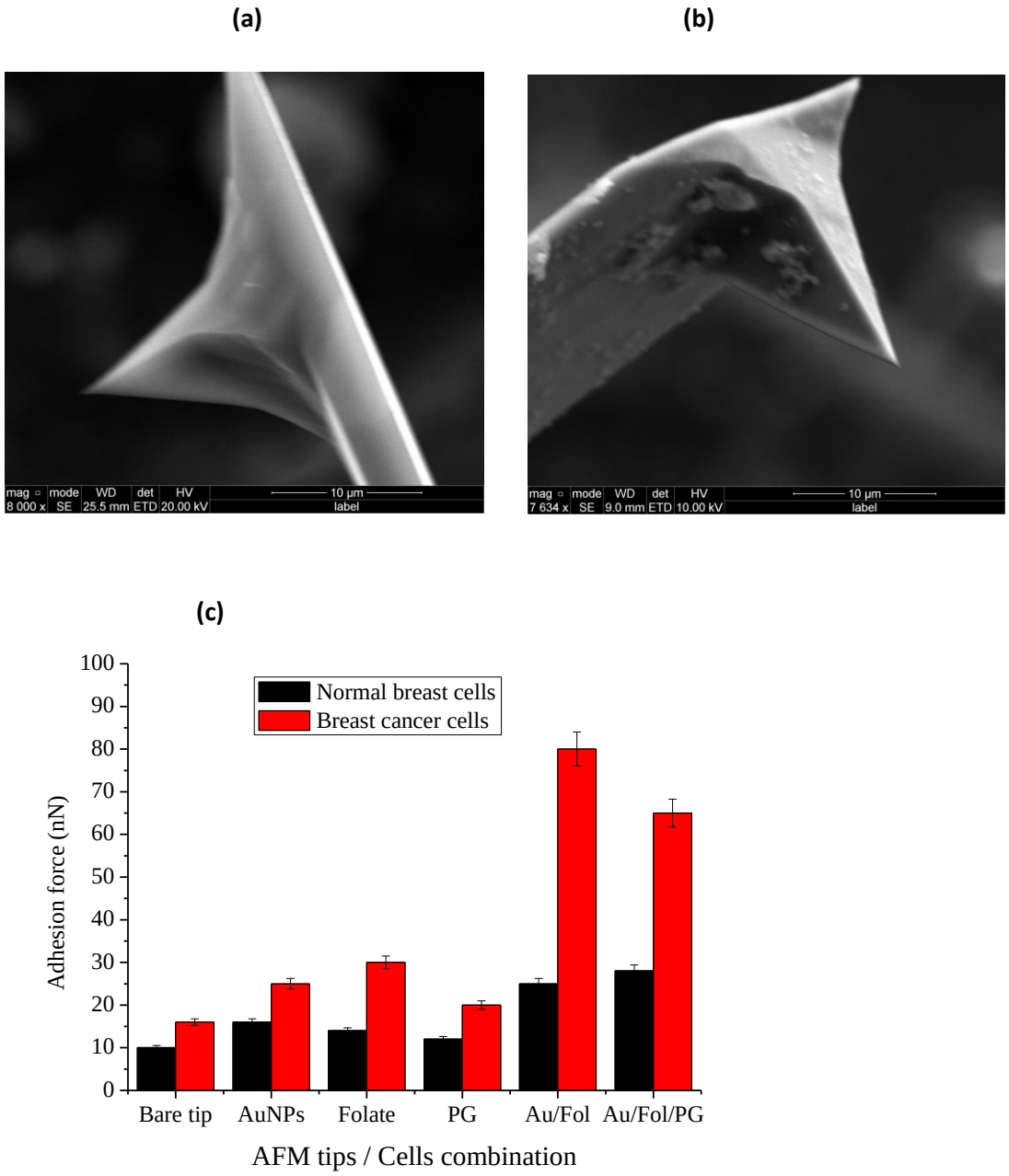

Fig.5. 11: Scanning Electron Microscopy images of (a) bare AFM tip and (b) AFM tip coated AuNPs (c) summary of Adhesion Force Measurements between normal breast and breast cancer cells and AFM tips with and without different coatings.

Table 5.1: DLS results of the conjugated gold nanoparticles synthesized from the conditioned medium of *Serratia marcescens* at pH 4.5 and 8.5 showing the Z-Average and PDI**.**

Sample	Z-Average mean (d.nm)	PDI mean
SM pH 4.5 + thiol + folate	57.93±0.24	0.215±0.009
SM pH 4.5 + thiol + folate + prodigiosin	58.71±0.39	0.224±0.002
SM pH 8.5 + thiol + folate	83.73±1.67	0.191±0.014
SM pH 8.5 +thiol + folate + prodigosin	85.44±1.07	0.166±0.003

Table 5.2: Showing the Z-Average and PDI of folate conjugated gold nanoparticles from *Nauclea latifolia* at varying pH with the anti-cancer drug prodigiosin attached.

Samples	Z-Average (nm)	PDI
NLO	58.9±0.3	0.26±0.004
NLO + thiol + folate	62.7±0.6	0.26±0.01
NLO + thiol + folate + prodigiosin	70.5±0.2	0.26±0.01
NL pH 6.5	97.8±1.8	0.29±0.003
NL pH 6.5 + thiol + folate	30.8±0.7	0.53±0.01
NL pH 6.5 + thiol + folate + prodigiosin	81.8±0.5	0.24±0.01
NL pH 7.5	28.1±0.8	0.48±0.04
NL pH 7.5 + thiol + folate	82.3±7.9	0.47±0.15
NL pH 7.5 + thiol + folate + prodigiosin	88.7±1.0	0.25±0.01
NL pH 8.5	23.7±0.3	0.46±0.01
NL pH 8.5 + thiol + folate	34.1±2.1	0.42±0.09
NL pH 8.5 + thiol + folate + prodigiosin	137.2±0.2	0.20±0.01
NL pH 9.5	33.8±1.0	0.45±0.03
NL pH 9.5 + thiol + folate	49.2±0.6	0.36±0.06
NL pH 9.5 + thiol + folate + prodigiosin	71.0±3.3	0.30±0.01

Table 5.3: Adhesion force measurement of the conjugated gold nanoparticles synthesized by SM at pH 8.5 conjugated with different ligands.

AFM Tip	Adhesion Force (nN)		
	Normal breast cells	Breast cancer cells	Approximate Increase
Bare tips	10±0.5	16±0.8	1.6
Folate	14±0.7	30 ±1.5	2.1
AuNPs	16±0.8	25±1.25	1.6
PG	12±0.6	20±1	1.7
AuNPs/folate/PG	28±1.4	65±3.25	2.3
AuNPs/Folate	25±1.25	80±4	3.2

CHAPTER 6

6.0 Extraction and Encapsulation of Prodigiosin in Chitosan Microspheres for Targeted Drug Delivery

6.1 Introduction

One of the biggest challenges of cancer therapy is the issue of non-specific anti-cancer drug delivery. It leads to the destruction of both cancerous cells and healthy cells [1]. Micro-encapsulation is a process by which small particles of solids, liquids or gases are enclosed within the thin walls of microscopic polymeric materials. Micro-encapsulation also enables the controlled release of drugs, with reduced side effects, reduced toxicity of drugs and also prevention of vaporization of many volatile drugs e.g. methyl salicylate and peppermint oil [2]. Micro-encapsulation is also used to mask the organoleptic properties of drugs, such as taste, odor or color of the substance and sometimes, to ensure safe handling of toxic materials [1-6]. Furthermore, the type of coating material used affects the properties of the microspheres. The polymer of choice should exhibit characteristics such as stability, reduced volatility, inertness with the active ingredients, and controlled release under specific conditions [7, 8].

To design a drug delivery system, there is need to consider the normal physiological scavenging processes that remove small foreign objects from the blood [9], hence, the need for micro-encapsulation. Renal clearance can also be avoided when the nanoparticulates are larger than the glomerular pore sizes [9-10]. Thus, the circulating half-lives of nanoparticles and their associated drugs can be prolonged by controlling their sizes. Controlled release systems maintain the concentration of drug in the blood, or in target tissues over a given period of time [11, 12]. This is often achieved by controlling the drug release kinetics [13]. Generally, the initial drug release rate is rapid, in order to achieve the effective therapeutic concentration of the drug. Then, the

drug release kinetics follows a well-defined behavior, in order to supply the maintenance dose, thus enabling the attainment of the desired drug concentration [14].

Chitosan is a linear polysaccharide that consists of β-(1-4)-linked D-glucosamine and N-acetyl-D-glucosamine. It is produced by alkaline de-acetylation of chitin, which is the main component of the exoskeleton of crustaceans, such as shrimps, crabs, and crawfish [15]. Chitin is the second most abundant natural polymer, after cellulose [16, 17]. The properties of chitosan depend on the degree of de-acetylation [18]. The degree of de-acetylation (DDA) of chitosan influences its physicochemical characteristics [18], its biodegradability [19] and its immunological activity [20]. Furthermore, chitosan is useful in medicine due to its biocompatibility [21], biodegradability, [19, 22] and low toxicity [23]. It enhances wound healing and exhibits other biological activities such as anti-microbial properties and the reduction of cholesterol level [24, 25]. The positive charge on chitosan, generated under physiological conditions, has been found to be responsible for its enhanced bioadhesion to negatively charged cell membranes. This enables the site-specific applications in controlled delivery systems [26–28].

In forming the microspheres, chitosan is often used, along with glutaraldehyde, as a cross linker. The reaction of chitosan with aldehyde groups often forms covalent imine bonds with the amino groups of chitosan. This is due to the resonance established with adjacent double ethylenic bonds [29] via a Schiff reaction. Covalent crosslinking leads to the formation of a permanent network, allowing for the free diffusion of water and enhancing the mechanical properties of the microspheres. Hence, the structure and mechanical properties of chitosan are in a range that is suitable for the controlled release of chemotherapeutic agents [30] within the therapeutic window.

Prodigiosin, a secondary metabolite, can be produced by the bacteria, *Serratia marcescens* (SM) and other bacteria such as *Zooshikella rubidus, Vibrio sp., Streptomyces griseoviridis, and Hahella chejuensis* [31-38]. It is a natural compound with a broad range of cytotoxic, anti-fungal, anti-bacterial, algicidal, anti-protozoal, anti-malarial, immunosuppressive, anti-cancer and anti-proliferative activities [39-41]. Prodigiosin has been reported to effectively induce apoptosis in hematopoietic cancer cells, as well as in cells derived from other human cancers (e.g. gastric and colon cancers), and has no marked toxicity in nonmalignant cell lines [42-44]. Furthermore, Francisco and co-workers (2003) [45] have reported the effects of PG on different human neuroblastoma cell lines (i.e. SH-SY5Y, LAN-1, IMR-32 (N-type) and SK-N-AS (S-type). Our interest in prodigiosin is in its anti-cancer property.

In this paper, we explore a procedure for the extraction, purification and encapsulation of prodigiosin, an anti-cancer agent, in chitosan microspheres. Prodigiosin is produced from *Serratia marcescens.* It is then encapsulated in chitosan using a water-in-oil emulsion (w/o) technique. The sizes and shapes of the microspheres are characterized, along with their encapsulation efficiency, drug loading, swelling ratio and drug release kinetics. The implications of the results are then discussed for the potential applications of the microspheres in localized chemotherapy.

6.2. Materials and Methods

6.2.1 Materials

All the following chemicals used in this project were of analytical grade:

Chitosan (Santa Cruz Biotechnology, Dallas, Texas, USA, Lot: A2913), Liquid paraffin (Lobal Chemie PVT Ltd, Mumbai, India, lot: LL10931112), Tween 20 (BDH Laboratory Supplies

Poole, BH15 ITD, England, lot: S2199087727), N-Hexane (Lobal Chemie PVT Ltd, Mumbai, India), and Acetone (Merck Chemicals, Germany). Absolute ethanol (JDH Guangdong Guanghua, Sci-Tec Co Ltd China), methanol (Sigma-Aldrich, Germany), chloroform (BDH Laboratory supplies, England), glutaraldehyde (Antares Chem Private Limited, Mumbai), acetic acid (Guangdong Guanghua Sci-Tech Co., Ltd), sodium bicarbonate and sodium carbonate anhydrous (EMD Chemical Inc. Gibbstown, NJ, USA)

6.2.2 Extraction and Purification of Prodigiosin

The bacteria, *Serratia marcescens* (SM) were cultured on peptone glycerol agar (constituted in the lab) and incubated at 30^{o}C for 24 h. A characteristic red pigment associated with prodigiosin [46] was observed after the incubation. The bacteria growing on the surface of the media were then scooped into 100 ml of absolute ethanol contained in a conical flask. This was shaken vigorously to extract the pigment into the ethanol. The solution was then centrifuged at 5000 rpm for 10 minutes. The supernatant was collected and placed in a rotary evaporator evaporator (BUCHI, Rotavapor® 114 with Water Bath B-480, Bristol, Wisconsin, USA) to separate the ethanol from crude prodigiosin.

Subsequently, the crude prodigiosin was purified using a column chromatographic technique [47]. The sample was dissolved in 2 ml of methanol and layered on a column packed with silica gel (Trade-Link (Mfg.Silica Gel, Mehsana District, India) as the stationary phase. Then, a mobile phase comprising a mixture of n-hexane, chloroform and methanol (in the ratio of 1:1:1), was used to elute the prodigiosin. Different fractions were collected in 10 ml aliquots. These were then scanned in the UV-Vis spectrophotometer to determine which fractions contained pure prodigiosin. The percentage purity was then determined, as reported in our earlier work [48].

6.2.3a Encapsulation Procedure

Chitosan microspheres containing prodigiosin were prepared using an emulsion cross-linking technique method developed by Roy *et al.*, [49], with some modifications. Briefly, 100 mg of chitosan was dissolved in 4 ml of 2% acetic acid solution (2.5 % (w/v) chitosan solution). Different formulations (S1, S2, S3 and S4), representing concentrations of the drug (prodigiosin) (1, 1.5, 2, 5 mg/ml) were dissolved in methanol-water (4:1). They were then added to chitosan solution and mixed thoroughly. The mixture was then degassed in a sonicator for 10 minutes. 150 ml of light liquid paraffin containing 0.5% Tween 20 was then poured into a 250 ml beaker, placed in the Sonicator, and stirred with a 4 blade mechanical stirrer at 2000 rpm.

The chitosan-drug solution was added drop-wisely, while still stirring, to form a w/o emulsion. After 20 min, 0.5 ml of 25% glutaraldehyde (cross linker) was added drop-wise at a rate of 0.125 ml per 15 min for 1 h. Stirring continued for 2.5 hours until the microspheres were obtained. The microspheres obtained were separated by centrifugation at 5000 rpm for 5 min. They were then decanted from the paraffin and washed 3 times with n-hexane, followed by acetone (x1), to remove the paraffin oil. Finally, the microspheres were washed with distilled water to eliminate the glutaraldehyde, prior to freeze-drying to obtain a free flowing microsphere powder.

6.2.3b Dissecting the Microspheres

To investigate inner surfaces of soft or hard materials, cryo fracture technique was adopted. This is a fast fracture method which involves simply breaking the specimen into two pieces after flash freezing in liquid nitrogen (LN2). 5 mg of the microspheres was place into a 5 ml beaker containing 2 ml of liquid nitrogen for 5 min. The microspheres were then filtered and quickly cut

open by pressing with a flat spatula. The fractured surfaces were viewed under the microscope using the SEM (Figure 6.1c).

6.2.4 Characterization of Drug-loaded Microspheres

6.2.4.1 Drug Concentration

A UV-Vis spectrophotometer (Biochrom Libra 522 spectrophotometer (Cambridge, England)) was used for the estimation of prodigiosin concentration. The drug (prodigiosin) was dissolved in methanol at a concentration of 1 mg/ml and scanned in-between the wavelengths 250-700 nm in the UV visible spectrophotometer. The maximum absorption was found to be 536 nm. This was selected for the preparation of a calibration curve within the range of 0-1 mg/ml. Subsequently, the concentration of the drug (prodigiosin) encapsulated was read off the calibration curve. Also the percentage of drug release from the microspheres was calculated from the curve.

6.2.4.2 Particle Size and Morphology

The sizes and morphology of the microspheres were characterized using a Phillips Model FEI XL30 field emission gun scanning electron microscope (SEM) (Phillips Electronics N.V., Eindhoven, the Netherlands). The dried microspheres were then mounted on carbon grids (Ted Pella, Inc. Redding, CA 96003-144), prior to scanning electron microscopy. The particle size distributions and morphologies were then analyzed using the Image J software (NIH, Bethesda, MD, USA).

6.2.4.3 Encapsulation Efficiency

The prodigiosin content in the microcapsules was determined by the digestion method [50]. 10 mg of the prodigiosin loaded microspheres was pulverized and placed in 10 ml

methanol/phosphate buffer (pH = 7.4). The mixture was then sonicated for 10 min and allowed to stand for 24 h at room-temperature. The suspension was then centrifuged at 5000 rpm for 10 minutes. The absorbance of the supernatant was measured in the UV-Vis spectrophotometer (Biochrom Libra 522 spectrophotometer, Cambridge, England) at a wavelength of 536 nm. The concentration of the prodigiosin was then determined from the drug concentration from the standard calibration curve. All of the samples were analyzed in duplicate. The percentage encapsulation efficiency of each drug concentration was determined from:

$$EE = \% \text{ Encapsulation efficiency} = \frac{\text{Amount of drug measured}}{\text{Theoretical amount of drug}} \times 100 \quad (1)$$

6.2.4.4 Drug Loading:

The drug loading capacity for each drug concentration was determined from:

$$DL = \% \text{ Drug loading} = \frac{\text{Amount of drug released from the lysed microspheres}}{\text{Amount of microspheres used for lysis}} \times 100 \quad (2)$$

6.2.4.5 Percentage Yield

The percentage yield was calculated as the ratio of the mass of microparticles obtained at the end of the process and the mass of initial substances added, including the drug and polymer.

$$PY = \text{Percentage Yield} = \frac{\text{Weight of microspheres}}{\text{Total expected weight of drug and polymer}} \times 100 \% \quad (3)$$

6.2.5 Swelling Index

The degree of swelling of the microspheres was studied by soaking 10 mg of the different chitosan microspheres in 10 ml of PBS (prepared in the lab) at a pH of 7.4. This was done at a temperature of 37˚C in different beakers and kept for 10 days. At daily intervals, the microspheres were filtered, blotted with a Whatman No.1 filter paper. They were then weighed using an analytical balance (O'Haus Analytical Plus, Switzerland). The experiments were performed in duplicate, and the swelling index of the microspheres was determined from:

$$\text{SI} = \text{Swelling index} = \frac{W_f - W_o}{W_o} \qquad (4)$$

where W_f is the final weight of microcapsules and W_o is the initial weight of microcapsules.

6.2.6 *In-vitro* Drug Release

10 mg of microspheres containing different concentrations of prodigiosin (1, 1.5, 2, 5 mg) were tied in muslin cloth (3 cm^2) and immersed in 10 ml of pH 7.4 PBS buffer in separate test tubes labelled S1 – S4. These were kept in a shaker incubator (that was set at 60 rpm and 37˚C throughout the experiment). At regular intervals, aliquots (5 ml) were removed for analysis and replaced with 5 ml of fresh buffer. The absorbance of the released drug was then measured using a UV-Vis Spectrometer (Biochrom Libra 522 Spectrometer, Biochrom Ltd, Cambridge, England) at 536 nm. The corresponding eluted drug concentrations were determined from a calibration curve that was obtained from known concentrations of purified prodigiosin.

6.2.7 Cell Viability Testing

The breast cancer cell line, MDA-MB-231, was used in this study, as reported in our previous work [51]. A dye exclusion assay for cell viability uses a dye or stain that can enter the cell and usually intercalates with the DNA in the nucleus. The mere entry of the dye into the cell assumes that the cell membrane has lost its integrity and that the cell is dead. In other words, live cells exclude the dye, while dead cells allow the dye to enter.

A 0.4% solution of trypan blue (Sigma Aldrich, St. Louis, MO, USA) in buffered isotonic salt solution, pH 7.2 to 7.3 (phosphate-buffered saline), was prepared. Then 0.1 mL of trypan blue stock solution was added to 1 mL of cells, mixed gently and incubated at room temperature for 1 minute. The cells were loaded immediately onto a hemocytometer and examined under an optical microscope at low magnification. The number of blue staining cells and the number of total cells were counted.

VC = % Viable Cells = [1.00 – (Number of blue cells ÷ Number of total cells)] × 100

6.3.0 Modeling

The drug release kinetics was studied by fitting the data into zeroth order, first order, Higuchi and Korsemeyer-Peppas [52 - 54] models. The most appropriate models were also determined on the basis of goodness of fit.

6.3.1 Zero Order Kinetics

The zeroth-order rate (Eq. 5) describes the systems in which the drug release rate is independent of concentration [55]. A plot of the amount of the drug released versus time will, therefore, be linear for zeroth-order kinetics. That gives:

$$C = k_0 t \qquad (5)$$

where k_0 is zeroth-order rate constant, expressed in units of concentration/time, and t is the duration.

6.3.2 First Order

First order rate kinetics describes release rates that are concentration dependent [56]. Hence, the plot of the log of the percentage of drug remaining versus time will be linear, with a negative slope [57].

$$\frac{dc}{dt} = - KC \qquad (6a)$$

where K is first order rate constant, expressed in units of time.$^{-1}$ Rearranging Equation 6a and taking logs of both sides gives:

$$\log C = \log C_0 - Kt / 2.303 \qquad (6b)$$

where C_0 is the initial concentration of drug and k is the rate constant. The first order rate constant, k , can be obtained from the slope of the plot of log C versus t. First order kinetics is often observed during the dissolution of water-soluble drugs in porous matrices [58-59].

6.3.3 Higuchi Models

Higuchi [52, 53] has proposed models that characterize the release of water soluble drugs incorporated into dilute semi-solid and solid matrices. For a planar system, with a homogeneous matrix, the flux (the amount of drug per unit area per unit time) is given by:

$$Q = [D (2C-C_s) C_s t]^{1/2} \quad (7a)$$

or

$$Q = Kt^{1/2} \quad (7b)$$

Where Q is the amount of drug released in time t per unit area, C is the initial drug concentration, Cs is the drug solubility in the matrix media and D is the diffusivity of drug molecules in the matrix substance. Higuchi describes drug release as a diffusion process that is well described by Fick's first law. For diffusion controlled processes, the plot of Q versus the square root of time exhibits a linear relationship.

6.3.4 Korsmeyer-Peppas Model

The release mechanism of prodigiosin from the microspheres was determined using the Korsmeyer-Peppas model [54]. Korsmeyer *et al.*, [54] have derived a simple relationship that describes drug release from a polymeric system Eq. (8). To obtain the mechanism of drug release, the data for the first 60% of drug release data was fitted with the Korsmeyer–Peppas model [54]. This gives:

$$M_t / M_i = Kt^n \quad (8)$$

Where M_t / M_i are fraction of drug released at time *t*, *K* is the rate constant and *n* is the release exponent. The *n* value is used to characterize different release mechanisms, as shown in Table 6.4. The constants *K* and *n* were obtained from a linear form of Equation (8) to give:

$$ln\left(m_t/m_i\right) = lnK + n \ln t \quad (9)$$

Where *log K* and *n* are the intercepts and the slopes of the plots of $\ln(m_t/m_i)$ versus ln*t*. Hence K and n can be obtained from the plots of $\ln(m_t/m_i)$ versus ln*t* (Figure 6.8). Furthermore, the mechanisms of drug release can be determined from the values of n (Table 6.4a).

6.4.0 Results and Discussion

6.4.1 Purity of Extracted Prodigiosin

The results of the UV-Vis measurements for the different fractions of extracted purfied prodigoisin showed that some fractions had their maximum absorbance at 536 nm, which is similar to the results from other studies [60-63]. These fractions were pooled together and later the liquid was evaporated to obtain pure prodigiosin. The purity of the extracted prodigiosin was determined (in percent) using methods described in our earlier publication [48]. The purity was found to be ~ 92.8%. A purity of ~ 94.66% was obtained for standard prodigiosin (pure PG (purity= 95%, Mw= 323.4 g/mol) was procured from Santa Cruz Biotechnology (CA, USA)).

6.4.2 Particle Sizes and Morphologies

The SEM images of the chitosan micro-particles loaded with prodigiosin are presented in Figures 6.1a – 6.1d. These images show spherical microspheres with rough surfaces (Figure 6.1a). The

roughness is attributed to the use of glutaraldehyde as a cross-linker [49]. The average particle sizes of the microspheres were between 40 µm and 60 µm (Figure 6.1b). The SEM images also revealed evidence of some dissected microspheres (by crogenic fracture), with micro-pores within the microspheres (6.1 c). These micropores enhanced the diffusion of drugs. The pore sizes of the microspheres, determined with the Image J 1.47v software package, are presented in a histogram in Figure 16.e. The most frequent (other pore sizes exist: i.e., the large peak at sizes 0 – 0.5) average pore sizes were between 1.1 µm and 1.5 µm.

6.4.3 Encapsulation Efficiency and Percentage Yield

The encapsulation efficiency (PEE) (in percent) of four formulations of prodigiosin (PG) in chitosan-based microparticles is presented in Figure 6.2a and Table 6.1. The encapsulation efficiency of PG increased with increasing drug: polymer ratio, with S4 (5 mg/ml prodigiosin) having a percentage encapsulation of 90 ±4% and S1 a percentage encapsulation ratio of 66.7 ±3.3% (Figure 6.2a and Table 6.1). The increase in the ratio of drug-to-polymer leads to the formation of large droplets with decreased surface areas. This results in slower diffusion of drugs, hence, higher encapsulation efficiencies [49]. The percentage yields of different formulations (S1 to S4) were also calculated. The yields were found to be in the range of ~ 42 ± 2.1% to 55.5±2.8 % (Figure 6.2b and Table 6.1) with yield decreasing as the drug:polymer ratio increased. The loss of material during the preparation of microspheres is attributed to the poor recovery process, especially during the filtration of the microspheres.

6.4.4 Swelling

In drug release systems, the swelling kinetics can determine the rate of drug release, which is dependent on pH, ionic strength of solution, or solution temperature [64-71]. In the current work, the average swelling index was plotted against time (Figure 6.3) . The plot shows that there was a steady increase in the size of the microspheres with time. This increase continues until the size reaches thermodynamic equilibrium [72]. This corresponds to the findings of Sadjia and Fatma [73], who noted that the swelling ratio increases with time, although later, constant swelling values were observed. These swelling values can be considered as an equilibrium swelling ratio [72].

In Figure 6.4, the swelling ratios of the different formulations of the microspheres are compared The results show a general increase in the swelling ratio, with increasing drug concentration [74]. The implication is that this will help in the formulation of the dosage of the drug. When treating a patient with aggressive or late stage cancer, there will be need for the system that can release the drugs at a faster rate and, as such, reduce the number of cancerous cells. Subsequently, the formulation with slower rate, will then be used for slower rate drug release

6.4.5 *In-vitro* Drug Release by Prodigiosin-Chitosan Microparticles

The percentage cumulative drug release profile is presented in Figure 6.5. The sample, S1, had the longest period of release (11 days). This is attributed to the higher polymer: drug concentration [75]. Hence, the drugs travel longer distances to be eluted. Since polysaccharides undergo dissolution in aqueous medium, due to solvent penetration, swelling, polymer chain disentanglement and relaxation [76], solute transport from polysaccharide-based material

systems (such as chitosan) can be driven by diffusion and/or dissolution. From the current results (Figures 6.6a – 6.6e), the release profile suggests diffusion-controlled release.

The initial drug released is due to diffusion and burst processes, as the drug can travel through the pores formed during the hardening phase. This is followed by a later degradation-controlled release for a smaller fraction of the drug (Figures 6.6a - 6.6e). Figure 6.6a shows a single microsphere before being immersed in the pH 7.4 drug release buffer. After 2 days, a crack was noticed to have initiated (6.6b). Then, by the fifth day, a higher incidence of cracks was observed (Figure 6.6c). By day 9, degradation had set in and most of the polymers appear to have broken down. Progressive degradation was observed on the 12^{th} day, as shown in Figure 6.6e. Hence, most of the drug release occurred by diffusion through the pores that formed during the hardening phase.

In the current studies, in the matrix-microspheres comprising the drug, prodigiosin, and the hydrophilic polymer chitosan, the release followed the following three steps: First, the dissolution medium penetrated into the microsphere matrix (hydration). This is followed by swelling, with instant or subsequent dissolution or erosion of the matrix. Finally, the transport of the dissolved drug occurred either through the hydrated matrix, or from eroded microspheres, to the surrounding dissolution medium [77]. The prodigiosin released on the first day for the different formulations (S1, S2, S3 and S4) were 4.4%, 10%, 3.5% and 6.25%. By the 6^{th} day, the percentage release had increased to 60.1%, 71.7%, 78.7% and 77.5%, respectively (Table 6.3).

The prodigiosin release data obtained from dissolution are plotted in Figure 6.7. They are plotted as prodigiosin concentration (mg/ml) versus time (days). In accordance with Eq. 5, a linear regression analysis of the data yielded a best fit with a straight line ($C = 8.06x - 3.01$) and a

regression coefficient of R^2 = 0.9559. According to Eq. 5, the slope of the line corresponds to a zeroth order release [55]. Therefore, the rate of dissolution is k_0 = 8.06 mg.ml^{-1} day^{-1}, while the rate of prodigiosin released per unit time (Q) can be obtained from Equation (10):

$$Q = k_0 \text{ x } V \qquad (10)$$

Where V is volume of dissolution medium (ml) and k_0 is the rate of dissolution.

6.4.6 Drug Release Kinetics

The release kinetics of prodigiosin from the microspheres was also determined based on best fit of the models tested, which include: zeroth- order and first-order models and the Higuchi model [78]. The R^2 values were obtained for the linear curves obtained via regression analysis of the plots (Figure 6.8a – 6.8c). The regression coefficients determined for different drug release kinetic models are : 0.964 for zeroth-order; 0.999 for the first-order models and 0.975 for the Higuchi model. The first order model, therefore, provides the best fit to the current data.

Hence, the first order release model was used to analyze the drug release from the different formulations (S1 - S4), as shown in Figure 6.9. The minimum drug contents obtained after release (Co) was calculated using Equation 11,

$$ln\, C = lnCo - Kt \qquad (11)$$

And the half-lives were equally determined using

$$t_{½} = \frac{ln2}{k} \qquad (12)$$

Where *lnCo* is the intercept, k is the slope (rate constant) and *t* corresponds to time. The results of the fit are presented in Table 6.2. These show that at concentration of 5 mg/ml (S4), 4.1 mg/ml, representing 82% of the drug, was released, leaving behind only 0.9 mg/ml (Co = 18%), while at the concentration of 1 mg/ml (S1), Co was 0.46 (46%). This further confirms the findings of prior researchers [73], who noted that the higher the drug-polymer ratio, the higher the swelling ratio, and the faster the drug elution rates from the microspheres. Also, the half-life (the time required for the drug concentration to drop to one-half its initial value) showed that the formulation, S2, had the longest half-life of 84 h. This was followed by S1with 23.76 h, and the least being S4, with 4.8 h.

The above results are consistent with the fact that the higher the concentration of the drug, the larger the pore sizes, and hence, the quicker the drug elution. The differences in the pore sizes are attributed to the effects of the cross-linking agent that was added. The same amount of the cross-linker (glutaraldehyde) was added in all of the formulations. The formulation with the highest polymer: drug ratio was more tightly linked than others. Hence, they have smaller pore sizes.

Also, the drug release mechanism was determined from the plot of ln (m_t/m_i) versus ln T (Figure 6.10). The value of n for the various formulations (Table 6.4a), is consistent with anomalous transport. Hence, the diffusion was non-Fickian diffusion.

6.4.7 Cell Viability

In our study, the effects of drug release from the prodigiosin-chitosan microspheres were tested on viable triple negative breast cancer cells (MDA-MB-231cells acquired from American Type Culture Collection (ATCC Manassas, KS, USA). The results showed that prodigiosin (released

from the microspheres) reduced the viability of the cancer cells, (Figure 6.11). The effects of drug concentration on the viability of the breast cancer cells were studied against a control (without drug). The results (plots of cell viability against time) (Figure 6.12) of the viability of breast cancer cells exposed to 1mg/ml (S1) and 5mg/ml (S4) of prodigiosin encapsulated in chitosan microspheres were compared with the cancer cells without prodigiosin treatment. A significant decrease in the cell viability was observed after 24 hours with both levels of prodigiosin treatment, while, in contrast, cell proliferation was observed in the control sample. Also, the decrease in cell viability with the 5 mg/ml prodigiosin was faster than the decrease in cell viability observed at the lower concentration (1 mg/ml).

The loss of cells' ability to divide was largely due to the release of the drug onto the cells. The reduction in the cell viability is attributed to the induced apoptosis associated with prodigiosin release [79, 80]. Prodigiosin has been found to promote apoptosis in a wide variety of human cancer cell lines, including hematopoietic, gastrointestinal, and breast and lung cancer cells, with no marked toxicity in nonmalignant cells [81-87]. The action of prodigiosin is through the intrinsic apoptotic pathway otherwise known as mitochondria-mediated apoptosis. Tsing-Fen et al. [88] have recently shown that prodigiosin down-regulates survivine-protein (member of the inhibitor of apoptosis family).

6.4.8 Implications

In this work, we have shown that – prodigiosin of high purity (92.8%) can be obtained from *Serratia marcescens.* We have also demonstrated that prodigiosin reduced the viability of the breast cancer cell line, (MDA-MB-231). Since prodigiosin can be readily produced from locally sourced bacteria, this approach could greatly reduce the cost and availability of drugs for cancer

treatment. The encapsulation efficiency studies incorporating prodigiosin into chitosan microspheres also showed that the S4 formulation had the highest encapsulation efficiency. This is consistent with the findings of Dhakar *et al.*, [89, 90], who noted that higher drug-polymer ratios increase the drug loading capacity. The percentage yield of the production of prodigiosin: chitosan microspheres were generally poor for all four formulations due to the recovery process. There is, therefore, a need to improve the recovery methodology. Finally, it is important to note that the good network of micropores (present within the microspheres), facilitated by the use of a cross-linker (glutaraldehyde), contributed to the efficient drug release that was observed. S1, with a drug concentration of 1mg/ml, had the longest half-life, while the mixture with highest drug concentration (5mg/ml), had the shortest half-life. Hence, different formulations can be administered, as appropriate, for different types or stages of cancer.

6.5.0 Summary and Concluding Remarks:

This paper presents the results of an experimental study of prodigiosin extraction and encapsulation in chitosan microspheres. The resulting structures, which have the potential to reduce the cost of localized cancer drug release, were used to study the release of cancer drugs (prodigiosin), from chitosan capsules. The formulation with the highest concentration of drug had the highest encapsulation efficiency. The percentage yield varied, due to the recovery method that was used. The drug release studies also showed that the primary mechanisms of drug release were diffusion and dissolution. The drug release kinetics was determined to be well described by first order kinetics.

REFERENCES

1. Rawat, M., Singh, D., Saraf, S.: Nanocarriers: promising vehicles for bioactive drugs. Biol Pharm Bull. 2006; 29: 1790–1798.

2. Nitika, A., Ravinesh, M., Chirag, G., Manu, A.: Microencapsulation – A Novel Approach in Drug Delivery: A Review Indo Global Journal of Pharmaceutical Sciences, 2(1): 1-20 (2012).

3. Ge, H., Hu, Y., Jiang, X., Cheng, D., Yuan, Y., Bi, H., Yang, C.: Preparation, characterization, and drug release behaviors of drug nimodipine-loaded poly(ε-caprolactone)- poly(ethylene oxide)-poly(ε-caprolactone) amphiphilic triblock copolymer micelles. J Pharm Sci.; 91:1463–1473 (2002).

4. Gref, R., Minamitake, Y., Peracchia, M.T., Trubetskoy, V., Torchilin, V., Langer, R.: Biodegradable long-circulating polymeric nanospheres. Science; 263:1600–1603 (1994).

5. Shin, I.G., Kim, S.Y., Lee, Y.M., Cho, C.S., Sung, Y.K.: Methoxy poly (ethylene glycol)/ε-caprolactone amphiphilic block copolymeric micelle containing indomethacin. I. Preparation and characterization. J Control Release; 51:1–11 (1998).

6. Jeong, J.C., Lee, J., Cho K. Effects of crystalline microstructure on drug release behavior of poly (ε-caprolactone) microspheres. J. Control Release; 92: 249–258 (2003).

7. Blanco, D., Alonso, M.J.: Protein encapsulation and release from poly(lactide-co-glycolide) microspheres: effect of the protein and polymer properties and of the co-encapsulation of surfactants. Eur J Pharm Biopharm; 45(3):285-94 (1998).

8. Jagtap, Y.M, Bhujbal, R.K, Ranade, A.N, Ranpise, N.S.: Effect of various polymers concentrations on physicochemical properties of floating microspheres". Indian journal of pharmaceutical sciences; 74: (6) 512-520 (2012).

9. Michelle, L., Peter, L.C., Hisataka, K.: Clearance Properties of Nano-sized Particles and Molecules as Imaging Agents: Considerations and Caveats. Nanomedicine (Lond.), 3(5) 703–717(2008).

10. Hak, S.C., Wenhao, L., Preeti, M., Eiichi, T., John, P. Z., Binil , I.I., Moungi, G.B., John, V. F. Renal Clearance of Nanoparticles. Nat. Biotechnol; 25(10) 1165–1170 (2007).

11. Langer, R. S., Wise, D. L(Eds).: Medical Applications of Controlled Release, Applications and Evaluation. Vol. I and II, CRC Press, Boca Raton, Florida (1984).

12. Pillai, O., Dhanikula, A. B., Panchagnula, R.: Drug delivery: An odyssey of 100 years. Current Opinion in Chemical Biology, 5 (4), 439-446 (2001).

13. Li, V.H. K., Lee, V. H. L.: Controlled drug delivery: Fundamentals and applications,(Robinson J R, Lee V H L, eds.) 2nd Ed., Marcel Dekker Inc., New York. 4 – 36, (1987).

14. Suvakanta, D., Padala, N. M., Lilakanta, N., Prasanta, C.: Kinetic modeling on drug release from controlled Drug delivery systems Acta Poloniae Pharmaceutica ñ Drug Research, 67(3) 217- 223 (2010).

15. Muzzarelli, R.: Chitosan, in: Muzzarelli, R (Ed.), Natural Chelating Polymers, Pergamon Press, Oxford, 144–176 (1973).

16. Illum, L. Chitosan and Its use as a Pharmaceutical Excipient. Pharm Res., 15:1326-1331 (1998).

17. Nunthanid, J., Puttipipatkhachorn, S., Yamamoto, K., Peck, G. E.: Physical Properties and Molecular Behavior of Chitosan Films. Drug Dev Ind Pharm., 27 (2): 143- 157 (2001).

18. Zydowicz, N, Vachoud, L. A., Domard, L.A. in: A. Domard, C. Jeuniaux, R. Muzzarelli, E. Roberts (editors), Advances in Chitin Science, 1, Lyon: Andre J; 262 (1996).

19. Nordtveit, R.J., Varum, K.M., Smidsrod, O.: Degradation of partially N-acetylated chitosans with hen egg white and human lysozyme. Carbohyd. Polym. 29, 163 (1996).

20. Peluso, G., Petillo, O., Ranie ri, M., Santin, M., Ambrosic, L., Calabro, D., Avallone, B., Balsamo, G.: Chitosan-mediated stimulation of macrophage function. Biomaterials, 15, 12-15 (1994).

21. Borchard, G., Junginger, H.E.: Modern drug delivery applications of chitosan. Adv Drug Del Rev., 52 (2): 103 (2001).

22. Shigemasa, Y., Saito, K., Sashiwa, H., Saimato, H.: Enzymatic degradation of chitins and partially deacetylated chitins. Int. J. Biol. Macromol. 16, 43 (1994).

23. Karlsen, J., Skaugrud, O.: Excipient properties of chitosan. Manuf. Chem. 62, 18 (1991).

24. Singla AK, Chawla M. Chitosan: some pharmaceutical and biological aspects-an update. J PharmPharmacol., 53 (8): 1047-1067 (2001).

25. Ueno, H., Mori, T., Fujinaga, T.: Topical formulations and wound healing applications of chitosan. Adv Drug Del Rev., 52 (2): 105-115 (2001).

26. Senel, S., Kremer, M .J., Kas, S., Wertz, P. W., Hincal, A. A., Squier, C. A. Enhancing effect of chitosan on peptide drug delivery across buccal mucosa. Biomaterials. 21, 2067–2071 (2000).

27. He P, Davis SS, Illum L. In vitro evaluation of mucoadhesive properties of chitosan microspheres. Int. J. Pharm. 166, 75–88 (1998).

28. Aksungur, P., Sungur, A., Unal, S., Iskit, A.B., Squier, C. A., Senel, S. J.: Chitosan delivery systems for the treatment of oral mucositis: In vitro and in vivo studies. J. Control Release; 98, 269–279 (2004).

29. Monteiro, O. A.C., Airoldi, C.: Some studies of crosslinking chitosan glutaraldehyde interaction in a homogeneous system, Int. J. Biol. Macromol. 26, 119–128. (1999).

30. Lindsey, A. S., Adam, M. D., Sarena, D, H., Nicholas, A, P.: Therapeutic applications of hydrogels in oral drug delivery. Expert Opin Drug Deliv. 11(6): 901–915 (2014).

31. Lewis, S.M., Corpe, W.A.: Prodigiosin-producing bacteria from marine sources. Applied and Environment Microbiology, 12 (1) 13-17 (1964).

32. Song, M.J., Bae, J., Lee, D.S., Kim, C.H., Kim, J.S., Kim, S.W., Hong, S.I.: Purification and characterization of prodigiosin produced by integrated bioreactor from Serratia sp. KH-95. Journal of Bioscience and Bioengineering 101, (21) 57-161 (2006).

33. Huh, J.E, Yim, J.H., Lee, H.K., Moon, E.Y., Rhee, D.K., Pyo, S.: Prodigiosin isolated from Hahella chejuensis suppresses lipopolysaccharide-induced NO production by inhibiting p38 MAPK, JNK and NF-κB activation in murine peritoneal macrophages. International Immunopharmacology 7, (13), 1825-1833 (2007).

34. Alihosseini, F., JU KS, Lango J, Hammock BD, Sun, G. Antibacterial colorants: Characterization of prodiginines and their applications on textile materials. Biotechnology Progress, 24, (3), 742-747 (2008).

35. Kawasaki, T., Sakurai, F., Hayakawa, Y.: A prodigiosin from the roseophilin producer *Streptomyces griseoviridis*. Journal of Natural Products, 71, (7), 1265-1267 (2008).

36. Kim, D., Kim, J.F., Yim, J.H., Kwon, S.K., Lee, C.H., Lee, H.K. Red to red - the marine bacterium Hahella chejuensis and its product prodigiosin for mitigation of harmful algal blooms. Journal of Microbiology and Biotechnology, 18, (10), 1621-1629 (2008).

37. Borić, M., Danevčič, T., Stopar, D.: Prodigiosin from Vibrio sp. DSM 14379: A new UV-protective pigment. Microbial Ecology, 62, (3), 528-536 (2011).

38. Lee, J.S., Kim, Y.S., Park, S., Kim, J., Kang, S.J., Lee, M.H., Ryu, S., Choi, J.M., Oh, T.K., Yoon, J.H.: Exceptional production of both prodigiosin and cycloprodigiosin as major metabolic constituents by a novel marine Bacterium, Zooshikella rubidus S1-1. Applied and Environmental Microbiology, 77, (14), 4967-4973 (2011).

39. Furstner, A.: Chemistry and biology of roseophilin and the Prodigiosin alkaloids: A survey of the last 2500 years. Chem Int Ed Engl, 42, 3582-3603 (2003).

40. Samrot, A.V., Chandana, K., Senthilkumar, P., Narendra, K. G.: Optimization of Prodigiosin production by *Serratia marcescens* SU-10 and evaluation of its bioactivity. International Research Journal of Biotechnology (ISSN: 2141-5153), 2(5), 128-133 (2011).

41. Cerdeno, A.M., Bibb, M.J., Challis, G.L.: Analysis of the prodiginine biosynthesis gene cluster of Streptomyces coelicolorA3 (2): new mechanisms for chain initiation and termination in modular multienzymes. Chem Biol, 8, 817-829 (2001).

42. Montaner, B., Pérez-Tomás, R.: Prodigiosin Induces Caspase-9 and Caspase-8 Activation and Cytochrome C Release in Jurkat T cells. Ann. NY Acad. Sci. 973, 246-249 (2002).

43. Pérez-Tomás, R., Montaner, B., Llagostera, E., Soto-Cerrato, V.: The Prodigiosins, Proapoptotic Drugs with Anticancer Properties. Biochem. Pharmacol. 66, 1447-1452 (2003).

44. Montaner, B., Navarro, S., Piqué, M., Vilaseca, M., Martinell, M., Giralt, E., Gil, J., Pérez-Tomás, R.: Prodigiosin from the Supernatant of *Serratia Marcescens* Induces Apoptosis in Hematopoietic Cancer Cell Lines. British J. Pharmacol. 131, 585-593 (2000).

45. Francisco, R., Perez-Tomas, R., Gimenez-Bonafe, P., Soto-Cerrato, V., Gimenez-Xavier, P., Ambosio, S.: Mechanisms of Prodigiosin Cytotoxicity in Human Neurobblastoma Cell Lines. European journal of Pharmacology. 572 (2-3) 111-119 (2007).

46. Kamble, K.D., Hiwarale, V. D.: Prodigiosin Production from *Serratia Marcescens* Strains obtained from Farm Soil. Int. J. Environmental Sci. 3(1) 631-638 (2012).

47. El-Bialy, H.A., El-Nour, S.A.: Physical and chemical stress on *Serratia marcescens* and studies on prodigiosin pigment production. Annals of Microbiology. 65 (1): 59–68 (2015).

48. Danyuo, Y., Ani, C.J., Obayemi, J.D., Dozie-Nwachukwu, S., Odusanya, O.S., Oni, Y., Anuku, N., Malatesta, K., Soboyejo, W.O.: Prodigiosin Release from an Implantable Biomedical Device: Effect on Cell Viability. Advanced Materials Research, 1132, 3-18 (2015).

49. Roy, S., Panpalia, S.G., Nandy, B.C., Rai, V.K., Tyagi, L.K., Dev, S., Meena, K.C.: Effect of Method of Preparation of Chitosan Microspheres of Mefanamic Acid. International Journal of pharmaceutical sciences and drug Research, (1), 36-42, (2009).

50. Sabitha, P., Ratna, J.V., Reddy, K.R.: Design and evaluation of controlled release chitosan-calcium alginate microcapsules of Anti tubercular drugs for oral use. Int. J. Chem.Tech Res. 2(1)88-98 (2010).

51. Obayemi, J.D., Danyuo, Y., Dozie-Nwachukwu, S., Odusanya, O.S., Anuku, N., Malatesta, K., Yug, W., Uhrich, K.E., Soboyejo, W.O.: PLGA-based microparticles loaded with bacterial-synthesized prodigiosin for anticancer drug release: Effects of particle size on drug release kinetics and cell viability. Materials Science and Engineering C, 66: 51–65 (2016)

52. Higuchi, T.: J Pharm Sci; 50:874-875 (1961).

53. Higuchi, T.: Mechanism of sustained action medication. Theoretical analysis of rate of release of solid drugs dispersed in solid matrices. J. Pharm. Sci., 52: 1145-1149 (1963).

54. Korsmeyer, R.W., Gurny, R., Doelker, E., Buri, P., Peppas, N .A.: Mechanisms of solute release from porous hydrophilic polymers. Int. J. Pharm, 15: 25-35 (1983).

55. Kalam, M. A., Humayun, M., Parvez, N., Yadav, S., Garg, A., Amin, S., Sultana, Y., Ali, A.: Continental J Pharm Sci 1: 30 – 35 (2007).

56. Bourne, DWA. Pharmacokinetics. In: Banker, G.S., Rhodes, C.T., Modern Pharmaceutics, 4th ed., Marcel Dekker Inc., New York, 67-92 (2002).

57. Kabir, A.L.K., Biswas, B.K., Rouf, A.S.S.: Design, Fabrication and Evaluation of Drug Release Kinetics from Aceclofenac Matrix Tablets using Hydroxypropyl Methyl Cellulose. Dhaka Univ J Pharm Sci. 8(1): 23-30 (2009).

58. Narashimhan, B., Mallapragada, S.K., Peppas, N. A.: Release kinetics, data interpretation, in: Encyclopedia of controlled drug delivery, Mathiowitz E. Ed., John Wiley and Sons, Inc, New York (1999).

59. Silvina, A.B., Lamas, M.C., Claudio, J.S.: In-vitro studies of diclofenac sodium controlled-release from biopolymeric hydrophilic matrices. J. Pharm. Pharm. Sci. 5(3):213-219 (2002) .

60. Ahmad, A.S., Ahmad, W.Y.W., Zakaria, Z. K., Yosof, N.Z.: Applications of bacterial pigments as colorant: the Malaysian perspective. New York: Springer Briefs in Molecular Science (2012)

61. Nakashima, T., Kurachi, M., Kato, Y., Yamaguchi, K., Oda, T.: Characterization of bacterium isolated from the sediment Coast area of Omura Bay in Japan and several biological activities of pigment produced by this isolated. Microbiol Immunol. 49, 407-415 (2005)

62. Giri, A.V., Anandkumar, N., Muthukumaran, G., Pennathur, G.: A novel medium for the enhanced cell growth and production of prodigiosin from *Serratia marcescens* isolated from soil. BMC Microbiology. 4:11 (2004).

63. Azambuja, P., Garcia, E.F.: Isolation of *Serratia marcescens* in the midgut of Rhodnius prolixus: impact on the establishment of the parasite Trypanosoma cruzi in the vector. Exper parasitol. 107:89-96 (2004)

64. Martínez-Ruvalcaba , A., Sánchez-Díaz, J.C., Becerra, F., Cruz-Barba, L.E., González-Álvarez, A.: Swelling characterization and drug delivery kinetics of polyacrylamide-co-itaconic acid/chitosan hydrogels. eXPRESS Polymer Letters. 3(1): 25–32 (2009)

65 Frank, S., Lauterbur, P.C.: Voltage-sensitive magnetic gels as magnetic resonance monitoring agents. Nature, 1993; 363: 334–336.

66. Peppas, N.A., Colombo, P.: Analysis of drug release behavior from swellable polymer carriers using the dimensionality index. Journal of Controlled Release. 1997; 45: 35–40

67. Tanaka, T.: Phase transitions of gels. in 'Polyelectrolyte gels: Properties, preparation and applications' (eds.: Harland R. S., Prud'homme R. K.) American Chemical Society, Washington, 480, 1–21 (1992).

68. Suzuki ,A., Ishii, T., Maruyama, Y.: Optical switching in polymer gels. Journal of Applied Physics, 80: 131– 136 (1996).

69. Khare , A.R., Peppas, N. K.: Swelling/deswelling of anionic copolymer gels. Biomaterials, 16: 559–567 (1995).

70. Zhong, X., Wang ,Y-X., Wang, S-C.: Pressure dependence of the volume phase-transitions of temperature sensitive gels. Chemical Engineering Science. 51: 3235–3239 (1996)

71. Peppas, N.A, Huang, Y.: Polymer and gels as molecular recognition agents. Pharmaceutical Research, 19: 578–587 (2002).

72. Danyuo, Y., Dozie-Nwachukwu, S., Obayemi, J.D., Ani, C.J., Odusanya, O.S., Oni, Y., Anuku, N., Malatesta, K., Soboyejo, W.O.: Swelling of poly (N-isopropylacrylamide) P (NIPA)-based hydrogels with bacterial-synthesized prodigiosin for localized cancer drug delivery. Mater Sci Eng C Mater Biol Appl. 59:19-29 (2015).

73. Bennour, S., Louzri, F.: Study of Swelling Properties and Thermal Behavior of Poly (N,N-Dimethylacrylamide-co-Maleic Acid) Based Hydrogels. Advances in Chemistry, Vol 2014, Article ID 147398, 1-10 (2014).

74. Patil, K.N., Upadhye, K.P.: Formulation development and evaluation of mucoadhesive micro-spheres of salbutamol sulphate by using a natural polymer. International Journal of Pharmaceutical Sciences and Research. 4(12): 4775- 4786 (2013).

75. Perumal, D.: Microencapsulation of ibuprofen and Eudragit RS 100 by the emulsion solvent diffusion technique, Int.J.Pharm, 218, 1-11 (2001).

76. Bonacucina, G., Cespi, M., Palmieri, G.F. Evaluation of dissolution kinetics of hydrophilic polymers by use of acoustic spectroscopy. Int J Pharm 377:153–158 (2009).

77. Kiortsis, S., Kachrimanis, K., Broussali, T., Malamataris, S.: Drug release from tableted wet granulations comprising cellulosic (HPMC or HPC) and hydrophobic component. Eur. J. Pharm. Biopharm. 59: 73-83 (2005).

78. Shoaib, M.S., Tazeen, J., Merchant, H.A., Yousuf, R.I.: Evaluation of Drug Release Kinetics from Ibuprofen Matrix Tablets using HPMC. Pak. J. Pharm. Sci., 19(2), 119-124 (2006).

79. Williams, N. R., Fineran, P. C., Leeper, F. J., Salmond, G. P.: The biosynthesis and regulation of bacterial prodiginines. Nat. Rev. Microbiol, 4, 887-889 (2006).

80. Pandi, S.K., Arul, D., Smiline, A. S. G., Hairul, I. V., Saravanan, S.V. G., Raghuraman, R.: Prodigiosin Induced Apoptosis and Inhibited Proliferation in Carcinoma Hsc-2 Cells. Int. J. of Current Research, 3(4): 151-156 (2011).

81. Montaner, B., Navarro, S., Pique, M., Vilaseca, M., Martinell, M., Giralt, E., Gil, J., Perez-Tomas, R.: Prodigiosin from the supernatant of Serratia marcescens induces apoptosis in haematopoietic cancer cell lines. Br J Pharmacol 131:585–593 (2000)

82. Campas, C., Dalmau, M., Montaner, B., Barragán, M., Bellosillo, B., Colomer, D., Pons, G., Pérez-Tomás, R., Gil, J.: Prodigiosin induces apoptosis of B and T cells from B-cell chronic lymphocytic leukemia. Leukemia 17:746–50 (2003).

83. Diaz-Ruiz, C., Montaner, B., Perez-Tomas R.:Prodigiosin induces cell death and morphological changes indicative of apoptosis in gastric cancer cell line HGT-1. Histol Histopathol 16: 415–21 (2001).

84. Montaner, B., Perez-Tomas, R.: Prodigiosin-induced apoptosis in human colon cancer cells. Life Sci 68: 2025–2036 (2001).

85. Soto-Cerrato, V., Llagostera, E., Montaner, B., Perez-Tomas, R.: Mitochondria- mediated apoptosis operating irrespective of multidrug resistance in breast cancer cells by the anticancer agent prodigiosin. Biochem Pharmacol 68:1345–52 (2004).

86. Llagostera, E., Soto-Cerrato, V., Joshi, R., Montaner, B., Gimenez-Bonafe, P., Perez-Tomas, R.: High cytotoxic sensitivity of the human small cell lung doxorubicin-resistant carcinoma

(GLC4/ADR) cell line to prodigiosin through apoptosis activation. Anticancer Drugs 16: 393–9 (2005).

87. Brenner, D., Mak, T.W.: Mitochondrial cell death effectors. Curr Opin Cell Biol 21: 871–877 (2009).

88. Tsing-Fen, H., Yu-Ta, P., Show-Mei, C., Shin-Chang, L., Bo-Lin, F., Chien-Hsing, L., Wan-Ju, Y., Jo-Shu, C., Chia-Che, C.: Prodigiosin down-regulates surviving to facilitate paclitaxel sensitization in human breast carcinoma cell lines. Toxicology and Applied Phamacology. 235: 253-260 (2009).

89. Dhakar, R.C., Maurya, S.D., Sagar, B.P.S., Bhagat, S., Prajapati, S.K., Jain, C.P.: Variables Influencing the Drug Entrapment Efficiency of Microspheres: A Pharmaceutical Review. Der Pharmacia Lettre, 2(5): 102-116 (2010).

90. Dhakar, R.C., Maurya, S.D., Saluja, V.: From Formulation Variables to Drug Entrapment Efficiency of Microspheres: A Technical Review. Journal of Drug Delivery & Therapeutics. 2(6), 128-133 (2012)

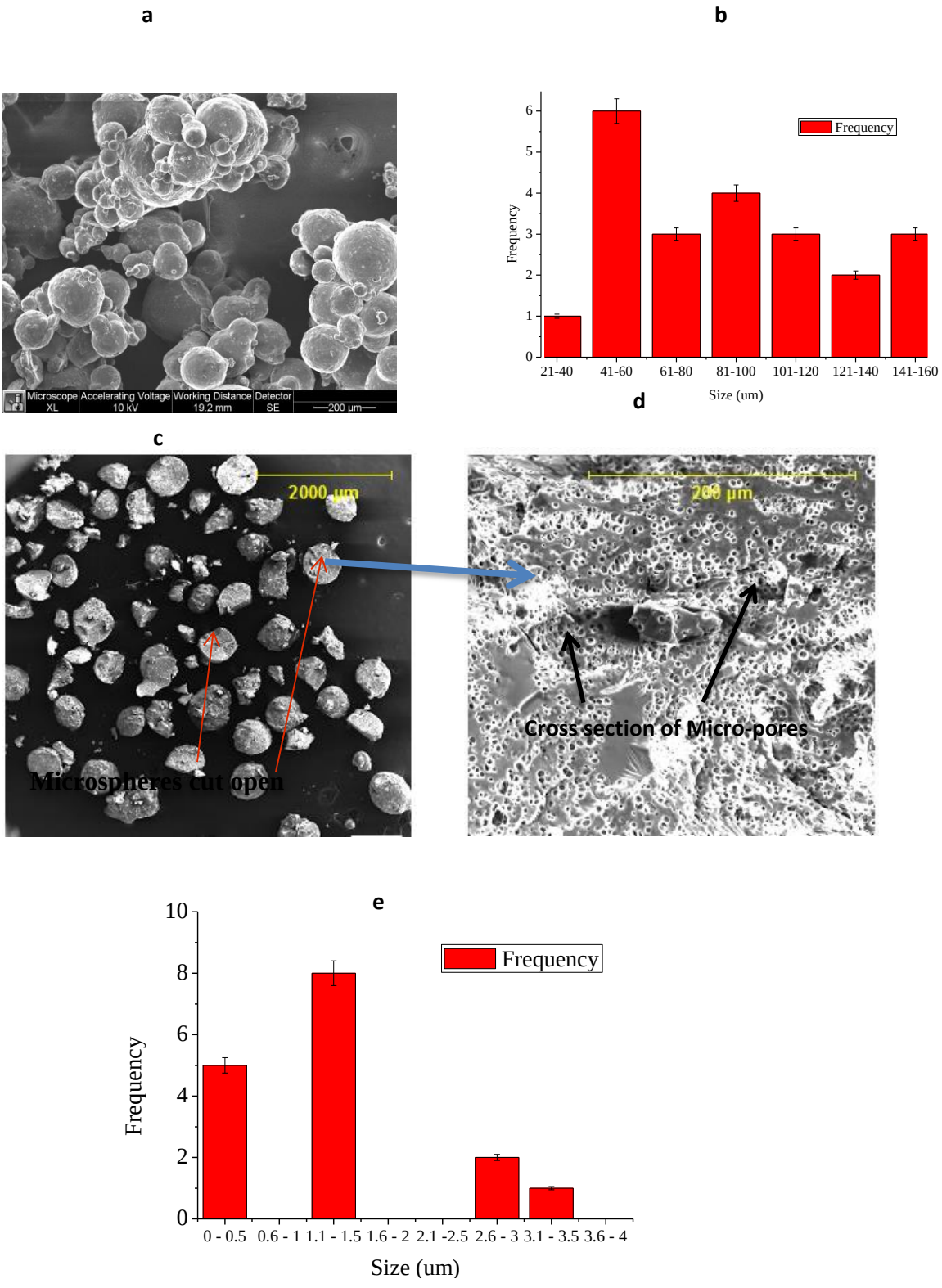

Figure 6.1: SEM images of (a) spherical shaped prodigiosin - chitosan microspheres (b) size distribution of chitosan microspheres (c) microspheres cut open (d) enlarged micropores within the microspheres and (e) histogram of size distribution for the micro-pores.

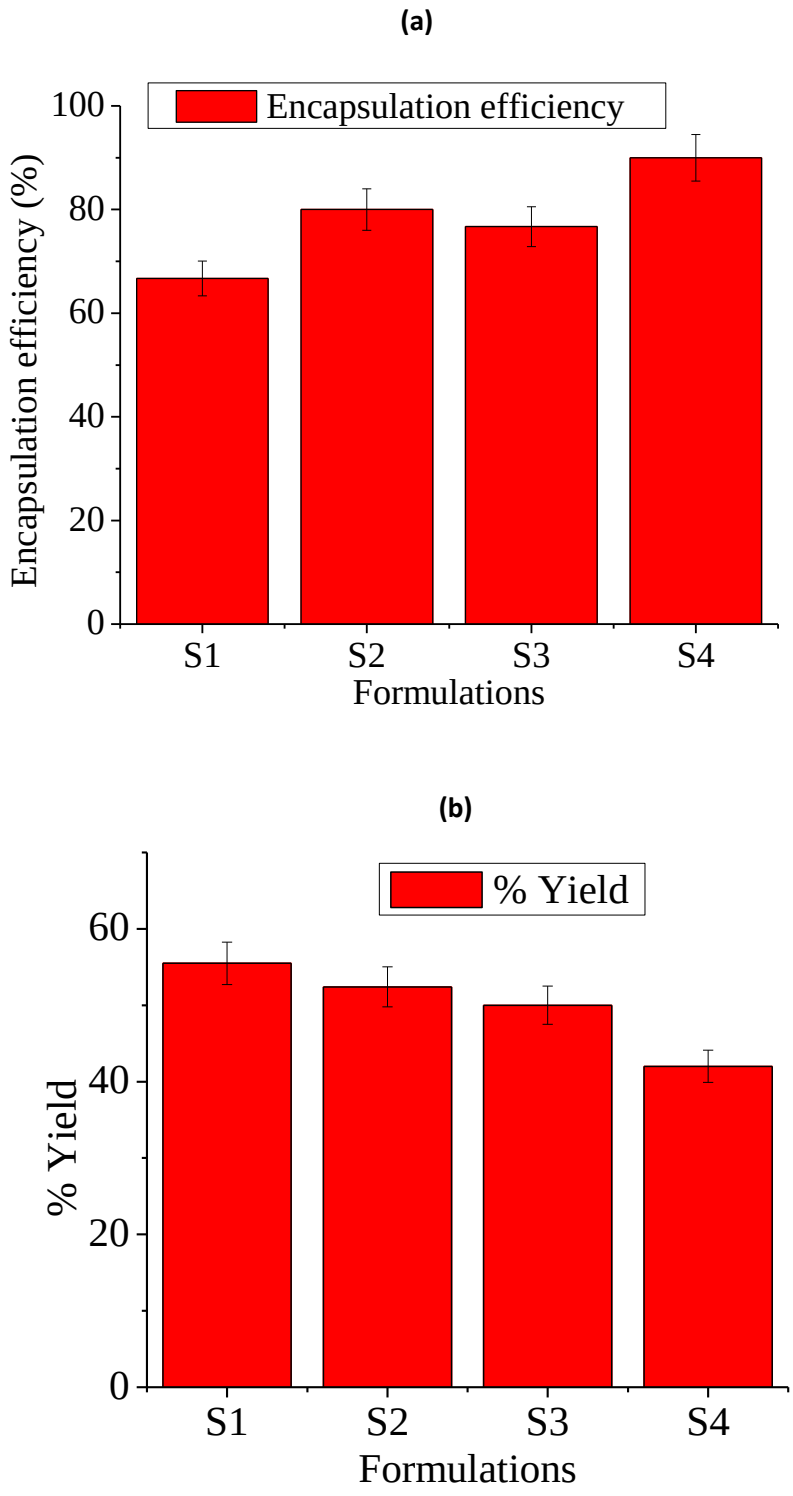

Figure 6.2: Showing (a) the percentage encapsulation efficiency and (b) % yield of the different formulations of prodigiosin-chitosan microspheres

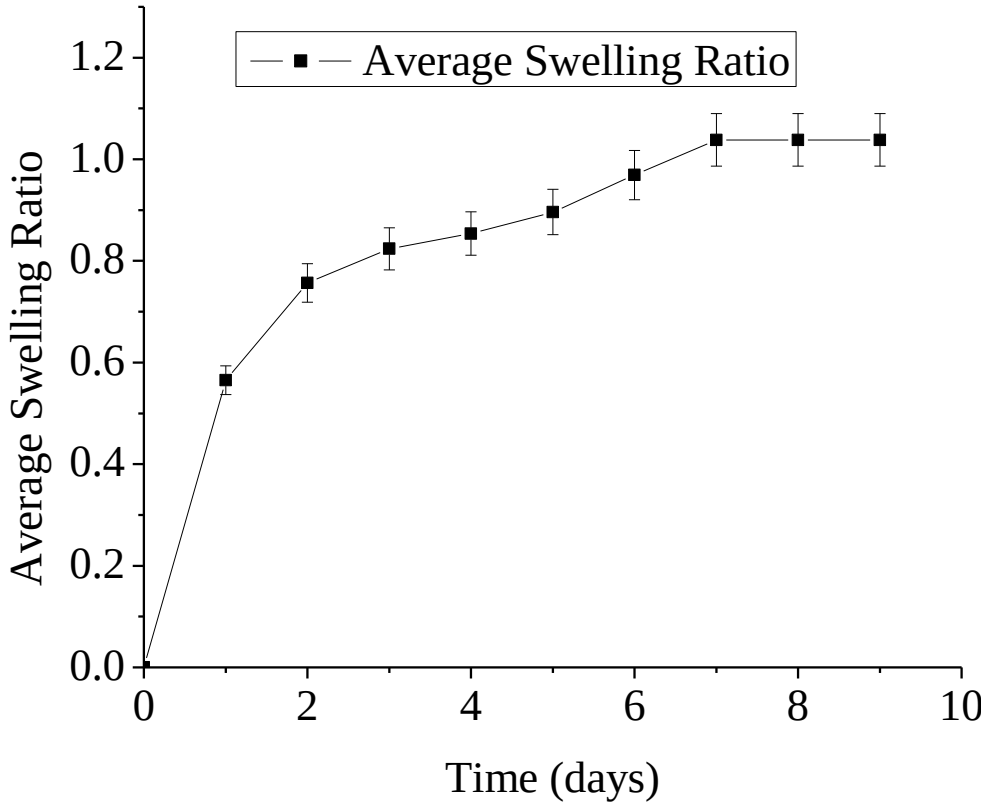

Figure 6.3: Average swelling ratio of the four formulations (S1 – S4) of prodigiosin-chitosan microparticles

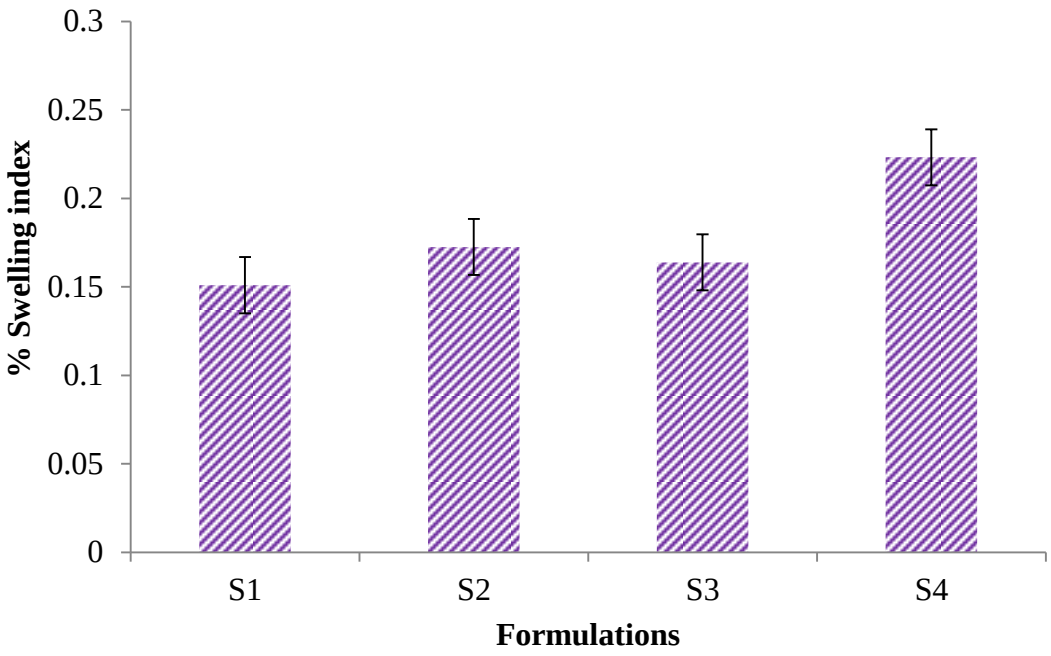

Figure 6.4: Comparison of swelling index of different formulation of prodigiosin-chitosan microspheres

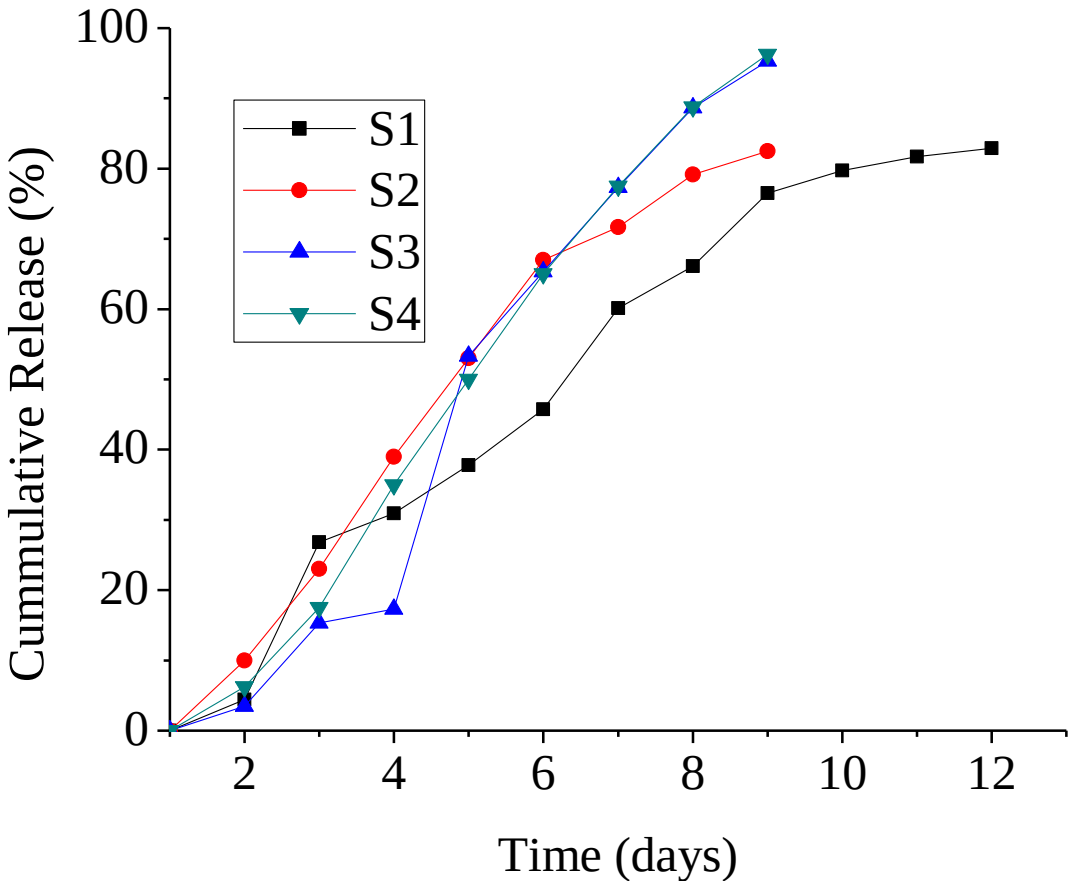

Figure 6.5: Release pattern of prodigiosin from the prodigiosin-chitosan microspheres

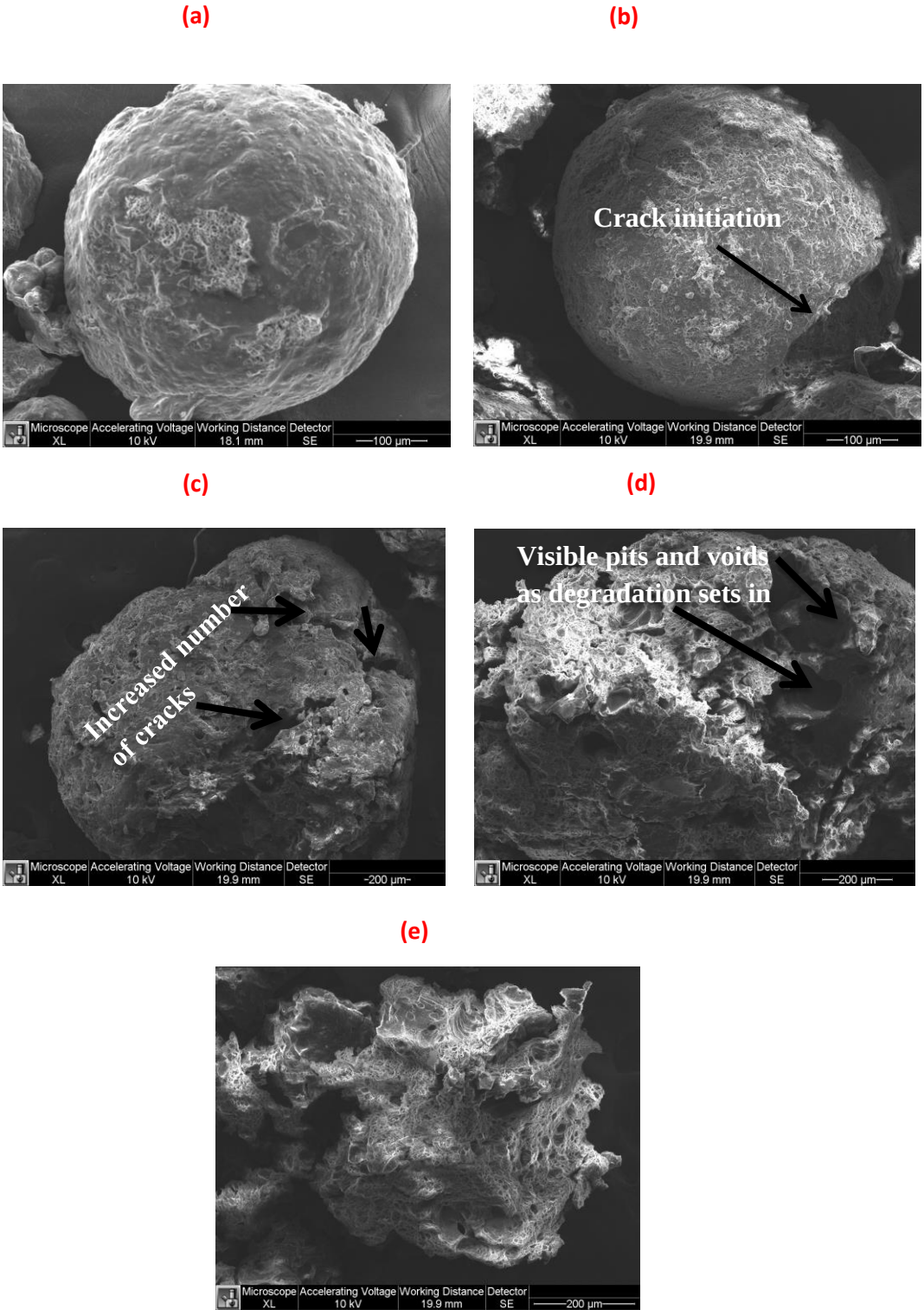

Figure 6.6: SEM Images showing the degradation process of the microspheres (a) microsphere before immersing in the pH 7.4 buffer (b) microsphere after 2 days in buffer, crack being initiated (c) increase in number of cracks after 5 days immersed in bufffer(d) at day 9 degradation has set in (e) after 12 days.

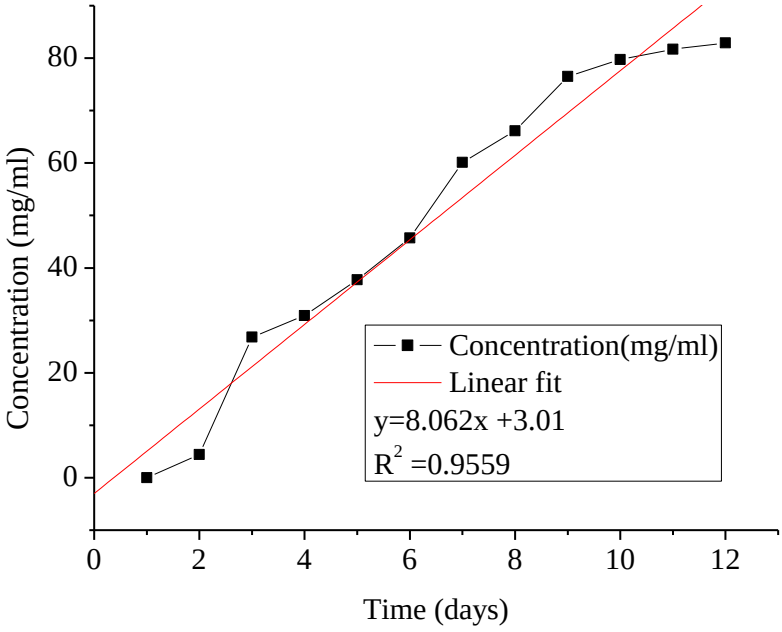

Figure 6.7: Prediction of prodigiosin drug release from microspheres using drug concentration (mg/l) versus time (days)

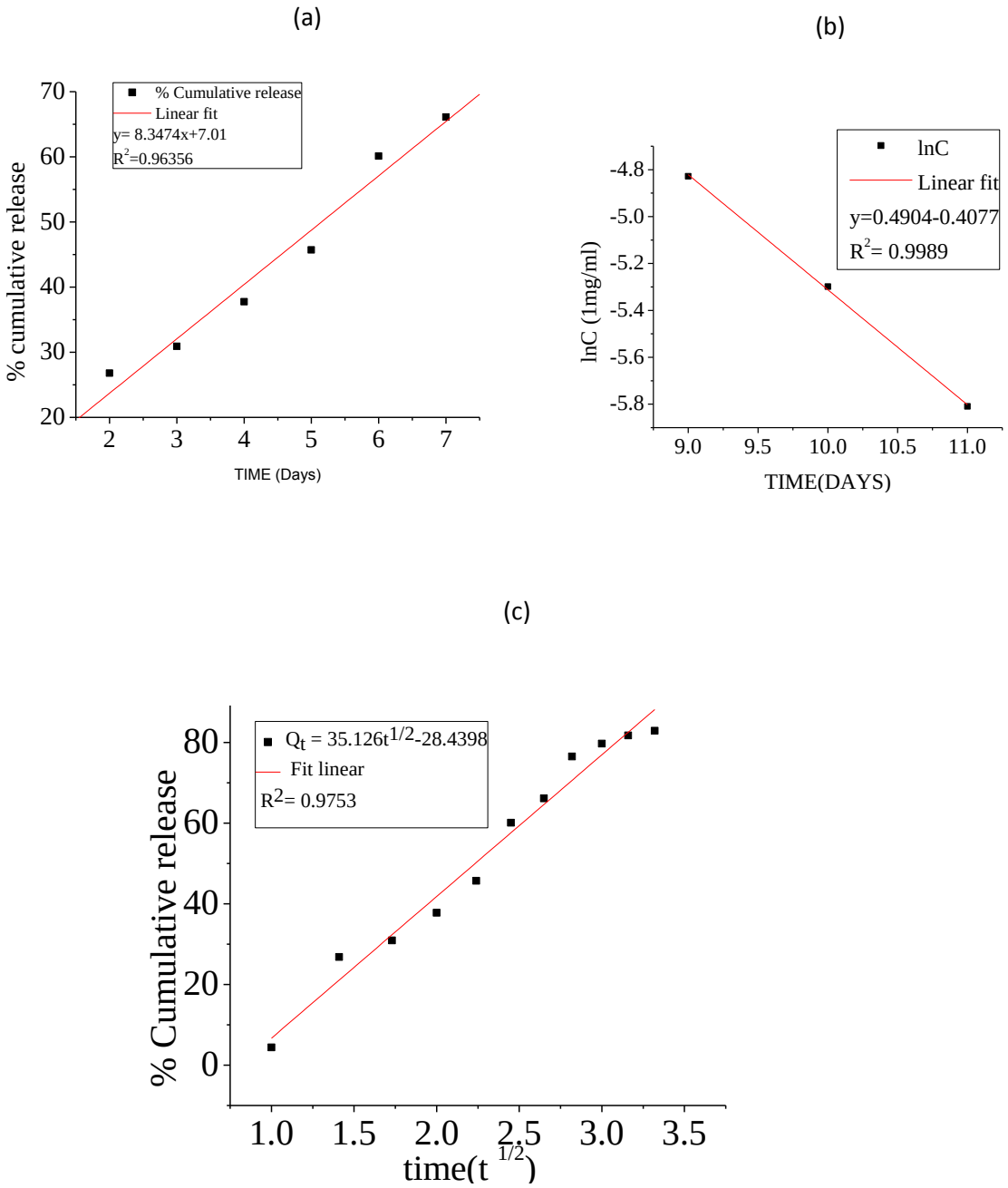

Figure 6.8: Estimation of Drug Release Model: (a) Zeroth Order (b) First- Order and (c) Higuchi model.

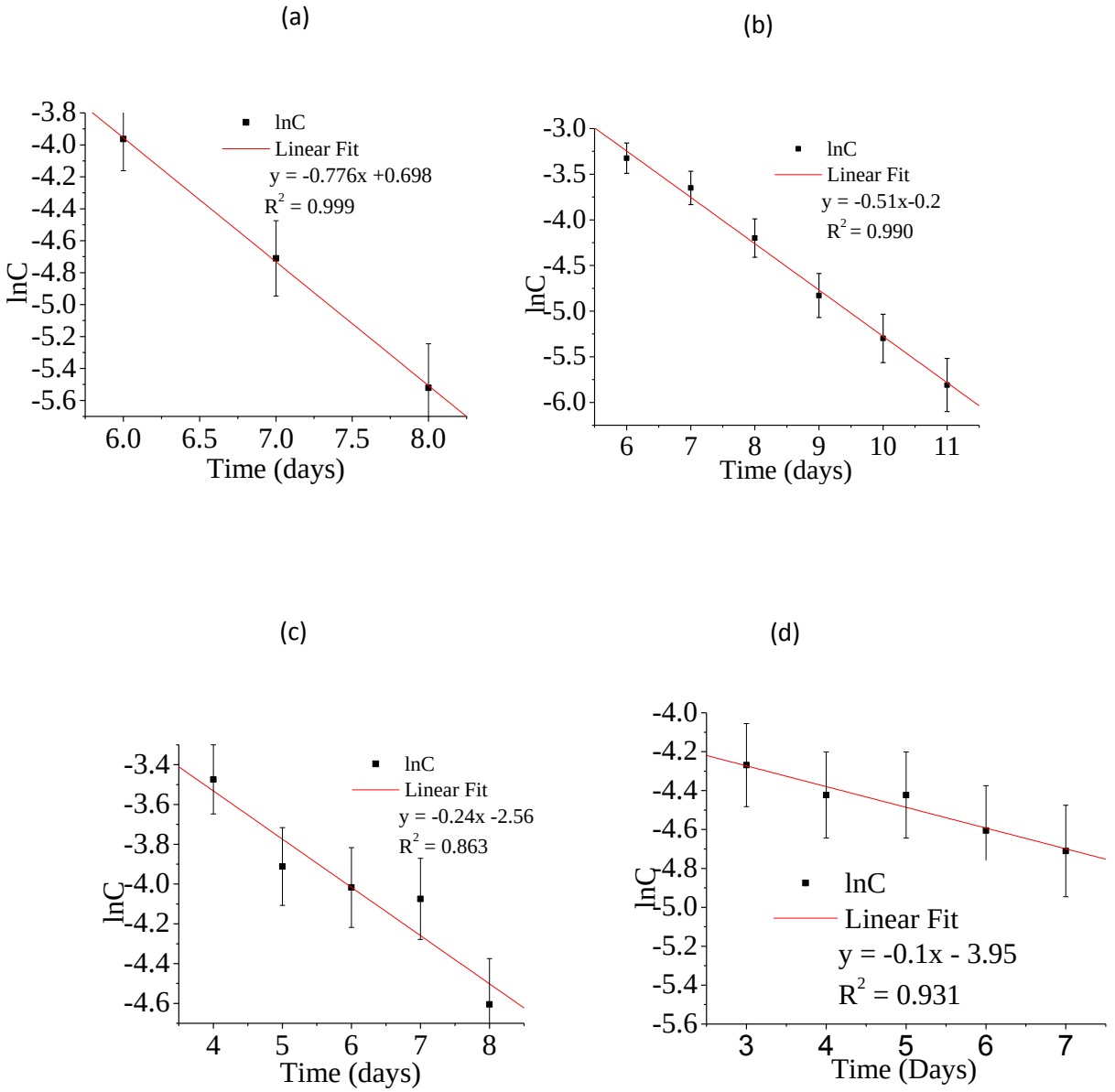

Figure 6.9: First Order Estimation of Drug Release. Plots of ln C versus Time for different prodigiosin chitosan in the microspheres: (a) S,1mg/ml, (b)S2, 1.5mg/ml, (c)S3, 2mg/ml and (d) S4,5mg/ml .

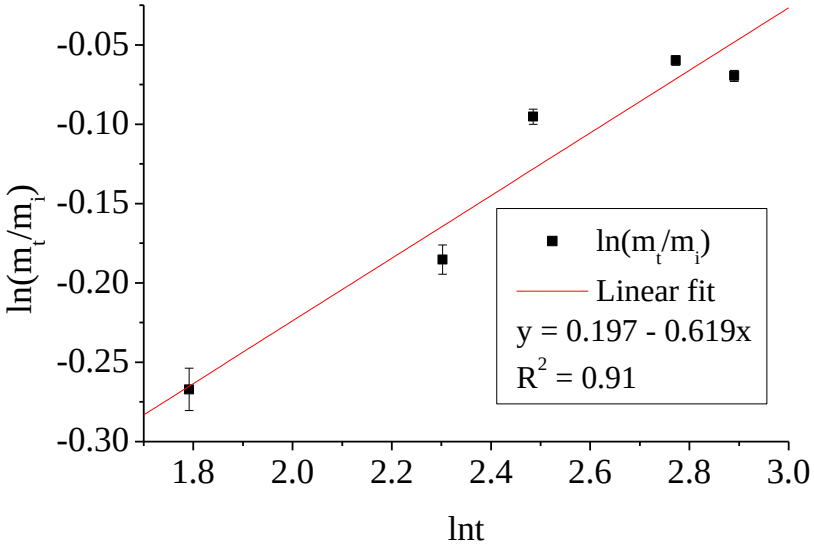

Figure 6.10: Diffusion fit for prodigiosin release from a plot of ln (m_t/m_i) versus ln T for prodigiosin - chitosan microspheres

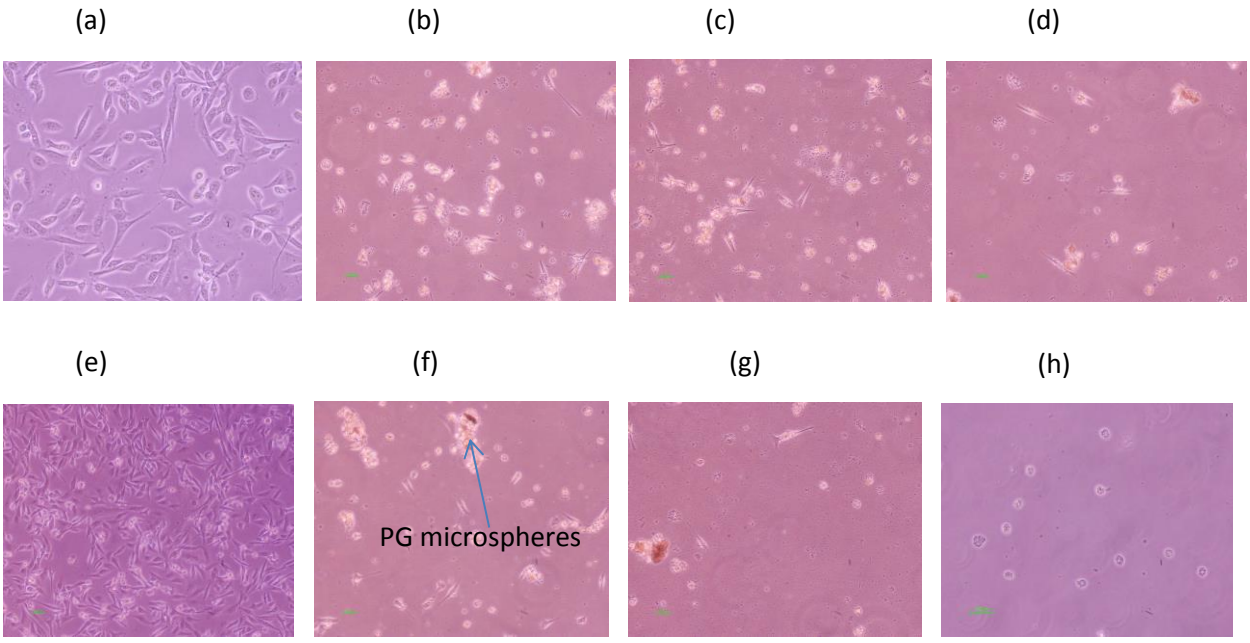

Figure 6.11: Cytotoxicity testing of the encapsulated prodigiosin in prodigiosin:chitosan microspheres using MDA-MB-231 cells. (a) MDA-MB-231 cells growing at 70% confluence. Figures (b) (c) and (d) show breast cancer cells treated with 1mg/ml prodigiosin (S1) encapsulated in chitosan microspheres at 24 h, 72 h and 96 h respectively, (e) control after 96 h, while Figures (f), (g) and (h) show breast cancer cells treated with 5mg/ml prodigiosin(S4) in prodigiosin:chitosan microspheres at 24h, 72 h and 96 h respectively..

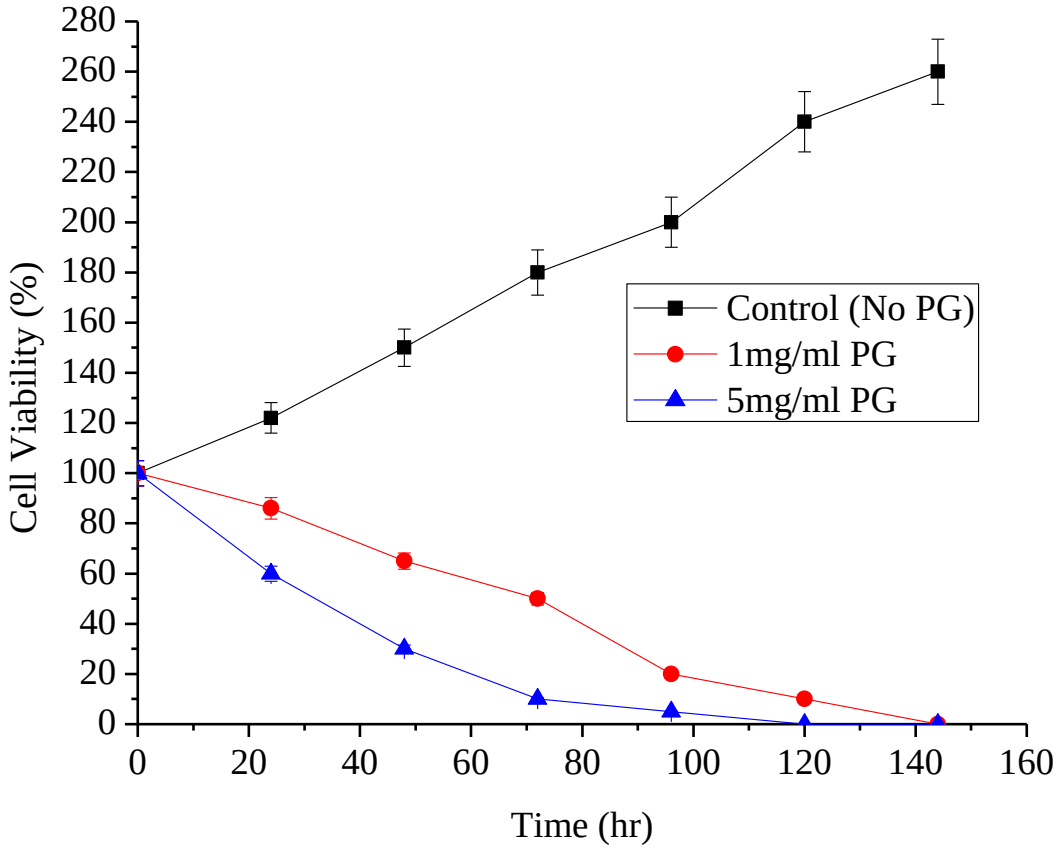

Figure 6.12: Cell Viability study of MDA-MB-231 Cell Line showing the effect incubation with different concentration of prodigiosin encapsulated in chitosan microspheres.

Table 6.1: Showing the encapsulation efficiency, drug loading capacity and % yield of the prodigiosin encapsulated chitosan microspheres

Samples (mg/ml)	S_1 (1mg/ml)	S_2 (1.5mg/ml)	S_3 (2mg/ml)	S_4 (5mg/ml)
% Encapsulation efficiency	66.7±3.3	80±4	76.7±3.8	90± 4
% Drug loading capacity	6.7±0.3	12±0.6	15.3±0.8	45± 2.3
% Yield	55.5±2.8	52.4±2.6	50±2.5	42±2.1

Table 6.2: showing the minimum drug content after release (Co) and the half-life

Drug Conc. (mg/ml)	C_o (mg/ml)	$t_{1/2}$ (Hours)	R^2
S_1(1 mg/ml)	0.46	23.76	0.999
S_2 (1.5 mg/ml)	0.6	8.4	0.983
S_3 (2 mg/ml)	0.79	7.2	0.863
S_4 (5 mg/ml)	0.9	4.8	0.931

TABLE 6.3: % Cumulative drug release

TIME (DAYS)	$T^{1/2}$	S1 (1 mg/ml)	S2 (1.5mg/ml)	S3 (2 mg/ml)	S4 (5 mg/ml)
1	1.00	4.4	10	3.5	6.25
2	1.41	26.8	23	15.33	17.5
3	1.73	30.92	39	17.33	35
4	2.00	37.76	53	53.33	50
5	2.24	45.72	67	66.67	65
6	2.45	60.12	71.67	78.67	77.5
7	2.65	66.12	79.17	90	88.75
8	2.82	76.52	82.5	96.67	96.25
9	3.00	79.72			
10	3.16	81.72			
11	3.32	82.92			

TABLE 6.4 (a): n values for the different formulations

	S1	S2	S3	S4
n	0.12	0.19	0.24	0.19
k	-0.36	-0.62	-0.48	-0.58
R^2	0.91	0.90	0.87	0.72

Table 4(b): Exponent n of the power law and drug release mechanism from polymeric controlled delivery systems of spherical geometry

Diffusion exponent (n)	Overall solute diffusion mechanism
0.43	Fickian diffusion
0.43 < n < 0.85	Anomalous (non-Fickian) diffusion
0.85	Case-II transport

CHAPTER 7

7.0 Concluding Remarks and Suggestions for Future Work

7.1 Summary and Concluding Remarks

This dissertation presented two approaches for the targeted drug delivery for the treatment of breast cancer. One approach was the use of gold nanoparticles functionalized with targeting moieties (LHRH and Folic Acid) and tethered with prodigiosin, an anti-cancer drug, to actively target cancerous cells through endocytosis. The second approach involved the use of encapsulated prodigiosin in chitosan microspheres for localized drug delivery. Some of the salient results and conclusions made in the course of this study are stated below.

The results from our preliminary work on the biosynthesis of gold nanoparticles from *Nauclea latifolia* leaf extracts showed that gold nanoparticles were synthesized in a record time of < 30 seconds [1] at pH 7.0. The TEM result revealed that most of the nanoparticles were spherical and that the sizes varied from 10nm - 60 nm, which is ideal for biomedical applications [2, 3]. In chapter 3, we presented the conjugation of the biosynthesized AuNPs with LHRH. Evidence of the actual conjugation was based on the comparison of unconjugated with the conjugated gold nanoparticles. The appearance of a second peak at 260 nm in the UV-Vis spectrum of the conjugated nanoparticles, together with the peak characteristic of AuNPs at 540 nm confirms the presence of the peptide, LHRH [4].

A comparison of the hydrodynamic diameters and the polydispersity index of the gold naonoparticles synthesized (before and after conjugation) were equally studied. The z-average increased with the addition of the ligand, LHRH and further still when the anti-cancer drug, prodigiosin (PG), was added (47.9 nm, 58.9 nm and 60.2 nm, respectively). The adhesion results showed that the adhesion force between LHRH-conjugated biosynthesized AuNPs and the breast

cancer cell line MDA-MB-231 was greater (by a factor of five) than that of LHRH-conjugated AuNPs to normal breast cells (cell line MCF-10A). This therefore defines the specificity of LHRH to cancer cells and hence increases its potential for use in selective and specific targeting and treatment of breast cancer.

The ability of the bacteria, *Serratia marcescens* to synthesize gold nanoparticles both intra-and extra-cellularly and was demonstrated in chapter 4. The cell-conditioned medium proved to be more effective than the biomass for the synthesis of gold nanoparticles, since nanoparticles synthesis with the conditioned medium requires lesser reaction times. The optimum pH for the synthesis was found to be pH 4. The secondary metabolite from *Serratia*, prodigiosin, was also used to synthesize AuNPs, and was shown to be responsible for the reduction of $HAuCl_4$ to form elemental Au. Most of the nanoparticles produced by prodigiosin have a PDI of between 0.2 and 0.3 meaning that they are mildly polydispersed.

The purpose of chapter 5 was to try to profer a solution to the particular type of breast cancer prevalent among black Americans, Hispanics and mostly African women. This type of cancer is called triple negative breast cancer (TNBC). From a review of the literature, it was found that TNBC over expresses folate receptors on their surfaces, hence the effort using folic acid as the targeting moity. AuNPs were conjugated to the folic acid through the N-hydroxy succinamide ester of folate. The conjugation was confirmed through a series of characterizations including UV-Vis spectroscopy, TEM, FTIR, DLS and HIM. The most interesting result was the image from the HIM analysis that showed clearly the ring of folate coating the AuNPs. FTIR analysis was performed to further confirm the conjugation of Folate-S-AuNPs. The results revealed carboxylic acid (C=O) stretching vibrations at 1670 cm-1 originating from folic acid. There was

also the appearance of double peaks at 1010 cm-1 and 930 cm-1 corresponding to carbonyl stretching (C=S) and –SH stretching which account for the presence of the thiol group in the reaction.

Adhesion measurements were done for the folate conjugated gold nanoparticles and the unconjugated moieties. The force of adhesion was compared between normal breast cells and TNBC cell line, MDA-MB-231. The highest adhesion was noticed in the AuNPs/folate conjugate with the adhesion force rising up to 80nN for the interaction with the triple negative breast cancer cells and 25 nN with the normal breast cells. These results clearly showed that conjugation of gold nanoparticles to the ligands improved their attachment to the cancer cells. In addition, the fact that the adhesion was higher with the cancerous cells than with the normal cells confirmed the specificity of the folate ligands.

In a bid to ensure total cure of breast cancer, we decided to consider multiple approaches to drug delivery, hence the idea of localized drug delivery (chapter 6). The extracted and purified prodigiosin was encapsulated in chitosan microspheres by a water-in-oil emulsion (w/o) technique. It was discovered that the drug: polymer ratio determined the encapsulation efficiency: the higher the drug: polymer ratio, the higher the PEE. The swelling ratio was also found to increase with the drug concentration, with the implication that patients with late stage or aggressive cancer will need the system that can release the drugs at a faster rate and, as such, reduce the number of cancerous cells. Subsequently, the drug design – with the slower release rate will then be used for early stage or less aggressive cancer. In terms of the cumulative drug release, the formulation with the higher polymer composition had the longest period of drug release. This was attributed to the smaller pore sizes which were due to the high level of cross

linking with chitosan. The initial drug release was due to diffusion and burst processes followed by a later degradation-controlled release for a smaller fraction of the drug. The release kinetics of prodigiosin from the microspheres was determined based on best fit of the models tested (zeroth-order and first-order models and the Higuchi model). The regression coefficients determined for the different models were: 0.964 for zeroth-order model; 0.999 for the first-order model and 0.975 for the Higuchi model. The first order model, therefore, was the best fit to the current data.

The effects of drug release from the microspheres were tested on viable breast cancer cells (MDA-MB-231cells), while breast cancer cells without drug were used as control. An appreciable decrease in cell viability was observed in the cancer cells while cell proliferation was observed in the control sample. The loss of cells' reproductive ability was largely due to the release of the drug onto the cells. The reduction in the cell viability is attributed to the induced apoptosis associated with prodigiosin release [5, 6].

In conclusion, a combination of / synergy between targeted drug using gold nanoparticles and localized drug delivery with the aid of encapsulated microspheres is a dependable method to ensuring a lasting solution to the menace of breast cancer. Secondly, the use of locally sourced materials in this study promises to reduce the cost of treatment while also making the drugs readily available especially in developing countries.

7.2 Suggestions for Future Work

In furtherance to the work covered by this desertation, the following suggestions are proferred as to future work.

7.2.1 Biosynthesis using *Nauclea latifolia.*

The leaf extracts of this plant were successfully used to synthesize gold nanoparticles within the shortest time ever recorded. However, the results from the TEM and the EDS indicated that some

impurities were present, so further purification processes need to be done before using the extract. Moreover, the phytochemical analysis of *Nauclea latifolia* showed that it contains alkaloids, flavonoids, tannins, saponins, phlobatanins, sterols and cyanogenic glycosides [7]. There is a need to evaluate these compounds to know the exact component or components that is involved in the actual reduction of the gold chloride. This will also help in achieving pure gold nanoparticles.

7.2.2 Use of folate for targeting triple negative breast cancer

From the work we have done, folic acid was successfully conjugated to gold nanoparticles. In addition, the adhesion measurements showed an increased adhesion of gold folate to the triple negative cell line (MDA-MB-231) compared to normal breast cells. However, we suggest that more TNBC cell lines be tested and also in addition to adhesion work, viability testing should be carried out to further validate the efficacy of folate in targeting TNBC.

7.2.3 Cell culture

In the course of this work, we have been able to achieve one very important feat, which is establishing a functional Human Cell Culture Laboratory for the first time in West Africa. This type of cell culture laboratory is essential for any meaningful biomedical research. At the present, we have the breast cancer cell line, MDA-MB-231, the normal breast cell line, MCF-10A under culture in the lab. We strongly suggest that more cell lines be acquired especially for other diseases so that many researchers and research into other diseases will benefit. Moreso, pertaining to the work in this dissertation, more in-depth cytology work needs to be done with the conjugated gold nanoparticles and the microspheres to study additional aspects of their interactions with normal cells and cancer cells.

7.2.4 Animal work.

The ultimate goal of this research is to use the results as a basis for human clinical trials and human use. To do this, additional processes and studies are necessary. First, is the *in vitro* study, which we have done with the cells, to test the efficacy of AuNPs-drug design. The next stage is to do *in-vivo* trials beginning with lower animals like mice before the human trials.

Virgin female Sprague-Dawley (SD) rats (6- 8weeks old), with weights of 180 - 200 g should be purchased. The animals will be housed two rats per plastic cages and allowed them to acclimate in standard conditions (under a 12 h light/dark cycle) for one week. The rats should be given free access to distilled water and food throughout the experiment. The breast cancer cell line, MDA-MB-231 should be maintained at 37°C in a humidified atmosphere of 5% CO_2 in L15 medium supplemented with 10% fetal bovine serum (FBS), and 1% penicillin/streptomycin. When the cells have reached 90% confluence, they should be harvested and suspended in 300 µl of phosphate buffered saline. The rats will be anesthetized by intraperitoneal injections. The cell suspension (6×10^6 cells in 300 µl PBS) should be drawn into 1ml insulin syringes without needles to minimize damage, lysis and death to the cells. The cell suspension should be inoculated subcutaneously into the mammary fat pad (right flank) of the SD rats using an insulin syringe with #26 gauge needle. The beds of rats should be supported with suitable heat lamp because animals may lose body heat during the procedure. The temperature, breathing and heart rates of animals should be monitored closely. To maintain a steady breathing rate, they should be gently turned over and back for 10 - 20 s and their position rotated every few minutes. Thereafter, animals should be palpated for the detection of mammary tumors twice each week. Tumors can be measured using digital calipers. They should then be weighed on a daily basis.
The latency period and the onset of tumor incidence should be noted as tumor growth landmarks [8]. All animals were monitored for mammary tumor development, followed by the injection of the gold nanoconjugate-drug design of various concentrations dispersed in de-ionized water. The effect of the drug design on the tumor cells at different time intervals

References

1. Dozie-Nwachukwu, S. O., Etuk-Udo, G., Obayemi, J. D., Anuku, N., Odusanya, O.S., Malatesta, K., Chi, C., Soboyejo, W.O. Biosynthesis of Gold Nanoparticles from *Nauclea Latifolia* Leaves. Advanced Materials Research, 1132; 36-50 (2015).

2. Ahmad, A., Mukherjee, P., Mandal, D., Senapati, S., Khan, M.I., Kumar, R., Sastry, M.: Enzyme mediated extracellular synthesis of CdS nanoparticles by the fungus, *Fusarium oxysporum.* J Am Chem Soc. **124,** 12108-12109, (2002).

3. Li, S.D., Huang, L.: Nanoparticles evading the reticuloendothelial system: role of the supported bilayer. Biochim Biphys Acta. **788**(10) 2259–2266 (2009).

4. Rogošić, M., Mencer, H.J., Gomzi, Z.: Polydispersity index and molecular weight distributions of polymers. European Polymer Journal. 32, (11), 1337–1344 (1996).

5. Williams, N. R., Fineran, P. C., Leeper, F. J., Salmond, G. P. The biosynthesis and regulation of bacterial prodiginines. Nat. Rev. Microbiol , 4; 887-889 (2006)

6. Pandi, S. K., Arul, D., Smiline, A. S. G., Hairul, I. V., Saravanan, S.V. G., Raghuraman, R: Prodigiosin Induced Apoptosis and Inhibited Proliferation in Carcinoma Hsc-2 Cells. Int. J. of Current Research, 3(4): 151-156 (2011).

7. Eze, S. O., Obinwa, E. Phytochemical and Nutrient Evaluation of the Leaves and Fruits of Nauclea latifolia (Uvuru-ilu). Communications in Applied Sciences; 2, (1), 8-24 (2014).

8. Riveraa, E.S., Andradeb, N., Martin, G., Melitoa, G., Cricco, G., Mohamada, N., Davioa, C., Caroa, R., Bergoc, R. M. Induction of mammary tumors in rat by intraperitoneal injection of NMU: histopathology and estral cycle influence. Cancer Lett. 86: 223-228 (1994).